The Dissertation Committee for Maria Andrea Miller Certifies that this is the approved version of the following dissertation:

Highly Concentrated, Nanoclusters of Self-crowded Monoclonal Antibodies for Low Viscosity, Subcutaneous Injections

Committee:

Keith P. Johnston, Supervisor

Jennifer Maynard, Co-Supervisor

Thomas Edgar

Thomas Truskett

Robert O. Williams, III

Highly Concentrated, Nanoclusters of Self-crowded Monoclonal Antibodies for Low Viscosity, Subcutaneous Injections

by

Maria Andrea Miller, B.S.

Dissertation

Presented to the Faculty of the Graduate School of

The University of Texas at Austin

in Partial Fulfillment

of the Requirements

for the Degree of

Doctor of Philosophy

The University of Texas at Austin

May 2011

Acknowledgements

No dissertation is ever truly the work of just one individual. There are many people who I need to thank for helping me to pursue a Ph.D. First off would be my family. Without the encouragement of my parents and husband, I would not be in the position I am today. In addition, to all of my friends who have seen me through the rough times and helped me along the way. I also need to thank all those who have helped me navigate the course of my studies. I wouldn't be where I am today without my advisor, Keith Johnston. I also need to thank, Jennifer Maynard for being a very helpful co-advisor with the work I have done with proteins. In addition, I need to thank Bill Williams for being a collaborator on the poorly water soluble drug project. In addition, many students in their groups including Jennifer Pai, Tarik Khan, Jamie Sutherland, Nicole Bienborn, Kevin O'Donnell, Wei Yang, and James DiNunzio as well as Michal Matteucci, Josh Engstrom, Jasmine Tam, Miguel Rodrigues, Mehul Patel in Dr. Johnston's group have taught me various techniques used in my studies and helped me along the way. I would never have been able to finish all the work in this dissertation without the additional help from, Michal Matteucci, Aileen Dinin, Ameya Bordwakar, Tarik Khan, Jamie Sutherland, Miguel Rodrigues, James DiNunzio, Kevin O'Donnell and undergraduate students, Brian Wilson, Kevin Kaczorowski, David Vier, Austin Irvin, Vidia Paramita, Baltej Ludher.

Highly Concentrated, Nanoclusters of Self-crowded Monoclonal Antibodies for Low Viscosity, Subcutaneous Injections

Publication No._____

Maria Andrea Miller, Ph.D.

The University of Texas at Austin, 2011

Supervisor: Keith P. Johnston

Co-Supervisor: Jennifer Maynard

Delivery of protein therapeutics is restricted to intravenous infusions due to protein-dependent problems including low solubilities, high viscosities, and physical instabilities. The ability to inject high concentrations of proteins via subcutaneous injections would increase accessibility and compliance. Large particles of a protein in a non-aqueous solvent can decrease the viscosity over a solution of equally concentrated individual protein molecules. The lower viscosity of a particle suspension is due to decreased surface area resulting in reduced electroviscous effects, solvation and deviations of the particle shape from a spherical geometry.

Additional studies show that aqueous-based dispersions of antibody nanoclusters can be formed by increasing the attractive interactions between protein molecules using the excluded volume effects of extrinsic crowding agents. These novel, equilibrium, nanoclusters are maintained by a balance of highly attractive interactions and weak electrostatic repulsive interactions near the protein's pI. These protein nanoclusters are

ideal for subcutaneous delivery as they have low interactions between the colloids, are reversible in nature, and dissolve rapidly upon dilution in a buffer media. Through *in vivo* mouse studies, the bioavailability of a monoclonal antibody in the dispersion is prolonged and higher doses can be administered versus a solution. Overall, these studies with high concentration, low viscosity subcutaneous injections of protein therapeutics open new opportunities in biotechnology.

For oral delivery of itraconzole, controlled flocculation of individual polymerically-stabilized nanoparticles is used to increase supersaturation. Flocculation of these nanoparticles is achieved by desolvating the polymer by changing the pH. The flocculated dispersions can then be easily filtered. The final amorphous powder maintains high supersaturation with simulated stomach and small intestine conditions and improves bioavailability of itraconazole, over the commercial product, Sporanox®.

Solutions of monoclonal antibodies are unstable for proper storage times, thus frozen storage stability of a monoclonal antibody is necessary. To create a representative small-scale model of freezing in a commercial tank, understanding of the effects of freezing rate, freeze-concentration, and exposure of the protein to interfaces on protein aggregation is essential. Studies of frozen storage stability at various freezing rates were conducted under different storage conditions for up to 1 year.

Table of Contents

List of Tables

List of Figures

Chapter 1: Introduction

Proteins for use as therapeutics have received much attention due to advances in recombinant DNA technology and synthetic techniques to manufacture them.[1-3] In addition, they are viewed to be less toxic and behave more predictably *in vivo* therefore expanding and improving patient treatment.[4, 5] Lagging behind however is the ability to effectively deliver these large macromolecules.[1] Proteins are readily denatured by a variety of stresses including heating, agitation, freezing, pH changes and exposure to interfaces and denaturants.[3, 6] In addition, proteins can be chemically modified by reactions such as hydrolysis and deamidation.[2, 6] Once denatured, the protein can aggregate to form soluble or insoluble, non-covalent or covalent, and reversible or irreversible aggregates.[3] On top of the effect of environmental conditions around the protein, the structure of the protein, both primary and secondary structures, may play a role in the ability and the degree of protein aggregation.[7, 8] Monoclonal antibodies (MAb) are of particular interest as therapeutics because they can successfully target distinct antigens and can potentially be used in the treatment of many diseases such as cancer, allergic diseases, asthma and other inflammatory diseases, cardiovascular, respiratory and infectious diseases.[9, 10] As a result, it is estimated that as of 2003 >20% of all biopharmaceuticals being evaluated in clinical trials were mAbs.[9]

To overcome the instabilities proteins encounter in solution, dry protein powders can be produced to improve shelf life of proteins at ambient temperatures.[11-13] Lyophilization has been a common method used to produce stable dry protein powders.[13, 14] During lyophilization, the liquid protein solution is slowly cooled until frozen and then water is removed by sublimation under vacuum (Figure 1.1).[11] The low

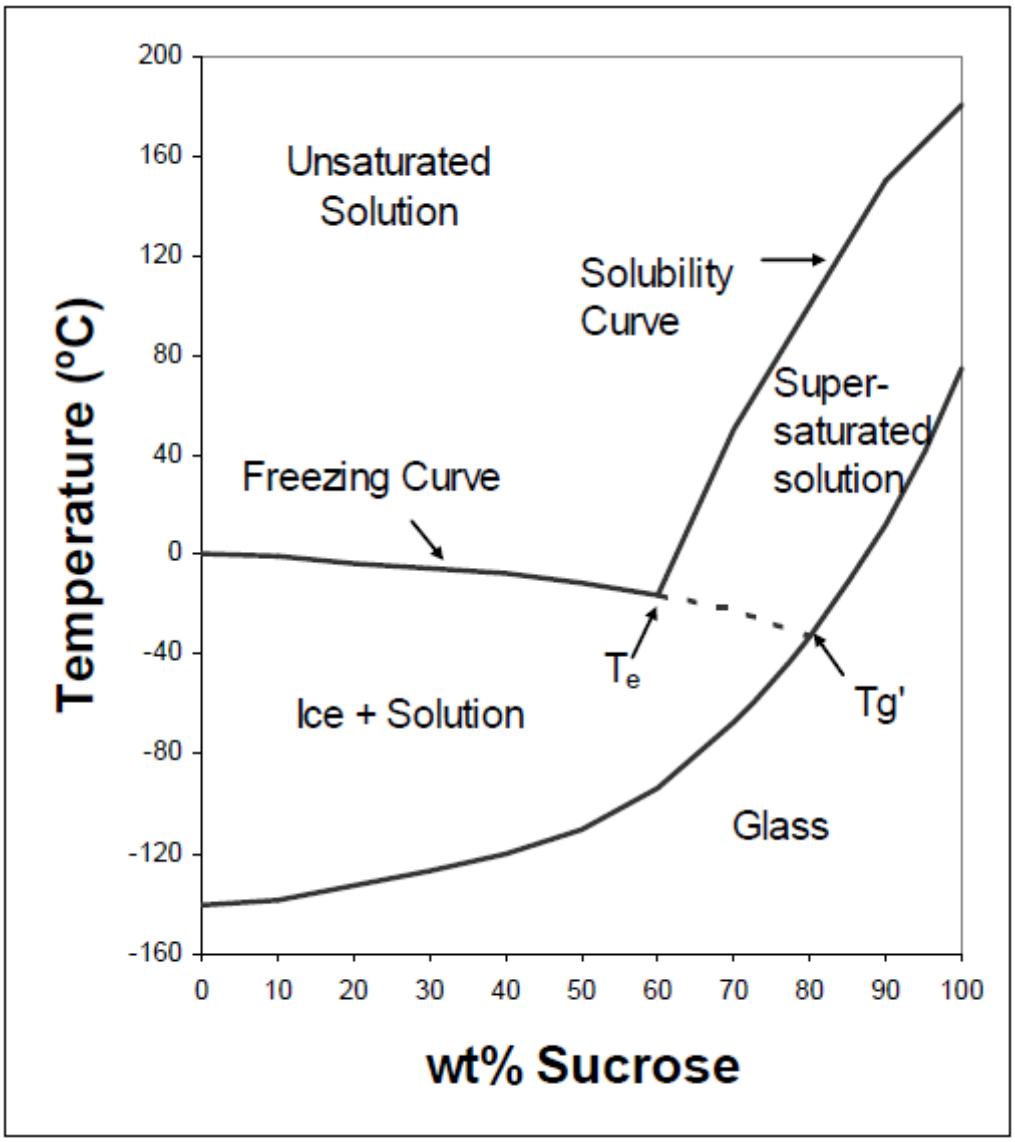

Figure 1.1 Solid-liquid diagram for the sucrose-water system. Adapted from figure 7 in Nail *et al.*[15]

specific surface area powder produced by lyophilization is typically reconstituted to a solution and delivered by an intravenous infusion.[16, 17] Formulation of protein therapeutics in general has often been limited to low concentration (<50 mg/mL) due to the chemical and physical instabilities of the active therapeutic.[4, 5, 9, 10, 18, 19] As a result, delivery of protein therapeutics has been typically limited to high volume intravenous injections (more than 2 mL) because a typical therapeutic dose is 100-1000 mg corresponding to several mg/kg dosing.[5, 9, 10] The primary focus of this dissertation is on the formation of highly concentrated, low viscosity suspensions of proteins suitable for subcutaneous delivery. Additional sections on increased supersaturation of amorphous poorly-water soluble drug particles, the formation of flocculated amorphous nanoparticles for oral delivery of itraconazole and on the relationship between freezing conditions and the stability of a monoclonal antibody over extended frozen storage follow.

1.1 CONCENTRATED PROTEIN SUSPENSIONS FOR SUBCUTANEOUS DELIVERY

To take full advantage of protein therapeutics, delivery techniques must be expanded to include some that are more readily accessible allowing for outpatient administration and home use, lowering the cost of treatment.[5, 9, 10, 19] Especially for mAbs (~150 kDa), large proteins are very unlikely candidates for non-invasive delivery routes including oral and pulmonary since membrane permeability and resulting bioavailability from these types of delivery is very low and has only barely been successful with small peptides.[10, 20, 21] Therefore, an alternative is to formulate a subcutaneous injection, similar to a relatively painless injection of insulin. However, for subcutaneous delivery, the maximum volume that can be administered is 1.5 mL, giving a necessary protein concentration greater than 100mg/mL for doses on the order of a few mg/kg.[5, 9, 10, 20, 22]

Currently, solution formulations have been explored to obtain a formulation with the necessary concentration range, however the increase in viscosity and the decrease in stability of the mAb are serious drawbacks to this approach.[5, 9, 18, 19, 23-26] MAbs reconstituted from a lyophilized powder or concentrated by techniques such as tangential flow filtration exhibit rapidly increasing viscosities at a concentration of approximately 125 mg/mL due to short-range attractive protein interactions, electrostatic effects, and excluded volume effects.[10, 22] Chemical reactions and physical interactions resulting in chemical modifications of the protein or physical aggregation of the protein have a linear or higher dependence on the concentration.[27] Thus, high concentrations of protein can increase the rates of physical aggregation and chemical modification of proteins.[27]

A novel approach is to create a low-viscosity suspension of the protein. Suspensions leave the mAb in the solid state and increase the stability of the protein by avoiding irreversible protein unfolding by decreasing protein flexibility, which is hypothesized to increase resistance to thermal denaturation and chemical degredation.[28] An increase in enzyme catalytic activity in nearly anhydrous organic solvents also attests to the stability of a protein in an organic solvent.[29, 30] In addition, suspensions of protein C and a proprietary mAb, in a polymer gel formulation and benzyl benzoate [31, 32] and factor IX, a therapeutic protein, in perfluorodecalin and perfluorotributylamine[23] have shown physical stability of the protein over an extended time of exposure to the organic solvents.

1.2 ISOLATION OF NANOPARTICLES OF A POORLY WATER SOLUBLE DRUG

A secondary objective of this dissertation is to improve oral drug delivery of a small molecule, poorly-water soluble drug, Itraconazole. It has been estimated 40% of drugs currently in development have poor water solubility, which leads to low

bioavailability of these therapeutic agents.[33, 34] For these poorly water soluble drugs, absorption into the blood stream from oral delivery is limited by low solubility in the GI tract.[35] Dissolution rates can be enhanced by increasing the surface area for adsorption, A, by reducing the particle size, as predicted by the Noyes-Whitney equation[36]

$$\frac{\partial M}{\partial t} = \frac{DA}{h}(\Delta C) \quad (1.1)$$

where M is the mass of undissolved drug, t is time, D is the average diffusion coefficient, and ΔC is the different between the equilibrium concentration of the drug adjacent to the particle surface and the concentration in the bulk. In addition, solutions of poorly water soluble drugs can be supersaturated by using the amorphous form.[37, 38] However, common techniques to form nanoparticles including mechanical milling[39] and high pressure homogenization[40] often require long processing times, risk contamination with impurities, and offer little control over the morphology of the final product.[41] Controlled, antisolvent precipitation (AP) to form polymerically stabilized nanoparticles of poorly water soluble drugs, offers more control over the production of amorphous particles with high drug loading with high process yields.[42-44] During AP, high surface area particles are produced by generating high levels of drug supersaturation to induce rapid nucleation in the presence of amphiphilic polymer stabilizers (Figure 1.2).[43, 44] The polymer stabilizer partitions to the interface introduced by the newly created drug surface to arrest particle growth and orients itself to increase steric stabilization.[44]

Polymerically stabilized aqueous nanoparticle dispersions of poorly water soluble drug may be isolated into a dry powder by a variety of methods. Spray drying has been used to isolate poorly water soluble drugs such as ketoconazole, itraconazole and ibuprofen particles.[45] However, the elevated temperatures (~90ºC), can result in crystallization of the therapeutic as the temperature approaches the glass transition temperature.[46] In addition, ultrafiltration with submicron polycarbonate membrane has

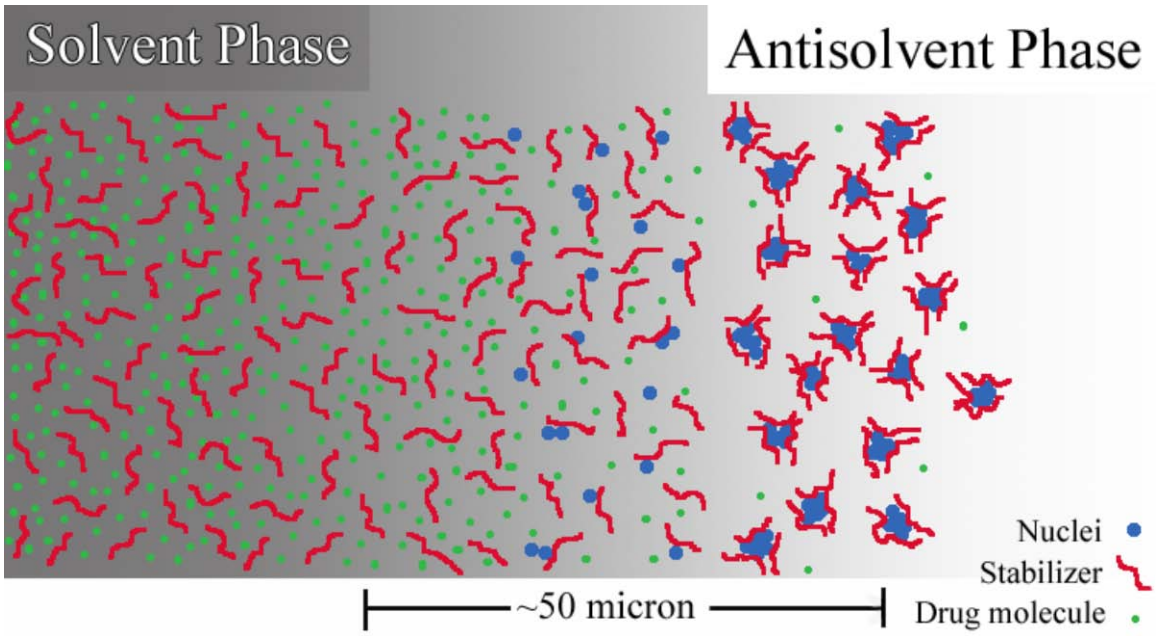

Figure 1.2 Controlled precipitation of drug particles in the presence of amphiphilic stabilizers.[43]

been used to isolate small microparticles of budesonide.[47] However, long processing times allow for possible agglomeration of the individual nanoparticles.

A third option is to rapidly flocculate polymer stabilized drug nanoparticle dispersions. The large flocs formed can be rapidly filtered to maintain the amorphous morphology of the drug.[8, 46] A critical flocculation temperature, corresponding to the cloud point temperature, may be observed for the stabilizing polymer in the aqueous nanoparticle dispersion.[48] This temperature can be decreased by the addition of inorganic salts, such as sodium sulfate.[49] Rapid flocculation of the nanoparticle dispersion with a constant overall volume fraction of solids results in the formation of open fractal flocs with a low fractal dimension (Figure 1.3).[46] In contrast, the particle volume fraction and the temperature increase during spray drying producing much denser flocs.[46] The differences in pathways in particle volume fraction and solvent conditions, as a function of temperature and salinity, is shown to have a profound effect on the particle size upon redispersion, and ultimately, the level of supersaturation as the particles dissolve.[46] However, in some cases the increase in salinity is not sufficient to reach the cloud point of the polymer at a reduced temperature; therefore there is a need to explore other methods to rapidly flocculate these amorphous nanoparticles. For example, the cloud point temperature can be readily accessible near room temperature for polymers where a change in dissociation with pH influences solvation.

1.3 OBJECTIVES

The primary goal for the first section of this dissertation is to improve the subcuanteous delivery of protein therapeutics, especially monoclonal antibodies, by

forming highly concentrated, non-aqueous and aqueous suspensions of model and therapeutic proteins. In the second section, the goal is to improve the oral delivery of the

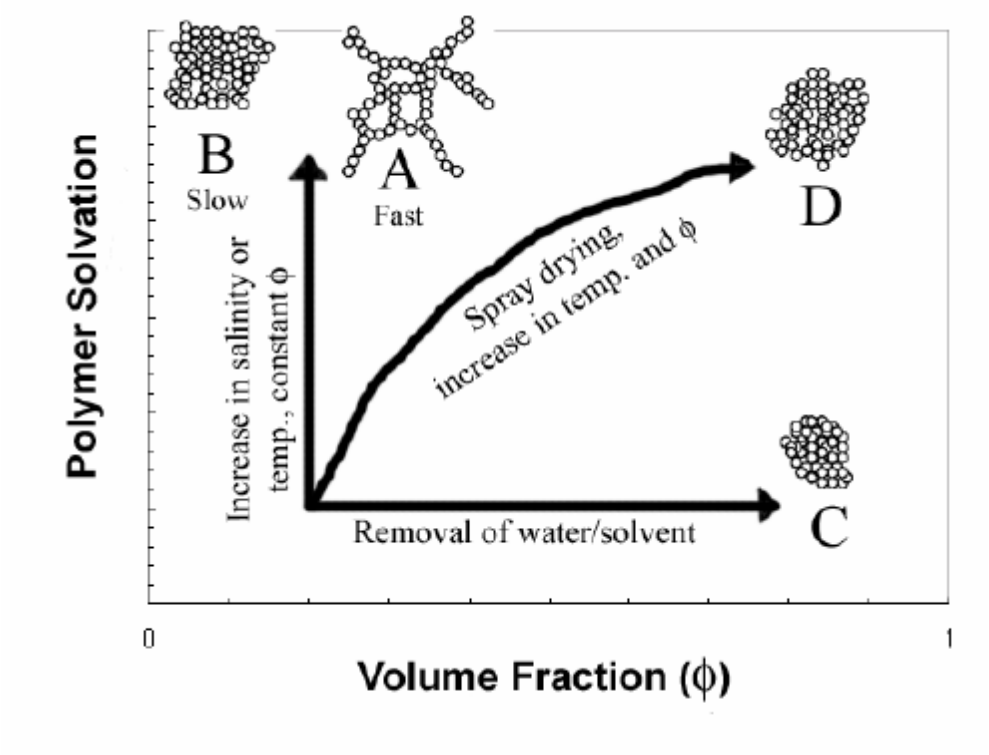

Figure 1.3 Floc structure as a function of polymer solvation and φ. Polymer solvency diminishes with increase in salinity or temperature.[46]

poorly water soluble drug, itraconazole, by using amorphous dry powders formed by antisolvent precipitation, flocculated, filtered and dried at room temperature. The final objective of this dissertation is to improve long term frozen storage of a monoclonal antibody therapeutic by analyzing the impact of freezing rate and freeze concentration on the stability of a monoclonal antibody over a time period of 2 months to a year.

To improve delivery of proteins by subcutaneous injections, the first objective is to form highly concentrated non-aqueous suspensions of the model protein lysozyme with apparent viscosities below 50 cP. Milled particles, smaller than 37 μm, of lyosyzme, were suspended in the non-aqueous solvent benzyl benzoate or a 50/50 volume mixture of safflower oil and benzyl benzoate at concentrations up to nearly 400 mg/ml. These highly concentrated suspensions produced apparent viscosities below 50cP due to their low intrinsic viscosity. The intrinsic viscosity, regressed from the Krieger-Dougherty model, is only slightly above the Einstein value of 2.5, indicating the increase in viscosity relative to that of the solvent was caused primarily by excluded volume. Thus, increases in viscosity from electrical double layer interactions, solvation of the particles, or deviations of the particle shape from a spherical geometry are minimal, and much smaller than typically observed for soluble protein aqueous solutions.

A second objective to improve delivery of proteins by subcutaneous injections is the formation of highly concentrated aqueous nanoclusters of an antibody. Here, we assemble a protein (sheep IgG) into translucent dispersions of 80-250nm nanoclusters at high concentrations, while simultaneously preserving the native folded state due to self-crowding. The design of slightly charged protein colloids at the isoelectric point is the opposite of the normal approach, where the protein is highly charged at a pH away from the isoelectric point to solubilize the protein monomer. The dispersions were formed by

gently stirring a mixture of lyophilized powder, with a mass ratio of protein/trehalose of 1/1 with a buffer solution, and in some cases, additional crowders. The size of the nanoclusters for an overall volume fraction, ϕ, up to 0.21 (275 mg/ml IgG) was varied by tuning the depletion attraction by varying the volume fraction of extrinsic crowder, ϕ_E, with trehalose as a single crowder, or with mixed crowders. At constant ϕ, the hydrodynamic diameters were equivalent at a given φ_E, upon changing φ_E along various pathways, upwards and downwards, suggesting an approach to thermodynamic equilibrium. Thus, concentrated equilibrium nanoclusters may be formed at the isoelectric point, where the short range attractive forces are strong enough to balance the repulsion from the small charge on the protein. Universality of the mechanism is shown by utilizing a second, potentially therapeutic monoclonal antibody, mAb1B7. Similar nanoclusters dispersions to those formed with the sheep IgG are formed. Additional *in vitro* stability of the mAb1B7 shows that the formation of nanoclusters does not impact the binding of mAb1B7 to Pertussis toxin. Further *in vivo* studies resulted in a favorable pharmacokinetic profile with a reduced burst phase, as compared to intravenous or subcutaneous injection of an antibody solution at the same concentration. Many people contributed to the completion of these chapters including Ameya Borwankar, Brian Wilson, Aileen Dinin, Tarik Khan, Kevin Kaczorowski, Jamie Sutherland, and Jamye O'Neal. In addition to running many of the experiments used in this study, Brian Wilson contributed significantly in the discovery and tunability of the translucent dispersions. Ameya Borwankar with the help of Thomas Truskett created the model for predicting cluster size and contributed significant time and effort to obtaining many of the dynamic light scattering results obtained. *In vivo* studies were conducted with the help of Tarik Khan and Jamye O'Neal.

To improve oral delivery of the poorly water soluble drug, itraconazole, the primary objective is to investigate an alternate recovery method for antisolvent precipitated nanoparticles using flocculation by changing the pH. Amorphous nanoparticle dispersions stabilized with a pH sensitive polymer, Eudragit®L100-55, are flocculated by the reduction of pH to 2.5 where the polymer is no longer charged. The rapid change in pH desolvates the polymeric stabilizer resulting in strong attractive forces between the nanoparticles to form open flocs. The particles are flocculated under constant volume of particles, without removing water. After flocculation, the flocs are rapidly filtered using high porosity filter paper and air drying to remove residual water. The particles remain amorphous throughout flocculation, filtration and drying with high yields. Previously, salt flocculation has been demonstrated with antisolvent precipitation of naproxen[8] and itraconazole[46, 50]. This dissertation extends the study of flocculation to form amorphous particles, by demonstrating the high sustained supersaturation and *in vivo* bioavailability of a powder formed by pH flocculation. The original salt flocculation process was the work of Michal Matteucci. The *in vivo* studies were conducted by James DiNunzio. In addition, the theory of the excess heat capacity leading to increased supersaturation is analyzed in depth for antisolvent precipitated nanoparticles of itraconazole. This work was originated and many of the calculations initially run by Michal Matteucci.

1.4 DISSERTATION OUTLINE

Chapter 2 presents apparent viscosities below 50 cP are reported for suspensions of milled lysozyme microparticles up to nearly 400 mg/ml in benzyl benzoate or benzyl benzoate mixtures with safflower oils through a syringe with a 25 to 27-gauge needle at room temperature. These apparent viscosities were confirmed using a cone-and-plate

rheometer. The intrinsic viscosity regressed from the Kreiger-Dougherty model was only slightly above the Einstein value of 2.5, indicating the increase in viscosity relative to that of the solvent was caused primarily by the excluded volume. Thus, the increases in viscosity from electrical double layer interactions (electroviscous effects), solvation of the particles, or deviations of the particle shape from a spherical geometry were minimal, and much smaller than typically observed for proteins dissolved in aqueous solutions. The small electroviscous effects are expected given the negligible zeta potential and thin double layers in the low dielectric constant organic solvent. The suspensions were resuspendable after a year, with essentially constant particle size after two months as measured by static light scattering. The lower apparent viscosities for highly concentrated protein suspensions relative to protein solutions, coupled with these favorable characteristics upon resuspension, may offer novel opportunities for subcutaneous injection of therapeutic proteins.

Chapter 3 shows how highly concentrated, polyclonal sheep IgG is crowded by extrinsic molecular crowders, into 80-250nm clusters to form aqueous dispersions. These dispersions allow protein self-crowding within the cluster to preserve the native folded state. These novel, equilibrium clusters are formed by balancing attraction from the extrinsic molecular crowders and the inherent specific short-range protein interactions against very weak electrostatic charging of the protein near the isoelectric point. Equally sized nanoclusters were formed by multiple techniques including dispersing a lyophilized protein powder to an aqueous solution containing additional molecular crowders and adding and removing crowders from a protein solution. A universal curve, based on the total φ of crowders in the dispersion but independent of the type of crowder used, can be formed from individual and multiple crowders, including trehalose, PEG300 and NMP. Since the φ of the protein within the nanoclusters is estimated to be at least 0.3, protein

self-crowding within the cluster is anticipated to prevent protein unfolding. The consistent, equilibrium size of the cluster allows the interactions to be viewed from the standpoint of a protein or the cluster as an individual entity. Thus, by changing the colloid size from a protein monomer (~1-15nm) to a submicron nanocluster (80-250nm), specific short-range attractive interactions on the protein, whose influence is important to ~1nm from the surface, and excluded volume effects from the extrinsic molecular crowders can be minimized. The decreased effect of specific short-range attractive interactions results in decreased viscosity of the nanocluster dispersion when compared to a protein solution.

In Chapter 4, the concept of forming highly concentrated, aqueous dispersions of mAbs is expanded to a therapeutic mAb1B7 to show universality of Chapter 3. Dispersions of antibody particles were created by rapid freezing and lyophilization, followed by particle suspension in a buffer that limits antibody dissolution. By changing the colloid size from a protein monomer (~10 nm) to a submicron cluster (~200 nm), the effects of specific short-range attractive interactions are minimized, resulting in decreased viscosity and increased colloidal and protein stability. This procedure provided antibody dispersions in high yield, with no detectable alteration of tertiary structure and full retention of biological activity *in vitro*. Subcutaneous administration of amorphous antibody dispersions resulted in a favorable pharmacokinetic profile with a reduced burst phase, as compared to intravenous or subcutaneous injection of an antibody solution at the same concentration. Moreover, antibody present in the serum retained full activity as measured by *in vitro* binding and cellular neutralization assays.

Chapter 5 presents the rapid flocculation of nanoparticle dispersions of a poorly water soluble drug, itraconazole (Itz). Rapid flocculation was utilized to produce amorphous powders with desirable dissolution properties for high bioavailability in rats.

Antisolvent precipitation (AP) was utilized to form Itz nanodispersions with high drug loadings stabilized with hydroxypropylmethylcellulose (HPMC) or the pH-sensitive Eudragit® L100-55 (EL10055). The HPMC dispersions were flocculated by desolvating the polymer through the addition of a divalent salt, and the enteric EL10055 by reducing the pH. The formation of open flocs by essentially diffusion limited aggregation, facilitated redispersion of the flocs at pH 6.8. Upon redispersion of the flocculated nanoparticles at pH 6.8, the particle size was modestly larger than the original size, on the order of 1 μm. High *in vitro* supersaturation (AUC) of the flocculated nanoparticle dispersions was observed in micellar media at pH 6.8, after 2 hours initial exposure at pH 1.2 to simulate the stomach, relative to the AUC for a commercially available solid dispersion Itz formulation, Sporanox. Greater *in vivo* bioavailability in rats was correlated directly to the higher *in vitro* AUC at pH 6.8 with micelles during the pH shift experiment for the flocculated nanoparticle dispersions relative to Sporanox. The ability to generate and sustain high supersaturation in micellar media at pH 6.8, as shown with the *in vitro* pH shift dissolution test, is beneficial for increasing bioavailability of Itz by oral delivery.

In Chapter 6, dissolution of pure solid itraconazole in metastable amorphous states was used to produce high supersaturation in low pH media. For a pre-wet dispersion of particles on the order of 1 μm produced by antisolvent precipitation, an experimental supersaturation of 63 times the crystalline solubility was achieved. This experimental value approached the calculated value of 95 from the configurational free energy, G_{conf}, which was determined from modulated differential scanning calorimetry measurements. A high fragility, quantitatively determined by the fragility parameter, γ_{cp}, is dependent on the configurational heat capacity, C_{pconf}, favoring a high G_{conf} and thus high supersaturation. However, high fragility also increases the driving force for

crystallization of the solid during dissolution. The relatively fragile pre-wet dispersions dissolved rapidly and produced high supersaturation without crystallizing, in contrast with much lower supersaturation values for slowly dissolving particles with low wet surface areas formed by spray drying or lyophilization of aqueous dispersions.

1.5 REFERENCES

1. Banerjee, P. S.; Hosny, E. A.; Robinson, J. R., Parenteral Delivery of Peptide and Protein Drugs. In *Peptide and Protein Drug Delivery*, Lee, V. H. L., Ed. 1991; Vol. 4, pp 487-543.

2. Manning, M. C.; Patel, K.; Borchardt, R. T., Stability of Protein Pharmaceuticals. *Pharm Res* **1989,** 6, (11), 903-918.

3. Wang, W., Protein aggregation and its inhibition in biopharmaceutics. *Int. J. Pharm.* **2005,** 289, 1-30.

4. Frokjaer, S.; Otzen, D. E., Protein Drug Stability: A Formulation Challenge. *Nat. Rev. Drug Discovery* **2005,** 4, 298-306.

5. Dani, B.; Platz, R.; Tzannis, S. T., High Concentration Formulation Feasibility of Human Immunoglubulin G for Subcutaneous Administration. *J. Pharm. Sci.* **2007,** 96, (6), 1504-1517.

6. Carpenter, J. F.; Izutsu, K.-i.; Randolph, T. W., Freezing and drying induced perturbations of protein structure and mechanisms of protein protection by stabilizing additives. In *Freeze Drying/Lyophilization of Pharmaceutical and Biological Products*, Rey, L.; May, J. C., Eds. Marcel Dekker, Inc.: New York, 2004; Vol. 137, pp 147-186.

7. Wang, W., Instability, stabilization, and formulation of liquid protein pharmaceuticals. *Int. J. Pharm.* **1999,** 185, 129-188.

8. Chennamsetty, N.; Voynov, V.; Kayser, V.; Helk, B.; Trout, B. L., Design of therapeutic proteins with enhanced stability. *PNAS* **2009,** 106, (29), 11937-11942.

9. Yang, M. X.; Shenoy, B.; Disttler, M.; Patel, R.; McGrath, M.; Pechenov, S.; Margolin, A. L., Crystalline monoclonal antibodies for subcutaneous delivery. *PNAS* **2003,** 100, (12), 6934-6939.

10. Liu, J.; Nguyen, M. D. H.; Andya, J. D.; Shire, S. J., Reversible Self-Association Increases the Viscosity of a Concentrated Monoclonal Antibody in Aqueous Solution. *Journal of Pharmaceutical Sciences* **2005,** 94, (9), 1928-1940.

11. Costantino, H. R.; Firouzabadian, L.; Hogeland, K.; Wu, C. C.; Beganski, C.; Carrasquillo, K. G.; Cordova, M.; Griebenow, K.; Zale, S. E.; Tracy, M. A., Protein spray-freeze drying. Effect of atomization conditions on particle size and stability. *Pharm Res* **2000,** 17, 1374-1383.

12. Maa, Y.-F.; Costantino, H. R., Spray freeze-drying of biopharmaceuticals: applications and stability considerations. In *Lyophilization of Biopharmaceuticals*, Costantino, H. R.; Pikal, M. J., Eds. American Association of Pharmaceutical Scientists: Arlington, 2004; Vol. 2.

13. Webb, S. D.; Golledge, S. L.; Cleland, J. L.; Carpenter, J. F.; Randolph, T. W., Surface adsorption of recombinant human interferon-gamma in lyophilized and spray-lyophilized formulations. *J Pharm Sci* **2002,** 91, 1474-1487.

14. Carpenter, J. F.; Chang, B. S.; Randolph, T. W., Physical Damage to Proteins During Freezing, Drying and Rehydration. In *Lyophilization of Biopharmaceuticals*, Costantino, H. R.; Pikal, M. J., Eds. AAPS Press: 2005; pp 423-442.

15. Nail, S. L.; Jiang, S.; Chongprasert, S.; Knopp, S. A., Fundamentals of freeze-drying. In *Pharmaceutical Biotechnology. 14. Development and Manufacture of Protein Pharmaceuticals*, Nail, S. L.; Akers, M. J., Eds. Kluwer Academic/Plenum Publishers: New York, 2002; pp 281-360.

16. Wang, W., Lyophilization and development of solid protein pharmaceuticals. *Int. J. Pharm.* **2000,** 2000, 1-60.

17. Leach, W. T.; Simpson, D. T.; Val, T. N.; Anuta, E. C.; Yu, Z.; Williams III, R. O.; Johnston, K. P., Uniform encapsulation of stable protein nanoparticles produced by spray freezing for the reduction of burst release. *J Pharm Sci* **2005,** 94, 56-69.

18. Defelippis, M. R.; Akers, M. J., Peptides and Proteins as Parenteral Suspensions: an Overview of Design, Development, and Manufacturing Considerations. In *Pharmaceutical Formulation Development of Peptides and Proteins*, Frokjaer, S.; Hovgaard, L., Eds. Taylor & Francis Limited: Philadelphia, 2000; pp 113-143.

19. Harris, R. J.; Shire, S. J.; Winter, C., Commercial Manufacturing Scale Formulation and Analytical Characterization of Therapeutic Recombinant Antibodies. *Drug Dev. Res.* **2004,** 61, 137-154.

20. Brown, L. R., Commercial challenges of protein drug delivery. *Expert Opin. Drug Deliv.* **2005,** 2, (1), 29-42.

21. Pawar, R.; Ben-Ari, A.; Domb, A. J., Protein and peptide parenteral controlled delivery. *Expert Opin. Biol. Ther.* **2004,** 4, (8), 1203-1212.

22. Shire, S. J.; Shahrokh, Z.; Liu, J., Challenges in the Development of High Protein Concentration Formulations. *Journal of Pharmaceutical Sciences* **2004,** 93, (6), 1390-1402.

23. Knepp, V. M.; Muchnik, A.; Oldmark, S.; Kalashnikova, L., Stability of Nonaqueous Suspension Formulations of Plasma Derived Factor IV and Recombinant Human Alpha Interferon at Elevated Temperatures. *Pharm. Res.* **1998,** 15, (7), 1090-1095.

24. Liu, J.; Nguyen, M. D. H.; Andya, J. D.; Shire, S. J., Reversible Self-Association Increases the Viscosity of a Concentrated Monoclonal Antibody in Aqueous Solution. *J. Pharm. Sci.* **2005,** 94, (9), 1928-1940.

25. Saluja, A.; Badkar, A. V.; Zeng, D. L.; Nema, S.; Kalonia, D. S., Ultrasonic Storage Modulus as a Novel Parameter for Analyzing Protein-Protein Interactions in High Protein Concentration Solutions: Correlation with Static and Dynamic Light Scattering Measurements. *Biophys J* **2007,** 92, 234-244.

26. Harn, N.; Allan, C.; Oliver, C.; Middaugh, C. R., Highly Concentrated Monoclonal Antibody Solutions: Direct Analysis of Physical Structure and Thermal Stability. *J. Pharm. Sci.* **2007,** 96, (3), 532-546.

27. Saluja, A.; Kalonia, D. S., Nature and consequences of protein-protein interactions in high protein concentration solutions. *Int. J. Pharm.* **2008,** 358, 1-15.

28. Stevenson, C. L., Characterization of Protein and Peptide Stability and Solubility in Non-Aqueous Solvents. *Current Pharmaceutical Biotechnology* **2000,** 1, 165-182.

29. McMinn, J. H.; Sowa, M. J.; Charnick, S. B.; Paulaitis, M. E., The Hydration of Proteins in Nearly Anhydrous Organic Solvent Suspensions. *Biopolymers* **1993,** 33, 1213-1224.

30. Halling, P. J., High-affinity binding of water by proteins is similar in air and in organic solvents. *Biochimica et Biophysica Acta* **1990,** 1040, 225-228.

31. Chen, G.; Luk, A.; Houston, P.; Li, L.; Sharon, M.; Garley, M.; Bannister, R.; Hill, B.; Lucas, C.; Volkin, D.; Dalmonte, P.; Qi, P.; Khossravi, M.; Blasie, C.;

Grousnick, K.; Huang, M.; Wang, D.; Zhao, H.; Zhu, Y.; Martin, P.; Treacy, G. In *Injectable nonaqueous suspension of highly concentrated proteins for non-IV administration*, AAPS Annual Meeting and Exposition, Nashville, TN, 2005; The AAPS Journal: Nashville, TN, 2005.

32. Chaubal, M. V.; Zhao, Z.; Bruley, D. F., Novel injectable gels for the sustained release of protein C. In *Advances in Experimental Medicine and Biology*, Kluwer Academic/Plenum Publishers: Baltimore, 2003; Vol. 540 (Oxygen Transport to Tissue XXV), pp 147-155.

33. Lipinski, C. A., Avoiding investment in doomer drugs, is poor solubility an industry wide problem? *Current Drug Discovery* **2001**, 17-19.

34. Lipinski, C. A., Poor aqueous solubility - an industry wide problem in drug discovery. *Am. Pharm. Rev.* **2002,** 5, 82-85.

35. Amidon, G. L.; Lennernas, H.; Shah, V. P.; Crison, J. R., A Theoretical Basis for a Biopharmaceutical Drug Classification: The Correlation of in Vitro Drug Product Dissolution and In Vivo Bioavailability. *Pharm Res* **1995,** 12, (3), 413-420.

36. Noyes, A. A.; Whitney, W. R., The rate of solution of solid substances in their own solutions. *Journal of the American Chemical Society* **1897,** 19, 930-934.

37. Matteucci, M. E.; Miller, M. A.; Williams III, R. O.; Johnston, K. P., Highly Supersaturated Solutions of Amorphous Drugs Approaching Predictions from Configurational Thermodynamic Properties. *Journal of Physical Chemistry B* **2008,** 112, (51), 166675-16681.

38. Hancock, B. C.; Parks, M., What is the True Solubility Advantage for Amorphous Pharmaceuticals? *Pharm Res* **2000,** 17, (4), 397-404.

39. Liversidge, E. M.; Liversidge, G. G.; Cooper, E. R., Nanosizing: a formulation approach for poorly-water-soluble compounds. *Eur J Pharm Sci* **2003,** 18, 113-120.

40. Zhang, F.; Skoda, M. W. A.; Jacobs, R. M. J.; Martin, R. A.; Martin, C. M.; Schreiber, F., Protein Interactions Studied by SAXS: Effect of Ionic Strength and Protein Concentration for BSA in Aqueous Solutions. *J Phys Chem B* **2007,** 111, 251-259.

41. Muller, R. H.; Jacobs, C.; Kayser, O., Nanosuspensions as particulate drug formulations in therapy: Rationale for development and what we can expect for the future. *Advanced Drug Delivery Reviews* **2001,** 47, 3-19.

42. Rogers, T. L.; Gillespie, I. B.; Hitt, J. E.; Fransen, K. L.; Crowl, C. A.; Tucker, C. J.; Kupperblatt, G. B.; Becker, J. N.; Wilson, D. L.; Todd, C.; Broomall, C. F.; Evans, J. C.; Elder, E. J., Development and Characterization of a Scalable Controlled Precipitation Process to Enhance the Dissolution of Poorly Water-Soluble Drugs. *Pharmaceutical Research* **2004,** 21, (11), 2048-2057.

43. Matteucci, M. E.; Hotze, M. A.; Williams III, R. O.; Johnston, K. P., Drug Nanoparticles by Antisolvent Precipitation: Mixing Energy Versus Surfactant Stabilization. *Langmuir* **2006,** 22, (21), 8951-8959.

44. Matteucci, M. E.; Brettmann, B. K.; Rogers, T. L.; Elder, E. J.; Williams III, R. O.; Johnston, K. P., Design of Potent Amorphous Drug Nanoparticles for Rapid Generation of Highly Supersaturated Media. *Molecular Pharmaceutics* **2007,** 4, (5), 782-793.

45. Rasenack, N.; Muller, B. W., Dissolution Rate Enhancement by in Situ Micronization of Poorly Water-Soluble Drugs. *Pharm Res* **2002,** 19, (12), 1894-1900.

46. Matteucci, M. E.; Paguio, J. C.; Miller, M. A.; Williams III, R. O.; Johnston, K. P., Flocculated Amorphous Nanoparticles for Highly Supersaturated Solutions. *Pharm Res* **2008,** 25, (11), 2477-2487.

47. Ruch, F.; Matijevic, E., Preparation of Micrometer Size Budesonide Particles by Precipitation. *J Colloid Interface Sci* **2000,** 229, 207-211.

48. Pelton, R. H., Polystyrene and polystyrene-butadiene latexes stabilized by poly(N-isopropylacrylamide). *Journal of Polymer Science, Part A: Polymer Chemisty* **1988,** 26, (1), 9-18.

49. Pandit, N.; Trygstad, T.; Croy, S.; Bohorquez, M.; Koch, C., Effect of Salts on the Micellization, Clouding, and Solubilization Behaviour of Pluronic F127 Solutions. *J Colloid Interface Sci* **2000,** 222, (2), 213-220.

50. Matteucci, M. E.; Paguio, J. C.; Miller, M. A.; Williams III, R. O.; Johnston, K. P., Highly Supersaturated Solutions from Dissolution of Amorphous Itraconazole Microparticles at pH 6.8. *Molecular Pharmaceutics* **2009,** 6, (2), 375-385.

Chapter 2: Low Viscosity Highly Concentrated Injectable Non-Aqueous Suspensions of Lyosyzme Microparticles

Subcutaneous injection of concentrated protein and peptide solutions, in the range of 100 to 400 mg/ml, is often not possible with a 25 to 27-gauge needle, as the viscosity can be well above 50 cP. Apparent viscosities below this limit are reported for suspensions of milled lysozyme microparticles up to nearly 400 mg/ml in benzyl benzoate or benzyl benzoate mixtures with safflower oils through a syringe with a 25 to 27-gauge needle at room temperature. These apparent viscosities were confirmed using a cone-and-plate rheometer. The intrinsic viscosity regressed from the Kreiger-Dougherty model was only slightly above the Einstein value of 2.5, indicating the increase in viscosity relative to that of the solvent was caused primarily by the excluded volume. Thus, the increases in viscosity from electrical double layer interactions (electroviscous effects), solvation of the particles, or deviations of the particle shape from a spherical geometry were minimal, and much smaller than typically observed for proteins dissolved in aqueous solutions. The small electroviscous effects are expected given the negligible zeta potential and thin double layers in the low dielectric constant organic solvent. The suspensions were resuspendable after a year, with essentially constant particle size after two months as measured by static light scattering. The lower apparent viscosities for highly concentrated protein suspensions relative to protein solutions, coupled with these favorable characteristics upon resuspension, may offer novel opportunities for subcutaneous injection of therapeutic proteins.

2.1 INTRODUCTION

Proteins and other polypetides therapeutics are on the rise in recent years given their lower toxicity and more predictable and selective behavior *in vivo* than for other

classes of drugs not naturally found in the body.[1,2] Delivery of high dosages (100-1000mg) of protein therapeutics has been limited primarily to dilute large volume intravenous injections. The high dilution helps prevent physical and chemical instabilities of proteins that would be encountered at high concentrations.[1-7] A potentially less invasive method of administration is a subcutaneous injection. Since the injection volume is limited to ~1.5 ml, the concentration of the protein therapeutic is often substantially above 100 mg/ml, where loss in stability can become a major issue.[2,3,5-8] In addition, the viscosity of a highly concentrated solution often increases markedly, typically well above 50 cP for proteins with non-spherical shapes, electrical double layer interactions, and hydration of the protein molecule in water, severely limiting the feasibility of subcutaneous injection.[5,7-11] Various electrostatic interactions due to the distortion of the double layer by shear and intramolecular and intermolecular double layer interactions, collectively called the electroviscous effects, can increase the viscosity markedly.[12,13] In some cases, the viscosity increase from electroviscous effects can be mitigated by adding sodium chloride to increase the ionic strength of the solution or by varying the buffer species and pH to reduce the surface charge on the protein.[2,5,7,14] Another limitation is that large excipient concentrations, often up to 20:1 excipient to protein by mass[15], are often needed to protect against denaturation and aggregation; however, the excipients occupy space in solution otherwise available to the protein.[3,5,8] An alternative to solutions is to form suspensions of an insoluble protein in a non-aqueous solvent. In some cases, smaller excipient levels are needed to stabilize the protein in the solid state relative to in solution and the storage time can be increased to that appropriate for pharmaceutical products.[3,16]

To date, relatively few examples of suspensions of proteins in non-aqueous media have been reported for medicinal purposes as the focus has been on aqueous protein

solutions. Highly viscous suspensions of bovine somatotropin, marketed to increase milk production in dairy cows, and a bovine growth hormone releasing factor analog, used to release somatotropin from the cow's pituitary gland, have been formulated in sesame oil and Miglyol oil, respectively.[4,17,18] These viscous suspensions require a large 14-16 gauge needle for injection, whereas the preferred needle size for humans is ~ 25 - 27 gauge. In addition, a few non-aqueous extended release formulations for the peptide insulin and for very stable proteins such as protein C and a proprietary monoclonal antibody have been produced with the aid of viscosity enhancers and gel forming polymers in the presence of diluents such as benzyl benzoate or benzyl alcohol.[4,19-21] However, injection of these suspensions with a larger 21-gauge needle causes significant pain leading to non-compliance. In addition, the high levels of excipients needed to stabilize the protein particles and form the gel reduce the overall concentration of the protein in the formulation.[19,21-23] Another option is to crystallize the protein or monoclonal antibody and to suspend the crystals in aqueous media.[3,4,24] However, crystallization of high molecular weight proteins can be very difficult due to the high degree of segmental flexibility, and is more feasible for small peptides that have a much lower degree of flexibility.[3,4]

The objective of this study was to produce highly-concentrated (up to 400 mg/ml) protein suspensions with viscosities below ~ 50 cp, the limit for a subcutaneous injection via a 25- to 27-gauge syringe, and to describe theoretically the reasons for the low viscosities. Suspensions of particles smaller than 37 μm of the model protein, lysozyme, with concentrations from 50 to 370 mg/ml were formulated with benzyl benzoate as the pure non-aqueous solvent or a 50/50 volume mixture of the pharmaceutically acceptable solvents safflower oil and benzyl benzoate. The organic solvents offer various advantages over aqueous solvents including low protein solubility and reduced electrostatic

interactions (electroviscous effects) due to the low dielectric constants of the solvent. The experimental apparent viscosities are correlated with the Krieger-Dougherty equation to determine the intrinsic viscosity. The regressed intrinsic viscosity will be shown to be near the Einstein value of 2.5 indicating primarily an excluded volume effect. Thus, the increases in viscosity from the effects of protein shape, solvation, and electroviscous effects are small. In contrast, increases in viscosities from these additional effects can be pronounced for aqueous protein solutions.[5,7] In addition, for successful delivery with concentrated suspensions, the particle size and suspension uniformity must be controlled in order to administer an accurate and uniform dose.[4] The uniform aliquots measured from the suspensions, as well as the slow settling rates, are shown to be sufficient to favor uniform doses. Colloidal stability of the particles is shown by consistent static light scattering measurements of particle size over months.

2.2 MATERIALS AND METHODS

2.2.1 Materials

Lysozyme in lyophilized powder form (L6876) was purchased from Sigma Chemical Company (St. Louis, MO). Bovine serum albumin (BSA) in lyophilized powder form (BP671), ACS grade acetonitrile and USP grade ethanol were used as received from Fisher Chemicals (Fairlawn, NJ). Food grade olive oil and safflower oil were used while benzyl benzoate was obtained from Acros Organics (New Jersey) and N.F. grade ethyl oleate from Spectrum Chemical Corp. (Gardena, CA).

2.2.2 Suspension Formation

Lysozyme powder as received was dry milled with a porcelain mortar and pestle for several minutes. The milled powder was then sieved through a number 400 mesh and particles smaller than 37 μm were collected. Samples of the particles were then weighed

and added to the measured amount of benzyl benzoate or a premixed 50/50 volume mixture of benzyl benzoate and safflower oil to give 50 to 400 mg/ml concentration of particles in the solvent. Each vial was then shaken by hand to disperse the powder evenly through the suspension without the need for sonication.

2.2.3 Particle Size Analysis

Particle size was measured by multiangle static laser light scattering using a Malvern Mastersizer-S (Malvern Instruments, Ltd., Worcestershire, UK). The size of the milled and sieved powder was measured upon suspension in acetonitrile in a large recirculation cell (~500ml) and also immediately after being added to ethanol in a small batch cell (Malvern, Worcestershire, UK, ~15ml). In each case the obscuration during the measurement was between 10-15%. After storing the suspensions for 2 months at room temperature, the particle size was measured again immediately after shaking and diluting the sample in ethanol in the small batch cell.

2.2.4 Viscosity Measurement

The viscosity was measured as the time to draw 1 ml of the sample into a 1ml BD tuberculin slip tip syringe with a 25 g 5/8" long or 27 g 1/2" long needle at room temperature. Each measurement was made at least 3 times and averaged, while maintaining the suction force by holding the end of the plunger at the 1ml mark each time. Liu *et al.* found this measurement time to be correlated linearly to viscosity.[5-7] Using known viscosities of each pure liquid, benzyl benzoate, ethanol, ethyl oleate and olive oil, the correlation between the time to draw 1 ml of solution and the viscosity was found for each needle size to give an r^2 value greater than 0.999 as expected from the Hagen-Poiseuille equation (Eq. 1 below). The apparent viscosity of the suspensions in each pure solvent was calculated from these correlations and the values for the two

separate needle sizes were averaged to give a final average apparent viscosity of each sample. Additional samples of the solvent mixture of benzyl benzoate and safflower oil were made from 10 to 90 percent benzyl benzoate by volume and the viscosity was calculated as described above.

2.2.5 Rheology Measurement

The change in viscosity at various shear stresses was measured using an AR 2000ex cone-and-plate rheometer (TA Instruments, New Castle, Delaware) for two of the pure benzyl benzoate suspensions (200 and 400 mg/ml particles). Approximately 1 ml of the suspension was placed on the peltier plate and the 40 mm 2° HAL aluminum cone was lowered to a final truncation gap of 55 μm. The excess suspension was removed prior to performing a measurement. 25 measurements between the shear stress of 5 and 100Pa were taken after the equipment equilibrated at room temperature (23ºC). The shear rate was measured up to 10^3 s^{-1} where inertial and edge effects began to introduce error. However the applied torque was within instrument specifications, giving a maximum 2-3% error in the viscosity measurement.

2.2.6 Average Settling Rate and Maximum Volume Fraction Measurement

The settling rate of the particles in the solvents was measured by shaking the suspension in a test tube 13 mm in diameter. Pictures were taken with a standard digital camera after 10 to 1440 minutes as the height of the sediment-supernatant interface decreased. To measure the final settling volume of the samples, the vials containing the suspensions were left undisturbed for 4 months and images of the settled suspension were taken. All images were analyzed using ImageJ software to determine the distance from the meniscus to the settling front. This approach has been used previously to measure the average settling rate of a concentrated suspension.[25] The maximum volume fraction for

the settled suspension was defined by dividing the volume fraction of particles in the overall suspension by the ratio of the volume containing particles after settling for 4 months to the overall volume.

2.2.7 Quantification of Protein Concentration

The concentration of lysozyme in an aqueous solution was measured following the protocols for the Micro BCA Protein Assay (Pierce, Rockford, IL). Each sample was measured in triplicate with relative standard deviations (%RSD) less than 2% in a General Assay 96 well plate. The absorbance was measured at 562 nm in a spectrophotometer (μQuant Model MQX200; Biotek Instruments Inc., Winooski, VT). A standard curve of untreated lysosyme was prepared at concentrations between 2 and 30 μg/ml.

2.2.8 Rate of Lysozyme Partitioning to Aqueous Phase

Partitioning and dissolution of lysozyme from the concentrated suspension was measured in pH 7.4 potassium phosphate buffer. The USP paddle method was used with a VanKel VK6010 Dissolution Tester with a Vanderkamp VK650A heater/circulator. 900 ml of dissolution media was preheated in large 1L capacity dissolution vessels (Varian Inc., Cary, NC) to 37°C. A sample of the concentrated suspension giving a total of 18 mg of lysozyme was added. At time increments of 2 to 240 minutes, 1 ml samples were taken and analyzed using the Micro BCA protein analysis mentioned earlier.

2.2.9 Optical Density Measurement

The lysozyme in suspension was dissolved in water, and the optical density was measured to determine whether large aggregates were present. 0.1 ml of the concentrated lysozyme suspension was added to a test tube with 4 ml of DI water. This mixture was then gently mixed and left for 3 days for the protein to partition to the water phase. The

water phase was then separated and a sample was diluted and tested for concentration using the Micro BCA Protein Assay as mentioned above. On the basis of the concentrations measured, the remaining aqueous solution was diluted to 1 mg/ml. This solution was tested for optical density using at least 3 200μl aliquots in a 96-well plate and analyzed using the μQuant spectrophotometer at 350 nm. A standard lysozyme aqueous solution was made at 1 mg/ml concentration and exposed to the pure benzyl benzoate solvent and the benzyl benzoate and safflower oil solvent mixture for 3 days and measured as the standard for oil-water interface induced aggregation of the protein. An aqueous solution never exposed to any organic solvent was also measured immediately after it was made and used as a standard for absorbance measurements.

2.2.10 Suspension Uniformity Measurement

Three separate 0.1 ml aliquots of the resuspended concentrated lysozyme suspensions were added to test tubes with 8 ml of DI water. These mixtures were then gently mixed and left for 1 day for the protein to partition to the water phase. The aqueous phase was then separated and diluted to a theoretical concentration of 20 μg/ml if 100% of the protein partitioned. The actual concentration was then analyzed using the Micro BCA protein assay mentioned above.

2.2.11 Karl Fischer Moisture Analysis

After being stored for four months, a sample of 0.1 ml of the redispersed concentrated suspension was inserted using a 19-gauge needle through the septum of the titration cell of an Aquatest 8 Karl-Fischer Titrator (Photovolt Instruments, Indianapolis, IN). Each suspension, pure benzyl benzoate and the benzyl benzoate and safflower oil solvent mixture was measured in triplicate and averaged.

2.2.12 Polarity Determination

An aliquot of the suspension was diluted with the solvent until individual particles were visible on a slide through an optical microscope (Bausch & Lomb, 10x magnification). Microelectrophoresis was used to determine if a charge was present on the particles. The diluted particle dispersion was placed between two parallel wire electrodes (0.01-in. diameter stainless steel 304 wire, California Fine Wire) spaced 1 mm apart. The electrodes were secured to a glass microscope slide and observed by optical microscopy. A potential of 10–100 V was applied with the polarity of the electrodes switched every 15–60 sec.

2.3 RESULTS

2.3.1 Formation of Suspensions

Prior to adding the milled and sieved lysozyme particles to the suspending media, the lysozyme mass percentage was determined to be 91.5% by weight of the particles, consistent with the manufacturers specifications, according to the micro BCA assay. The average particle size found to be approximately 20 μm, according to static light scattering measurements (Figure 2.1). For the average particle size measurement, a minor secondary submicron peak was also visible in all measurements. However since the 15 ml small batch cell is only calibrated for particle sizes down to 500 nm, this peak was not included in the analysis. Upon adding the suspending media, a uniform suspension was formed by shaking by hand as shown in Figure 2.2b. Thereafter, the particles settled slowly enough to remain partially suspended even after 24 hours (Figure 2.2c) and took up a significant portion of the volume even after 2 months (Figure 2.2a).

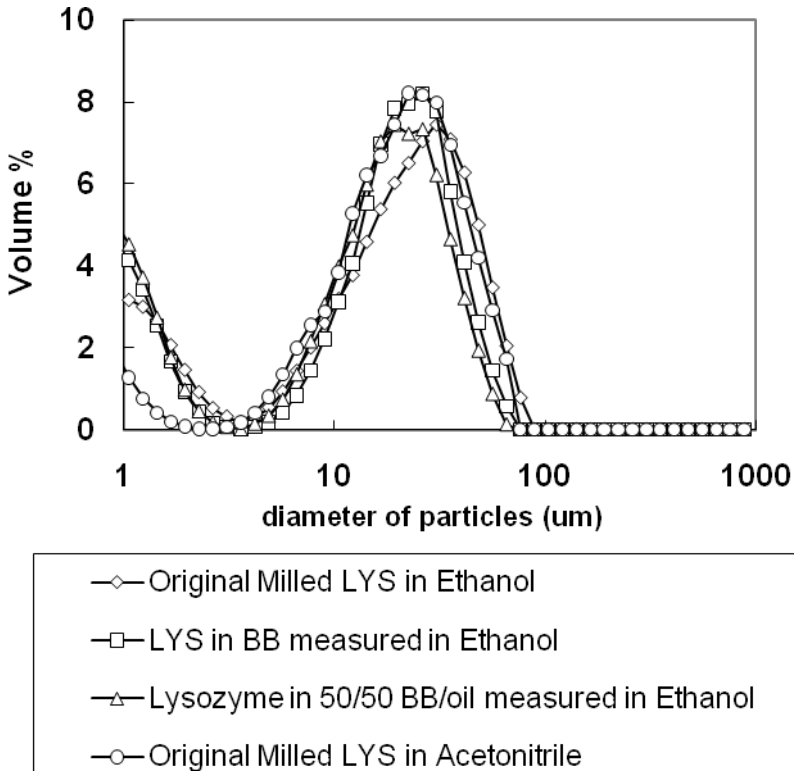

Figure 2.1 Volume % of particles versus size measured for the original lysozyme (LYS) milled particles in acetonitrile (○) and ethanol (◊) and after 2 months of storage for the suspensions in pure benzyl benzoate(BB) (□) and a mixture of benzyl benzoate and oil (BB/oil) (▲) both measured immediately after being diluted in ethanol to 10-15% obscuration by light scattering

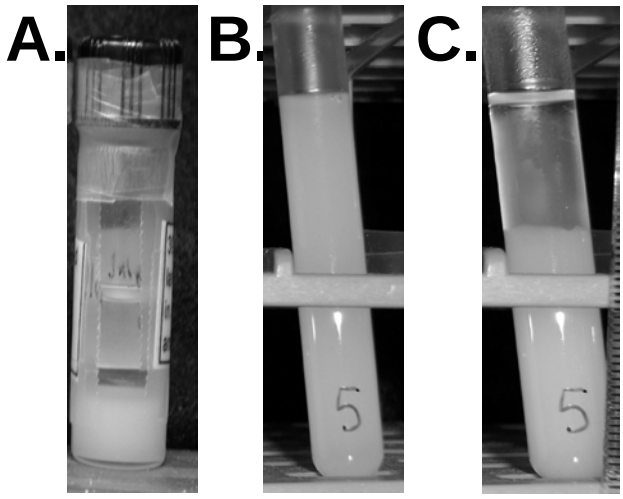

Figure 2.2 Pictures of the 300mg/mL suspension of lysozyme particles in 50/50 Benzyl Benzoate and Safflower Oil A) in vial after being left for 2 months B) after being shaken and resuspended in a test tube C) after being allowed to settle for 24 hours

2.3.2 Apparent Viscosity of Solvent Mixture and Suspensions

Using the known viscosities of pure solvents, a correlation between the time to draw 1 ml of the sample and viscosity was generated. This type of correlation has been described by Shire and coworkers on the basis of the Hagen-Poiseuille equation, assuming steady, laminar, isothermal flow along the axis of the needle and no slip at the walls [5-7]

$$< v >= \frac{R^2}{8\eta}\left(\frac{|\Delta P|}{L}\right) \qquad (2.1)$$

where υ is the velocity, R is the inner radius of the needle, η is the viscosity, and $\Delta P/L$ is the average pressure drop over the length of the needle. To ensure that the entrance pressure drop was negligible, the entry distance was calculated. The resulting value of 0.0001 cm was significantly less than the 1.27cm or 1.58cm length of the needle (see supplemental information for calculation). Ensuring that the average pressure drop over the length of the needle remains constant for each sample by maintaining the same suction pressure inside the syringe, the inverse of the velocity of the fluid multiplied by the cross-sectional area gives the time to draw up a specified volume of liquid, in this case 1 ml. This time is proportional to the viscosity as shown by the Hagen-Poiseuille equation, and has been very accurately correlated by Shire *et al.* to the viscosity.[5,7] Using the approximation for shear rate (γ) in a capillary,

$$\dot{\gamma} = \frac{4Q}{\pi R^3} \qquad (2.2)$$

where Q is the volumetric flow rate and R is the radius of the needle, the shear at the wall over the length of the capillary for both needle sizes was calculated to be on the order of 10^3 s^{-1}. In this shear rate range for two of the suspensions formulated, the apparent viscosity was approximately that measured using a cone-and-plate rheometer at the

appropriate shear rate (Figure 2.5). Because only this high shear rate range is relevant to subcutaneous injection, additional samples were measured with the syringe method alone.

The measured viscosities of the solvent mixtures of benzyl benzoate and safflower oil at room temperature are shown in Figure 2.3. In this case, since the minimum and maximum values are the for the pure solvents, the generalized mixing rule should follow the form

$$f(\eta_m)_L = \sum_i x_i f(\eta_i)_L \quad (2.3)$$

where η_m is the viscosity of the mixture, i is the number of components, x_i is the liquid volume, weight, or mole fraction, and η_i is the viscosity of the i^{th} component. $f(\eta)_L$ can be η_L, ln (η_L), 1/ η_L etc.[26] For our data, the best correlations were obtained with $f(\eta)_L$ = ln (η_L). This theoretical result is shown by the dotted line in Figure 2.3, assuming no water was present in the system. As will be discussed below, the small amount of residual moisture below 100 μg/ml in the solvent may be expected to change the viscosity by less than 1%.

The apparent viscosities of the suspensions with increasing concentration were measured for both the pure benzyl benzoate system and the solvent mixture of 50/50 benzyl benzoate and safflower oil. Figure 2.4 presents the resulting apparent viscosities, averaged from the measurements using two syringe sizes (left y-axis), and the average time to draw 1 ml from the 25-gauge syringe (right y-axis) as a function of the concentration of lysozyme particles. For subcutaneous delivery, 50 cP is an appropriate maximum viscosity where it will take approximately 20 seconds for 1 ml of the suspension to be expelled via a 26-gauge syringe.[3] From Figure 2.4, the highest apparent viscosity measured was approximately 50 cP, where it took approximately 55 seconds to draw 1 ml into a 25-gauge syringe. The disparity in the times measured reflects the

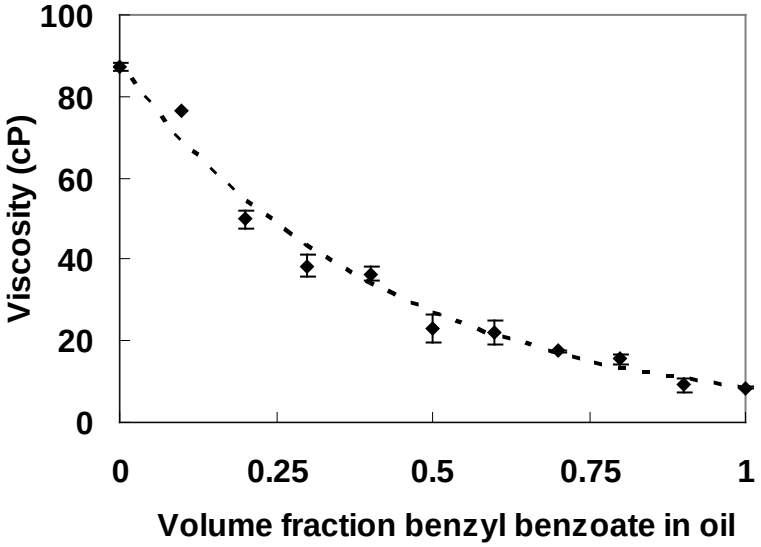

Figure 2.3 Viscosity of a solution of benzyl benzoate and safflower oil at room temperature at varying concentrations measured experimentally and correlated with eq. 2.3. Error bars indicate the standard deviation of each measurement.

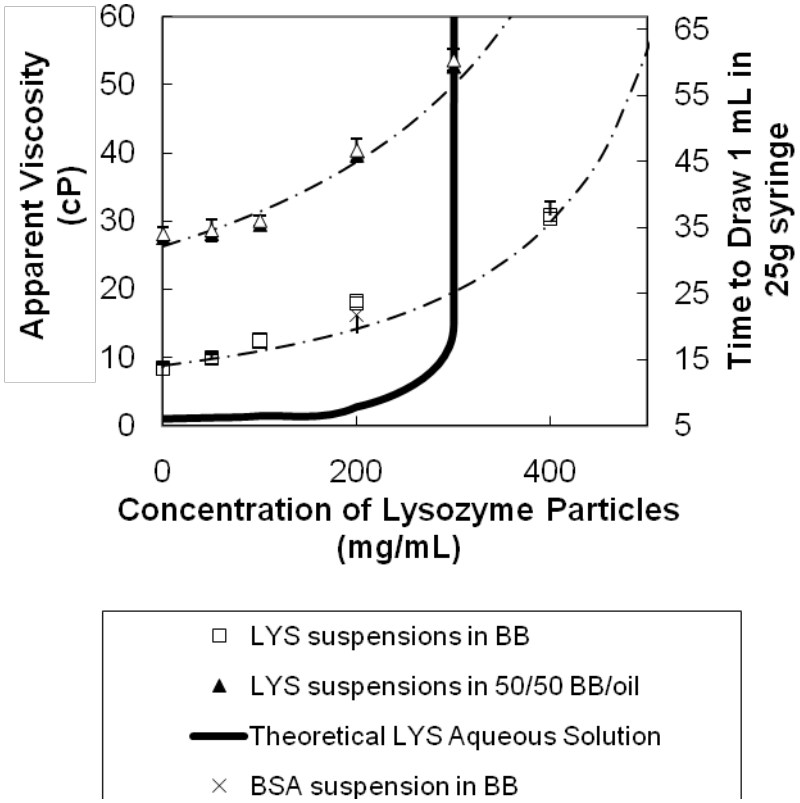

Figure 2.4 The apparent viscosity as a function of concentration of particle in suspensions of the non-aqueous solvents, benzyl benzoate (BB) (■) and 50/50 benzyl benzoate and safflower oil (BB/oil) (▲) with there correlations based on the Kreiger-Dougherty equation (eq. 2.4) and the theoretical viscosity of an aqueous lysozyme (LYS) solution, calculated using the hard quasisphere model (eq. 2.8) (solid line)

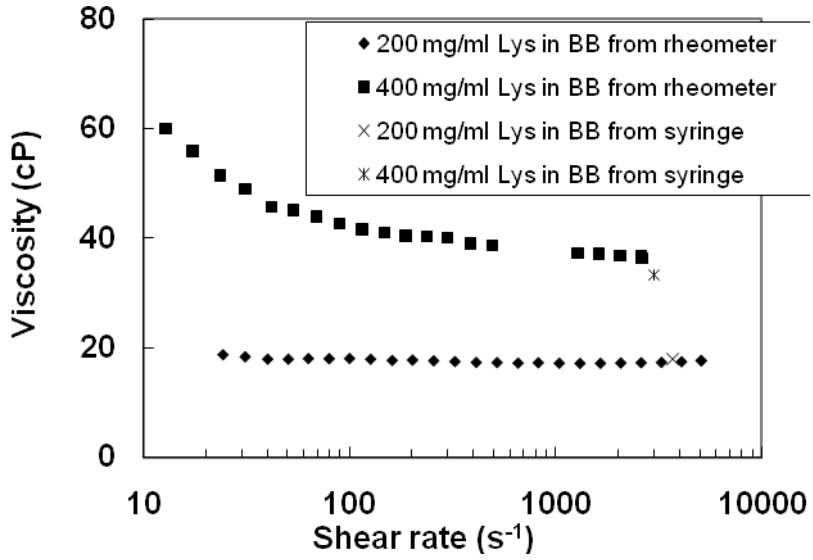

Figure 2.5 Viscosity confirmation of syringe viscosity measurements using the AR 2000ex rheometer.

smaller suction force that can be applied to draw the volume into the syringe relative to the larger force available to expel the solution from the syringe.

The correlation of the apparent viscosity with the free solvent volume fraction, $1 - (\phi/\phi_{max})$, was modeled using the Kreiger-Dougherty equation

$$\frac{\eta}{\eta_o} = \left[1 - \left(\frac{\phi}{\phi_{\max}}\right)\right]^{-[\eta]\phi_{\max}} \quad (2.4)$$

where η is the apparent viscosity of the dispersion, η_o the solution viscosity, φ the volume fraction of particles, φ_{max} the maximum packing fraction, and $[\eta]$ the intrinsic viscosity (Table 2.1). φ_{max} was approximated experimentally after gravitational settling of the particles over 4 months. It was approximately 0.50 for the pure benzyl benzoate solvent solution and 0.52 for the benzyl benzoate and safflower oil solvent for low shear rates. Using these values, the intrinsic viscosity of the suspension, $[\eta]$, was determined to be 2.7 for the pure benzyl benzoate suspensions and 2.3 for the benzyl benzoate and safflower oil suspensions. Since the exponent, $-[\eta]\varphi_{max}$ was used to determine $[\eta]$, uncertainty in the approximation of φ_{max} of about 20% can introduced a similar uncertainty in $[\eta]$. However, this uncertainty is small when compared with changes in $[\eta]$ of more than an order of magnitude for proteins with strong interactions in solutions.

2.3.3 Particle Stability of the Suspension

The stability of the particles in suspension was measured by numerous different techniques. First the average settling rate was measured and compared to the calculated theoretical Stokes settling rate (U_s) for the average particle size (r)

$$U_s = \frac{2r^2 \Delta\rho g}{9\eta_o} \quad (2.5)$$

Table 2.1 Comparison of the two solvent systems used for highly concentrated suspensions for the exponents for the Krieger-Dougherty equation, the experimental or assumed (*) maximum packing fraction, and intrinsic viscosity average plus or minus the standard deviation

Solvent system	**Exponent for Krieger-Dougherty equation $-[\eta]\Phi_{max}$**	**Maximum volume packing fraction Φ_{max}**	**Intrinsic viscosity $[\eta]$**
Benzyl benzoate suspension	-1.36 ± 0.09	0.50	2.7 ± 0.18
50/50 Safflower Oil and Benzyl Benzoate suspension	-1.2 ± 0.06	0.52	2.3 ± 0.12

where Δρ is the difference in densities between the solvent and the particles, and g is acceleration due to gravity. For a high concentration of particles, the particle crowding will reduce the settling rate to yield

$$U = U_s(1-\phi)^{6.55} \qquad (2.6)$$

This modified average Stokes settling rate and the experimentally measured values were found to be within a factor of two for most concentrations lower than 300 mg/ml as shown in Table 2.2. However, for a concentration of 400 mg/ml the experimental values was an order of magnitude lower than the predicted rate (Table 2.2). At this high concentration, the increase in apparent viscosity at the very low shear rates found in settling ($\sim 10^{-5}$ s^{-1})[27] is much more pronounced, leading to an increased settling time (Figure 2.5). Shear thinning is expected in concentrated suspensions, as high shear will overcome interparticle forces and rearrange the particles to a more ordered configuration.[27-29]

Three aliquots were taken of an organic suspension to determine the uniformity of the protein within the suspension. The organic suspension was added to an aqueous phase to form a two-phase system as described in the experimental section. The system was equilibrated for 1 day, to be conservative; as it appeared that the partitioning reached equilibrium in 60 minutes. The aqueous phase was then diluted approximately 1000 times, and the concentration of protein was measured. For 8 ml of aqueous phase equilibrated with 0.1 ml of the concentrated non-aqueous suspension, at least 80% of the protein partitions into the aqueous phase in 24 hours (Table 2.3). The %RSD for the amount of extracted protein were typically below 5% indicating reasonable uniformity of the protein particles in the redispersed suspension. The %RSD was slightly larger for the highly concentrated 300 mg/ml sample in the mixed solvent.

Table 2.2 Comparison of experimental settling rates and settling rates quantified by the modified Stokes settling equation accounting for particle interactions (eq. 2.5,2.6)

Safflower oil concentration (% of solvent) (remainder is benzyl benzoate)	Protein concentration (mg/ml)	Volume fraction of particles (Φv)	Experimental settling rate (cm/hr)	Modified Stokes settling rate (cm/hr)
50	46	0.03515	1.85	0.85
50	92	0.0703	1.32	0.67
50	183	0.1406	0.32	0.40
50	275	0.2109	0.043	0.23
0	46	0.03515	3.91	2.24
0	92	0.0703	1.64	1.76
0	183	0.1406	0.52	1.05
0	366	0.2812	0.031	0.32

Table 2.3 Percent of sample recovered in aqueous phase and % relative standard deviation (%RSD) of 3 samples for suspensions formed in benzyl benzoate with and without safflower oil

Safflower oil concentration (% of solvent) (remainder is benzyl benzoate)	Particle Concentration (mg/ml)	% protein recovered in aqueous	% RSD
50	50	84.4%	2.21%
50	100	85.8%	6.61%
50	200	93.8%	3.20%
50	300	83.3%	9.45%
0	50	93.1%	1.52%
0	100	100%	3.46%
0	200	100%	3.65%
0	400	88.7%	4.29%

The particles in suspension were stored for extended time periods to determine whether the particle size changed due to aggregation or other processes including Ostwald ripening. The original particle size was measured via static light scattering immediately after the particles were sieved and resuspended in both acetonitrile, where lysozyme is very insoluble, and ethanol, where lysozyme is slightly soluble.[30] The uniformity of the two measurements ensures that the time scale of the measurement is much quicker then the time scale of growth of the particles in ethanol (Figure 2.1). Following 2 months of storage, the samples were diluted in ethanol and immediately tested. The particle size was found to be essentially constant during storage (Figure 2.1). The visual inspection of one formulated suspension after storage for a year and redispersion by shaking confirms that the particles could be redispersed.

The potential effect of electrostatic interactions on the particle stability was tested. However the lysozyme particles did not display organized movement when the current was reversed for voltages from 10 to 100 V for two electrodes spaced 1 mm apart in the benzyl benzoate solvent. Thus the charge on the particles was small as expected given the low dielectric constant of the solvent.

2.3.4 Protein Stability in the Suspension by Optical Density

Protein aggregation was investigated by measuring the optical density on sample aliquots that partitioned from the organic to the water phase. The protein was diluted to a concentration of 1 mg/ml, confirmed by dilution of an aliquot to 20 μg/ml with the micro BCA assay. Additional lysozyme samples in an aqueous solution at the same concentration were exposed to the solvent to measure the effect of the oil-water interface on aggregation. All these solutions were checked for large protein aggregates by comparison with a fresh lysozyme solution at the same concentration. The absorbance at

350 nm of the standard solution, without exposure to the non-aqueous solvent (0.047 ± 0.005), was approximately the same as that for the particles in the pure benzyl benzoate solvent (0.051) and the mixed benzyl benzoate/safflower oil solvent (0.052). As this is within the error of the experiment, it suggests that the particles did not undergo significant formation of large aggregates over the four to five month month time period tested. Since lysozyme is a very stable model protein, additional protein denaturation and aggregation studies were not conducted.

Quantification of the moisture content may be used to determine the free and bound water in the suspension. The moisture content was measured for each suspension after being exposed to atmospheric conditions for 2 months. The linear correlations found between the moisture content and suspension concentration indicates that the moisture is directly associated with the protein (Figure 2.6). The benzyl benzoate solvent contains an average of 20 μg of water per 0.1 ml of solution or approximately 0.02% by weight. The safflower oil and benzyl benzoate mixture contains approximately 74 ug of water in the same volume sample or approximately 0.074%. The sample with the highest concentration of protein in benzyl benzoate, 400 mg/mL, contained the most moisture, an average of 4450 μg of water per 0.1 ml of suspension giving an absolute maximum concentration of 4.5% by weight of the suspension after being stored for 2 months.

2.4 DISCUSSION

2.4.1 Colloidal Stability of the Protein in Suspension

A key concern for an injectable suspension is the ability to redisperse the particles after settling with gentle agitation.[4] For the various aliquots of the protein in water extracted from the redispersed suspensions, the relatively constant protein concentrations indicate that the suspensions were uniform after gentle shaking. The lack of particle

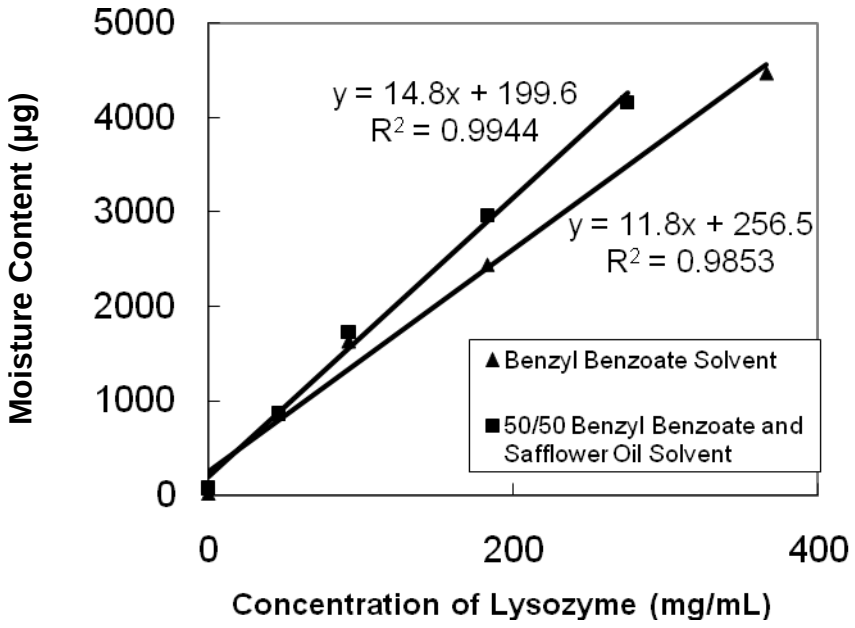

Figure 2.6 Karl Fisher moisture content analysis of the non-aqueous suspension in benzyl benzoate (▲) and benzyl benzoate and safflower oil (■)

aggregation as measured by static light scattering (Figure 2.1) and lack of caking of the suspended particles demonstrate significant storage stability. The lack of sintering of the particles is favored by the fact that the hydrophobic poor solvent does not soften the protein chains. The lack of particle growth from Ostwald ripening is not surprising since the protein is almost completely insoluble in these non-aqueous solvents[30] and will therefore undergo little diffusion. Furthermore, the lack of particle aggregation is favored by the weak hydrophobic interactions between the protein particles in a low dielectric constant organic solvent.

The average particle size of ~10 μm is optimal to balance the need for sufficiently small particles to flow through the needle versus large particles to minimize the particle surface area. Milled nanoparticles (~300 nm diameter) were found to produce a highly viscous paste. The high surface area led to stronger interactions between the particles, which increased the viscosity (results not shown).[31] In addition, particles not milled through the 37μm sieve caused clogging of the syringe (results not shown). Therefore, an aspect ratio compared to the needle of ~ 0.1 provided the proper balance of low particle surface area for weak particle interactions (low [η]) and small enough particles to prevent mechanical clogging of the needle.

The concept of protein particle engineering for the formation of low viscosity suspensions may be generalized beyond the milling technique in this study. For example, micron-sized protein particles may be formed by lyophilization or spray drying. In addition they may be encapsulated in polymer microspheres[18,24] for controlled delivery.

2.4.2 Effects of excluded volume, shape, solvation and electroviscous effects on viscosities of proteins in solution versus protein suspensions

In the Einstein model for the viscosity of a dilute colloidal dispersion of solid spheres ($\varphi<0.03$) [27,32], the slope of the viscosity ratio of the suspension over the solvent versus φ is 2.5. This slope signifies the excluded volume increment of viscosity due to the addition of dispersed particles, the intrinsic viscosity, $[\eta]$. The $[\eta]$ of concentrated protein colloids and protein suspensions may be regressed from the Kreiger-Doughety equation to give an indication of the effects of excluded volume and other interparticle forces (Equation 3).[27,28] The $[\eta]$ can increase from the Einstein value of 2.5 depending on the effects of solvation, particle shape, and electrical double layer forces (electroviscous effects), as well as the shear rate.[1,27] The values near 2.5 for the benzyl benzoate and the benzyl benzoate and safflower oil mixture suspensions in Table 2.1 indicate that the viscosity increase is governed primarily by the excluded volume effect. The value of 2.3 for the 50/50 benzyl benzoate and safflower oil mixture is slightly below the minimum Einstein 2.5 limit due to experimental uncertainty.

The solvation of protein molecules by a solvent will increase the volume fraction by

$$\frac{\phi_{solvated}}{\phi_{dry}} = \left[1+\left(\frac{m_{1,b}}{m_2}\right)\left(\frac{\rho_2}{\rho_1}\right)\right] \quad (2.7)$$

where $m_{1,b}$ is the mass of the bound solvent, m_2 is the mass of the particle, ρ_2 is the density of the particle and ρ_1 is the density of the solvent.[27] In the case of the Krieger-Dougherty equation, this solvation is manifested as an increase in $[\eta]$.[13,27] For the organic solvents in the present study, the increase in ϕ may be expected to be much smaller than in the case of water, which is a much stronger solvent for solvating proteins.

Since the solvated volume fraction is often unknown, the analysis of protein solutions is typically done using mass concentrations (g/ml) rather than volume fractions,

leading to values of the intrinsic viscosity in units of cm^3/g and different higher order relationships derived from the virial expansion.[5,33] For example, a hard quasi-spherical model has been shown to accurately predict viscosities of various protein solutions[5,9,10,34]

$$\frac{\eta}{\eta_o} = \exp\left(\frac{[\eta]c}{(1-\frac{k}{\upsilon}[\eta]c)}\right) \qquad (2.8)$$

where c is the mass protein concentration, k is a crowding factor and υ is the Simha parameter accounting for the change in shape from a sphere. For various proteins in solution, [η] varies from 2.7 for lysozyme to over $200cm^3/g$.[33] Even for lysozyme, a protein with a small axial ratio of 1.5[33], this model shows a dramatic increase in viscosity around a concentration of 300mg/ml (Figure 2.4). For glass fibers with axial ratios, 7, 14 and 21, the intrinsic viscosity increases from 3.8 to 5.03 to 6.0, respectively.[28] Our lower values of [η] are consistent aspect ratios close to 1, as expected for particles formed by milling.

The electroviscous effect caused by the charge on a protein surface and the associated double layer interactions often produces a marked increase the viscosity of a protein aqueous solution as a function of pH and salinity. The electroviscous effects are: primary, from distortion to the diffuse double layer surrounding the protein molecule, secondary, from interparticle double-layer interactions, and tertiary, from changes in intramolecular double layer interactions that affect the geometry of the system.[12-14,27] The primary electroviscous effect on the intrinsic viscosity, for the case of small zeta potentials (<25 mV) and large distortions of the double layer is given by

$$[\eta] = 2.5\left\{1+\frac{6(\varepsilon_r\varepsilon_0\zeta)^2}{k\eta_0 R_s^2}\frac{1}{1+Pe^2}\right\} \qquad (2.9)$$

where ε_r is the relative permittivity, ε_0 is the permittivity of free space, ζ is the zeta potential, k is the specific conductivity of the continuous phase, R_s is the radius of the colloid, and *Pe* is the Peclet number.[12,27] For aqueous protein colloids, assuming low ionic strength, an increase in ζ as the pH moves away from the pI, will raise [η].[14] For a protein in a lower dielectric solvent, as has been shown for a polymer in methanol[35], the primary electroviscous effect, as shown in equation 2.9, has a reduced impact on [η]. In addition, the [η] has been shown previously to approach the Einstein value of 2.5 upon screening the surface charges on nanoparticles with ligands that adsorb on the charged sites.[36] In our case of non-aqueous protein suspension in low dielectric solvents, the negligible ζ observed experimentally, as a consequence of the low ε, leads to an insignificant increase in [η] from this electroviscous effect. Furthermore, secondary and tertiary electroviscous effects may also be ameliorated by lowering the dielectric constant thus lowering the surface charge and decreasing the thickness of the double layer.

The negligible elecroviscous effects and increase in φ from solvation for organic solvents can be attractive for achieving low [η], thereby increasing the achievable volume fraction of particles for a viscosity below 50 cP. These lower apparent viscosities in benzyl benzoate suspensions have also been seen for other milled proteins including bovine serum albumin (Figure 2.4). Benzyl benzoate and safflower oil are known solvents for parenteral delivery.[37,38] These solvents have been found in formulations including a testosterone propionate solution and a hydroxyprogesterone benzoate preparation for intramuscular delivery, but are much less common than water.[38] Benzyl Benzoate has been found to be completely nontoxic in a formulation with 50% or less benzyl benzoate in a fixed (nonvolatile) oil and non-irritating to the skin when injected at 10% benzyl benzoate in oil.[39,40] FDA approval of the use of benzyl benzoate as a pure solvent for subcutaneous delivery awaits further testing.

2.4.3 Destabilization of Protein Molecules in Suspension

It is challenging to prevent denaturation and aggregation of peptides and proteins at high concentrations, whether in solution or suspension form.[17,41-43] Oxidation due to the oil has been visible for Factor IX in soybean oil whereas miglyol oil has been used as the solvent to suspend a bovine growth hormone releasing factor analog for 10 weeks with no reported loss in stability measured by reverse-phase HPLC and FTIR.[17,41] In addition, at high concentrations (up to 300 mg/ml) the stability of bovine somatotropin in sesame oil was confirmed by fluorescence, Raman and FTIR spectroscopy.[42] In benzyl benzoate, insulin, protein C, and a proprietary monoclonal antibody are stable in sustained release polymer formulations.[19-21]

For the suspensions in this study, insoluble protein aggregates were not visible by optical density for lysozyme at any concentration after 2 months of storage at ambient conditions. Thus, the protein particles redissolved after being in suspension. As the optical density test was conducted in water, this also indicates that the exposure of the protein to the oil-water interface generated between the non-aqueous solvents and an aqueous environment, as will occur upon injection, did not produce insoluble aggregates. Additional characterization of the stability of lysoyzme was not performed, since lysozyme is very stable. Thus lysozyme would not be a good indicator of the stability of more fragile proteins, both with regard to denaturation and the formation of irreversible protein soluble and insoluble aggregates.[41,42,44-46] However, the moisture content in the suspension was examined, as it is an important factor that influences protein stability. The moisture controls protein hydration in the solid state, which is known to have a large effect on protein stability. For example, the reduced stability of Factor IX in another non-aqueous solvent, methoxyflurane, was attributed to water mediated reaction and conformational changes.[41] On the opposite end, studies of enzymatic activity in organic

solvents at low hydration levels have shown increased activity when the protein was only partially hydrated. The increase in activity has been attributed to reduced protein unfolding at low water levels.[47,48] For the suspensions studied, the values measured by Karl Fischer titration indicate that the water incorporated within the suspension tracked the concentration of the protein, therefore the slope describes the hydration of the protein in the solvent. In pure benzyl benzoate solvent, slightly less sorption of water was observed (~ 100 μg water/mg of protein), versus 140 μg water/mg of protein for benzyl benzoate/safflower oil after 4 months of storage at room temperature (~23°C) with no control over the humidity. Both of these values are above that needed for full hydration of the lysozyme protein molecules(~ 20 μg water/mg of protein).[47]

To achieve the optimum partially hydrated conditions for increased protein stability using the present suspensions, storage of proteins suspensions at lower temperatures and/or low humidities may maximize the stability of a protein in these organic solvents. At these low levels of protein hydration, the sorption of water from organic solvents has been found to be similar to that for solid protein particles exposed to air.[47,49] Since lysozyme and many other proteins have been shown to be stable in the solid phase with the proper excipients and storage conditions, the stability of the protein in the non-aqueous suspension may also be favorable.[44-46]

2.5 CONCLUSIONS

The viscosities of concentrated suspensions up to 300-400 mg/ml of ~10 μm milled particles of the model protein, lysozyme, were below 50 cp, the limit for subcutaneous injection through a 25 to 27-gauge needle. The apparent viscosity was correlated with volume fraction at all conditions according to the Krieger-Dougherty equation with an intrinsic viscosity close to 2.5, indicating weak interparticle interactions.

The various factors that produce large increases in viscosity for proteins in aqueous solution, including electroviscous effects from double layer interactions, an increase in ϕ from solvation, and deviations of the particle shape from a spherical geometry, have almost negligible effects for the non-aqueous protein suspensions in this study. The small electroviscous effects are a consequence of the small zeta potential and thin double layers in the low dielectric constant organic solvent. An average particle size of ~10 μm with an aspect ratio compared to the needle of ~ 0.1 provided the proper balance of low particle surface area for weak particle interactions (low [η]) and small enough particles to prevent mechanical clogging of the needle. Static light scattering of the suspensions demonstrated that the protein particle size did not vary for at least 2 months when stored at atmospheric conditions. The low settling rate of the particles (< 2 cm/hr) contributed to the excellent dose uniformity of 0.1 ml aliquots. The demonstration of injectable low viscosity supsensions with good collidal stability and dose uniformity is an important advancement for the ultimate goal of subcutaneous delivery of therapeutic proteins.

2.6 REFERENCES

1. Frokjaer, S.; Otzen, D. E., Protein Drug Stability: A Formulation Challenge. *Nat. Rev. Drug Discovery* **2005,** 4, 298-306.

2. Dani, B.; Platz, R.; Tzannis, S. T., High Concentration Formulation Feasibility of Human Immunoglubulin G for Subcutaneous Administration. *J. Pharm. Sci.* **2007,** 96, (6), 1504-1517.

3. Yang, M. X.; Shenoy, B.; Disttler, M.; Patel, R.; McGrath, M.; Pechenov, S.; Margolin, A. L., Crystalline monoclonal antibodies for subcutaneous delivery. *PNAS* **2003,** 100, (12), 6934-6939.

4. Defelippis, M. R.; Akers, M. J., Peptides and Proteins as Parenteral Suspensions: an Overview of Design, Development, and Manufacturing Considerations. In *Pharmaceutical Formulation Development of Peptides and Proteins*, Frokjaer, S.; Hovgaard, L., Eds. Taylor & Francis Limited: Philadelphia, 2000; pp 113-143.

5. Liu, J.; Nguyen, M. D. H.; Andya, J. D.; Shire, S. J., Reversible Self-Association Increases the Viscosity of a Concentrated Monoclonal Antibody in Aqueous Solution. *J. Pharm. Sci.* **2005,** 94, (9), 1928-1940.

6. Harris, R. J.; Shire, S. J.; Winter, C., Commercial Manufacturing Scale Formulation and Analytical Characterization of Therapeutic Recombinant Antibodies. *Drug Dev. Res.* **2004,** 61, 137-154.

7. Shire, S. J.; Shahrokh, Z.; Liu, J., Challenges in the Development of High Protein Concentration Formulations. *J. Pharm. Sci.* **2004,** 93, (6), 1390-1402.

8. Harn, N.; Allan, C.; Oliver, C.; Middaugh, C. R., Highly Concentrated Monoclonal Antibody Solutions: Direct Analysis of Physical Structure and Thermal Stability. *J. Pharm. Sci.* **2007,** 96, (3), 532-546.

9. Ross, P. D.; Minton, A. P., Hard Quasispherical Model for the Viscosity of Hemoglobin Solutions. *Biochem. Biophys. Res. Commun.* **1977,** 76, (4), 971-976.

10. Ross, P. D.; Minton, A. P., Analysis of Non-ideal Behavior in Concentrated Hemoglobin Solutions. *J. Mol. Biol.* **1977,** 112, 437-452.

11. Saluja, A.; Badkar, A. V.; Zeng, D. L.; Kalonia, D. S., Ultrasonic Rheology of a Monoclonal Antibody (IgG2) Solution: Implications for Physical Stability of Proteins in High Concentration Formulations. *J. Pharm. Sci.* **2007,** 96, (12), 3181-3195.

12. Hunter, R. J., *Zeta Potential in Colloid Science*. Academic Press Inc.: New York, 1981; p 386.

13. Saluja, A.; Kalonia, D. S., Nature and consequences of protein-protein interactions in high protein concentration solutions. *Int. J. Pharm.* **2008,** 358, 1-15.

14. Saluja, A.; Badkar, A. V.; Zeng, D. L.; Nema, S.; Kalonia, D. S., Application of High-Frequency Rheology Measurements for Analyzing Protein-Protein Interactions in High Protein Concentration Solutions using a Model Monoclonal Antibody (IgG2). *J. Pharm. Sci.* **2006,** 95, (9), 1967-1983.

15. Lee, S. L.; Hafeman, A. E.; Debenedetti, P. G.; Pethica, B. A.; Moore, D. J., Solid-State Stabilization of alpha-Chymotrypsin and Catalase with Carbohydrates. *Ind. Eng. Chem. Res.* **2006,** 45, 5134-5147.

16. Carpenter, J. F.; Chang, B. S.; Garzon-Rodrigues, W.; Randolph, T. W., Rational design of stable lyophilized protein formulations: theory and practice. In *Pharmaceutical Biotechnology. 13. Rational Design of Stable Protein*

Formulations, Carpenter, J. F.; Manning, M. C., Eds. Kluwer: New York, 2002; Vol. 13, pp 109-133.

17. Yu, L. X.; Foster, T. P.; Sarver, R. W.; Moseley, W. M., Preparation, Characterization, and in Vivo Evaluation of an Oil Suspension of a Bovine Growth Hormone Releasing Factor Analog. *J. Pharm. Sci.* **1996,** 85, (4), 396-400.

18. Foster, T. P.; Moseley, W. M.; Caputo, J. F.; Alaniz, G. R.; Leatherman, M. W.; Yu, X.; Claflin, W. H.; Reeves, D. R.; Cleary, D. L.; Zantello, M. R.; Krabill, L. F.; Wiest, J. R., Sustained elevated serum somatotropin concentrations in Holstein steers following subcutaneous delivery of a growth hormone releasing factor analog dispersed in water, oil or microspheres. *J. Controlled Release* **1997,** 47, 91-99.

19. Kang, F.; Singh, J., In vitro release of insulin and biocompatibility of in situ forming gel systems. *Int. J. Pharm.* **2005,** 304, 83-90.

20. Chaubal, M. V.; Zhao, Z.; Bruley, D. F., Novel injectable gels for the sustained release of protein C. In *Advances in Experimental Medicine and Biology*, Kluwer Academic/Plenum Publishers: Baltimore, 2003; Vol. 540 (Oxygen Transport to Tissue XXV), pp 147-155.

21. Chen, G.; Luk, A.; Houston, P.; Li, L.; Sharon, M.; Garley, M.; Bannister, R.; Hill, B.; Lucas, C.; Volkin, D.; Dalmonte, P.; Qi, P.; Khossravi, M.; Blasie, C.; Grousnick, K.; Huang, M.; Wang, D.; Zhao, H.; Zhu, Y.; Martin, P.; Treacy, G. In *Injectable nonaqueous suspension of highly concentrated proteins for non-IV administration*, AAPS Annual Meeting and Exposition, Nashville, TN, 2005; The AAPS Journal: Nashville, TN, 2005.

22. Ballard, B. E., Biopharmaceutical Considerations in Subcutaneous and Intramuscular Drug Administration. *J. Pharm. Sci.* **1968,** 57, (3), 357-378.

23. Brown, L. R., Commercial challenges of protein drug delivery. *Expert Opin. Drug Deliv.* **2005,** 2, (1), 29-42.

24. Pechenov, S.; Shenoy, B.; Yang, M. X.; Basu, S. K.; Margolin, A. L., Injectable controlled release formulations incorporating protein crystals. *J. Controlled Release* **2004,** 96, 149-158.

25. Lopez-Lopez, M. T.; Gomez-Ramirez, A.; Duran, J. D. G.; Gonzalez-Caballero, F., Preparation and Characterization fo Iron-Based Magnetorheological Fluids Stabilized by Addition of Organoclay Particles. *Langmuir* **2008,** 24, (14), 7076-7084.

26. Reid, R. C.; Prausnitz, J. M.; Sherwood, T. K., *The Properties of Gases and Liquids*. 3 ed.; McGraw-Hill Book Company: New York, 1977; p 688.

27. Hiemenz, P. C.; Rajagopalan, R., *Principles of Colloid and Surface Chemistry*. 3rd ed.; Marcel Dekker, Inc.: New York, 1997; p 650.

28. Barnes, H. A.; Hutton, J. F.; Walters, K., *An Introduction to Rheology*. Elsevier: New York, 1989; Vol. 3, p 199.

29. Bender, J. W.; Wagner, N. J., Optical Measurement of the Contributions of Colloidal Forces to the Rheology of Concentrated Suspensions. *J. Colloid Interface Sci.* **1995,** 172, 171-184.

30. Stevenson, C. L., Characterization of Protein and Peptide Stability and Solubility in Non-Aqueous Solvents. *Curr. Pharm. Biotechnol.* **2000,** 1, 165-182.

31. Bergstrom, L., Shear thinning and shear thickening of concentrated ceramic suspensions. *Colloids Surf., A* **1998,** 133, 151-155.

32. Larson, R. G., *The Structure and Rheology of Complex Fluids*. Oxford University Press: New York, 1998; p 688.

33. Cantor, C. R.; Schimmel, P. R., *BioPhysical Chemistry. Part II: Techniques for the Study of Biological Structure and Function*. W. H. Freeman and Company: San Francisco, 1980; p 846.

34. Minton, A. P., The Effective Hard Particle Model Provides a Simple, Robust, and Broadly Applicable Description of Nonideal Behavior in Concentrated Solutions of Bovine Serum Albumin and Other Nonassociating Proteins. *J. Pharm. Sci.* **2007,** 96, (12), 3466-3469.

35. Santini, C. M. B.; Hatton, T. A.; Hammond, P. T., Solution Behavior of Linear-Dendritic Rod Diblock Copolymers in Methanol. *Langmuir* **2006,** 22, (18), 7487-7498.

36. Studart, A. R.; Amstad, E.; Gauckler, L., Colloidal Stabilization of Nanoparticles in Concentrated Suspensions. *Langmuir* **2007,** 23, (3), 1081-1090.

37. Strickley, R. G., Solubilizing Excipients in Oral and Injectable Formulations. *Pharm. Res.* **2004,** 21, (2), 201-230.

38. Spiegel, A. J.; Noseworthy, M. M., Use of Nonaqueous Solvents in Parenteral Products. *J. Pharm. Sci.* **1963,** 52, (10), 917-927.

39. Lopatin, P. V.; Safonov, V. P.; Litvinova, T. P.; Yakimenko, L. M., Use of Nonaqueous solvents to Prepare Injection Solutions. *Khim.-Farm. Zh.* **1972,** 6, (11), 36-47.

40. Radwan, M., In vivo screening model for excipients and vehicles used in subcutaneous injections. *Drug Dev. Ind. Pharm.* **1994,** 20, (17), 2753-2762.

41. Knepp, V. M.; Muchnik, A.; Oldmark, S.; Kalashnikova, L., Stability of Nonaqueous Suspension Formulations of Plasma Derived Factor IV and Recombinant Human Alpha Interferon at Elevated Temperatures. *Pharm. Res.* **1998,** 15, (7), 1090-1095.

42. Harn, N. R.; Jeng, Y. N.; Kostelc, J. G.; Middaugh, C. R., Spectroscopic Analysis of Highly Concentrated Suspensions of Bovine Somatotropin in Sesame Oil. *J. Pharm. Sci.* **2005,** 94, (11), 2487-2495.

43. Weiss IV, W. F.; Young, T. M.; Roberts, C. J., Principles, Approaches, and Challenges for Predicting Protein Aggregation Rates and Shelf Life. *J. Pharm Sci.* **2009,** 98, (4), 1246-1277.

44. Yu, Z.; Johnston, K. P.; Williams, R. O., III, Spray freezing into liquid versus spray-freeze drying: Influence of atomization on protein aggregation and biological activity. *Eur. J. Pharm. Sci.* **2006,** 27, 9-18.

45. Engstrom, J. D.; Lai, E. S.; Ludher, B. S.; Chen, B.; Milner, T. E.; Williams, R. O., III; Kitto, G. B.; Johnston, K. P., Formation of Stable Submicron Protein Particles by Thin Film Freezing. *Pharm. Res.* **2008,** 25, (6), 1334-1346.

46. Engstrom, J. D.; Simpson, D. T.; Cloonan, C.; Lai, E. S.; Williams III, R. O.; Kitto, G. B.; Johnston, K. P., Stable high surface area lactate dehydrogenase particles produced by spray freezing into liquid nitrogen. *European Journal of Pharmaceutics and Biopharmaceutics* **2007,** 65, 163-174.

47. McMinn, J. H.; Sowa, M. J.; Charnick, S. B.; Paulaitis, M. E., The Hydration of Proteins in Nearly Anhydrous Organic Solvent Suspensions. *Biopolymers* **1993,** 33, 1213-1224.

48. Partridge, J.; Moore, B. D.; Halling, P. J., Alpha-Chymotrypsin stability in aqueous-acetonitrile mixture: is the native enzyme thermodynamically or kinetically stable under low water conditions? *J. Mol. Catal. B: Enzym.* **1999,** 6, 11-20.

49. Halling, P. J., High-affinity binding of water by proteins is similar in air and in organic solvents. *Biochim. et Biophys. Acta* **1990,** 1040, 225-228.

Chapter 3: Weakly interacting, equilibrium nanoclusters of stable protein at high concentration

Highly concentrated, polyclonal sheep IgG is crowded by extrinsic molecular crowders, into 80-250nm clusters to form dispersions, while the protein self-crowding within the cluster preserves the native folded state. These novel, equilibrium clusters are formed by balancing attraction from the extrinsic molecular crowders and the inherent specific short-range protein interactions against very weak electrostatic charging of the protein near the isoelectric point. Equally sized nanoclusters were formed by multiple techniques including dispersing a lyophilized protein powder to an aqueous solution containing additional molecular crowders and adding and removing crowders from a protein solution. A universal curve, based on the total φ of crowders in the dispersion but independent of the type of crowder used, can be formed from individual and multiple crowders, including trehalose, PEG300 and NMP. Since the φ of the protein within the nanoclusters is estimated to be ~0.3, protein self-crowding within the cluster is anticipated to prevent protein unfolding. The consistent, equilibrium size of the cluster allows the interactions to be viewed from the standpoint of a protein or the cluster as an individual entity. Thus, by changing the colloid size from a protein monomer (~1-15nm) to a submicron nanocluster (80-250nm), specific short-range attractive interactions on the protein, whose influence is important to ~1nm from the surface, and excluded volume effects from the extrinsic molecular crowders can be minimized. The decreased effect of specific short-range attractive interactions results in decreased viscosity of the nanocluster dispersion when compared to a protein solution. While this concept is demonstrated for a particular antibody, the formation of nanocluster dispersions by increasing the total attractions between protein molecules, close to the isoelectric point, to increase protein stability and decrease protein viscosity is applicable to any protein.

3.1 INTRODUCTION

Concentrated proteins in aqueous media (100 to 500 mg/ml) are of widespread interest in colloid and biophysical chemistry[1], biochemistry[2], cellular processes[3], protein crystallization[4, 5], protein processing and storage[6], drug delivery by subcutaneous injection and other routes[7, 8], and medicine[9, 10]. At these concentrations where the average spacing between protein molecules is ~5 nm, hydrophobic,[11] hydrogen bonding, and fluctuating charge dipole[12] attractive interactions (~3kT) with a range of ~1nm limit solubilities markedly.[2, 13] Even when the proteins are soluble, these specific short range interactions often produce protein aggregates[3, 14], or viscous gels[15], as described with colloidal phase diagrams.[5, 13, 16-19] Extensive protein specific studies have addressed these problems by manipulating the sequence of amino acids.[20, 21] A complimentary alternative would be to utilize concepts in colloid chemistry to form dispersions of insoluble protein particles, as reported recently in organic solvents.[22] In principle this approach may be applicable to large classes of proteins, including therapeutic antibodies, if the protein remains folded within the particles.

Even though proteins have complex structures and short-range interactions, colloidal phase diagrams are similar for proteins and simple spherical particles with short-range attraction.[5, 13, 19] For uncharged spherical polymer colloids with a diameter σ, of 560nm, the strength and range ($\Delta\sigma$ < 100 nm) of the short range attraction have been adjusted independently to map transitions from individual particles to polydipserse clusters and ultimately equilibrium phase separation to form gels.[1, 23, 24] In the case of very slightly charged spherical polymer particles (~10^{-3} charges/particle) in a low dielectric constant organic solvent, distinct equilibrium clusters of 10^3 particles[23, 25] were formed by balancing of short range attraction and repulsion, from self-charging within the cluster. To our knowledge these types of large equilibrium clusters have rarely been

reported in aqueous media, with recent examples of charge-screened biodegradable gold clusters[26] and sugar[27] of unknown charge. For concentrated solutions (ϕ = 0.2) of highly charged lysozyme at pH 7.0 (isoelectric point, pI= 11), dilute dynamic clusters about 2.5 times larger than the monomer, or ~15 nm have been observed by neutron spin echo and small angle neutron scattering[28, 29] and dynamic light scattering (DLS)[30]. To form much larger protein clusters, the charge on the protein would have to be smaller to reduce electrostatic repulsion. However, the attractive interactions between the clusters must also be sufficiently weak and balanced by electrostatic repulsion to avoid aggregation of nanoclusters resulting in viscous gels. The ability to design the proper balance of colloidal interactions for the formation of stable nanoclusters of proteins at high concentrations would provide an alternative to solutions of individual protein molecules.

The folded state of dilute proteins is stabilized by excluded volume (depletion) effects with the addition of crowding agents, for example sugars and polysaccharides, relative to the larger unfolded state.[31-33] In cells, the high total volume[34, 35] fraction of these extrinsic crowders, ϕ_E, enhances the folded state.[3] The excluded volume interactions or likewise depletion attraction between two particles is driven by the gain in entropy as a cosolute (often called crowder[3]) is excluded from the depletion zones (overlap region) between two solutes. Thus, the depletion force compresses the protein to assume the more compact folded state, with the smaller depletion zone.[31, 32, 34-36] Recent *in vitro* experiments have related the force for unfolding a dilute globular protein ubiquitin to the concentration of the extrinisic crowder, dextran, up to ϕ_E = 0.4 with atomic force microscopy.[37, 38] Depletion attraction from self-crowding of proteins (in contrast with extrinsic crowders) may be expected to stabilize the folded state, as demonstrated by simulation and theory, at ultra high protein concentrations (φ>0.15).[11, 39] However, the limited solubility of proteins in solution has prevented verification of these

predictions experimentally. If protein nanoclusters with controlled size could be formed, and self-crowding within the nanoclusters prevented unfolding, highly concentrated dispersions could be designed as an alternative to protein solutions.

Here, we assemble a protein (sheep IgG) into translucent dispersions of 80-250nm nanoclusters at high concentrations, while simultaneously preserving the native folded state due to self-crowding. Equilibrium nanoclusters are formed near the pI, where the short range attractive forces are strong enough to balance the repulsion from the small charge on the protein. This novel concept is the opposite of the typical approach to solubilize highly charged protein in the monomer state away from the pI. The dispersions were formed by gently stirring a mixture of lyophilized powder, with a mass ratio of protein/trehalose of 1/1 with a buffer solution near the pI, in some cases with additional crowers including polyethyelene glycol (Mw = 300) (PEG300) and n-methyl-2-pyrrolidone (NMP). The hydrodynamic diameter of the clusters, D_h, was measured by dynamic light scattering at 160 or 165^o to minimize multiple scattering. At constant ϕ_I, the values of D_h were equivalent at a given φ_E or upon changing φ_E along various pathways, upwards and downwards, suggesting an approach to thermodynamic equilibrium. For an overall ϕ_I up to 0.21 (275 mg/ml IgG), D_h was tuned from 85 to 260nm by varying the depletion attraction via the volume fraction of extrinsic crowder, ϕ_E. In another type of experiment, the protein was diluted at constant crowder concentration, to determine the ϕ_I where the protein became monomer. We define this value as the “DLS solubility” of the protein. The lack of formation of aggregates of the nanoclusters is demonstrated *in situ* with DLS and SEM micrographs, as well as a repulsive osmotic second virial coefficient for the intercluster interaction from static light scattering (SLS). The weak intercluster interactions limit viscosities for the nanocluster dispersion to ~50 cp even with protein concentrations up to 275 mg/ml where $\phi_I = 0.21$.

The self-crowding (depletion attraction) of the proteins within the clusters prevented protein unfolding, as demonstrated by tryptophan (TRP) fluorescence in the concentrated dispersions. As predicted by theory,[11, 39] the concentrations of protein in the clusters, around 0.29 for various cluster sizes from 85 to 258nm respectively, as characterized by static light scattering, were sufficiently high to provide self-crowding. Furthermore, after dilution in buffer, the protein remained stable according to an enzyme-linked immunorsorbent assay (ELISA), and the presence of only a sharp monomer peak by DLS, in addition to TRP fluorescence.

The mechanism of cluster formation and stability is explained in terms of a hierarchy of attractive intracluster and repulsive intercluster colloidal interactions, along with a new free energy model. The predictions of the cluster size with the free energy model are in semi-quantitative agreement with the experimental data. The electrostatic repulsion is shown to be relatively weak for the weakly charged protein monomer, but simultaneously strong between the clusters, given their much larger charge. Simultaneously, the depletion and specific short range attractive interactions are strong enough at the protein molecule scale to hold the clusters together (intracluster), yet very weak at the intercluster scale. This hierarchy of electrostatic and attractive interactions provides two key goals: (1) formation of equilibrium nanoclusters of protein monomer and (2) weak interactions between the nanoclusters for stable dispersions with low viscosities. The range of the specific short range and depletion interactions, ~1 nm, is essentially independent of protein particle size. Thus, these intercluster attractive interactions are much weaker for 100 nm clusters where the average spacing is 50 nm at $\phi_I = 0.2$, relative to 5 nm for 10 nm protein molecules. The design of these concentrated dispersions of equilibrium stable protein nanoclusters is based on universal colloid scaling concepts for hierarchical short-ranged interactions balanced by electrostatic

repulsion, and thus may be expected to be applicable to wide classes of proteins. The low viscosity (<50 cp) and high molecular stability are of great interest in subcutaneous injection of protein therapeutics with a 25-28 gauge needle, where high dosages of greater than 100 mg/ml are desired in an injection volume of only 1-1.5 ml.[6]

3.2 MATERIALS AND METHODS

3.2.1 Materials

Polyclonal sheep IgG (Product No. I5131) was purchased from Sigma-Aldrich, Inc.(St. Louis, MO) and further purified by size-exclusion, fast protein liquid chromatography (FPLC) (details in Appendix 1.2). α-α trehalose, polyethylene glycol with an average molecular weight of 300 (PEG 300), n-methyl 2-pyrrolidone (NMP), and all other chemicals were purchased from Fisher Chemicals (Fairlawn, NJ).

3.2.2 Powder and dispersion formation

The pI of the protein was determined to be 6.4 from the zeta potential in 20mM histidine buffer at a pH of 5.5, 6.4 and 7.4 and confirmed by isoelectric focusing gel electrophoresis (Figure A1.2.1) (see Appendix 1.2 for procedure). The IgG solution, purified by FPLC, (see Appendix 1.2 for details), at an initial concentration of 20 mg/ml in histidine buffer, pH 5.5, with 1:1 wt ratio of α-α trehalose, was slowly frozen over 6 hours in 8 ml vials on a pre-cooled lyophilizer tray at -40°C (VirTis Advantage Plus Benchtop Freeze Dryer). The sample was then lyophilized to form a dry powder at 100mTorr with 12 hours of primary drying at-40°C followed by a 6 hour ramp to 25°C and an additional 6 hours of secondary drying at 25°C. Scanning electron microscopy images of the powders formed upon lyophilization are included in the supplementary section (Figure A1.2.2). Between 0.039 and 0.08g ± 0.0005g of powder were compacted with a spatula into a 0.1ml conical vial (Wheaton Science Products No. 986211). 100 $\pm$ 1

µl of an aqueous-based buffer were added to the conical vial with a 20-200 µl micropipet to yield a total dispersion volume of ~0.1ml. NaCl was added to 50 mM pH 6.4 phosphate buffer (the pI of sheep IgG[40]) to yield a total ionic strength of 154mM. The mixture of powder and buffer was stirred gently, at low shear, with the tip of the 25g needle to remove air pockets and form a translucent dispersion without the appearance of any visible inhomogeneities (Figure 3.1) using the naked eye. It was assumed that the highly soluble trehalose in the powder dissolved and became an extrinsic crowding agent in the dispersion. In certain experiments, the aqueous buffer contained a known volume of PEG300 as an additional crowder, or mixture of PEG300 and NMP. The total volumes of the various components in the concentrated dispersions are given in Table A1.2.1, based on known masses and densities (from partial molar volumes) of IgG and trehalose and known added volumes of the other (liquid) components. The volume fractions of the components (φ, I for IgG, T for trehalose, P for PEG300, and N for NMP) are given in Table 3.1. This basic procedure was also used to determine volume fractions throughout the study.

3.2.3 Characterization of the dispersions

Hydrodynamic diameters, D_h, of nanoclusters and/or protein monomer in the aqueous crowder solutions were measured by dynamic light scattering (DLS) at various concentrations on a custom-built (Brookhaven) apparatus with a 632.8 nm laser, a fiber optic detector and an avalanche photodiode[41] at various scattering angles and a temperature of ~23ºC, unless otherwise specified. The measurements at high ϕ ranging

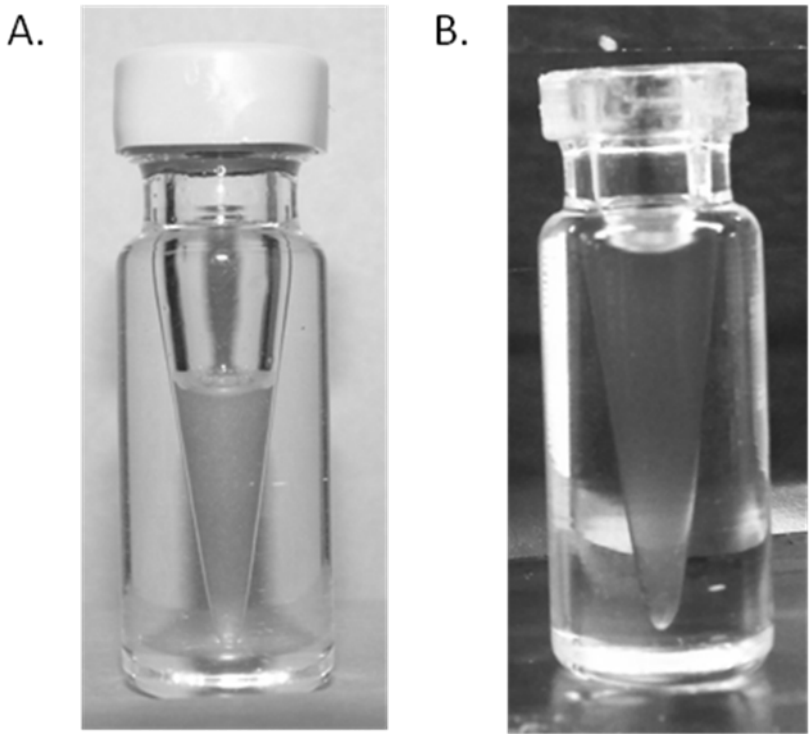

Figure 3.1 Digital image of translucent dispersion. A) 157 mg/ml – 0.08 φ_P/0.16 φ_N B) 275 mg/ml. All dispersions in Table 3.1 looked very similar.

Table 3.1. Hydrodynamic diameter of clusters, protein monomer solubility by DLS dilution, and viscosities in pH 6.4 50mM phosphate buffer. The volume fractions were calculated assuming ideal mixing; actual masses in the dispersions are given in Table A1.2.1.

IgG (c_i) or trehaolse concentration (mg/ml)	**φ_I**	**φ_T**	**φ_P**	**φ_N**	**φ_E (total extrinsic crowders)**	**Hydrodynamic Diameter, D_h (nm)**	**DLS Solubility (mg/ml)**	**Dispersion Viscosity (cP)**	**Solvent Viscosity (cP)**	**Intrinsic Viscosity**
214	0.16	0.13	0	0	0.13	85 ±25	31-50	37	1.5	17
275	0.21	0.17	0	0	0.17	88 ± 9	31-50	63	2.1	14
157	0.12	0.09	0.16	0	0.25	111 ± 10	ND	51 ± 7	3.4	20
162	0.12	0.10	0.24	0	0.34	111 ± 10	<1	48 ± 1	3.5	19
157	0.12	0.10	0.08	0.16	0.33	258 ± 24	1.25-2.5	25 ± 5	4.3	13
204	0.15	0.12	0.07	0.14	0.34	ND	1.25-2.5	102	5.6	16

from 0.12 to 0.21 were made at 160-165° scattering angle to minimize multiple scattering[42] with a specialized ~60 µl sample cell (Beckman Coulter Part # A54094) to minimize the amount of protein required. To ensure that multiple scattering was minimized for the concentrated dispersion, additional measurements at a second scattering angle of 135° were conducted and found to give a D_h within 10% of the measurement at 160°. Data analysis was performed with CONTIN using a digital autocorrelator (Brookhaven BI-9000AT). DLS measurements in Table 3.1 were performed in triplicate. Reported average diameters corresponded to the D_{V50}, or diameter at which the cumulative sample volume was under 50%. All samples contained one peak with a narrow distribution resulting in a relative standard deviation in peak width of less than 20% (see supplemental table A1.2.2 for detailed analysis). The particular samples containing PEG300 without NMP (lines 3 and 4 in Table 3.1) were measured in the same cell, but with a Delsa Nano Particle Size Analyzer (Beckman Coulter, Fullerton, CA) at a scattering angle of 165º. The technique was validated with a polystyrene standard ($\phi \leq$ 0.3) as shown in Figure A1.2.3. A variety of experiments were performed with much lower concentrations of protein (1 mg/ml) in 2 ml ampoules (Wheaton Scientific product #176776) at a scattering angle from 30° to 90° as previously reported.[26] In addition, the average count rate for the larger volume, low concentration dispersions was recorded as the measured intensity for static light scattering (SLS) to determine the porosity and second osmotic virial coefficient.

To further characterize particle morphology by scanning electron microscopy (SEM) and scanning transmission electron microscopy (STEM) the aqueous dispersions were diluted to 40 mg/ml and lyophilized as described in the supplemental section. The degree of folding of the IgG within the concentrated dispersed particles was monitored from the λ_{max} in fluorescence of the tryptophan residues in the fully unfolded protein

(350nm) versus the folded protein (336nm).[43] A standard curve of the sheep IgG unfolding versus the concentration of a denaturant, urea, is included in the supplemental (Figure A1.2.4). The protein activity was characterized by a polyclonal capture enzyme-linked immunosorbent assay (ELISA), after 10 μl of the dispersion was diluted to 1 mg/ml in a phosphate buffer, as described in detail in the supplemental section. These samples were also measured by DLS at 30º to characterize the protein monomer peak and to identify the presence of any irreversible aggregates. The monomeric peak obtained by DLS was also verified by size exclusion chromatography (SEC), described in the Appendix A1.2 and Table A1.2.3.

3.2.4 Viscosity measurement

The apparent viscosity of the IgG nanocluster dispersions was measured in triplicate with 10% relative standard deviation using a 25 gauge (ID = 0.1mm) 1.5" long needle attached to a 1ml tuberculin slip tip syringe, according to the Hagen-Pouiselle equation. The velocity through the needle was determined with a video camera (Image J software) on the basis of the time to draw the dispersion from a height 0.4" from the bottom of the cone to a height 0.1" (~50 μl). The time was measured to within 0.05 seconds at least 3 times and averaged, while maintaining a nearly constant suction force by holding the end of the plunger at the 1ml mark. A maximum volume of 10% of the cavity in the syringe was filled with dispersion to minimize variation in the pressure drop. A linear correlation between the time to draw 0.05 ml from the conical vial and the viscosity of various calibration fluids is shown in Figure A1.2.5.[21, 22] The mixed aqueous-based solvent mixture viscosity (without protein) was measured using a Cannon-Fenske calibrated viscometer tube (Fisherbrand Catalog No. 13-617B) at least 3 times and averaged.

3.3 RESULTS

3.3.1 Formation of highly concentrated nanocluster dispersions

A translucent dispersion was formed upon gentle stirring of high concentrations of the lyophilized IgG:trehalose (1:1) particles in aqueous pH 6.4 phosphate buffer (Figure 3.1). This translucent appearance is a consequence of the unusually low difference in refractive indices between the protein (~1.42) and the aqueous solvent (~1.33-1.37), despite the high protein concentration, c_i, of 150-275 mg/ml. The low turbidity enables visual observation that macroscopic particles were not present in all cases, which would be an important heuristic for the use of these dispersions for parenteral therapy.

The DLS results are first presented for the highly concentrated dispersions in Table 3.1, followed by more specialized studies to determine the "DLS solubility" of the IgG and to vary pathways to prove that the clusters reached equilibrium. At a scattering angle of 160^o, the D_h of the protein nanoclusters was approximately an order of magnitude larger than the value of 10nm for individual IgG molecules[44] (Table 3.1). For the simplest cases in the first two rows with trehalose as the only extrinsic crowder, D_h ~85-88 nm for c_i and trehalose concentrations of 214 and 275 mg/ml (Figure 3.2A and Table 3.1). The ability to accurately measure D_h at a scattering angle of 160° with a concentrated dispersion was determined by additional measurements at angles of 145° and 135° confirming the average particle size within 10%. In addition, a polystyrene standard with φ of 0.3 was used to confirm that the accuracy of the particle size to within 15%. In Figure 3.2A for one representative DLS run at each crowder condition, no larger aggregates are observed in the size distribution and the peak width had a relative standard deviation of less than 10%. All D_h values reported in Table 3.1 are the average and standard deviation of 3 or more individual runs provided in the Appendix 1.2 (Table

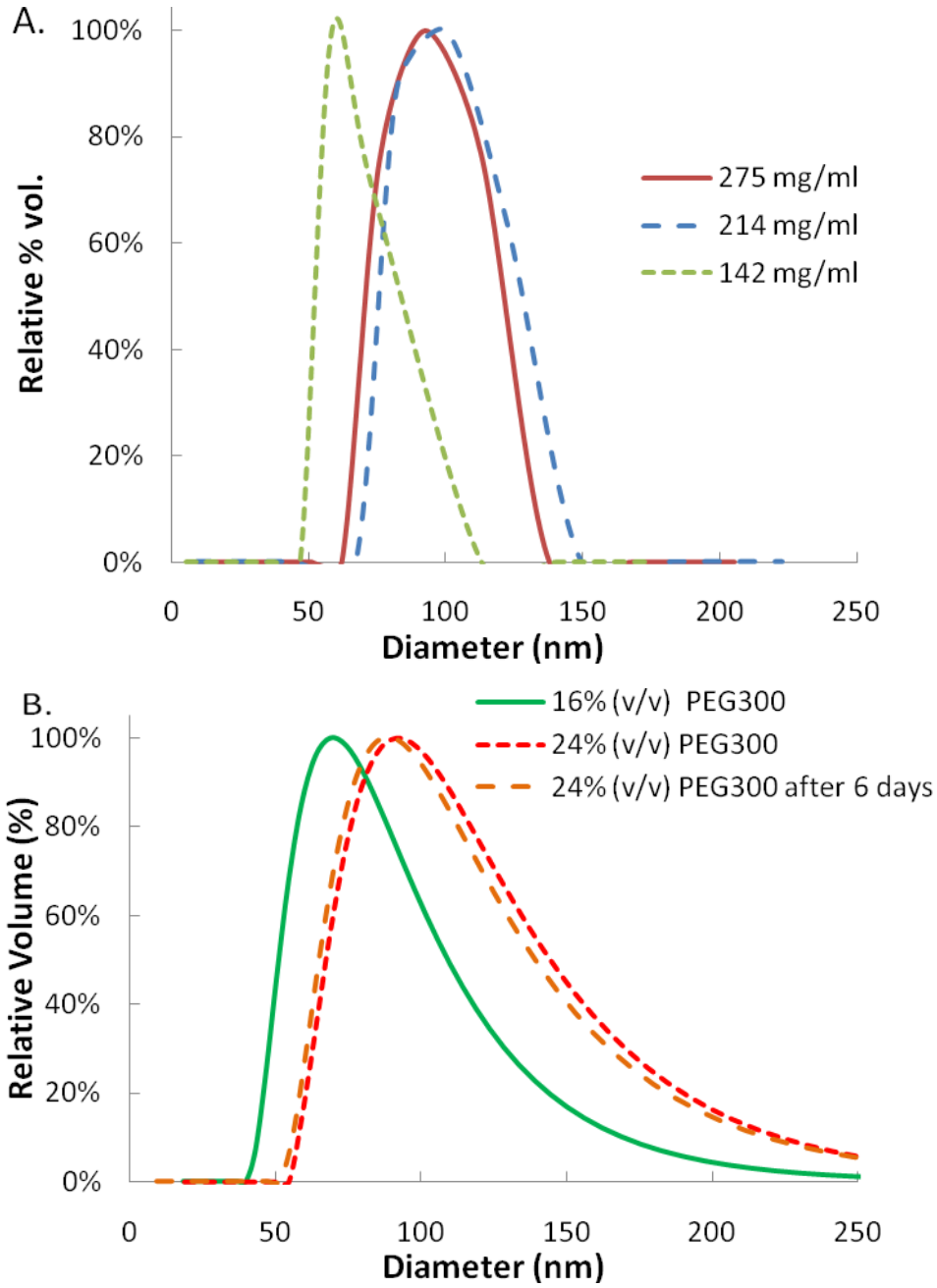

Figure 3.2. DLS hydrodynamic diameters of protein nanoclusters. A) Trehalose is only extrinsic crowder. (At 142 mg/ml IgG, $\varphi_T = 0.09$) B) 157 mg/ml IgG dispersion with $\varphi_P = 0.16$ or 0.24. Additional sample information in Table 3.1.

A1.2.2). For a lower concentration of trehalose as a crowder and a c_i of 142 mg/ml (φ_T = 0.09), smaller 58 nm clusters were formed (Figure 3.2A). When PEG300 was added (ϕ_N = 0.16-0.24) to raise the total extrinsic crowder volume fraction, $\phi_{E,}$ to 0.25 and 0.34, the D_h increased modestly to 111 nm (Figure 3.2B). Even larger 258 nm clusters were observed with a mixture of φ_p = 0.08 and φ_N = 0.16 despite a similar total ϕ_E of 0.33 as for the case without NMP.

The IgG concentration, c_i, in the dispersion was diluted at constant compositions of all extrinsic crowders to define the "DLS solubility", as shown in Figure 3.3. The c_i where the D_h shifted from greater than ~50nm, to the hydrodynamic diameter of the IgG, 11nm[44], was defined to be the solubility of the IgG in the extrinsic crowder solution. By this DLS solubility technique, the IgG solubility at the pI (pH 6.4) with 250 mg/ml trehalose (φ_T = 0.15) was between a c_i of 31 and 50 mg/ml as the large clusters were still visible at 50 mg/ml, however only the soluble monomer was visible at 31 mg/ml (Figure 3.3A). When 0.16 φ_N and 0.08 φ_P with 200 mg/ml trehalose are used in combination as crowders (φ_E = 0.34), the IgG solubility decreased by 1 order of magnitude, to between 1.25 and 2.5 mg/ml (Figure 3.3B). The DLS solubility at other crowder conditions, including the extrinsic crowder combination of PEG300 and trehalose, was also investigated (Table 3.1). Using the DLS IgG dilution method, the solubility was detected to be less than 1 mg/ml for an added 0.24 φ_P (Table 3.1). Solubilities of less than 1 mg/ml could not be detected by the DLS as the intensity of the scattered laser light was too weak.

Rapidly frozen and lyophilized SEM and STEM images of the concentrated nanocluster dispersions confirm the particle size and show the morphology of the clusters formed with added extrinsic crowders 0.16 φ_N and 0.08 φ_P (φ_E = 0.33, Figure 3.4). As

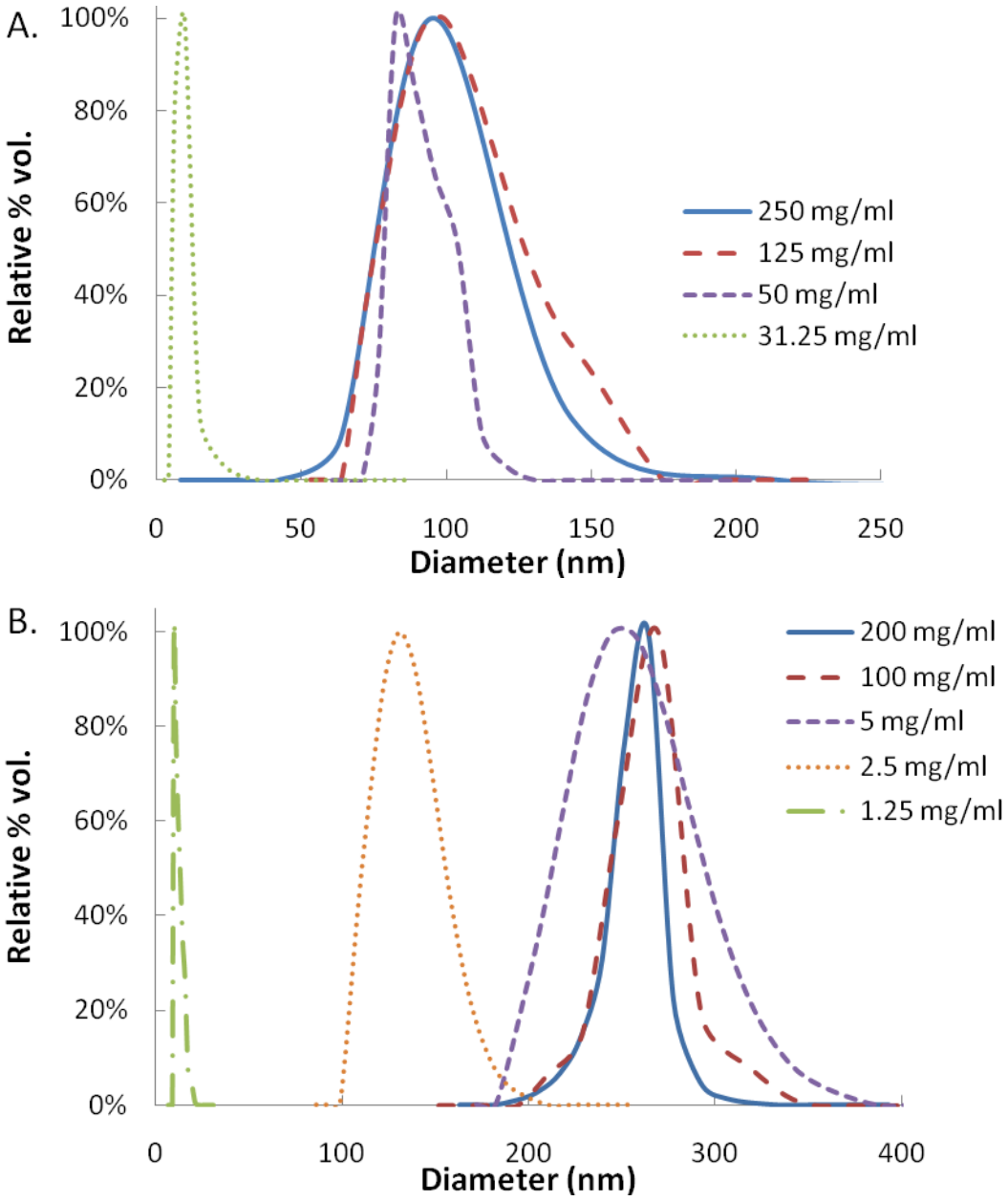

Figure 3.3. DLS hydrodynamic diameters at constant extrinsic crowder concentrations versus protein to determine protein solubilities. A) initial 250 mg/ml IgG in pH 6.4 buffer with 250 mg/ml trehalose (φ_T = 0.15). The protein monomer solubility is between ~31 m and 50 mg/ml. B) initial 200 mg/ml IgG in pH 6.4 buffer with 0.16 ϕ_N/0.08 ϕ_P and 200 mg/ml trehalose (φ_E = 0.34). The protein monomer solubility is between ~1.5 and 2.5 mg/ml.

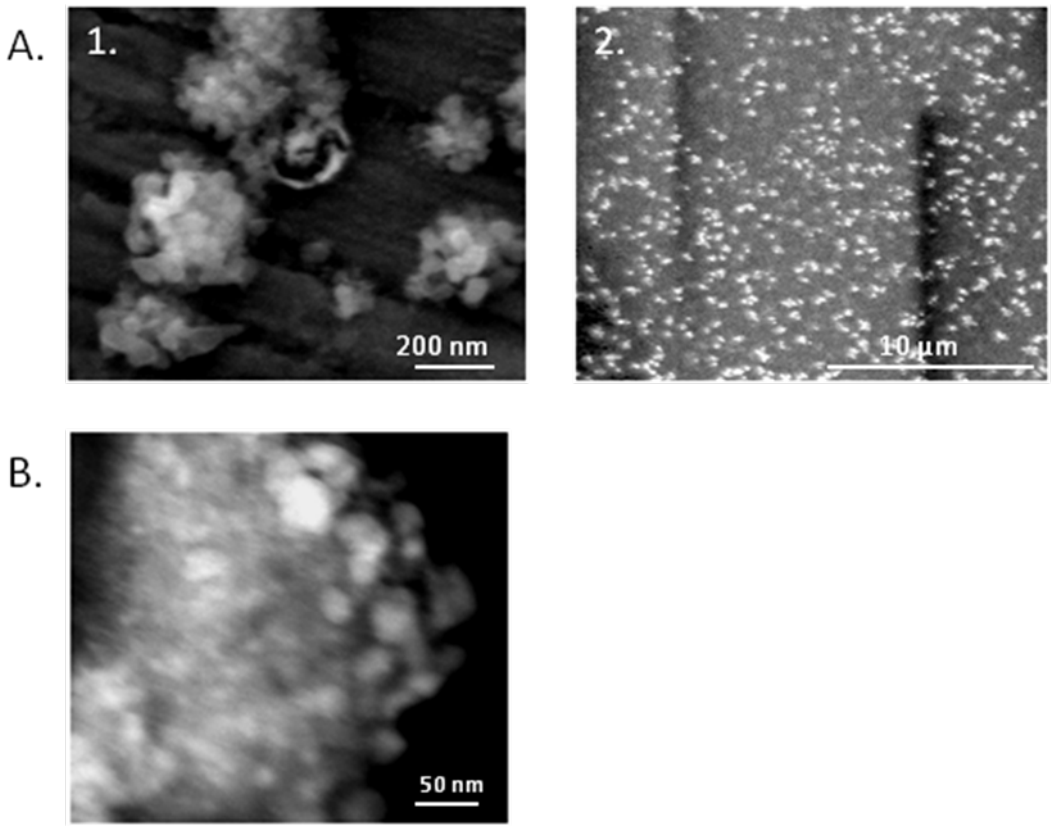

Figure 3.4 A) Cryo-SEMs and B)STEM images of the 157 mg/ml - 0.08 φ_P/0.16 φ_N IgG dispersion in Table 3.1

seen by both SEM (Figure 3.4A1) and STEM (Figure 3.4B), the particles are clusters formed of ~50nm and below primary particles. From SLS measured concurrently with the DLS at various scattering angles (30°, 45°, 75° and 90°), the fractal dimension of the nanoclusters can be determined as the exponent from a log-log plot of the scattering vector and the SLS intensity (see Appendix 1.2 for details).[45] The fractal dimension of a cluster, D_f, characterizes the structure of a flocculated particle by relating the volume fraction of solid in the particle, φ_I, to the primary particle diameter, d, and the cluster diameter, d_k.[46]

$$\phi_I = \left(\frac{d_k}{d} \right)^{D_f - 3} \qquad \text{Eq. 3.1}$$

For a cluster composed of densely packed particles, D_f approaches 3. For the nanoclusters formed with 250 mg/ml trehalose (φ_T = 0.15), a D_f of 2.4 was measured experimentally by SLS (Figure A1.2.6) resulting in a φ_I of individual proteins of 0.29 (Table 3.2). For the clusters formed with $0.16\varphi_N$ and $0.08\varphi_P$ (φ_E = 0.34), a φ_I of 0.29 was calculated (Table 3.2) using the measured Df of 2.6 (Figure A1.2.6).

3.3.2 Effect of crowder concentration on equilibrium nanocluster diameter

The effect of the total extrinsic crowder volume fraction (φ_E) on the size of the protein nanoclusters was determined by increasing and decreasing φ_E by a variety of paths at a constant c_i (Figure 3.5). In Figure 3.5A path 1, φ_T was increased from 50 mg/ml up to 300 mg/ml by adding trehalose from a concentrated solution of trehalose (500 mg/ml trehalose). At each point, the c_i was maintained at 50 mg/ml by simultaneously adding a small volume of a 200 mg/ml concentrated protein dispersion with 200 mg/ml trehalose prior to measuring the D_h. The average D_h and standard deviation of 3 individual measurements at each condition is shown in Figure 3.5. The

Table 3.2. Characterization of protein stability. Maximum emission wavelength (λ_{max}) for concentrated protein dispersions from tryptophan fluorescence assay where λ_{max} for fully folded protein is 336nm and for fully unfolded protein is 349nm. For ELISA and DLS, dispersions were diluted in pH 7.0 buffer to 1 mg/ml.

Dispersion name	**φ protein within nanocluster from SLS**	**φ_E (extrinsic)**	**TRP λ_{max} (nm)**	**ELISA Relative EC_{50}***	**DLS - Hydrodynamic Diameter (nm)**
275 mg/ml	0.29	0.17	336 ± 1	1.1 ± 0.1	9 ± 2
157 mg/ml - 0.08 φ_P/0.16 φ_N	0.29	0.33	336 ± 1	1.1 ± 0.2	10 ± 1

*Relative EC_{50} was calculated as the difference between the EC_{50} of the reconstituted dry powder to the original purified solution prior to processing.

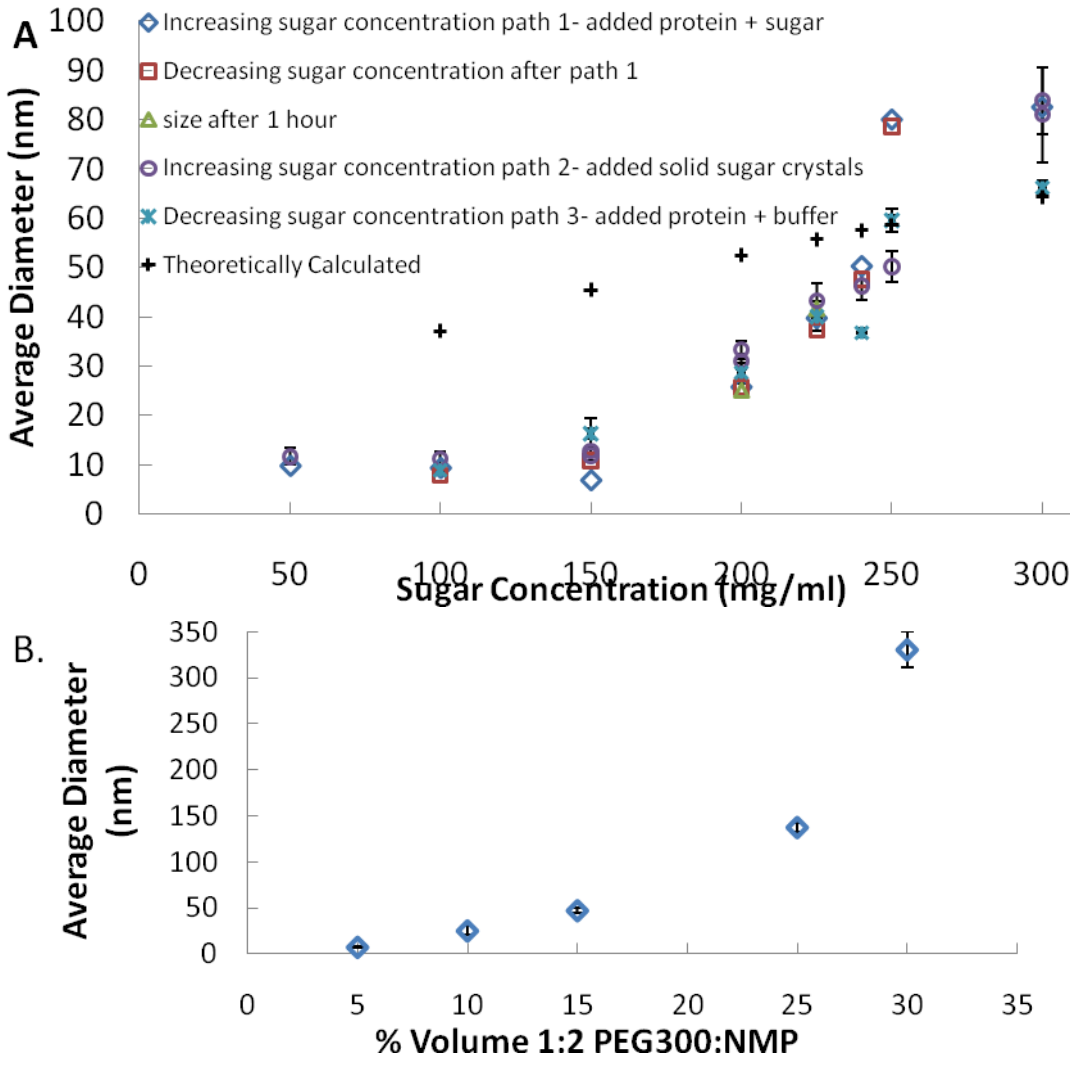

Figure 3.5. A) D_h of protein nanoclusters at a constant c_i of 50 mg/ml. In path 1, trehalose concentration was increased with 500 mg/ml trehalose in pH 6.4 phosphate buffer along with constant c_i. For decreasing sugar concentration, pure buffer was added while maintaining constant c_i. In path 2, solid sugar crystals were added. In path 3, trehalose concentration was decreased using pure pH 6.4 phosphate buffer and 200 mg/ml IgG dispersion with trehalose. The values for the cluster diameters obtained from theory (Eq. 3.14-3.17) are also superimposed on the plot. B) IgG and trehalose concentration constant at 30 mg/ml. φ_N and φ_P were increased by adding a 1:2 volume solution of PEG300:NMP while maintaining constant IgG and trehalose concentrations.

individual DLS runs and peak width of these measurements is included in Table A1.2.4. By DLS, the protein at a concentration of 50 mg/ml trehalose was present as a monomer, as seen from the D_h of ~ 10 nm, up to a trehalose concentration of 150 mg/ml. Above 150 mg/ml of trehalose, the protein formed clusters as shown by the increasing D_h. The protein cluster diameter increased linearly with trehalose concentration and reached ~ 80 nm at a trehalose concentration of 300 mg/ml (Figure 3.6). In Figure 3.7, the mass of trehalose was converted to φ_T by using the mass density of trehalose (1.64 g/ml[47]). To verify the reproducibility of the cluster size by a separate pathway, the trehalose concentration starting from 300 mg/ml was decreased by adding a pure buffer solution. Again, the c_i was maintained at 50 mg/ml by adding slight amounts of the concentrated protein dispersion mentioned above. The experimentally measured cluster size decreased at the same rate, based on φ_T, as it had increased while adding trehalose (Figure 3.5A decreasing sugar concentration after path 1). In a separate experiment (Figure 3.5A path 2), an alternate method was used to increase the trehalose concentration. Trehalose crystals were dissolved directly in the protein solution at 50 mg/ml IgG and 50 mg/ml trehalose to increase the trehalose concentration. At each trehalose concentration, the size of the protein clusters produced by both methods, whether increasing or decreasing trehalose concentration, closely agreed. In addition, a third path, path 3, was tried where an initial trehalose concentration of 300 mg/ml and a constant IgG concentration of 50 mg/ml was diluted to 100 mg/ml IgG by using pH 6.4 phosphate buffer with the requisite small amounts of a 200 mg/ml IgG dispersion to maintain the IgG concentration at 50 mg/ml. All these different paths yield sizes that agree well with each other at the different trehalose concentrations that were tried and seem to fall on the same straight line.

A second crowder composition, a 1:2 by volume solution of PEG300 and NMP, was also used to determine particle size at various total φ_E. In this case, a measured

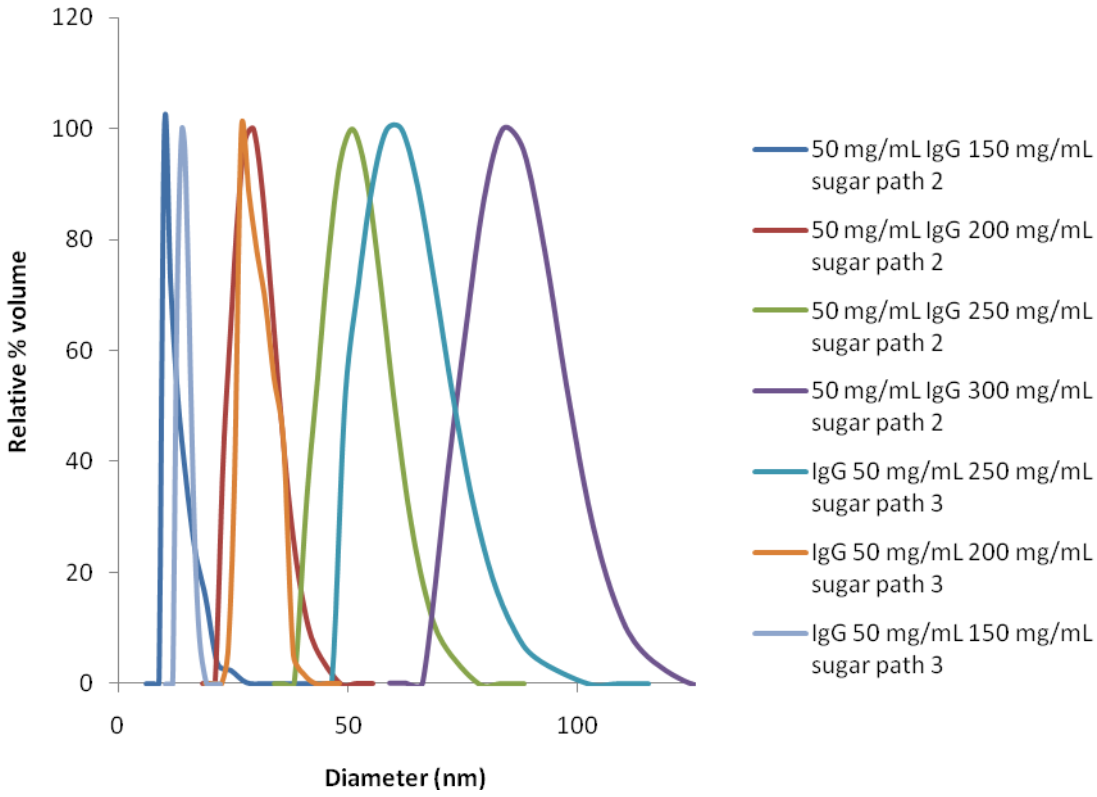

Figure 3.6. Distribution of the hydrodynamic diameter from DLS for selected samples from Figure 3.5A at different concentrations of trehalose and various pathways

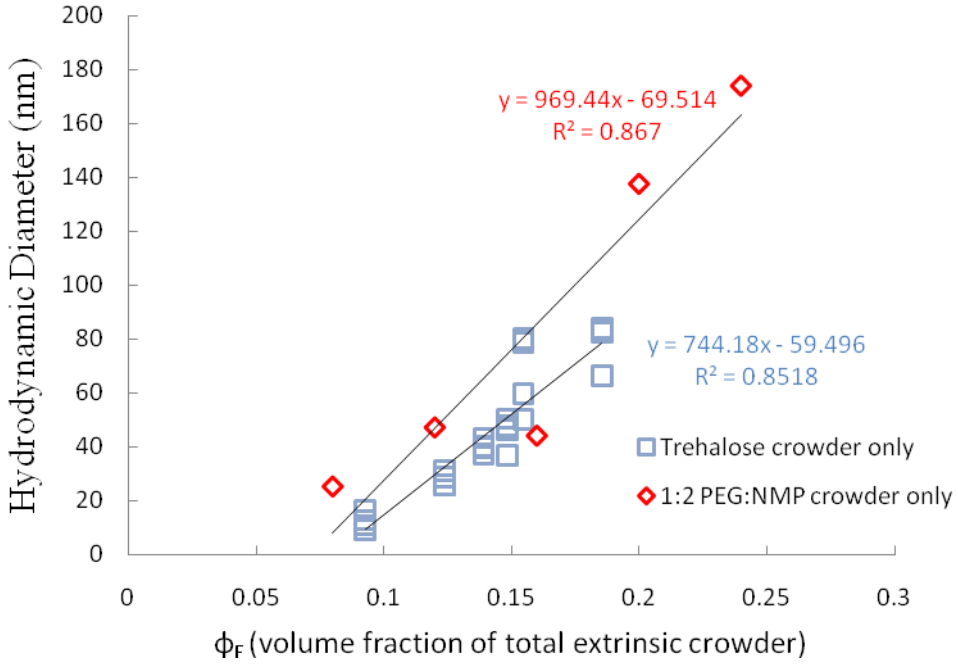

Figure 3.7 Universal scaling of hydrodynamic diameter measured by DLS for data in Figure 3.5 with increasing trehalose concentration (□) and constant φT with increasing NMP/PEG300 (◊).

volume of the 1:2 volume solution of PEG300 and NMP was added to increase total φ_E, while constant protein and trehalose concentrations of 30 mg/ml were maintained by the addition of a small amount of the 1:1 wt ratio protein to trehalose lyophilized powder. Cluster growth was observed as the φ_E of PEG300 and NMP was increased to 0.15 and higher. The largest particles of ~250nm were seen at a φ_E of PEG300 and NMP of 0.3. Actual hydrodynamic diameter distributions for some selected samples in Figure 3.5A obtained by DLS are shown in Figure 3.6. The distributions are fairly narrow with a relative standard deviation of less than 10% over the mean. Also, not only do the cluster sizes for different paths match up well as shown in Figure 3.5A but the distributions also are fairly consistent (Figure 3.6). The size of the protein clusters formed for both the trehalose crowder only and the 1:2 PEG 300:NMP crowder system was plotted against the total extrinsic crowder volume fraction in Figure 3.7. Both types of crowder systems give very comparable linear growth of the protein cluster size as shown in Figure 3.7. In fact, both crowder systems fall nearly on the same line.

3.3.3 Properties of the nanocluster dispersions (low viscosity and high molecular stability)

Syringable viscosities (< 50 cP) were obtained for most of conditions in Table 3.1, except the final row with 204 mg/ml IgG (0.08 φ_P/0.16 φ_N). The viscosities for the samples with φ_P between 0.16-0.24 were modestly higher than those for the NMP-PEG mixtures. Even higher volume fractions of PEG300, 0.50, increased the viscosity to the point where it was not syringeable at 150 mg/ml IgG (results not shown). When only trehalose was used as an extrinsic crowding agent, the viscosity of the protein dispersion at 214 mg/ml, was 37 cP. Viscosities this low have rarely been reported, if reported at all,

for therapeutic proteins at such a high concentrations.[6, 21, 48] Furthermore, solutions often cannot be formed at 200-300 mg/ml as the protein solubilities are not this high.[2, 20]

The apparent dispersion viscosity is commonly described as a function of the intrinsic viscosity, [η], maximum volume fraction of particles, φ_{max}, and the solvent viscosity, η_0, using the Krieger-Dougherty equation (Eq. 3.2).[22, 45]

$$\frac{\eta}{\eta_o} = \left[1 - \left(\frac{\phi_I}{\phi_{\max}}\right)\right]^{-[\eta]\phi_{\max}} \qquad \text{Eq. 3.2}$$

The η may be reduced by lowering η_0, or [η], which is a minimum of 2.5 for hard sphere colloids, and increasing φ_{max}. In table 3.1, φ_I is the volume fraction of protein and ϕ_{max} = 0.55. Because we have an equal mass of trehalose as protein present in the solvent, the solvent viscosity is increased to account for the soluble sugar.[49] For the samples with trehalose as the only extrinsic crowding agent, the solvent viscosity was approximated from a standard curve of trehalose solution viscosities[49], while all other extrinsic crowder in buffer solutions were measured experimentally. For each of the PEG-NMP formulations, [η] was fairly low, between 13 and 16. At a concentration of 275 mg/ml IgG with only sugar as a crowder, the [η] for the protein dispersion is around the same value, 14. For the three experiments with only PEG as an added crowder, the [η] values are a little larger (19-20) than for the NMP-PEG samples but still smaller than for many reported proteins with intrinsic viscosities as high as 100.

Given that the dispersions offer low viscosities at high concentrations, the protein stability within the dispersion and upon dilution is examined. At a c_i of 100 mg/ml, diluted from the concentrated dispersions with the crowders present, a fluorescence assay was utilized to show protein folding in the concentrated dispersion.[43] Isolated protein amino acid side chains, tryptophan and to a lesser extent tyrosine, excited at 295nm, will emit a maximum signal at 350nm.[43] Due to the local environment within a fully folded

protein, the maximum emission wavelength (λ_{max}) will shift to 336nm for the sheep IgG (Figure A1.2.4). Upon full unfolding of the protein, the local environment of the amino acid residues will change and λ_{max} will increase to 350nm. Thus a scan of the emission at wavelengths between 336 and 350 where the dispersed particles are excited at 295nm and λ_{max} is recorded will indicate the folding of the protein within the nanoclusters. For both dispersions with pure sugar crowder and with NMP and PEG, the λ_{max} of 336nm indicates the fully folded state of the protein (Table 3.2). High retention of monomeric protein and antibody activity for the protein diluted and dissolved to 1 mg/ml in a pH 7.0 phosphate buffer from the aqueous dispersion, is also shown in Table 3.2. As the sheep IgG used in these initial studies does not bind a single target, a polyclonal anti-sheep IgG capture ELISA was used to monitor loss of conformational epitopes due to denaturation.[7, 50] The relative EC_{50} ~ 1. 1 indicates similar binding to the standard IgG, within error of the experiment (Table 3.2). The relative EC_{50} values close to 1 indicate a negligible change in activity. According to DLS measurements for the dissolved IgG from nanoclusters at 1 mg/ml, the protein dissolves to a D_h of ~10nm, the D_h of the sheep IgG[44] (Table 3.2). Additional size exclusion chromatography to quantify the % monomer of the protein upon dilution into a pH 7.0 buffer is found in the supplementary material (Table A1.2.3).

3.3.4 Protein nanocluster interactions

Interparticle interactions of the nanoclusters in dispersion were quantified by measuring the second virial coefficient, B_2, by static light scattering (SLS). Since it was necessary to dilute the concentrated dispersion to remove multiple scattering, only the NMP-PEG system was utilized. A plot of $KcP(\theta)/R_\theta$ versus c was used to determine B_2 with the relationship

$$\frac{Kc}{R_\theta} = \frac{1}{P(\theta)}\left(\frac{1}{M_w} + 2B_2c\right) \qquad \text{Eq. 3.3}$$

where K is an optical constant

$$K = \frac{4\pi^2 n_0^2 (\frac{dn}{dc})^2}{N_A \lambda^4} \qquad \text{Eq. 3.4}$$

Here n_0 is the refractive index of the solvent and λ is the wavelength of the incident beam. The Rayleigh ratio (R_θ) for each sample was calculated based on the known R_θ of toluene[51] and the experimentally measured count rates for toluene and the sample. The refractive index increment (*dn/dc*) for the nanoclusters was taken to be the same as that for protein aqueous solutions (0.185 ml/g[52, 53]), as additional crowders and the formation of the nanoclusters are not anticipated to affect the value of *dn/dc* (for additional information see Appendix 1.2 and Figure A1.2.7). In the nanoclusters, intraparticle interference influences the measured intensity. To reduce this effect, an additional factor, P(θ), was added to eq. 3.4 to account for the change from pure Rayleigh scattering to Debye scattering (Eq. 3.5).[45, 54]

$$\frac{1}{P(\theta)} = 1 + \frac{16\pi^2 \overline{R_g^2}}{3\lambda^2} sin^2\left(\frac{\theta}{2}\right) \qquad \text{Eq. 3.5}$$

A low scattering angle, 30°, was chosen to reduce the second term of the 1/P(θ) equation (Eq. 3.5). The slope in Figure 3.8 indicates a positive B_2 of 6.6 *10^{-5} mol*ml/g^2 thus signifying that the nanocluster interparticle interactions are slightly repulsive. The repulsive nature of the nanocluster interparticle interactions is supported by other indirect characterization techniques. If the nanocluster interparticle interactions were attractive, we may not have seen discrete individual particles by SEM or DLS.

3.4 Discussion

3.4.1 Potential of mean force between two protein colloids in crowded solution

The total potential of mean force for two protein molecules includes depletion (dep)[35], van der Waals (VDW) and specific short-range (SSR) attraction along with electrostatic repulsion (EL).[2, 13, 18]

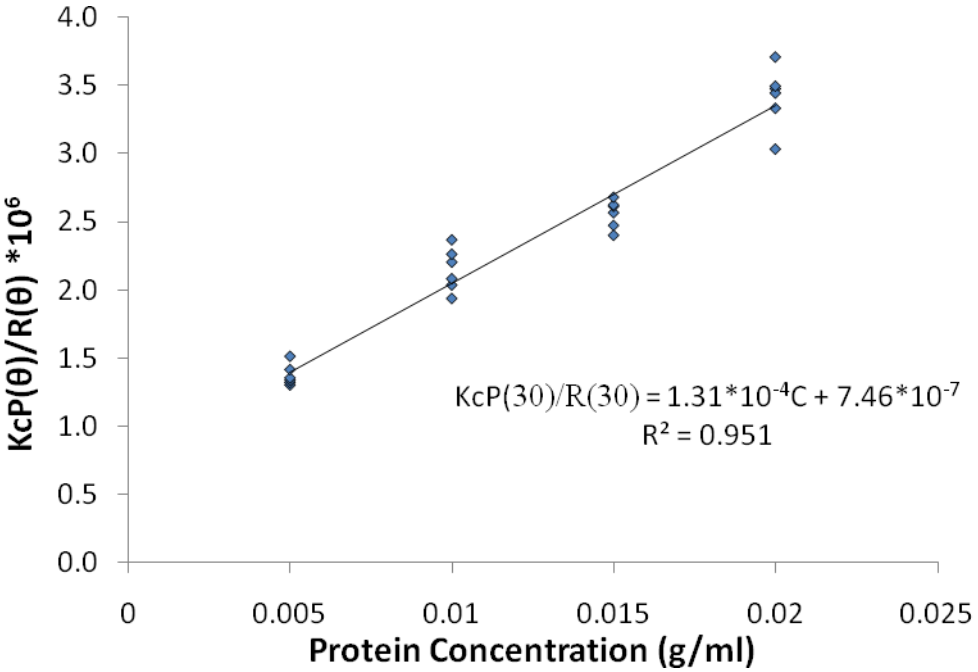

Figure 3.8 Static light scattering (SLS) data on dilutions of the protein/trehalose nanocluster dispersions with constant $0.08\varphi_P/0.16\ \varphi_N$

$$V = V_{dep} + V_{VDW} + V_{SSR} + V_{EL}$$ Eq. 3.6

The depletion attraction (also termed crowding) between two particles arises from a gain in entropy as cosolutes (crowders) are excluded from the overlap region between the particles.[55] For the Asakura-Oosawa potential:

$$\frac{V_{dep}}{k_B T} = -\frac{2}{3}\pi n_C R_{PHS}{}^3 \left(1 - \frac{r-\sigma}{2R_{PHS}}\right)^2 \left(2 + \frac{3R}{R_{PHS}} + \frac{r-\sigma}{2R_{PHS}}\right)$$ Eq. 3.7

n_C and R_{PHS} are the number density and radius of extinisic crowders, approximated as a penetrable hard sphere, r is the center to center distance between two protein molecules and R is the radius of the colloid.[56] The van der Waals attraction for two spheres of equal radii[45]

$$V_{VDW} = \frac{-A}{6}\left[\frac{2R^2}{(r-\sigma)(r+\sigma)} + \frac{2R^2}{r^2} + \ln\left[\frac{(r-\sigma)(r+\sigma)}{r^2}\right]\right]$$ Eq. 3.8

where A is the Hamaker constant. The attractive specific short-range interactions, which include hydrophobic interactions, hydrogen bonding and fluctuating charge dipoles, are often modeled with a square-well potential:

$$V_{SSR}/k_B T = \begin{cases} \infty & r < \sigma \\ -\varepsilon/k_B T & \sigma \le r \le (1+\Delta)\sigma \\ 0 & r > (1+\Delta)\sigma \end{cases}$$ Eq. 3.9

where $\varepsilon/k_B T$ is the depth (~2.7 for a monoclonal antibody[57]) with a width ($\Delta\sigma$) of ~1nm in which σ is the diameter of the protein molecule.[5, 18, 19, 28, 58] For a typical protein, it is reasonable to assume that the width, $\Delta\sigma$, is independent of colloid size as the range of hydrophobic interactions and hydrogen bonds does not scale with the size of the colloid.[18, 59, 60] For an 11 nm protein molecule and a 0.5 nm crowding agent such as trehalose, the range of all of these potentials is similar, ~1nm (Figure 3.9A, 3.9B). The electrostatic repulsion can be modeled as

$$V_{EL} = \frac{64\pi R k_B T \Gamma_0^2 \eta_\infty}{\kappa^2} \exp(-\kappa(r-\sigma)$$ Eq. 3.10

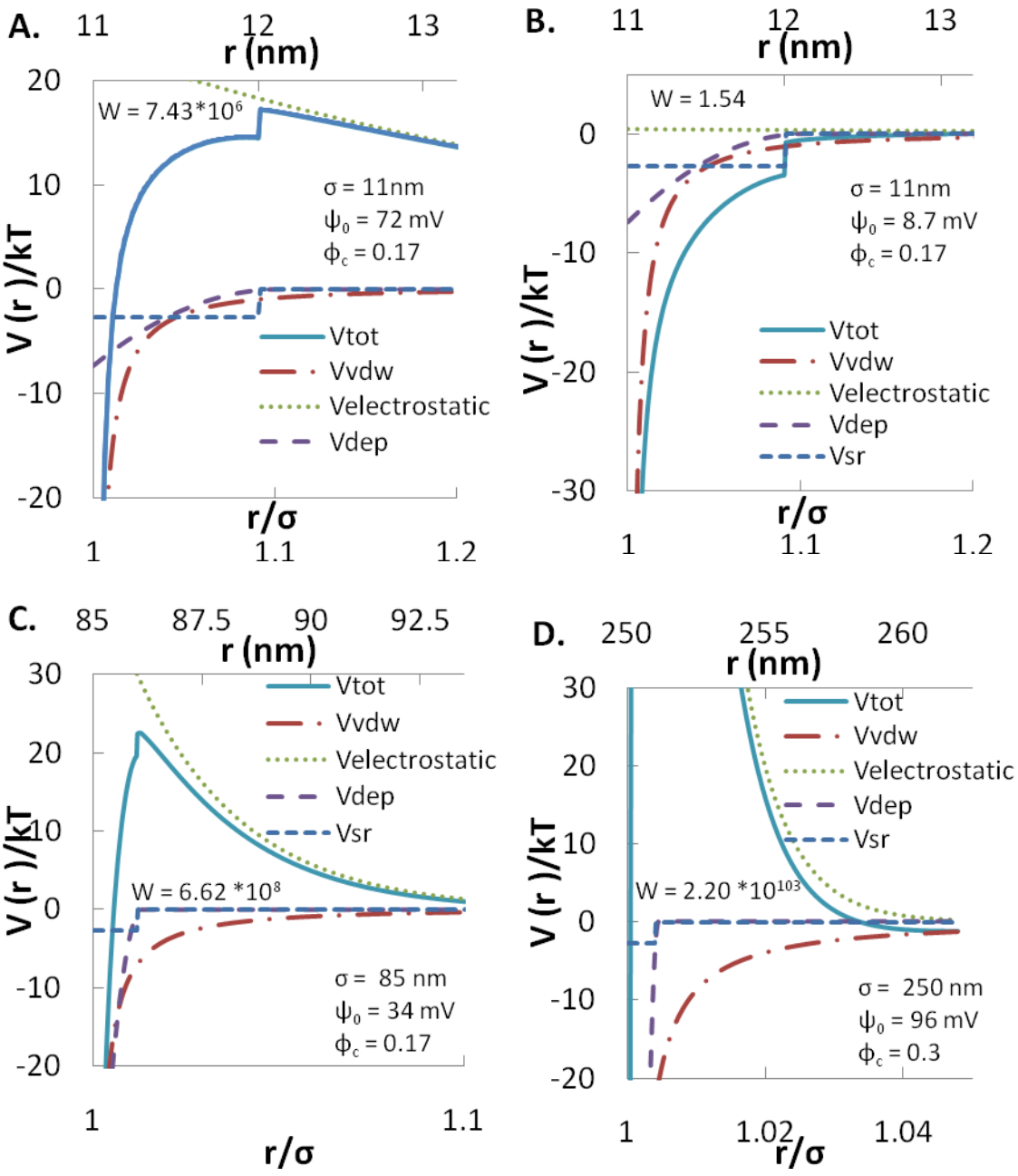

Figure 3.9. Total potential (Vtot (r)), attractive potentials from van der Waals, Vvdw(r), specific short-range attraction, Vsr(r), and depletion-attraction, Vdep(r) for a 0.5 nm radius crowder and electrostatic repulsive potential, Velectrostatic, for A) electrostatically stabilized protein monomer B) unstable protein monomer near the pI C) an electrostatically stabilized protein nanocluster near the pI D) an electrostatically stabilized protein nanocluster near the pI

where $\Gamma_0 = \frac{exp\left[\frac{z_I e \psi_0}{2 k_B T}\right]-1}{exp\left[\frac{z_I e \psi_0}{2 k_B T}\right]+1}$ Eq. 3.11

and n_∞ is the bulk ion concentration, κ^{-1} is the Debye length, z_I is the valence of the electrolyte, e is the charge on an electron, and ψ_0 is the surface potential of the protein. The charge is related to ψ_0 by

$$Q = zne = 4\pi\varepsilon\varepsilon_0 R\psi_0(1+\kappa R) \quad \text{Eq. 3.12}$$

where ε is the dielectric constant and ε_0 is the permittivity through free space.[61] The stability ratio for a colloid is defined as the ratio of fast, diffusion controlled aggregation to slow, kinetically-controlled aggregation[45, 62]

$$W = 2R\int_{2R}^{\infty} \frac{\frac{D_\infty}{D(u)}\left[exp\left(\frac{V_{Total}}{k_B T}\right)\right]}{r^2} dr \quad \text{Eq. 3.13}$$

where u is defined as r/R and the ratio $D_\infty/D(u)$ is a hydrodynamic correction factor.

The colloidal interactions between two protein monomers are shown in Figures 3.9A and B in terms of the various contributions to V_{tot} for a fixed φ_c of 0.17, corresponding to data in Table 3.1. Both r and the reduced range (r/σ) are indicated. In all cases throughout this study, the range of the specific short-ranged interactions $\Delta\sigma$ was 1 nm and the range of V_{DEP} < 1nm for the extrinsic crowders. In Figure 3.9A for a protein molecule >2 pH units away from the pI, the charge/protein molecule ~50[63], and consequently, V_{EL} is dominant over the sum of all attractive interactions. The large repulsive barrier results in a high value of the stability ratio, W, 7 x 10^6, which is about the same with or without the V_{DEP} term. This scenario with a large V_{EL} and low sugar concentrations to minimize V_{DEP} is typically utilized to form colloidally stable solutions of individual protein molecules. However, despite the highly repulsive V_{tot}, protein solubilities are often limited to ~150-200 mg/ml as described on phase diagrams of second virial coefficients, B_2/B_2^{HS}.[2, 19] In our unusual case near the pI of a protein, the

charge/protein molecule decreases to less than 10. Here, the zeta potential is small and not well defined.[60, 63] Thus, we assumed a value of 6 charges/protein molecules, which results in a surface potential of 8.7mV. With this low charge, the strength of electrostatic repulsion was negligible relative to either the V_{DEP} or V_{SR} or V_{VDW} attraction, as shown in Figure 3.9B, and thus W was ~ 1. With this strong attraction near the pI, concentrated solutions of protein monomer may not be formulated.[19, 60, 64] In our case, we intentionally use the attraction to form nanoclusters of the protein monomer, as is described in the next section.

3.4.2 Free energy model for equilibrium cluster size

Groenewold and Kegel[25] proposed a model to predict the equilibrium aggregation number for large clusters of colloidal particles, in which short range attraction is balanced by long range electrostatic repulsion. This balance must satisfy simultaneously a secondary requirement that the colloidal interactions between clusters do not cause the clusters to aggregate to form gels. The free energy of a spherical cluster consisting of *n* colloidal particles per protein molecule is[25]

$$\frac{\beta F_{Cl}}{n} = -\frac{\beta \varepsilon z}{2} + \frac{4\pi\gamma R_c^2}{n} + \frac{3Qnq}{5R_c} + 2q\left[\ln\left(\frac{q}{q_0}\right) - 1\right] \qquad \text{Eq. 3.14}$$

where F_{Cl} is the free energy of a protein cluster, $\beta = 1/k_BT$, ε is the pairwise interaction potential between two protein molecules, z is the co-ordination number for the protein in the cluster, γ is the surface tension for the cluster, ($\gamma = \epsilon/4\pi R^2$ where R is the radius of a protein monomer and $\epsilon\beta(\varepsilon)$ is the attractive pair potential between two protein molecules), R_c is the radius of the cluster, n is the number of protein molecules in a cluster, Q is the Bjerrum length, q is the charge on a protein molecule, q_0 is the value in the absence of Coulombic interactions. The first term describes the interaction potential between adjacent protein molecules in the cluster. The second or surface tension term

describes the missing attractive interactions at the cluster surface. The third term is the Coulombic repulsion for a homogeneously charged sphere in terms of Q at which the interaction between two elementary charges is k_BT. At room T, Q ~ 56/ε_r nm, where ε_r is the dielectric constant inside the cluster. The last term describes the combinatorial and translational entropy gain for the dissociating ions. The value of q_0 is given by the equation[25]

$$q_0^2 = \frac{v\sigma_c s}{b^3 e^{\beta\epsilon} + 2\varphi} \qquad \text{Eq. 3.15}$$

where v is the volume of a single protein molecule, σ_c is the number of dissociable sites per surface area of the molecule, s is the surface area of the protein molecule, b is the typical distance between an ion pair, ϵ is the energy required to dissociate an ion pair (=Q/b) and φ is the colloid volume fraction in the solution. For the purpose of the further derivation, it is assumed that z~z_0.

To take into account the porosity of the clusters, we refine the model in terms of the fractal dimension D_f according to the relationship

$$R_c = \left(\frac{n}{k}\right)^{\frac{1}{D_f}} R \qquad \text{Eq. 3.16}$$

The minimization of $f_C = F_{Cl}/n$ by setting $\frac{d\left(\frac{\beta F_{Cl}}{n}\right)}{dn} = 0$ yields the number of monomers in the cluster at equilibrium

$$n^* = k^{\frac{3}{3-2D_f}} \left\{\frac{3(D_f-2)\beta\epsilon R_p}{3(D_f-1)Qq^2}\right\}^{\frac{D_f}{2D_f-3}} \qquad \text{Eq. 3.17}$$

which in the limit of D_f =3 gives the result obtained in Groenewold and Kegel.[25] Eventually, at the point where the electrostatic repulsion becomes insufficient to balance the attractive forces, the protein forms a gel.[65] The gel point may be defined by the spinodal curve, where the second derivative of the free energy per protein molecule with respect to q is zero (that is $\frac{d^2\left(\frac{\beta F_{Cl}}{n}\right)}{dq^2} = 0$), as been shown experimentally.[24]

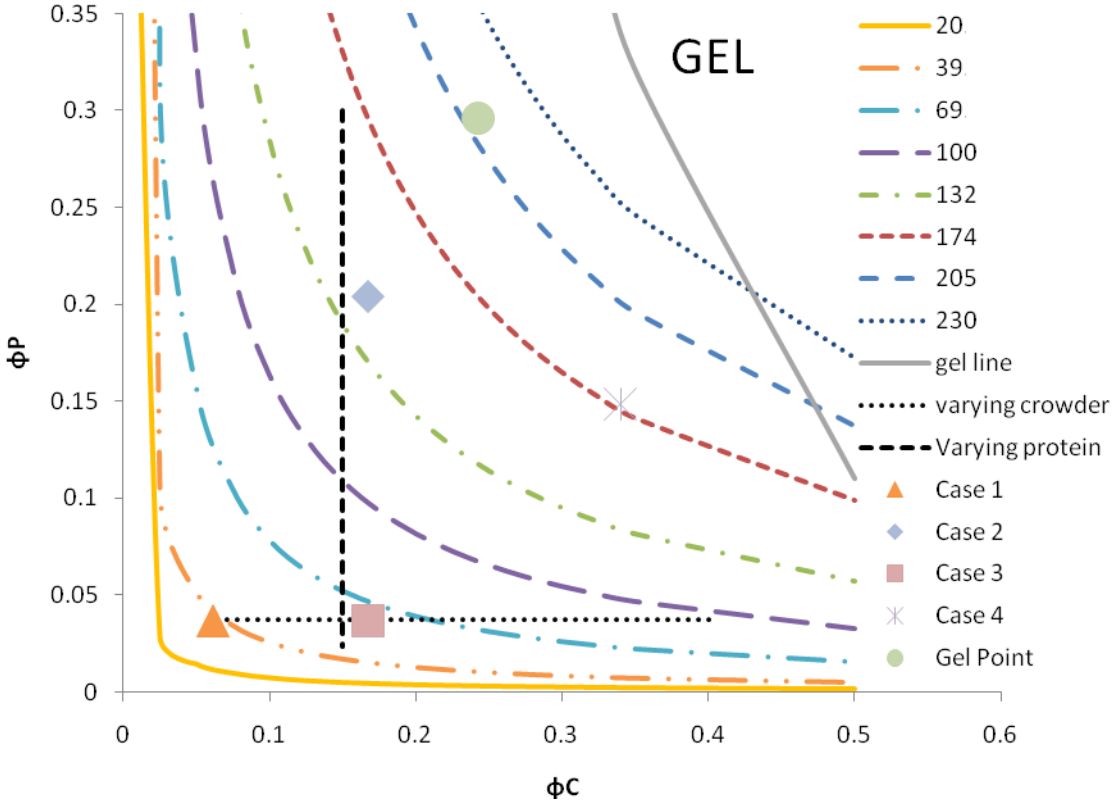

Figure 3.10. Phase diagram for a protein dispersion based on the equilibrium theory described in Eq. 3.14-3.17. The steep solid line is the gel line above which the solution forms a gel phase. Each curve indicates clusters of the same size or aggregation number, indicated by the diameter of the cluster in nm in the legend.

Figure 3.10 presents a set of contours for cluster sizes ranging from 20 to 230 nm, for a given φ_p, as a function of φ_c. The calculated q_0, which depends upon φ_p, as shown in the appendix, is on the order of one charge/protein molecule near the pI.[25, 63] Given the uncertainty in ε_r and q_o, the value of ϵ was approximated as the contact value for the depletion potential in eq. B, which depends upon φ_C, while the other attractive terms were neglected as they are not influenced by crowding. Horizontal and vertical pathways for varying either φ_p or φ_c, which were also used in the experimental studies, are shown explicitly in Figure 3.10. For a given φ_p, an increase in φ_c raises the depletion attraction between protein monomer and hence increases the cluster diameter, D, in reasonable agreement with the data shown in Figure 3.5A given the simplicity of the model. For instance, the model does not consider charge screening, differences in ε_r inside and outside the cluster, and variations in the attractive interaction with increasing the distance from the surface. Similarly, at a given φ_c when φ_p increases, D increases as shown by the vertical dashed black line, corresponding to the experimental data in Figure 3.3. Here larger clusters are the result of a decrease in q_0 with φ_p, thus a decrease in the Coulombic repulsion. A few specific cases are also denoted. For Case 1 at 100 mg/ml sugar and a φ_p of 0.037 (Table 3.3), the predicted R_c is ~35 nm while the experimental value was 10 nm (Figure 3.5A). For 275 mg/ml sugar and a φ_p of 0.037, the predicted and measured values of R were ~60 nm. For Case 3 (row 2 Table 3.1, 275 mg/ml sugar and protein) R ~140 nm compared to the experimentally measured size of 88 nm. Case 4 from Figure 3.3B has a predicted size of 174 nm compared with 250 nm observed experimentally. The calculated spinodal curve or gel line and an experimental condition which results in a gel of equilibrium nanoclusters (gel point) also correspond. The translucent dispersion formed at the gel point (300 mg/ml c_i with 300 mg/ml trehalose) could not be drawn

Table 3.3 Input and output variables for the equilibrium cluster model proposed.

	Case 1 Figure 3.10	**Case 2 Figure 3.10**	**Example from Kegel[25]**
D_f	2.5	2.5	3
Dielectric constant ($Є_r$)	15	15	10.72
Bjerrum Length (Q) (nm)	3.733	3.733	5.22
Number of dissociable sites per unit area of colloid surface (σ_C) (nm^{-2})	0.2	0.2	0.15
Distance between opposite charges in an ionic bond (b) (nm)	0.2	0.2	0.134
Radius of primary particle (R) (nm)	5.5	5.5	Disc (75 x 15)
φ_C	0.061	0.167	NA
Attractive energy (Є/kT)	2.63	7.26	7.5
Surface Tension (γ)	0.006919	0.01910	0.002122
φ_E	0.037	0.204	0.3
z_0	0.435	0.185	0.0004
Z	9	116	80
Aggregation number (n)	21	627	200,000

through a 25 gauge needle with a syringe. The location of the gel curve relative to the experimental point is quite reasonable given the simplicity of the model and complexity of the electrostatic interactions with the cluster.

Table 3.3 provides the model input variables for the some of the cases described above, along with the calculated q_0 and n. The total number of dissociable sites on the protein monomer at a given pH, $\sigma_c s$ (where σ_c is the number of dissociable sites per unit surface area s), was chosen as 50 based on literature.[63] Thus for a spherical protein with R = 5.5 nm, σ_c is ~ 0.2, as for cases 1 and 2 in Table 3.3. The ε_r was chosen as 15 given the low local dielectric constant of a pure protein. For this low ε_r, the V_{rep} inside the cluster is long ranged given the large value of κ^{-1}, a necessary requirement for formation of an equilibrium cluster with a well defined radius. In the case of ε_r for pure water, the range of repulsion would be too short for formation equilibrium clusters.

The large clusters may be contrasted with small clusters of highly charged lysozyme monomer at a pH of about 8, far from the isoelectric point, with aggregation numbers < 5 and lifetimes of ~25 ns.[28, 29, 66] The small size and short lifetime are consistent with the dominance of the large repulsion for the highly charged particles relative to the attractive forces. In Table 3.3, results are shown for clusters of Boehmite rods in ortho-dichlorobenzene (ε_r = 10.12) where several of the parameters are similar to the protein clusters.[25, 67] However, the low q_0 results in massive clusters with an aggregation number of 200,000 as observed experimentally and described theoretically.[25] The nanoclusters in the current study have a charge intermediate between these two cases, which results in long lived equilibrium clusters with n ~ 10^2 to 10^3. However, the size could be further manipulated by varying φ_c at a given φ_P.

3.4.3 Intercluster interactions

Since the number of protein monomers is well defined for an equilibrium nanocluster below the gel point, the nanocluster may be viewed as an individual colloidal particle. A sufficient repulsive V_{tot} between two nanoclusters is required to prevent aggregation of the clusters and to maintain a low viscosity. As shown in Figure 3.9C, a large repulsive barrier is present for an 85nm protein nanocluster near the pI, consistent with the stable nanocluster dispersions for the case of $\varphi_c = 0.17$ in Table 3.1. In contrast, the protein monomer dispersion was unstable in Figure 3.9B, where the following parameters were held constant: 6 charges/protein monomer, $\Delta\sigma$= 1nm, and $\varphi_c = 0.17$. For ~231 protein molecules within the cluster, the large charge of ~ 1380 produces a surface potential of ~34mV according to eq. 3.12, well above the value for the monomer of only 8.7 mV. Thus, V_{EL} is substantial for the nanocluster, despite the proximity to the pI, and simultaneously, negligible for the monomer. Furthermore, V_{EL} scales as R_p such that the range of repulsion is much longer than for V_{DEP} (<1 nm) and V_{SSR}. Since the range of these attractive forces is not influenced significantly by R_p, it is similar for the protein monomer and the nanoclusters. Thus, the reduced range, r/σ, of these attractive interactions (< ~1.01) for the nanocluster is far below that of ~1.1 for the protein monomer. In contrast, V_{EL} is relatively insensitive to r/σ. Since V_{EL} is dominant for the nanoclusters, they do not aggregate and remain colloidally stable with a W of $6*10^8$.

Of the various attractive interactions for the nanoclusters, the range of the VDW interaction is the longest as it scales with R. However, since the nanocluster are porous, as shown in the SEM and STEM images (Figure 3.4), the Hamaker constant is reduced.[68] In Figure 3.9C and 3.9D, the Hamaker constant is reduced two fold to 2.5kT. Even with including the VDW attractions, the electrostatic interactions were much stronger and longer-ranged than the total attractive interactions.[8] For a 250nm protein nanocluster

formed with a higher crowder volume fraction of 0.3 (similar to the experimental conditions in row 5 Table 3.1), electrostatic repulsion was even more dominant as shown in Figure 3.9D. With ~5870 protein monomers, the larger charge corresponded to a higher surface potential of ~96mV, and W reached 10^{103}. Experimentally, repulsive interactions between the nanoclusters were measured by SLS, with a B_2 of 6.6 x 10^{-5} mol*ml/g^2 (Figure 3.8). However, theoretical determination of B_2 from V_{tot} is poorly defined as the contributions from V_{DEP} and V_{VDW} diverge at very small r.

In summary, a direct comparison of the potentials in Figure 3.9B and 3.9C reveals a novel concept of hierarchical interactions where V_{tot} is strongly attractive for protein monomer and simultaneously, highly repulsive for the nanoclusters, consistent with the experimental data. This difference is due primarily to the increase in the range and strength of V_{EL} with an increase in Q and R_p, relative to a negligible change in the range of interaction for V_{SSR} and V_{DEP}. The strongly attractive intracluster interactions at r/σ = 1.1 are necessary to generate the nanoclusters, whereas the weak intercluster attraction at the same r/σ prevent aggregation and gelation of the clusters. This ability to control the hierarchical colloidal interactions may be expected to be universal and applicable to a wide variety of peptides and proteins.

3.4.4 Stability of the protein within the nanocluster dispersion

At high protein concentrations, ϕ_I, simulation with a coarse-grained model[11] indicates crowders tend to stabilize the native state due to excluded volume effects, regardless of any other interactions with the protein. In the presence of a crowder, the protein will attempt to minimize its excluded volume. Thus, the protein will prefer to be in its folded or native state.[34, 35] In the unfolded state, the protein has a greater degree of surface hydrophobicity and hence displays increased protein-protein interactions leading

to the unfolded state being favored.[69, 70] Therefore according to Cheung and Truskett[11], at higher protein concentrations, the protein shows an increased tendency to be in the native state due to the balance between destabilizing protein-protein interactions and the stabilizing entropic crowding.[69] In the interior of the cluster, the protein concentration is very high (~0.29) and therefore it favors the folded state. Also at such high concentrations, protein self–crowding plays a role. Measurements by tryptophan fluorescence confirm the present of the protein folded state within the nanocluster dispersions (Table 3.2).

For therapeutic proteins to retain activity without inducing adverse immunogenic reactions, it is essential to maintain the native three-dimensional conformation during recovery and formulation.[8, 71] Currently, antibodies are challenging to formulate at high concentrations as solutions, since the high-level of protein mobility facilitates protein denaturation and exposure of internal hydrophobic patches, leading to reversible intermolecular association and, eventually, irreversible aggregation.[14, 32, 72] However, excluded volume interactions from added crowding agents thermodynamically increase the stability of the native protein state.[33, 37, 38] As the φ_c increases, the protein molecule will entropically favor the reduced volume of the natively folded state over the unfolded state.[34] For sugar as a crowding agent, the increase in the stability of a protein solution has been observed in terms of the negative preferential binding parameter between the protein and sugar.[31, 32, 73] Thus the extrinsically crowded solution environment of the protein nanoclusters will prevent unfolding of the protein molecules. Upon dilution into a pure buffer, DLS confirms the presence of the monomeric protein and ELISA does not detect a difference in protein binding. These protein specific tests indirectly confirm that no changes occurred in the folding of the protein during the formation and dilution of the

nanoclusters that affected the binding of the protein or resulting in the formation of irreversible aggregates.

The low levels of protein denaturation observed are achieved by stabilization of the protein native state during sample processing. Lyophilization is widely used in biopharmaceutical processing and has been shown to stabilize the protein native state by kinetically trapping protein molecules in an amorphous solid[74-76], thus reducing protein mobility which can lead to aggregation. Addition of the crowder, trehalose, during lyophilization further stabilizes the protein native state in solution by excluded volume and upon dehydration by forming hydrogen bonds with protein.[33, 77, 78] Within the protein nanoclusters, the solid state is maintained, restricting protein mobility both in the particles and on the particle surface, relative to a solution.[72, 79-82] Particle dissolution upon dilution occurs rapidly (~1 second), given the high particle surface area and solubility of the protein monomer in physiological buffers (upon dilution of the crowding agents). The presence of the diluted crowders such as trehalose and PEG300 in the dissolution buffer, further prefers the native protein state by entropically favoring it by excluded volume.[72, 75, 78, 83]

3.4.5 Decreased viscosity in nanocluster dispersions versus protein solutions

For protein molecules in solution at high concentrations, for example ϕ_I = 0.1 to 0.3, the strong short-range specific attractive interactions[24, 29], often produce viscosities 5 to 100 times the hard sphere value to the Krieger-Dougherty eq. 2.[21, 84] For monoclonal antibody solutions with concentrations of 150 mg/mL, viscosities greater than 100cP have been attributed to reversible self association of protein molecules, on the basis of measurements by analytical ultracentrifugation.[21, 59] In contrast, the low viscosities in the present study for the nanocluster dispersions may be shown to be consistent with the

weak interactions between the nanoclusters, as suggested by the low intrinsic viscosities in Table 3.1.

For hard spheres, gelation, the result of increased clustering, does not occur until at least a φ of 49%.[85] Since nanocluster dispersions act more like hard spheres due to the decreased attractive interactions between nanoclusters, the viscosity should remain lower for nanoparticle dispersions at the same φ if the solvent viscosity remains the same. From the Krieger Dougherty equation (Eq. 3.2), the intrinsic viscosity ([η]) is used to compare the increase in viscosity due to the addition of particles.[45] In the hard sphere limit, [η] approaches 2.5, where the increase in viscosity due to the particles is solely due to the excluded volume, as seen previously for non-aqueous protein suspensions.[22] All values are significantly lower than the [η] reported for protein solutions, which can increase to greater than 50 cm^3/g.[86] Hydrogen bonding between the protein molecule and water molecules ("bound water"), up to now lumped together with hydrophobic effects and fluctuating charge-dipoles as specific attractive interactions, in addition increases the effective φ of the protein colloid, whether in solution or dispersion.[8, 45] If the hydration layer is approximated as a 0.1nm increase to the radius of the protein colloid[18], the ratio of φ_{eff} to φ will be 1.12 for the protein molecular solution but remain close to 1 (1.002) for the nanocluster dispersion. Since in the Krieger-Dougherty equation, an increase in φ_{eff} over the expected φ will be incorporated as an increase in $[\eta]$[45], the decrease in hydration for the nanocluster dispersions versus a protein solution by itself results in a lower [η] for the nanocluster dispersions.

In addition to specific attractive interactions, electroviscous as well as shape effects can also increase the intrinsic viscosity of a protein molecule when compared to the protein nanocluster dispersion. In the aqueous protein nanocluster dispersions, the surface charge is decreased by lowering the dielectric constant of the solution and

operating at the isoelectric point of the protein which results in a decrease the thickness of the double layer.[8, 45, 61, 87] The decreased thickness of the double layer will reduce any electroviscous effects, known to contribute to the increased viscosity for protein solutions at high zeta potentials.[21, 45, 60, 87-90] The molecular shape factor proportionally increases the intrinsic viscosity[45] and is a function of the aspect ratio of the solution.[8, 45, 86] At its minimum, spherical particles do not increase the intrinsic viscosity over the expected value.[45, 86] In the case of protein solutions, the shape of the molecule in solution is dependent on the protein itself.[8, 86] However, for the protein dispersion formed, the shape of the particle is dependent on the particle formation technique, and can therefore be tailored to be very spherical. Thus, for nanocluster dispersions, both the electroviscous and shape effects can be tailored to be insignificant increases to the viscosity.

3.5 CONCLUSIONS

Proteins may be crowded by extrinsic crowders into 80-250nm clusters to form highly concentrated dispersions, while the protein self-crowded state within the nanocluster preserves the native folded protein. These novel, equilibrium clusters are formed by balancing attraction from specific short-range attractive protein interactions and extrinsic crowders against very weak electrostatic charging near the isoelectric point of the protein. These large equilibrium clusters with aggregation numbers on the order of hundreds are formed at high protein concentrations in a molecularly crowded solution with a φ of total crowders > 0.13. In contrast, previously, small (n~10), dynamic clusters of lyozyme are formed at unsaturated conditions at a pH far from the pI of the protein which results in a large electrostatic repulsion preventing the formation of large, stable clusters.[29, 91] The size of various equilibrium clusters, determined by DLS and confirmed by SEM, fall on a universal curve with increasing total φ crowder regardless of the

crowder type or combination of crowders used (trehalose, PEG300, and/or NMP). The highly self-crowded environment within the nanocluster (φ protein within the cluster ~0.29) prevents unfolding of the protein, as predicted previously.[11, 39] The stability of the native state is confirmed experimentally by a tryptophan fluorescence assay within the crowded environment and upon dilution into buffer by ELISA and DLS. In contrast, in a protein solution at the same concentration without forming nanoclusters, low solubility prevents a sufficiently high φ to allow for protein self-crowding.

The hierarchy of strong intracluster interactions used to form the nanoclusters and the weak intercluster interactions result in high colloidal stability and low viscosities despite high protein concentrations reaching 275 mg/ml. Protein molecules are clustered together due to high specific attractive protein interactions and the additional attraction due to the added molecular crowders. Since the ~ 1 nm range of these attractive interactions is essentially independent of particle size, the specific short-ranged interactions and the depletion-attraction from the molecular crowders have a negligible attractive effect on the nanoclusters. A weakly repulsive B_2 confirms the weak interactions between nanoclusters experimentally. Decreased intercluster interactions result in particles that are more like hard spheres and thus should demonstrate lower viscosities than protein solutions at the same concentration.[22] The viscosity, estimated through a 25 gauge needle, confirms relatively low intrinsic viscosities for the nanoclusters. The low viscosity (<50 cp) and high molecular stability for the highly concentrated nanocluster dispersions are of great interest in subcutaneous injection of protein therapeutics with a 25-28 gauge needle, where high dosages of up to 500 mg/ml are desired in an injection volume of only 1-1.5 ml.[6] This hierarchical protein nanocluster concept is based on general scaling of short-ranged and crowding intermolecular and

intercluster interactions, and thus, may be expected to be applicable to a wide variety of protein and peptides.

3.6 REFERENCES

1. Lu, P. J.; Conrad, J. C.; Wyss, H. M.; Schofield, A. B.; Weitz, D. A., Fluids of Clusters in Attractive Colloids. *Phys Rev Let* **2006,** 96, 028306.

2. Prausnitz, J. M., Molecular thermodynamics for some applications in biotechnology. *J Chem Thermodynamics* **2003,** 35, 21-39.

3. Cheung, M. S.; Klimov, D.; Thirumalai, D., Molecular crowding enhances native state stability and refolding rates of globular proteins. *PNAS* **2005,** 102, (13), 4753-4758.

4. George, A.; Wilson, W. W., Predicting Protein Crystallization from a Dilute Solution Property. *Acta Cryst.* **1994,** D50, 361-365.

5. ten Wolde, P. R.; Frenkel, D., Enhancement of Protein Crystal Nucleation by Critical Density Fluctuations. *Science* **1997,** 277, 1975-1978.

6. Shire, S. J.; Shahrokh, Z.; Liu, J., Challenges in the Development of High Protein Concentration Formulations. *J. Pharm. Sci.* **2004,** 93, (6), 1390-1402.

7. Yang, M. X.; Shenoy, B.; Disttler, M.; Patel, R.; McGrath, M.; Pechenov, S.; Margolin, A. L., Crystalline monoclonal antibodies for subcutaneous delivery. *PNAS* **2003,** 100, (12), 6934-6939.

8. Saluja, A.; Kalonia, D. S., Nature and consequences of protein-protein interactions in high protein concentration solutions. *Int. J. Pharm.* **2008,** 358, 1-15.

9. Nguyen, H. D.; Hall, C. K., Spontaneous Fibril Formation by Polyalanines; Discontinuous Molecular Dynamics Simulations. *JACS* **2006,** 128, 1890-1901.

10. Berland, C. R.; Thurston, G. M.; Kondo, M.; Broide, M. L.; Pande, J.; Ogun, O.; Benedek, G. B., Solid-liquid phase boundaries of lens protein solutions. *Proc. Natl. Acad. Sci.* **1992,** 89, 1214-1218.

11. Cheung, J. K.; Truskett, T. M., Coarse-Grained Strategy for Modeling Protein Stability in Concentrated Solutions. *Biophys J* **2005,** 89, 2372-2384.

12. Sear, R. P., Interactions in protein solutions. *Current Opinion in Colloid & Interface Science* **2006,** 11, 35-39.

13. Rosenbaum, D. F.; Zukoski, C. F., Protein interactions and crystallization. *J Cryst Growth* **1996,** 169, 752-758.

14. Young, T. M.; Roberts, C. J., Structure and thermodynamics of colloidal protein cluster formation: Comparison of square-well and simple dipolar models. *J Chem Phys* **2009,** 131, 125104.

15. Areas, E. P. G.; Areas, J. A. G.; Hamburger, J.; Peticolas, W. L.; Santos, P. S., On the High Viscosity of Aqueous Solution of Lysozyme Induced by Some Organic Solvents. *J Colloid Interface Sci* **1996,** 180, 578-589.

16. Gast, A. P.; Hall, C. K.; Russel, W. B., Polymer-Induced Phase Separations in Nonaqueous Colloidal Suspensions. *J Colloid Interface Sci* **1983,** 96, (1), 251-267.

17. Mahadevan, H.; Hall, C. K., Experimental analysis of protein precipitation by polyethylene glycol and comparison with theory. *Fluid Phase Equilibria* **1992,** 78, 297-321.

18. Curtis, R. A.; Prausnitz, J. M.; Blanch, H. W., Protein-Protein and Protein-Salt Interactions in Aqueous Protein Solutions Containing Concentrated Electrolytes. *Biotechnology and Bioengineering* **1998,** 57, (1), 11-21.

19. Kulkarni, A. M.; Dixit, N. M.; Zukoski, C. F., Ergodic and non-ergodic phase transitions in globular protein suspensions. *Farady Discuss.* **2003,** 123, 37-50.

20. Trevino, S. R.; Scholtz, J. M.; Pace, C. N., Measuring and increasing protein solubility. *J Pharm Sci* **2008,** 97, (10), 4155-4166.

21. Liu, J.; Nguyen, M. D. H.; Andya, J. D.; Shire, S. J., Reversible Self-Association Increases the Viscosity of a Concentrated Monoclonal Antibody in Aqueous Solution. *J. Pharm. Sci.* **2005,** 94, (9), 1928-1940.

22. Miller, M. A.; Engstrom, J. D.; Ludher, B. S.; Johnston, K. P., Low Viscosity Highly Concentrated Injectable Nonaqueous Suspensions of Lysozyme Microparticles. *Langmuir* **2010,** 26, (2), 1067-1074.

23. Sedgwick, H.; Egelhaaf, S. U.; Poon, W. C. K., Clusters and gels in systems of sticky particles. *J. Phys.: Condens. Matter* **2004,** 16, S4913-S4922.

24. Lu, P. J.; Zaccarelli, E.; Ciulla, F.; Schofield, A. B.; Sciortino, F.; Weitz, D. A., Gelation of particles with short-range attraction. *Nature* **2008,** 453, 499-503.

25. Groenewold, J.; Kegel, W. K., Anomalously Large Equilibrium Clusters of Colloids. *J Phys Chem B* **2001,** 105, 11702-11709.

26. Tam, J. M.; Murthy, A. K.; Ingram, D. R.; Nguyen, R.; Sokolov, K. V.; Johnston, K. P., Kinetic Assembly of Near-IR-Active Gold Nanoclusters Using Weakly Adsorbing Polymers to Control the Size. *Langmuir* **2010,** 26, (11), 8988-8999.

27. Sidebottom, D. L.; Tran, T. D., Universal patterns of equilibrium cluster growth in aqueous sugars observed by dynamic light scattering. *Physical Review E* **2010,** 82, 051904.

28. Stradner, A.; Sedgwick, H.; Cardinaux, F.; Poon, W. C. K.; Egelhaaf, S. U.; Schurtenberger, P., Equilibrium cluster formation in concentrated protein solutions and colloids. *Nature* **2004,** 432, 492-495.

29. Porcar, L.; Falus, P.; Chen, W.-R.; Faraone, A.; Fratini, E.; Hong, K.; Baglioni, P.; Liu, Y., Formation of the Dynamic Clusters in Concentrated Lyoszyme Protein Solutions. *J. Phys. Chem. Lett.* **2010,** 1, 126-129.

30. Pan, W.; Vekilov, P. G.; Lubchenko, V., Origin of Anomalous Mesoscopic Phases in Protein Solutions. *J Phys Chem B* **2010,** 114, (22), 7620-7630.

31. Lee, J. C.; Timasheff, S. N., The stabilization of proteins by sucrose. *Journal of Biological Chemistry* **1981,** 256, (14), 7193-7201.

32. Kendrick, B. S.; Carpenter, J. F.; Cleland, J. L.; Randolph, T. W., A transient expansion of the native state precedes aggregation of recombinant human interferon-γ. *PNAS* **1998,** 95, 14142-14146.

33. O'Connor, T. F.; Debenedetti, P. G.; Carbeck, J. D., Stability of proteins in the presence of carbohydrates; experiments and modeling using scaled particle theory. *Biophysical Chemistry* **2007,** 127, 51-63.

34. Zhou, H.-X.; Rivas, G.; Minton, A. P., Macromolecular Crowding and Confinement: biochemical, biophysical and potential physiological consequences. *Annu. Rev. Biophys.* **2008,** 37, 375-397.

35. Davis-Searles, P. R.; Saunders, A. J.; Erie, D. A.; Winzor, D. J.; Pielak, G. J., Interpreting the Effects of Small Uncharged Solutes on Protein-Folding Equilibria. *Annu. Rev. Biophys. Biomol. Struct.* **2001,** 30, 271-306.

36. Mittal, J.; Best, R. B., Dependence of Protein Folding Stability and Dynamics on the Density and Composition of Macromolecular Crowders. *Biophys J* **2010,** 98, 315-320.

37. Ping, G.; Yang, G.; Yuan, J.-M., Depletion force from macromolecular crowding enhances mechanical stability of protein molecules. *Polymer* **2006,** 47, 2564-2570.

38. Pincus, D. L.; Thirumalai, D., Crowding Effects on the Mechanical Stability and Unfolding Pathways of Ubiquitin. *J Phys Chem B* **2009,** 113, 359-368.

39. Shen, V. K.; Cheung, J. K.; Errington, J. R.; Truskett, T. M., Insights into Crowding Effects on Protein Stability from Coarse-Grained Model. *Journal of Biomechanical Engineering* **2009,** 131, 071002 (7pg).

40. Newcombe, A. R.; Cresswell, C.; Davies, S.; Watson, K.; Harris, G.; O'Donovan, K.; Francis, R., Optimised affinity purification of polyclonal antibodies from hyper immunised ovine serum using a syntehtic Protein A adsorbent, MAbsorbent® A2P. *Journal of Chromatography B* **2005,** 814, 209-215.

41. Ryoo, W.; Webber, S. E.; Johnston, K. P., Water-in-Carbon Dioxide Microemulsions with Methylated Branched Hydrocarbon Surfactants. *Ind. Eng. Chem. Res.* **2003,** 42, 6348-6358.

42. Horn, F. M.; Richtering, W.; Bergenholtz, J.; Willenbacher, N.; Wagner, N. J., Hydrodynamic and Colloidal Interactions in Concentrated Charge-Stabilized Polymer Dispersions. *J Colloid Interface Sci* **2000,** 225, 166-178.

43. Giteau, A.; Venier-Julienne, M.-C.; Marchal, S.; Courthaudon, J.-L.; Sergent, M.; Montero-Menei, C.; Verdier, J.-M.; Benoit, J.-P., Reversible protein precipitation to ensure stability during encapsulation within PLGA microspheres. *Eur. J. Pharm. Biopharm.* **2008,** 70, 127-136.

44. Harn, N.; Spitznagel, T.; Perkins, M.; Allan, C.; Shire, S.; Middaugh, C. R., Biophysical Signatures of Monoclonal Antibodies. In *Current Trends in Monoclonal Antibody Development and Manufacturing*, Shire, S. J., Ed. DOI 10.1007/978-0-387-76643-0_14: 2010; pp 229-246.

45. Hiemenz, P. C.; Rajagopalan, R., *Principles of Colloid and Surface Chemistry*. 3rd ed.; Marcel Dekker, Inc.: New York, 1997; p 650.

46. Larson, R. G., *The Structure and Rheology of Complex Fluids*. Oxford University Press Inc.: New York, 1999.

47. Miller, D. P.; de Pablo, J. J.; Corti, H., Thermophysical Properties of Trehalose and its Concentrated Aqueous Solutions. *Pharmaceutical Research* **1997,** 14, (5), 578-590.

48. Dani, B.; Platz, R.; Tzannis, S. T., High Concentration Formulation Feasibility of Human Immunoglubulin G for Subcutaneous Administration. *J. Pharm. Sci.* **2007,** 96, (6), 1504-1517.

49. Uchida, T.; Nagayama, M.; Gohara, K., Trehalose solution viscosity at low temperatures measured by dynamic light scattering method: Trehalose depresses molecular transportation for ice crystal growth. *J Crystal Growth* **2009,** 311, 4747-4752.

50. Brickelmaier, M.; Hochman, P. S.; Baciu, R.; Chao, B.; Cuervo, J. H.; Whitty, A., ELISA methods for the analysis of antibody responses induced in multiple sclerosis patients treated with recombinant interferon-beta. *J Immunol Methods* **1999,** 227, (1-2), 121-135.

51. Itakura, M.; Shimada, K.; Matsuyama, S.; Saito, T.; Kinugasa, S., A Convenient Method to Determine the Rayleigh RAtio with Uniform Polystyrene Oligomers. *Journal of Applied Polymer Science* **2006,** 99, 1953-1959.

52. Saluja, A.; Badkar, A. V.; Zeng, D. L.; Nema, S.; Kalonia, D. S., Ultrasonic Storage Modulus as a Novel Parameter for Analyzing Protein-Protein Interactions in High Protein Concentration Solutions: Correlation with Static and Dynamic Light Scattering Measurements. *Biophys J* **2007,** 92, 234-244.

53. Salinas, B. A.; Sathish, H. A.; Bishop, S. M.; Harn, N.; Carpenter, J. F.; Randolph, T. W., Understanding and Modulating Opalescence and Viscosity in a Monoclonal Antibody Formulation. *J Pharm Sci* **2010,** 99, (1), 82-92.

54. Sandler, S. R.; Karo, W.; Bonesteel, J.-A.; Pearce, E. M., *Polymer Syntehsis and Characterization: A Laboratory Manual*. 1 ed.; Academic Press: San Diego, 1998; p 212.

55. Vrij, A., Polymers at Interfaces and the Interactions in Colloidal Dispersions. *Pure & Appl. Chem.* **1976,** 48, 471-483.

56. Tuinier, R.; Rieger, J.; De Kruif, C. G., Depletion-induced phase separation in colloid-polymer mixtures. *Advances in Colloid and Interface Science* **2003,** 103, 1-31.

57. Bajaj, H.; Sharma, V. K.; Kalonia, D. S., A High-Throughput Method for Detection of Protein Self-Association and Second Virial Coefficient Using Size-Exclusion Chromatography Through Simultaneous Measurement of Concentration and Scattered Light Intensity. *Pharm. Res.* **2007,** 24, (11), 2071-2083.

58. Rosenbaum, D. F.; Kulkarni, A. M.; Ramakrishnan, S.; Zukoski, C. F., Protein interactions and phase behavior: Sensitivity to the form of the pair potential. *J Chem Phys* **1999,** 111, (21), 9882-9890.

59. Kanai, S.; Liu, J.; Patapoff, T. W.; Shire, S. J., Reversible Self-Association of a Concentrated Monoclonal Antibody Solution Mediated by Fab-Fab Interaction That Impacts Solution Viscosity. *J Pharm Sci* **2008,** 97, (10), 4219-4227.

60. Yadav, S.; Liu, J.; Shire, S. J.; Kalonia, D. S., Specific Interactions in High Concentration Antibody Solutions Resulting in High Viscosity. *J Pharm Sci* **2010,** 99, (3), 1152-1168.

61. Hunter, R. J., *Zeta Potential in Colloid Science*. Academic Press Inc.: New York, 1981; p 386.

62. Russel, W. B.; Saville, D. A.; Schowalter, W. R., *Colloidal Dispersions*. Cambridge University Press: New York, 1995; p 525.

63. Chari, R.; Jerath, K.; Badkar, A. V.; Kalonia, D. S., Long- and Short-Range Electrostatic Interactions Affect the Rheology of Highly Concentrated Antibody Solutions. *Pharm. Res.* **2009,** 26, (12), 2607-2618.

64. Chi, E. Y.; Krishnan, S.; Kendrick, B. S.; Chang, B. S.; Carpenter, J. F.; Randolph, T. W., Roles of conformational stability and colloidal stability in the aggregation of recombinant human granulocyte colony-stimulating factor. *Protein Science* **2003,** 12, 903-913.

65. Lu, P. J.; Zaccarelli, E.; Ciulla, F.; Schofield, A. B.; Sciortino, F.; Weitz, D. A., Gelation of particles with short-range attraction. *Nature* **2008,** 453, (7194), 499-503.

66. Vekilov, P. G.; Feeling-Taylor, A. R.; Petsev, D. N.; Galkin, O.; Nagel, R. L.; Hirsch, R. E., Intermolecular Interactions, Nucleation and Thermodynamics of Crystallization of Hemoglobin C. *Biophys J* **2002,** 83, 1147-1156.

67. Buitenhuis, J.; Dhont, J. K. G.; Lekkerkerker, H. N. W., Static and Dynamic Light-scattering by Concentrated Colloidal Suspensions of Polydisperse Sterically Stabilized Boehmite Rods Expeirments. *Macromolecules* **1994,** 27, (25), 7267-7277.

68. Laven, J.; Vissers, J. P. C., The Hamaker and the Lifshitz approaches for the Van der Waals interaction between particles of composite materials dispersed in a medium. *Colloids and Surfaces A: Physicochemical and Engineering Aspects* **1999,** 152, 345-355.

69. Cheung, J. K.; Truskett, T. M., Coarse-grained strategy for modeling protein stability in concentrated solutions. *Biophysical Journal* **2005,** 89, (4), 2372-2384.

70. Cheung, J. K.; Raverkar, P. S.; Truskett, T. M., Analytical model for studying how environmental factors influence protein conformational stability in solution. *Journal of Chemical Physics* **2006,** 125, (22).

71. Maas, C.; Hermeling, S.; Bouma, B.; Jiskoot, W.; Gebbink, M. F., A role for protein misfolding in immunogenicity of biopharmaceuticals. *J Biol Chem* **2007,** 282, (4), 2229-2236.

72. Frokjaer, S.; Otzen, D. E., Protein Drug Stability: A Formulation Challenge. *Nat. Rev. Drug Discovery* **2005,** 4, 298-306.

73. Krishnan, S.; Chi, E. Y.; Webb, J. N.; Chang, B. S.; Shan, D.; Goldenberg, M.; Manning, M. C.; Randolph, T. W.; Carpenter, J. F., Aggregation of Granulocyte Colony Stimulating Factor under Physiological Conditions: Characterization and Thermodynamic Inhibition. *Biochemistry* **2002,** 41, 6422-6431.

74. Souillac, P. O.; Middaugh, C. R.; Rytting, J. H., Investigation of protein/carbohydrate interactions in the dried state. 2. Diffuse reflectance FTIR studies. *Int J Pharm* **2002,** 235, 207-218.

75. Carpenter, J. F.; Chang, B. S.; Randolph, T. W., Physical Damage to Proteins During Freezing, Drying and Rehydration. In *Lyophilization of Biopharmaceuticals*, Costantino, H. R.; Pikal, M. J., Eds. AAPS Press: 2005; pp 423-442.

76. Wang, B.; Tchessalov, S.; Warne, N. W.; Pikal, M. J., Impact of Sucrose level on Storage Stability of Proteins in Freeze-Dried Solids: I. Correlation of Protein-Sugar Interaction with Native Structure Preservation. *J Pharm Sci* **2009,** 98, (9), 3131-3144.

77. Carpenter, J. F.; Crowe, J. H., The Mechanism of Cryoprotection of Proteins by Solutes. *Cryobiology* **1988,** 25, (3), 244-255.

78. Timasheff, S. N., Stabilization of Protein Structure by Solvent Additives. In *Stability of Protein Pharmaceuticals: Part B.*, Ahern, T. J.; Manning, M. C., Eds. Springer: 1992; Vol. 3, pp 265-285.

79. Costantino, H. R.; Langer, R.; Klibanov, A. M., Moisture-Induced Aggregation of Lyophilized Insulin. *Pharm Res* **1994,** 11, (1), 21-29.

80. Desai, U. R.; Klibanov, A. M., Assessing the Structural Integrity of a Lyophilized Protein in Organic Solvents. *J Am. Chem. Soc.* **1995,** 117, 3940-3945.

81. Klibanov, A. M., Improving enzymes by using them in organic solvents. *Nature* **2001,** 409, 241-246.

82. Roberts, C. J.; Debenedetti, P. G., Engineering Pharmaceutical Stability with Amorphous Solids. *AIChE Journal* **2002,** 48, (6), 1140-1144.

83. Stagg, L.; Zhang, S.-Q.; Cheung, M. S.; Wittung-Stafshede, P., Molecular crowding enhances native structure and stability of α/β protein flavodoxin. *PNAS* **2007,** 104, (48), 18976-18981.

84. Lafleche, F.; Durand, D.; Nicolai, T., Association of Adhesive Spheres Formed by Hydrophobically End-Capped PEF. 1. Influence of the Presence of Single End-Capped PEO. *Macromolecules* **2003,** 36, 1331-1340.

85. Dawson, K. A., The glass paradigm for colloidal glasses, gels, and other arrested states driven by attractive interactions. *Current Opinion in Colloid & Interface Science* **2002,** 7, 218-227.

86. Cantor, C. R.; Schimmel, P. R., *BioPhysical Chemistry. Part II: Techniques for the Study of Biological Structure and Function*. W. H. Freeman and Company: San Francisco, 1980; p 846.

87. Saluja, A.; Badkar, A. V.; Zeng, D. L.; Nema, S.; Kalonia, D. S., Application of High-Frequency Rheology Measurements for Analyzing Protein-Protein Interactions in High Protein Concentration Solutions Using a Model Monoclonal Antibody (IgG2). *J Pharm Sci* **2006,** 95, (9), 1967-1983.

88. Adamczyk, Z.; Jachimska, B.; Kolasinska, M., Structure of colloid silica determined by viscosity measurements. *J Colloid Interface Sci* **2004,** 273, 668-674.

89. Russel, W. B., The rheology of supsensions of charged rigid spheres. *J Fluid Mech* **1978,** 85, (2), 209-232.

90. Russel, W. B., Structure-Property Relations for the Rheology of Dispersions of Charged Colloids. *Ind. Eng. Chem. Res.* **2009,** 48, 2380-2386.

91. Gliko, O.; Pan, W.; Katsonis, P.; Neumaier, N.; Galkin, O.; Weikauf, S.; Vekilov, P. G., Metastable Liquid Clusters in Super- and Undersaturated Protein Solutions. *J Phys Chem B* **2007,** 111, 3106-3114.

Chapter 4: Dispersions of Antibody Nanoparticles with Low Viscosity and High Concentration retain Activity and *in vivo* Bioavailability

Monoclonal antibodies continue to command a large market share with numerous entities in clinical trials for a variety of therapeutic indications. In many cases, the doses required for therapeutic efficacy are large, limiting options for antibody delivery and administration. We have developed a novel formulation strategy based on dispersions of submicron antibody particles that allows for subcutaneous injection of highly concentrated antibody (190 mg/ml). A solution of monoclonal antibody 1B7 was rapidly frozen and lyophilized using a novel spiral-wound *in situ* freezing technology (SWIFT) technique to generate amorphous particles. Upon gentle stirring a translucent dispersion of protein formed rapidly in buffer containing the pharmaceutically acceptable crowding agents, trehalose, polyethylene glycol and n-methyl-2-pyrrolidone. Formulation near the antibody isoelectric point minimizes the charge per molecule, such that the attractive forces were sufficient to form large particles, specifically clusters composed of protein molecules (~200nm diameter), with a low apparent viscosity (~24 cp). Within each particle, there are no detectable changes in antibody tertiary structure, as the protein native state is stabilized by self-crowding of the protein, limiting unfolding and aggregation. Upon *in vitro* dilution of the dispersion, the particles revert to monomeric protein with full activity, as monitored by dynamic light scattering and ELISA. When administered to mice as an intravenous solution, subcutaneous solution or subcutaneous dispersion at similar doses (4.6-7.3 mg/kg), the distribution and elimination kinetics were similar. The dispersion formulation makes ultra-high dosages possible (51.6 mg/kg); this also exhibited a similar pharmacokinetic profile. Moreover, analysis of the terminal serum samples by *in vitro* binding and cellular neutralization assays indicates antibody

delivered as a subcutaneous dispersion retains full activity over the 14-day study period. Overall, this method of generating high concentration, low viscosity dispersions of submicron antibody particles is readily generalizable and could lead to improved administration and patient compliance, providing new opportunities for the biotechnology industry.

4.1 INTRODUCTION

Monoclonal antibodies have generated considerable interest as therapeutics because they specifically target distinct antigens with favorable pharmacokinetic, production, and safety profiles.[1, 2] Currently, 28 monoclonal antibodies have received FDA-approval for treatment of a wide variety of diseases, commanding an annual market size of over $20 billion dollars.[3, 4] Despite advances in protein drug development which allow tailoring of key biophysical properties, such as solubility[5], stability[6], and binding affinity[7] via recombinant DNA techniques, few options have been developed to deliver these macromolecules at desired dosages (>2mg antibody/ kg body weight). Typically, large volumes of dilute protein solutions are delivered intravenously to avoid the chemical and physical destabilization and resulting loss in protein activity associated with high concentration formulations.[1, 8] For instance, Rituxan doses of 100-500 mg are currently administered by intravenous infusion of a 10 mg/ml solution.[9] Self-administered subcutaneous injections offer several major advantages over intravenous infusion, including increased accessibility and patient compliance, along with reduced pain and cost. However, the required therapeutic dosages would indicate protein concentrations in excess of 100 mg/ml, given the maximum subcutaneous injection volume of 1.5 ml.[10, 11]

Formulation of therapeutic proteins at these high concentrations is intrinsically difficult, demanding solutions customized for each new product. Frequently, formulation at high concentrations is not possible due to low protein solubility[5, 12], protein instability[13-15] and high solution viscosity[1, 16, 17] resulting from short-range attractive protein-protein interactions. These interactions, which include hydrophobic interactions, hydrogen bonds and fluctuating charge dipoles[17], act over distances up to ~1 nm[18]. At high protein concentrations (over 150 mg/ml), the average separation distance between individual antibody molecules is reduced to less than 10 nm.[19] Thus, the probability that two protein molecules will be less than 1nm apart is high and the effect of the short-range attractive interactions between protein molecules becomes significant.[19] This leads to the concentration-dependent formation of reversible and irreversible aggregates with potential adverse effects on protein activity, pharmacokinetics and immunogenicity. Most troubling are irreversible aggregates, high molecular weight aggregates comprised of monomers with altered native structure and reduced activity, which can result in a turbid solution or precipitation. The formation of these aggregates is highly protein specific[20] and can be formed through phsycial mechanisms, via partially unfolded monomers with exposed hydrophobic residues[21] or through chemical mechanisms, via formation of intermolecular bonds mediated by reactive thiols on cysteine or methionine residues[22].

Protein structure and activity in low viscosity formulations can be preserved at high protein concentrations by minimizing the effects of these short-range interactions. For example, concentrated suspensions of protein microparticles in water-insoluble organic solvents[23] and aqueous suspensions of protein crystals[1] with low viscosity have been reported. These formulations succeed by using micron-sized (5-20 μm) particles of proteins as opposed to protein monomers, thus increasing the average distance between protein particles for a given protein concentration. However, formulations of proteins in

organic solvents are not patient-friendly as they require large-bore needles and can result in additional side effects such as redness and swelling at the injection site.[24] In addition, while highly concentrated aqueous suspensions of crystalline insulin have a history of clinical use[24], it is challenging to routinely crystallize large protein molecules such as immunoglobulins due to their high molecular weight, surface oligosaccharides, and high degree of segmental flexibility.[1, 24, 25] Similarly, controlled release formulations in which proteins are encapsulated in polymeric matrices with non-aqueous[26] or aqueous media[27, 28] have also been explored. In these cases, the low loadings of protein within the particle (~15-20 mass %) result in a low deliverable dose even at high particle volume fractions.[29] Moreover, most polymeric delivery systems suffer from challenges with sterility, protein stability, incomplete protein release, and increased immunogenicity.[30-32]

Previously, we have reported a novel approach to preserve protein activity at high concentrations while achieving a low viscosity, in the form of concentrated dispersions of amorphous protein nanoclusters.[19, 33] The addition of trehalose as a “crowder” molecule occupies a large volume and increases the short-range protein-protein attractive interactions.[33] Consequently, most of the protein molecules are concentrated into densely packed equilibrium nanoclusters.[19, 33] The mechanisms of nanocluster formation and stabilization were explained in terms of the specific short-ranged attraction, van der Waals and depletion attraction balanced against weak electrostatic repulsion. The weak electrostatic repulsion was accomplished by, formulation near the protein isoelectric point (pI) where the protein was only slightly charged. Simultaneously, the nanoclusters do not aggregate, since their large size reduces the impact of the short range attractive interactions between nanoclusters. Furthermore, the electrostatic repulsion increases from the cumulative effect of hundreds to thousands of slightly charged protein monomers.[19] This hierarchy of attractive and repulsive interactions results in a colloidally stable

protein nanocluster dispersion with low viscosity.[19] In addition, the high volume fraction of the protein within the nanocluster, much higher than is possible with a protein solution, maintains the protein native structure due to a self-crowding, entropic stabilizing mechanism.[34, 35] To date, only a single extrinisic crowder, trehalose, has been reported for formation of nanoclusters of a therapeutic protein and the pharmacokinetics of that formulation.[33] Currently, it is unclear whether a single extrinisic crowder will be sufficient to optimize protein formulations for the desired therapeutic properties for wide classes of proteins. A recent study suggests that multicomponent crowder mixtures provide further control over nanocluster properties, but only *in vitro* studies for a single polyclonal sheep antibody have been performed.[19]

In this study, we demonstrate that a multicomponent mixture of three crowding agents can be used to create stable dispersions of highly concentrated, active monoclonal antibody particles which retain high activity and bioavailability upon subcutaneous administration in mice. Multicomponent crowding agent mixtures provide flexibility in formulation in response to specific biochemical characteristics of a particular protein such as high protein solubility. Murine IgG2a monoclonal antibody 1B7, which binds and neutralizes the pertussis toxin (PTx) associated with whooping cough infection[36, 37], was selected to demonstrate applicability to a therapeutically relevant molecule. The amorphous protein particles were generated via a new freezing method, spiral-wound in-situ freezing technique (SWIFT). In contrast, previous protein nanocluster studies used tray freezing to produce the protein particles.[19, 33] As opposed to traditional tray freezing lyophilization, the much more rapid SWIFT freezing may offer advantages for achieving high protein stability, as has been shown for spray freeze drying[38], spray freezing into liquids[39], and thin film freezing[40]. Unlike the other rapid freezing processes, in SWIFT, the particles are produced in the actual dosage vial to simplifying processing.[40] Next,

these particles were gently dispersed in a dispersion buffer comprised of histidine buffer adjusted to the approximate 1B7 pI augmented with three pharmaceutically acceptable crowding agents, water-soluble organic n-methyl-2-pyrrolidone (NMP), polyethylene glycol (PEG), and trehalose to confer low viscosity and limit 1B7 solubility to prevent particle dissolution. Under these conditions, the translucent dispersion exhibits a low viscosity even at high antibody concentrations (<50 cP at 200 mg/ml), with ~200 nm 1B7 particles in equilibrium with 2.5-5 mg/ml dissolved 1B7, as measured by DLS. Importantly, the protein native structure is preserved, as SDS-PAGE and ELISA analysis of diluted dispersions exhibit the same activity as untreated 1B7.

Last, we performed an *in vivo* murine pharmacokinetic study to compare the bioavailability of three different subcutaneously administered dispersions with traditional IV and SQ administration of antibody solutions. To compare the dispersion and solution controls at similar dosages, we administered a standard dosage (~5 mg/kg) in a large 100 µl volume. The 1B7 distribution and elimination half-lives were very similar for these three groups, while the time to peak serum concentration (t_{max}) was delayed for the SQ injections, consistent with the expected slower diffusion kinetics from this injection site. We then prepared the dispersion at high concentration (200 mg/ml) to compare the pharmacokinetics resulting from a small volume (1 µl), standard dose injection and a large volume (100 µl), high-dose (52 mg/kg) injection. Again, the pharmacokinetic profiles were remarkably similar for all SQ groups, although the small volume injection had a slightly shorter t_{max}, indicating that the more rapid diffusion kinetics of a small injection may impact the overall pharmacokinetics, consistent with results for the single crowder, trehalose, system[33]. Remarkably, analysis of terminal serum samples for total 1B7 protein and specific PTx binding activity by ELISA, as well as an *in vitro* PTx neutralization test, were unable to detect a loss in 1B7 activity or development of anti-

1B7 immune responses over a 14-day period. The high protein stability during injection, residence in the subcutaneous tissue and transport into the bloodstream is shown to be consistent with *in vitro* data previously reported[19, 33], whereby folded protein molecules rapidly diffuse away from the surface of the equilibrium nanoclusters. The ability to achieve high stabilities for the severe test of extremely high dosages may offer new opportunities for more modest increases in dosages in subcutaneous injection. Dispersions are a promising approach to highly concentrated, low viscosity protein formulations that preserve activity and confer favorable pharmacokinetics. Moreover, dispersions can achieve dosages at least 10-fold higher than can be attained via solutions and can be formulated with a variety of pharmaceutically acceptable agents.

4.2 MATERIALS AND METHODS

4.2.1 Antibody expression, purification and biotinylation

Murine hybridoma cells producing the IgG2a antibody 1B7 were grown in T-flasks in Hybridoma-SFM serum-free media at *37˚C with* 5% CO_2 until cell death, as reported previously[33, 37]. Briefly purification of the antibody consisted of centrifugation at 3000 rpm for 20 minutes, followed by filter sterilization using a 0.45 µm filter, dilution 1:1 with binding buffer (20 mM pH 7.0 sodium phosphate) and loading with binding buffer onto a pre-equilibrated Protein-A column (GE Healthcare). After baseline stabilization, 1B7 was eluted into collection tubes containing 1 M Tris pH 8.0 using an elution buffer (0.1M glycine pH 2.7). Protein concentration was measured with micro-bicinchonoinic acid (BCA) assay (Pierce, Rockford, IL), while non-reducing SDS-PAGE verified protein preparation homogeneity and purity. Purified 1B7 was labeled with biotin using EZ-link® Sulfo-NHS-LC-Biotin (Pierce, Rockford, IL). A 5 mM solution of the biotin reagent was added at a 5:1 molar ratio to a 1 mg/ml solution of the 1B7 in PBS at

room temperature and allowed to react for 30 minutes. Excess biotin was removed by buffer exchange using 50,000 MWCO Centricon concentrators with PBS.

4.2.2 Particle formation by spiral wound in-situ freezing technology (SWIFT)

Purified and biotinylated 1B7 was buffer exchanged into 20mM pH 5.5 histidine buffer using Centricons, as above. The protein concentration was measured again, solid α-α trehalose was added to a 1:1 wt ratio as a cryoprotectant and gently mixed to dissolve. The resulting solution was filter sterilized (0.22 μm), diluted to 20 mg/ml protein and transferred to a sterile 8ml (1.9 cm x 4.8 cm) glass vial for SWIFT freezing. During SWIFT, the base of the vial was contacted with liquid nitrogen while rotating the vial on its side (~1 revolution/second), resulting in a thin film of frozen solution on the inside edge of the vial, with subsequent thin films freezing in a spiral towards the center of the vial (Figure 4.1A). After the entire volume was frozen (~10-40 seconds), the samples were placed upright on a pre-cooled lyophilizer shelf at -40°C. The samples were then lyophilized for 12 hours at -40°C at 100mTorr, followed by a 6 hour ramp to 25°C at 50 mTorr, and maintained for secondary drying at 25°C at 50 mTorr for at least an additional 6 hours. To assess protein activity after freezing, powder was reconstituted at 5 mg/ml in PBS for analysis by dynamic light scattering (DLS) and enzyme-linked immunosorbent assay (ELISA) as described below. Samples of the dry powders after lyophilization for scanning electron microscopy (SEM) analysis were placed on adhesive carbon tape to fix the sample to the SEM stub. Each sample for SEM was platinum-palladium sputter coated using a Cressington 208 bench top sputter coater to a thickness of 10nm. Micrographs were taken using a Zeiss Supra 40 VP scanning electron microscope with an accelerating voltage of 5 kV. Further characterization of particles formed by SWIFT freezing is found in the supplemental.

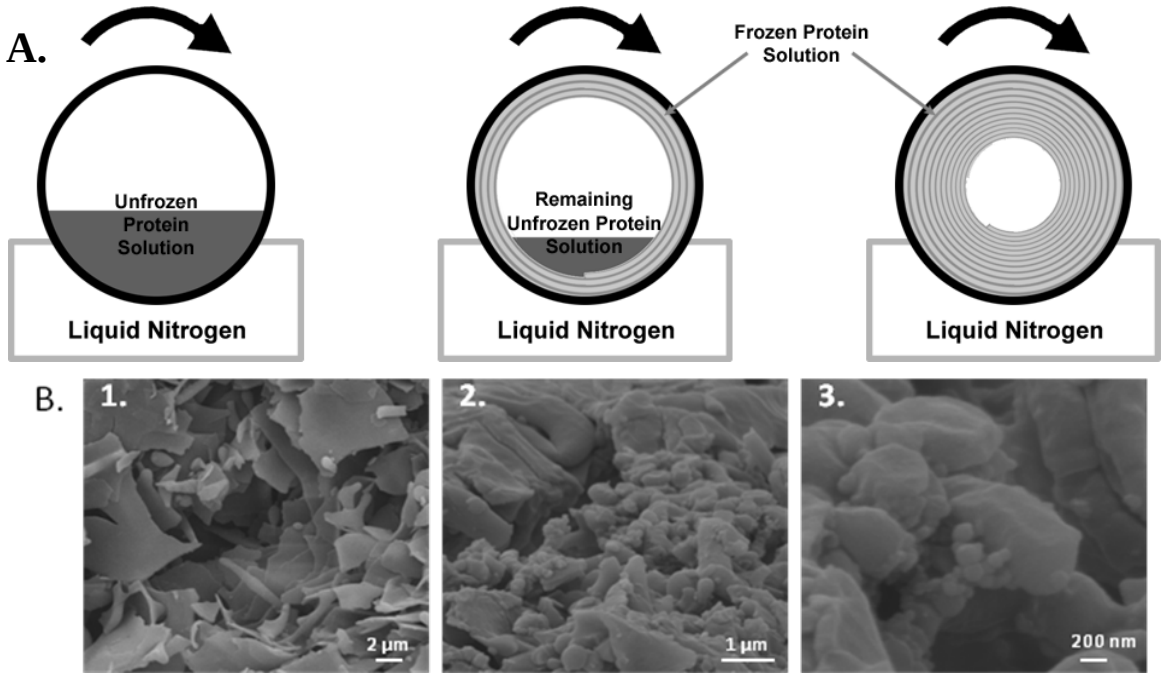

Figure 4.1 Schematic of SWIFT freezing process and dry powder SEM. A) The unfrozen protein solution in a cylindrical vial is placed on its side and rolled while exposed to liquid nitrogen. This causes a thin film of the protein solution to freeze on the inside edge of the vial followed by subsequent films towards the center of the vial resulting in a frozen annulus of protein solution which is placed in the lyophilizer to remove water. B) Morphology of SWIFT powder after lyophilization by SEM.

4.2.3 Dispersion formation

To form the dispersion, SWIFT frozen and lyophilized 1B7 protein powder was compacted into 0.1ml conical vials (Wheaton Science Products No. 986211) such that the total powder weight was 0.04 ± 0.001g. An aqueous-based solvent dispersion buffer, containing 10% (v/v) PEG300 and 20% (v/v) n-methyl-2-pyrrolidone (NMP) in a 50mM phosphate buffer with the pH adjusted to match the measured antibody pI (pH 7.2, see Figure S1), was added to the lyophilized protein. Gentle stirring with the tip of a needle removed air pockets, to yield a uniform, optically clear dispersion with a final 1B7 concentration of 160-200 mg/ml. Neither sonication nor violent mixing was necessary to form a uniform translucent dispersion.

4.2.4 Viscosity measurement

The apparent viscosity of the 1B7 dispersion was measured as the time to draw 50 μl of the dispersion into a 25 gauge 1.5” long needle attached to a 1ml tuberculin slip tip syringe, as reported previously for sheep IgG dispersions[19]. Briefly, videos of the conical vial containing the dispersion were taken and the time to draw from a height 0.4” from the bottom of the cone to a height 0.1” from the bottom of the cone was measured using Image J software. A standard curve using known solutions with various viscosities provided a linear correlation between the time to draw 0.05 ml from the conical vial to the viscosity with an r^2 value greater than 0.99[19]. These results are consistent with previous work with suspensions of model proteins and protein solutions which found that the time to draw up a specified amount of the sample in a syringe was correlated linearly to viscosity.[16, 19, 23]

4.2.5 Colloidal size determination/characterization

Dynamic light scattering (DLS) was used to measure the sizes of particles present in the purified 1B7 preparation, concentrated 1B7 dispersion and dilutions of the dispersion using a custom-built DLS apparatus[41] modified to include backscattering angles up to 165°[19, 33]. Particle sizes in the concentrated dispersion were measured with a small volume cell (60 μl, Beckman Coulter #A54094) at ~23°C and a 160° scattering angle, while all other measurements were made in a standard 1 ml cell at ~23°C and scattering angles optimized to detect the relevant particle size. To estimate the solubility of 1B7 in the dispersion buffer, the 200 mg/ml dispersion was diluted 1:40, 1:80 and 1:160 in dispersion buffer and particle sizes measured at a 90° scattering angle. We define the concentration of 1B7 at which the protein monomer peak is observed by DLS as the solubility.[19] To mimic the effects of dilution on particle size and detect formation of aggregates, the dispersion was diluted 1:40 in PBS to give a final 5 mg/ml 1B7 concentration and the resulting particle sizes measured at a scattering angle of 30°. The size of purified 1B7 monomeric antibody in PBS was measured at 5 mg/ml and a scattering angle of 30°.

4.2.6 *In vitro* antibody activity and aggregation assays

The 1B7 tertiary structure within the dispersed particles was assessed by intrinsic tryptophan fluorescence, as the emission maximum shifts based on the local environment of the tryptophan side chain.[42] A SpectraMax M5 spectrophotometer (Molecular Devices) was used to fluoresce protein samples at a wavelength of 295nm, with the emission spectrum recorded at 1nm increments between 310-380nm. For 1B7, a shift in the emission maximum is observed from 342 nm for folded protein to 350 nm for fully unfolded protein. This approach was used to qualitatively look for evidence of an altered tertiary protein structure of the protein dispersed in 200nm particles at 200 mg/ml.[43]

All subsequent assays of protein activity and structural stability were conducted on 1B7 dispersion diluted to 1 mg/ml in PBS. Controls included lyophilized 1B7 (reconstituted in PBS at 1 mg/ml) and purified 1B7 with no further processing (1 mg/ml in PBS). First, the formation of insoluble and di-sulfide linked aggregates was monitored by non-reducing SDS-PAGE. Briefly, 3 µg 1B7 sample was combined with loading buffer and separated on a 4-20% precast linear gradient polyacrylamide gel (Bio-Rad) and stained with Gel-Code Blue (Bio-Rad).

To monitor ligand-binding activity, an indirect PTx ELISA was employed as reported previously.[33, 37] High-binding ELISA plates (Costar) were coated with 50 µl pertussis toxin (PTx, List Biological Laboratories) at 0.75 µg/ml in PBS and incubated at 4°C overnight. Wells were blocked with assay buffer (PBS-1% milk) for 1hr, prior to addition of 1B7 samples in a√10 serial dilution scheme from 50 µg/ml in assay buffer. After one hour incubation at room temperature and triplicate washes with PBS-0.05% Tween 20, 50 µl goat anti-mouse IgG-horseradish peroxidase conjugate (1:2000 dilution in assay buffer, Sigma) was incubated for one hour at room temperature. Plates were washed in triplicate and signal developed with tetramethylbenzidine dihydrochloride (TMB) substrate (Pierce), quenched with 1N HCl and the resulting absorbance at 450 nm recorded using a SpectraMax M5 instrument. The EC_{50} value was calculated from the linear range of the dose-response curve as the antibody concentration corresponding to 50% of the maximum absorbance (Eq. 4.1).

$$EC_{50} = \frac{C(A_{450,max}) - C(A_{450,min})}{2} \qquad \text{Eq. 4.1}$$

For comparison between samples, the relative EC_{50} was calculated as the ratio of the sample EC_{50} to unprocessed control antibody EC_{50}. All samples were run in triplicate.

4.2.7 *In vivo* bioavailability in BALB/c mice

An *in vivo* pharmacokinetic study of the 1B7 dispersion and control solution was performed over a 14 day period using four to six healthy 24-27g, female BALB/c mice per group. Mice were administered a single 1 or 100 µl subcutaneous (SQ) injection of 1B7 at low (4.6-7.3 mg 1B7/kg body weight) or high (51.6 mg/kg) doses. The five sample groups compared in this study included two groups (1) IV and (2) SQ injections of 100 µl of a 1B7 solution (1.4 mg/ml solution for a final 5.6 mg/kg dose) reported previously[33], as well as (3,4) SQ injections of 100 µl antibody dispersion at low (4.6 mg/kg) and high (51.6 mg/kg) doses; and (5) SQ injection of 1 µl at a low (7.3 mg/kg) dose of the antibody dispersion in the dispersion buffer. The previously reported solution samples (groups 1 and 2) were prepared from a 20 mg/ml 1B7 solution in PBS diluted to 1.4 mg/ml in PBS[33] while the dispersion samples were diluted in the dispersion buffer from a 200 mg/ml 1B7 dispersion to a concentration of 1.2 mg/ml for group 3, 12.9 mg/ml for group 4, and 182 mg/ml for group 5 immediately prior to injection.

Prior to the injection and at eight additional timepoints between 12 and 336 hours, mice were weighed and a blood sample (~20 µl) collected from the tail vein. After collection, the samples were allowed to clot, centrifuged at 5000rpm for 10 minutes and serum transferred to a new tube. At the terminal timepoint (336 hours), mice were anaesthetized and between 0.2 and 1 ml serum collected by cardiac puncture. These samples were used in ELISA assays, to measure the total and active concentrations of 1B7 in the serum and, for the terminal time point, to measure antibody activity via an *in vitro* neutralization assays and to provide an initial estimate of mouse anti-1B7 responses. This study was performed with approval by the Institutional Animal Care and Use Committee at the University of Texas at Austin (protocol #AUP-2010-00070) in compliance of guidelines from the Office of Laboratory Animal Welfare.

4.2.8 Measurement of 1B7 in serum samples

To determine the concentration of active 1B7 in serum samples, a standard ELISA approach was used with the following modifications as previously reported[33, 44]. ELISA plates were coated with PTx at 1.5 μg/ml in PBS. The assay buffer used as diluent in all steps consists of 4% bovine serum albumin, 4% fetal bovine serum (FBS), 0.05% Tween 20, in PBS, pH 7.4. After blocking with assay buffer, 2.3 μl serum sample was serially 1:√10 diluted in 50 μl per well assay buffer. Each plate included mouse serum (Sigma) as a negative control and a 1B7 standard curve diluted to an initial concentration of 100 μg/ml in mouse serum. Additional samples were analyzed for total protein detected using a streptavidin coating on the ELISA plates to detect the biotinylated 1B7 (results not shown).

After measurement of the resulting absorbances, SoftMax Pro v5 was used to calculate EC_{50} values based on the serum dilution using a 4 parameter logistic (4PL) model for each individual curve. Concentrations of active 1B7 in each serum sample were calculated from a linear correlation between the log [(sample EC_{50})/ (standard EC_{50})] versus the log of the known 1B7 concentration in the standard curve. A linear correlation with a fit > 0.95 from at least 5 independent standard curves was determined (Figure A1.3.2).

4.2.9 Measurement of active antibody by CHO cell neutralization assay

As an orthogonal activity measurement to determine the concentration of serum 1B7 able to neutralize PTx activity *in vitro*, we employed a CHO cell neutralization assay modified from Gillenius *et al.*[37, 45] The concentration of neutralizing antibody was measured as the sera dilution that completely inhibited PTx-induced CHO cell clustering relative to a standard curve of purified 1B7 with known concentration. Briefly, 50 μl of 1.5 ng/ml pertussis in Dulbecco's Modified Eagle Medium (DMEM) with 10% FBS was

added directly to each well of a sterile 96 well tissue culture plate. Terminal serum samples (2.3 µl) were serially diluted using a 1/10 dilution scheme to maintain a constant PTx concentration. After incubation for 30 minutes at 37°C and 5% carbon dioxide, 100 µl / well of freshly trypsinized CHO cells at 10^5cells/ ml were seeded in each well. After 24 h of incubation at 37°C and 5% CO_2, wells were scored for CHO clustering using 0-3 scale, with 0 as elongated (non-clustered) and 3 as completely clustered.

4.3 RESULTS AND DISCUSSION

Here, we report formation of highly concentrated, low viscosity dispersions of antibody nanoclusters, in which the antibody retains native structure and binding activity upon dilution and in vivo subcutaneous administration. In contrast to our prior work, we used a novel freezing technique to form particles and multiple crowding agents to tune particle size. The combination of these innovations allowed us to administer subcutaneous antibody dispersions to mice at typical therapeutic doses (5-7 mg/kg) as well as an ultra-high dose, more than 10-fold higher than current practice (51.6 mg/kg).

4.3.1 Stable protein particles made by SWIFT freezing

The first step in preparation of concentrated aqueous dispersions is the formation of a dried powder of protein particles. The choice of freezing method is critical to both protect antibody structure and activity during freezing as well as to produce particles of the appropriate size and morphology to yield a colloidally stable dispersion. To address these concerns, we developed a novel freezing technique, SWIFT, which rapidly freezes an antibody solution directly in the final packaging vial prior to lyophilization (see Figure 4.1A). The rationale in developing this technique is that two major sources of protein denaturation during freezing are exposure to liquid-gas interfaces during spray-freeze

drying and the slow rate of freezing in larger volumes which can result in freeze concentration and subsequent concentration-dependent aggregation.[38, 39, 46, 47] By rotating the vial of protein solution while in contact with liquid nitrogen, each concentric layer freezes in less than a second. The remaining liquid is gently mixed due to rotation, normalizing any concentration gradients.

We used SWIFT followed by lyophilization to form submicron particles of the 1B7 antibody used in the dispersions. To prevent protein aggregation during freezing, the protein solution was adjusted to contain a 1:1 weight ratio of trehalose as a cryoprotectant.[48] The buffer selected, 20 mM histidine pH 5.5, is commonly used during lyophilization steps and will not crystallize resulting in large pH variations.[49] SEM analysis of the frozen and lyophilized 1B7 clearly indicates the presence of submicron particles, similar to the size desired in the final dispersion (Figure 4.1B). Importantly, antibody processed in this manner retains native conformation and activity upon reconstitution with PBS at 5 mg/ml. At this concentration, DLS detected a single species with a ~10nm hydrodynamic diameter, as expected for an antibody monomer[50] (Figure 4.2A). The absence of larger particles indicates that the antibody did not form irreversible aggregates during SWIFT and lyophilization. In addition, an ELISA to monitor the specific PTx-binding activity of the reconstituted antibody revealed no significant change in activity due to these processing steps versus the untreated control (Figure 4.3A).

The SWIFT process was designed to produce particles of the desired morphology while protecting protein structure and activity. This is achieved via rapid freezing with minimal liquid-air interface, goals inspired by related process, thin film freezing (TFF)[39, 40]. In SWIFT, each film layer, corresponding to a single vial revolution, is ~200nm thick (see Appendix B). Indirect contact with liquid nitrogen as a heat sink confers cooling rates of ~10^2 K/s. In TFF, a small volume of protein solution is deposited on a

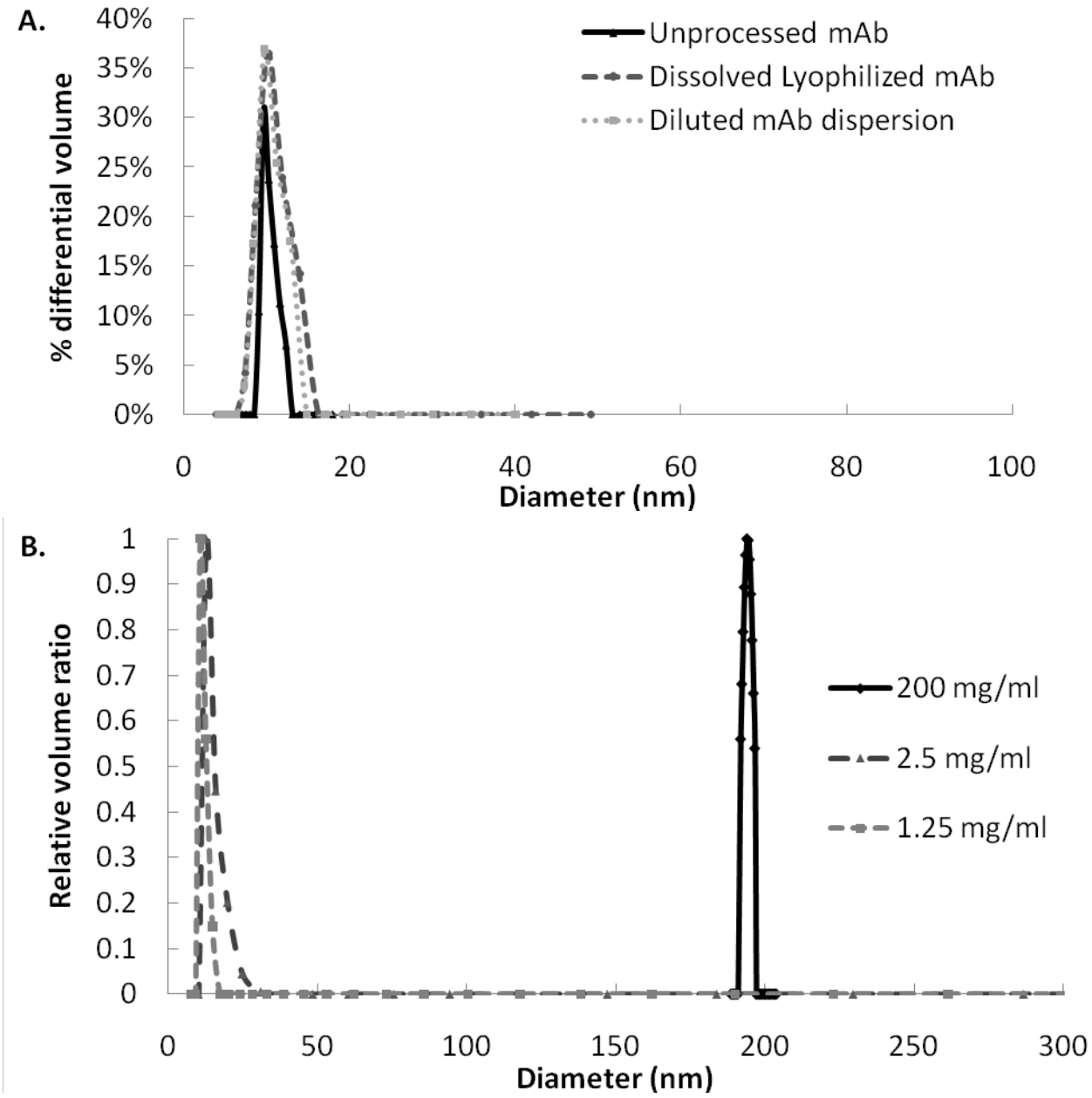

Figure 4.2 Size distribution of antibody particles. A) Comparison of unprocessed, lyophilized and dispersed 1B7 by DLS. All samples were diluted to 5 mg/ml in PBS. B) Effect of antibody concentration on particle size in dispersion buffer. At high concentration (200 mg/ml) in dispersion buffer, dynamic light scattering (DLS) detects only large particles of ~200 nm. Upon dilution below the solubility limit in the dispersion buffer, concentrations of 2.5 and 1.25 mg/ml detect only particles of ~10 nm size, the expected size for monomeric IgG.

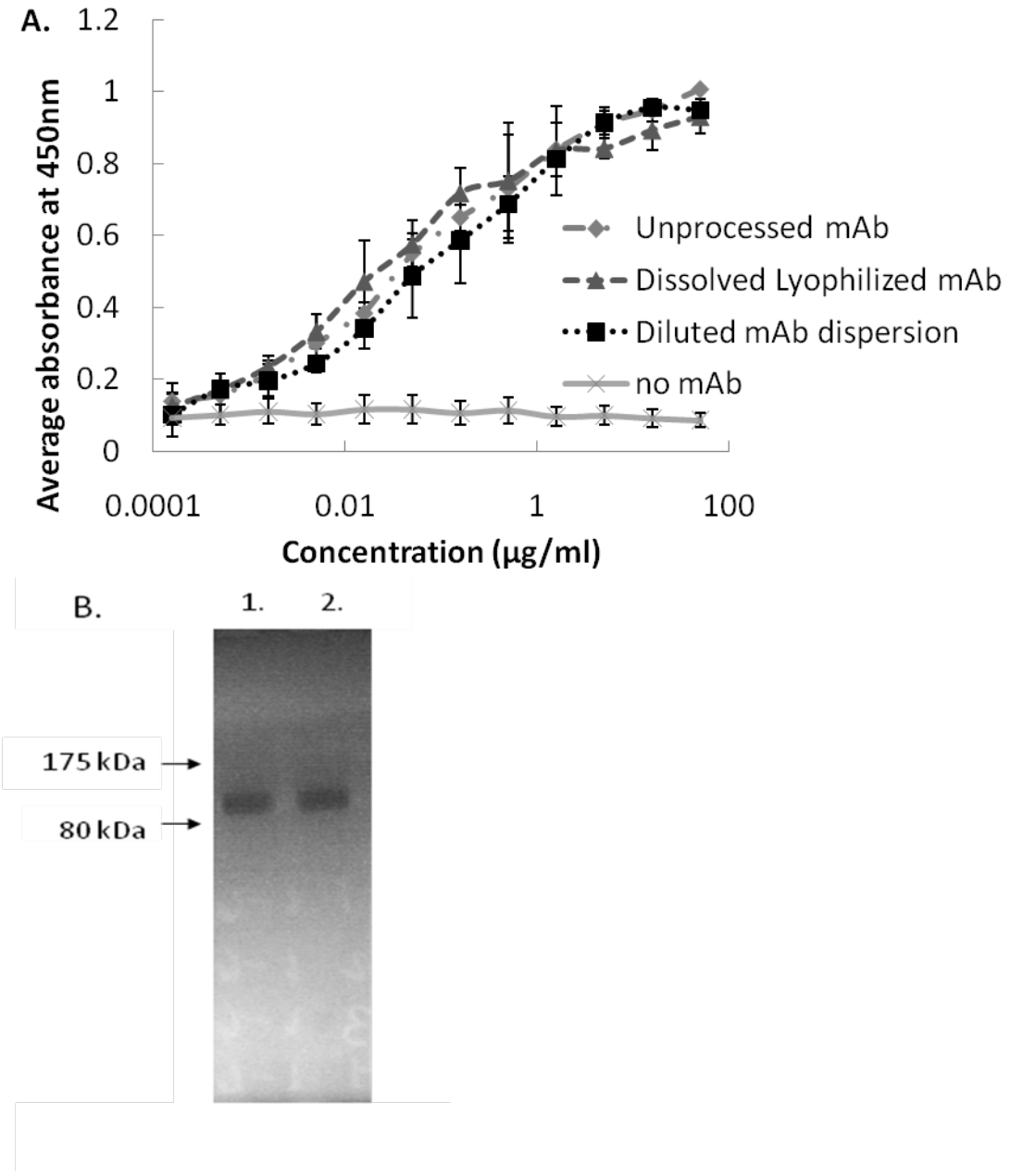

Figure 4.3 Characterization of antibody recovered from dispersion. A) Comparison of unprocessed, lyophilized and dispersed 1B7 by PTx ELISA to monitor antibody activity. B) SDS-PAGE gel comparing unprocessed, purified mAb1B7 (lane 1) and dispersion diluted from 200 to 1 mg/ml in PBS (lane 2).

cryogenically cooled surface, where it spreads to ~210 nm thickness, freezing within a single second[40]. Scaling-up to compare freezing times for equal volumes, TFF freezes at a rate of ~5.1 seconds per ml of protein solution, while SWIFT results in a similar rate, ~7.5 seconds/ml (Appendix B.1.3).

As a result of the similarities in freezing rates and film thicknesses, TFF and SWIFT processing of similar protein solutions yields dry particles with similar morphologies (Figure 4.1B).[40] As with TFF, the rapid cooling and freeing rates generate high supersaturation, thus a large number of ice nuclei and the formation of many thin liquid channels between the frozen water domains, containing the remaining unfrozen solution. The rapid vitrification of the thin liquid channels then decreases the number of collisions between protein and sugar particles thus inhibiting growth by coagulation of particles relative to traditional tray freezing lyophilization, which contains much larger liquid channels.[40] In addition, as the concentrations of the protein and sugar are increased in the unfrozen liquid, the rapid increase in viscosity will further reduce the mobility of the growing particle nuclei. Thus smaller submicron protein particles, as shown in Figure 4.1B, are formed during SWIFT freezing versus standard tray freezing lyophilization.

With both SWIFT and traditional tray lyophilization, low levels of protein denaturation and aggregation are achieved by kinetic and thermodynamic stabilization of the native protein structure during freezing and lyophilization. The native protein state is stabilized during lyophilization by kinetically trapping protein molecules in an amorphous solid[48, 51, 52], thereby reducing protein mobility which can lead to aggregation. Addition of the lyoprotectant trehalose during lyophilization further thermodynamically stabilizes the protein native state during freezing by entropically favoring the native folded state[51-53] and during dehydration by forming hydrogen bonds with proteins.[54, 55] However, processes to form submicron protein particles such as spray freeze drying

(SFD), have been shown to increase protein aggregation versus standard tray freezing lyophilization due to the large gas-liquid interface in the spraying step.[38, 56] The large area/volume of the gas-liquid interface of ~6000 cm^{-1} in SFD for 10 μm sprayed droplets can lead to protein adsorption at the interface, denaturation and aggregation.[38, 40, 48, 57, 58] In the case of SWIFT, the gas-liquid interface is minimized as the only exposure of the liquid protein solution to the air is the liquid interface inside the glass vial. As a result, the estimated gas-liquid interface decreases 3 orders of magnitude when compared to SFD to ~4 cm^{-1}. Thus the 1B7 was anticipated and found to remain stable upon reconstitution to monomer from the dry powder form after SWIFT freezing and lyophilization.

One practical advantage of SWIFT freezing is the ability to freeze directly in the final dosage vial when compared to other rapid freezing techniques such as TFF and SFD.[40, 46, 47] This approach avoids the need for costly, solid transfer steps while maintaining aseptic conditions. In this case, if a dosage of 80 mg of the protein is required at a concentration of 20 mg/ml, the 8 ml vial used in the study can serve as both the freezing and reconstitution vial. However, since the cooling rate SWIFT freezing is governed by the liquid cryogen used and the thickness of the glass vial, as well as the heat transfer coefficients of the materials used, the vial can be readily scaled-up or down to meet dosage requirements. In addition, by removing the transfer step to the final vial, all of the protein can be recovered after lyophilization and utilized in the formation of the final dosage.

4.3.2 Colloidal characterization of 1B7 particles in dispersion

To form the colloidally stable, translucent dispersion, the dry, sub-micron particles of antibody and trehalose produced via SWIFT were combined with a specially

formulated dispersion buffer. To reduce protein solubility, this includes a 50 mM phosphate buffer adjusted to the antibody pI (pH 7.2) and two additional crowding agents: 20% n-methyl-2-pyrrolidone (NMP) and 10% polyethylene glycol 300 (PEG300) by volume. After combining the SWIFT particles and dispersion buffer, the trehalose contained in the dry powder will dissolve. A fraction of the trehalose will diffuse into the solution, increasing the volume fraction of crowding agents as observed previously for sheep IgG[19]. Sufficient dispersion buffer was added to the dry powder to yield a final antibody concentration of 190 mg/ml with a final volume fraction (φ) of crowding agents of 0.34.

Under these conditions, DLS analysis of the dispersion using a low volume (60μL) cell identifies a single population of particles with a ~200 ± 14 nm diameter. This colloid size was reproduced in three separate experiments, measured each time in triplicate, with a representative curve shown in Figure 2B. This particle size was further confirmed by SEM images of the dispersion after dilution to 100 mg/ml in the dispersion buffer, rapid freezing and lyophilization onto an SEM stage (Figure 4.4B). This image shows nanoparticles of a size consistent with DLS measurements, but a different shape due to coating with crystallized trehalose. Previously, SEM and STEM images of dispersed sheep IgG and 1B7 particles at lower trehalose concentrations, visualized the dispersed particles as clusters of smaller particles[19]. We were able to obtain similar images for the current formulation after adding dispersion buffer to reduce the trehalose concentration, simultaneously reducing the 1B7 concentration to 40 mg/ml (Figure 4.4C). To confirm that these results are not affected by dissolution of the 1B7 nanoparticles, we measured the 1B7 solubility in dispersion buffer, using methods reported previously.[19] Starting with the 200 mg/ml dispersion, we progressively added dispersion buffer to reduce the protein concentration and measured the resulting particle sizes by DLS (Figure

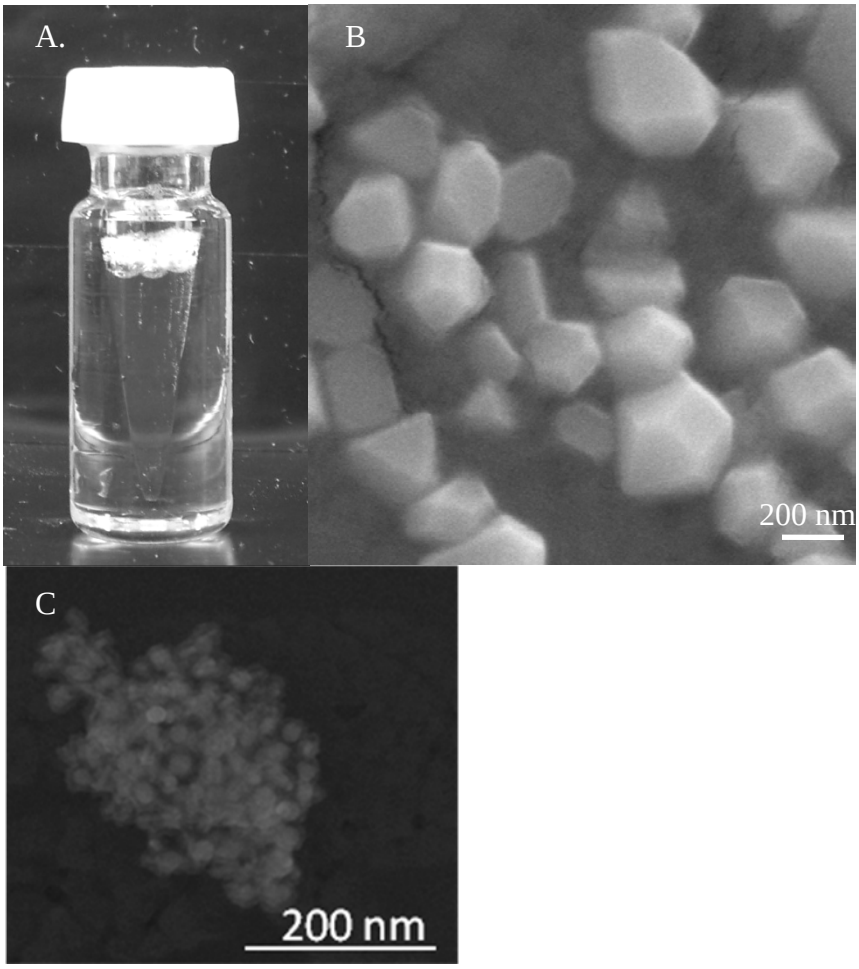

Figure 4.4 Visual appearance of dispersion. A) Digital image of suspended particles B) SEM image of the 1B7 dispersion (200 mg/ml) when diluted to 100 mg/ml in the dispersion buffer, rapidly frozen with the water removed by lyophilization and C) Highly magnified SEM image of a 1B7 particle diluted to 40 mg/ml prior to freezing and lyophilization

4.2B). We observed a single peak at ~200 nm until the protein concentration was reduced to 2.5 mg/ml or less. At this concentration, only a single ~10nm peak at is present, corresponding to the hydrodynamic diameter of a single monoclonal antibody molecule[59-61] From these data, we conclude that the solubility of 1B7 this dispersion buffer is ~2.5 mg/ml and that 1B7 nanoparticles formed with trehalose, PEG and NMP are fully reversible.

The dispersed particles were formed and exhibited colloidal stability due to a balancing of the intermolecular attractive and repulsive interactions at the protein molecular and colloidal levels, respectively.[19] Briefly, individual protein molecules are subject to highly attractive depletion and specific short-ranged interactions such as hydrophobic interactions, hydrogen bonding and charge-dipole interactions[62, 63] resulting in low protein solubility.[19] Near the 1B7 pI, electrostatic repulsion is relatively weak and thus the attraction force dominates between individual protein molecules. However, once these molecules assemble into nanoclusters, the interactions between particles are slightly repulsive, stabilizing the dominant size.[19] Each protein monomer on the cluster surface will have a small number of charges, thus the repulsive interactions become significant when summed over all the monomers[19]. Attractive specific and short-range depletion-attraction interactions between clusters are minimized as the average distance between clusters increases as the colloid size increases, but the distance over which these forces act is fixed. To exert the same force, an interaction with a range of 1 nm on a 10nm protein monomer would need to act over 20 nm on a 200 colloid. Between clusters, short-range attractive interactions are negligible relative to electrostatic repulsion resulting in a colloidally-stable dispersion of protein nanoclusters, as has been previously shown for sheep IgG.[19]

To formulate a stable antibody dispersion and balance repulsive forces, the depletion attraction forces can be fine-tuned by varying the concentrations of the crowding agents.[19, 64, 65] As observed here and previously[19], an increase in crowder concentrations dramatically reduces 1B7 solubility due to depletion-attraction interactions. While 1B7 and the sheep IgG dispersions could both be formulated with a single crowding agent, trehalose, the ternary crowder system used here may provide additional flexibility to tune solubility and formulate dispersions with highly soluble proteins or to further control the nanocluster size, protein stability, dispersion viscosity and nanocluster degradation during delivery.

The low apparent viscosity, 24 cP, of the ~190 mg/ml 1B7 dispersion was measured as the viscosity through a 25 gauge 1.5 inch needle (Table 4.1). This viscosity measurement was previously characterized for subcutaneous injections of highly concentrated solutions of monoclonal antibodies[16] and non-aqueous suspensions of lyosyzme[23]. The apparent dispersion viscosity is commonly described as a function of the intrinsic viscosity, [η], maximum volume fraction of particles, φ_{max}, and the solvent viscosity, η_0, using the Krieger-Dougherty equation (Eq. 4.2).[23, 66]

$$\frac{\eta}{\eta_o} = \left[1 - \left(\frac{\phi}{\phi_{\max}}\right)\right]^{-[\eta]\phi_{\max}} \qquad \text{Eq. 4.2}$$

The η may be reduced by lowering η_0, or [η], which has a minimum of 2.5 for hard sphere colloids, and increasing φ_{max}. For protein molecules in solution at high concentrations, for example ϕ = 0.1 to 0.3, strong short-range specific attractive interactions[63, 67], often produce viscosities 5 to 100 times the hard sphere value.[16, 68] For monoclonal antibody solutions with concentrations of 150 mg/mL, viscosities greater than 100cP have been attributed to reversible self-association of protein molecules, on the basis of measurements by analytical ultracentrifugation.[16, 69] In contrast, the low viscosities

Table 4.1 Biophysical characterization of 1B7 dispersions

Dispersion buffer	Protein Concentration (mg/ml)	mAb Solubility (mg/ml)	Colloid Diameter (nm)	Apparent Viscosity (cP)	Relative EC_{50}	λ_{max} (nm)*
20% NMP 10% PEG300	190 ± 20	>2.5	196 ± 14	24 ± 7	1.50 ± 0.32	340 ± 2

*Maximum emission wavelength (λ_{max}) of protein within the nanocluster excited at 295nm. Native, fully folded protein had a maximum emission wavelength of 342nm ± 1.5 and the full unfolded protein had a maximum emission wavelength 350nm

observed in the present study for the nanocluster dispersions may be consistent with the weak interactions between the nanoclusters, as suggested previously[19].

In addition to specific attractive interactions, shape effects can also increase the intrinsic viscosity of a protein molecule when compared to the relatively spherical protein nanoclusters in the dispersion. The molecular shape factor proportionally increases the intrinsic viscosity[66] and is a function of the aspect ratio of the molecule.[66, 70, 71] At its minimum, spherical particles do not increase the intrinsic viscosity over the expected value.[66, 70] In the case of protein solutions, the shape of the molecule in solution is dependent on the protein itself.[70, 71] However, for the nanocluster dispersion in the current study, surface tension forces will favor a relatively favorable spherical shape.

4.3.3 *In vitro* molecular stability of 1B7 in dispersion

The conformation of antibody contained within the dispersion and after dilution was assessed using multiple techniques. Tryptophan fluorescence assay, As reported previously for sheep IgG[19], no change in the maximum emission wavelength solvent exposed tryptophans was observed, measured by a tryptophan fluorescence assay, suggesting preservation of the active protein structure within the dispersed particles. After 10-fold dilution from the 200 mg/ml dispersion into PBS, DLS measured a single species with a ~10nm hydrodynamic diameter, as expected for a single antibody monomer[50] (Figure 4.2A). As with the 1B7 reconstituted from the SWIFT frozen and lyophilized powder, a lack of larger particles suggests that the antibody does not form irreversible aggregates upon dispersion and can recover its individual monomer size upon rapid dilution. This is further confirmed by non-reducing SDS-PAGE (Figure 4.3B), in which a single band is observed, with a molecular weight corresponding to that of an

antibody monomer, ~150 kDa[72], indicating an absence of irreversible thiol-linked and SDS-resistant aggregates. Finally, an ELISA to monitor the specific PTx-binding activity of the antibody reveals no significant change in activity due to the formation or dilution of the dispersion versus untreated control (Figure 4.3A).

To maintain therapeutic efficacy without inducing an adverse immunogenic response upon *in vivo* injection[71, 73], the conformational stability of the antibody must be maintained through every processing and delivery step: from creation of the dry, lyophilized powder to dispersing of the powder in the dispersion buffer. While instability of protein molecules includes both chemical degradation as well as physical denaturation, the higher order dependence on protein concentration of physical denaturation is expected to be a more severe challenge for the successful development of stable high protein concentration formulations and thus is examined in further detail.[10, 71] As discussed above, the protein powder formed by SWIFT freezing and lyophilization did not lose activity or develop aggregates after reconstitution in buffer. Stability of the protein within the dispersed particles is maintained due to the high volume fraction of protein within each particle. A high protein volume fraction allows protein self-crowding effects to result in the thermodynamic favoring of the natively-folded lowest surface area conformation of the protein.[19, 34, 35] This anticipated result is shown by the tryptophan fluorescence assay where no additional solvent exposed tryptophan residues are observed when the protein is dispersed. The concept of self-crowding to increase the fraction of natively folded proteins is similar to the idea that within cells proteins are stabilized by a high concentration of molecular crowding agents.[74, 75] In the case of self-crowding, the only difference is that the protein acts as its own molecular crowding agent.[34, 35] As a result when compared to a solid protein crystal, the difference between the amorphous protein particles formed in this case and crystalline protein particles does not lead to a

reduction in the stability of the native conformation of the protein, as expected by Yang and coworkers[1]. The entropic stabilization of the native protein state from self-crowding has been shown previously in theoretical arguments[34, 35], however, as protein solutions cannot achieve the high (>0.15) volume fractions necessary, it has only been realized recently for protein dispersions[19, 33]. In addition, unfolding and aggregation of the protein molecules in the dispersion are also reduced by decreased protein mobility of the solid state versus the solution state.[8, 76, 77] Kinetically, the protein molecules on the outside of the particles in the dispersion are also stabilized by the reduction in collisions which could lead to the formation of aggregates.[13, 19, 78]

The retention of active protein and lack of detectable aggregates of the protein upon dilution from the concentrated dispersion is an important indication of potential *in vivo* protein stability. The predicted dissolution time in PBS using the Noyes-Whitney equation for high surface/volume 200nm particles with a solubility of greater than 50 mg/ml is less than 1 second. In a previous study, a misfolded protein refolded during the slow dissolution process.[79] In the present study, the protein starts out in the folded state and has little time to unfold during the rapid dissolution. In addition, the molecular crowders present in the dispersion formulation will also be present simultaneously in the boundary layer surrounding the protein particles and help preserve the folded state.[80] For 1B7, high protein stability was observed upon diluting the protein at a constant crowder concentration by DLS and ELISA measurements, consistent with this rapid dissolution/crowding mechanism.[33] The fact that the clusters are natively-folded and reversible is highly beneficial for maintaining protein stability during dissolution of the clusters. With sheep IgG, at a constant protein concentration, a steady decrease in nanoparticle size was achieved upon diluting a single low molecular weight crowder, trehalose, to weaken the attractive forces.[19] At each step the protein in the cluster was

found to be folded and full activity of the protein upon dissolution of the cluster was confirmed by ELISA.[19] The protein molecules on the cluster surface are crowded by interior protein molecules and on the exterior by sugar molecules. As the folded molecules rapidly diffuse off the cluster surface into the PBS media, they remain folded as shown by the DLS and ELISA experiments.

4.3.4 *In vivo* bioavailability of stable 1B7 from dispersions

No reliable *in vitro* models exist to mimic *in vivo* dissolution of the rapidly dissolving (<1 second predicted dissolution time) dispersion after subcutaneous injection. Thus, we proceeded to a mouse model to measure the pharmacokinetic parameters as well as the specific activity of *in vivo* dissolved antibody material. The five treatment groups included three control groups to allow direct PK comparison, a low volume, high concentration and large volume, high concentration dispersion test groups. The control groups received a standard antibody dose (4.6-5.6 mg/kg delivered in 100 μl) to allow for a direct comparison of pharmacokinetics resulting from a subcutaneous dispersion injection and intravenous and subcutaneous delivery of an antibody solution. In order to deliver the same total amount of antibody in the same volume, the dispersion preparation was diluted in dispersion buffer to 1.4 mg/ml, a concentration readily achieved with antibody solution controls[33]. The fourth group was designed to assess the combined effects of dispersion concentration and delivered volume on *in vivo* dissolution rates and the resulting pharmacokinetics. These mice received a standard dose (7.3 mg/kg) administered as a high concentration dispersion (182 mg/ml) in a small 1 μl volume. The fifth group was designed to administer an ultra-high dose, which can only be achieved with high concentration, low viscosity formulations such as dispersions. These mice received a ten-fold higher dose than the other groups (51.6 mg/kg in 100 μl). For all

groups, serum samples were collected from the tail vein over 14 days, with the concentrations of total and active 1B7 antibody in each sample measured by streptavidin and PTx capture ELISAs, respectively. The efficacy of antibody present at the terminal time point was also assessed using an *in vitro* activity assay, based on antibody-mediated inhibition of toxin activity.

Overall, the 1B7 pharmacokinetic profile is quite similar for all groups, with nearly identical distribution and elimination kinetics. The primary differences result from the injection site and injection volume, affecting the time to reach the maximum concentration (tmax) and the value of the maximum concentration (Cmax/ dose). Looking first at the three control groups, delivery via subcutaneous dispersion resulted in a reduced burst phase (lower C_{max}/dose and delayed t_{max}) as compared to IV and SQ delivery of solutions (Table 4.2; Figure 4.5A). The IV solution group reached a maximum serum concentration at the first measured time point (12 hours), followed by a rapid decrease as the antibody is distributed throughout the tissues.[33] In comparison, the SQ solution group displayed a slightly reduced C_{max}/dose (24 versus 18 ug/ml/ mg/kg) and statistically significant delayed t_{max} (12 versus 21 hrs; $p<0.05$). While IV-administered material is instantly diluted in the blood volume, material administered SQ must diffuse from the injection site through interstitial fluid to reach the lymphatic and blood vessels before distribution in the blood volume, delaying these PK parameters (Figure 4.4A).[33, 81] The SQ dispersion injections exhibit similar trends as the SQ solution but with a lower Cmax and delayed tmax when compared to the SQ solution. This may reflect the effects of the dispersion buffer on mixing and antibody diffusion, as the effect is minimized with SQ dispersion 2, which was injected as a 1 ul volume instead of a 100 ul volume. For this sample, the tmax was identical (within error) to that of the SQ solution.

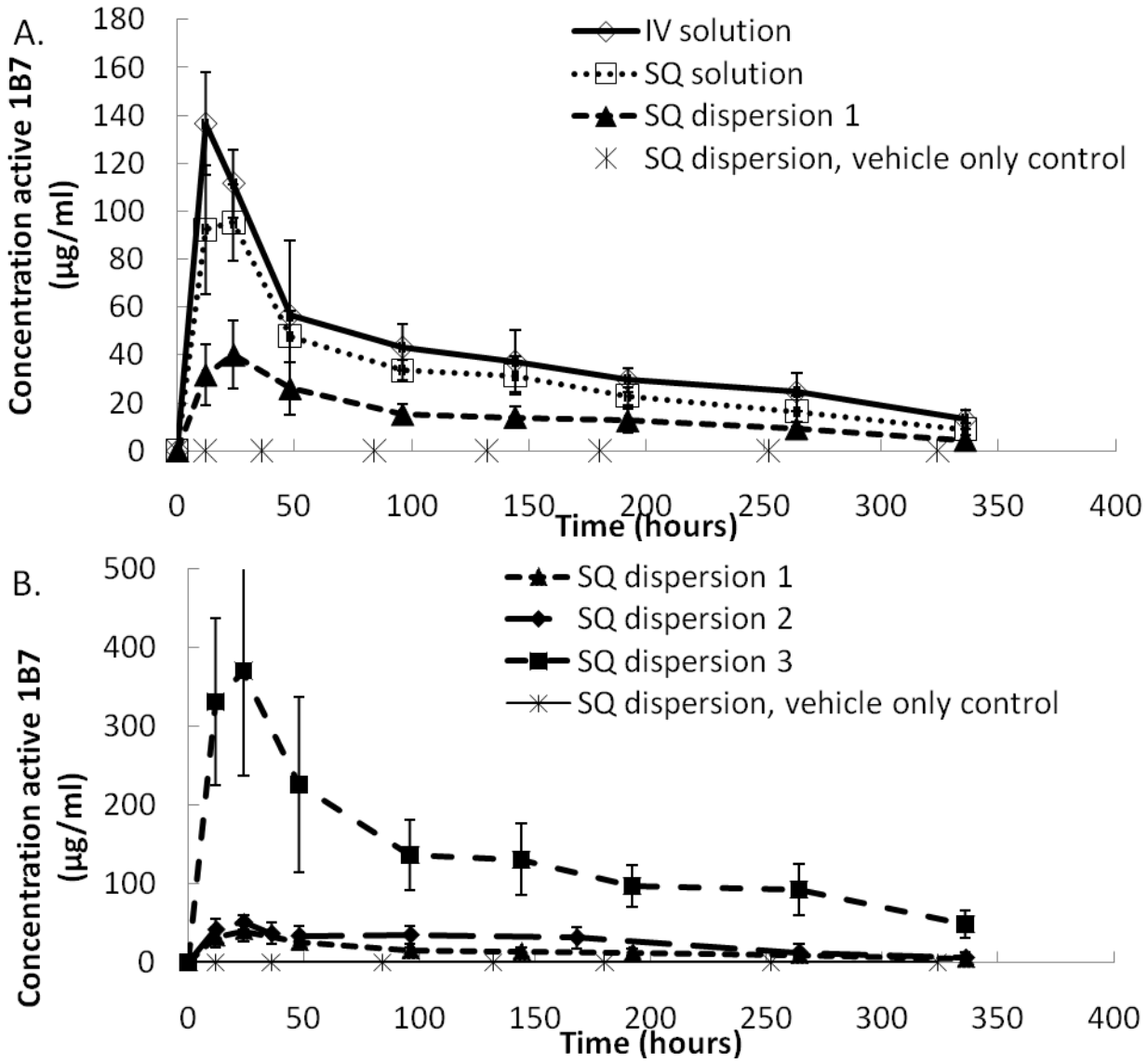

Figure 4.5 Serum concentrations of mAb after delivery. A) Comparison of mAb1B7 delivered via 100 µl injection of an IV solution (5.6 mg/kg dose), subcutaneous solution (5.6 mg/kg), subcutaneous dispersion (4.6 mg/kg) or dispersion buffer only SQ control (0 mg/kg). B) Comparison of mAb1B7 pharmacokinetics when delivered via subcutaneous dispersion with varying concentrations and injection volumes. SQ dispersion 1 is 4.6 mg/kg dose with a 100 µl injection volume, SQ dispersion 2 is 7.3 mg/kg dose with a 1 µl injection volume, and SQ dispersion 3 is a 51.6 mg/kg dose with 100 µl injection volume.

Table 4.2 Pharmacokinetic parameters for mAb 1B7 formulations.

Injection	N	Injection volume (µl)	Dose (mg/kg)	C_{max}/dose (µg/ml)/ (mg/kg)	$AUC_{0\text{-}14day}$/dose (µg*hr/ml)/ (mg/kg)	t_{max} (hours)	$t_{1/2,\alpha}$ (hours)	$t_{1/2,\beta}$ (hours)	In vitro neutralization titer
IV solution	6	100	5.6	24 ± 4	2070 ± 360	12 ± 0	46± 23	227 ± 25	500
SQ solution	4	100	5.6	18 ± 4	1630 ± 200	21 ± 6	43 ± 17 *	210 ± 17	400
SQ dispersion 1	5	100	4.6	8.7 ± 3.0	925 ± 260	29 ± 11	54 ± 21 *	219 ± 25	400
SQ dispersion 2	5	1	7.3	7.1 ± 1.2	1174 ± 470	22 ± 5	49 ± 29*	180± 16	ND
SQ dispersion 3	6	100	51.6	7.3 ± 2.6	757 ± 290	30 ± 15	51 ± 23 *	250± 24	5900

ND- not determined

* $t_{1/2,\alpha}$ determined from 2 points for some mice

Once the maximum serum concentration is attained, all groups show similar 1B7 pharmacokinetics. As seen in Figure 5, these data fit a biphasic exponential profile, with α distribution and β elimination time constants that are within experimental error for all groups, based on 1B7 concentrations measured by the PTx ELISA (Table 4.2). The β elimination half-life was also within error for all groups when measured using a total protein ELISA assay (results not shown). The distribution phase represents passive antibody diffusion from the well-mixed blood volume into other tissues, driven by the 1B7 concentration gradient and the elevated vascular pressure, while antibody elimination rates are controlled by interactions with specific receptors such as the FcRn. Notably, both mechanisms require a monomeric, properly folded antibody molecule. A soluble aggregate will have a larger size and consequently larger diffusion constant and slower $t_{1/2\alpha}$, while a misfolded monomer or soluble aggregate will exhibit different binding kinetics for the FcRn and a different $t_{1/2\beta}$. The similar kinetics observed for all groups indicate that the antibody delivered as a SQ dispersion is able to dissociate from the nanocluster and diffuse away from the injection site while retaining an active, monomeric form, similar to the *in vitro* observation in which active 1B7 monomer is rapidly recovered upon dispersion dilution.

These experiments were performed in mice, where the large allowed injection volume per body mass (100 µl/25g) allows for direct comparisons between solutions and dispersions formulated at the same concentration. A similar comparison is not possible in humans, as SQ injections are restricted to ~1.5 ml volume. To demonstrate that dispersions can achieve dosages relevant for humans, we prepared group 4 as a scaled-down version of a human dose. Here, a 1 µl volume of highly concentrated dispersion

(182 mg/ml) was administered subcutaneously, for a final 7.6 mg/kg murine dosage. Scaling-up to calculate the human dosage, in which a 182 mg/ml dispersion could be administered in a 1.5 ml volume, this is equivalent to a 4.3 mg/kg human dose, exceeding current dosing guidelines (2 mg/kg). To evaluate the potential for dispersions to result in less-frequent administration of ultra-high antibody dosages, which are not currently achievable with solutions, group 5 mice received a large, 100 µl injection volume of dispersion (12.9 mg/ml), for a 51.6 mg/kg dose. This group also exhibited similar pharmacokinetics (similar t_{max}, $t_{1/2,\alpha}$, $t_{1/2,\beta}$) and 1B7 bioavailability indicating concentration and dose-independent pharmacokinetics.

To provide an orthogonal measurement of antibody quality to complement antigen ELISA, we measured 1B7 biological activity with an *in vitro* CHO cell neutralization assay using sera from the terminal time point. Free PTx will bind cell-surface receptors, undergo receptor-mediated endocytosis and eventually ADP-ribosylation of $G_{i/o}$ coupled receptors; phenotypically, this results in loss of contact inhibition and CHO cells grow in a clustered morphology. Antibody-mediated neutralization of PTx blocks toxin entry into cells, protecting normal growth phenotype. Sera were diluted in the presence of a fixed PTx concentration, CHO cells added and, after 24 hrs growth, scored for normal or clustered morphology. The highest sera dilution completely preventing CHO cell clustering was recorded and compared versus purified control 1B7 antibody. This assay resulted in no statistically significant differences between groups on titre per µg antibody basis. Based on this assay, there is no evidence for a loss in antibody efficacy as a result of injection site (SQ vs. IV) or formulation (Table 4.2). Western blot analysis was used to demonstrate the absence of gross physical

changes in serum antibody due to formulation and administration route, such as formation of insoluble or disulfide bonded aggregates (Figure A1.3.5).

As shown by both *in vitro* and *in vivo* data, the protein within the dispersion shows no detectable loss of native conformation during any processing step or after dissolution and systemic absorption. As described previously within the dispersion, the native conformation is maintained by protein self-crowding and the addition of crowding agents entropically stabilizing the native conformation.[35] For aggregation to occur upon dissolution, the native protein must reversibly unfold to an aggregation-prone intermediate and collide with another aggregation-prone protein molecule to form an aggregate, which leads to irreversible inactivation of the protein.[21] As in the *in vitro* dilution experiments, initially *in vivo* the crowders within the dispersion (trehalose, PEG, and NMP) are still present as the particles dissolve and thus entropically prevent the protein from unfolding.[53, 82] Due to the fast dissolution time, the nearby crowders from the dispersion will help prevent unfolding of the protein. *In vivo*, as the crowders from the dispersion are diluted, additional crowders in the extracellular environment around the SQ injection or in the blood stream will help maintain the protein stability. Thus during the *in vivo* particle dissolution and distribution of 1B7 near the injection site, stabilizing crowders, either from the injection or naturally occurring within the body, reduce the number of aggregation-prone protein intermediates. Furthermore the fast dissolution kinetics will dilute the therapeutic protein and decrease the number of collisions that lead to the formation of aggregates. As the dissolved crowder is diluted upon injection, if individual protein molecules diffuse away from the nanocluster surface, as in the in-vitro experiments, stabilization by self-crowding will still be present in the

remaining protein molecules in the nanocluster. Preliminary immunogenicity studies support this conclusion as no propensity for the generation of anti-drug antibodies is detected in any sample (Figure A1.3.6). Therefore, with the result from the CHO assay, the protein particles from dispersion likely retain the native antibody state even after *in vivo* injection.

4.4 CONCLUSIONS

Nanocluster dispersions allow formulation of a monoclonal antibody at high concentration and low viscosity, with no detectable loss in antibody structure or activity *in vitro* or in vivo and similar pharmacokinetics when administered subcutaneously to mice. Highly concentrated ~200 mg/ml aqueous-based dispersions of a therapeutically relevant antibody, 1B7[37], were formed from stable, submicron protein particles containing a 1:1 weight ratio of trehalose in an aqueous buffer with multiple crowding agents, including trehalose, PEG and NMP. These particles were produced by rapid freezing in a dosage vial using spiral-wound in-situ film technology (SWIFT) to minimize protein denaturation and aggregation. The solubility of 1B7 was lowered in the aqueous-based solvent by adding pharmaceutically acceptable crowding agents, PEG300 and NMP, along with the trehalose from the dry powder to facilitate formation of the dispersion. The protein particles retain their native conformation in the dispersion as shown by fluorescence of the tryptophan residues on the protein. Additional analyses, ELISA, DLS and SDS-PAGE upon dilution of the dispersion into a pure buffer, indicate that the protein rapidly recovers monomeric form with full activity. The apparent viscosity through a 25 g 1.5” needle of the 190 mg/ml IgG dispersion with NMP and PEG was only 24 cP, as a consequence of the starting solution viscosity below 2 cP and

the low intrinsic viscosity. Similar *in vivo* distribution and elimination half-lives were measured from the dispersion and solution formulations at similar doses, while the time to peak serum concentration (t_{max}) was delayed for the SQ injections, consistent with the expected slower diffusion kinetics from this injection site. Remarkably, in the terminal serum samples, testing for specific PTx binding activity by ELISA, as well as an *in vitro* PTx neutralization test, was unable to detect a loss in 1B7 activity or development of anti-1B7 immune responses. In combination with previous work with sheep IgG[19] and 1B7[33], the mechanism of excluded volume from crowding agents, which results in formation of reversible nanoclusters of stable protein that dissociate upon dilution, is shown to be applicable for multiple IgG proteins with multiple crowding agents, demonstrating flexibility in formulation for other therapeutic proteins. The ability to form stable, highly concentrated dispersions of a protein therapeutic with low viscosities and favorable bioavailability will increase the potential use of subcutaneous injection, possibly for treatment of many chronic diseases.

4.5 REFERENCES

1. Yang, M. X.; Shenoy, B.; Disttler, M.; Patel, R.; McGrath, M.; Pechenov, S.; Margolin, A. L., Crystalline monoclonal antibodies for subcutaneous delivery. *PNAS* **2003,** 100, (12), 6934-6939.

2. Reichert, J. M.; Rosensweig, C. J.; Faden, L. B.; Dewitz, M. C., Monoclonal antibody successes in the clinic. *Nature Biotechnology* **2005,** 23, (9), 1073-1078.

3. Reichert, J. M., Probabilities of success for antibody therapeutics. *mAbs* **2009,** 1, (4), 387-389.

4. Nelson, A. L.; Dhimolea, E.; Reichert, J. M., Development trends for human monoclonal antibody therapeutics. *Nat Rev Drug Disc* **2010,** 9, 767-774.

5. Trevino, S. R.; Scholtz, J. M.; Pace, C. N., Measuring and increasing protein solubility. *J Pharm Sci* **2008,** 97, (10), 4155-4166.

6. Chennamsetty, N.; Voynov, V.; Kayser, V.; Helk, B.; Trout, B. L., Design of therapeutic proteins with enhanced stability. *PNAS* **2009,** 106, (29), 11937-11942.

7. Maynard, J. A.; Maassen, C. B. M.; Leppla, S. H.; Brasky, K.; Patterson, J. L.; Iverson, B. L.; Georgiou, G., Protection against anthrax toxin by recombinant antibody fragments correlates with antigen affinity. *Nature Biotechnology* **2002,** 20, 597-601.

8. Frokjaer, S.; Otzen, D. E., Protein Drug Stability: A Formulation Challenge. *Nat. Rev. Drug Discovery* **2005,** 4, 298-306.

9. *RITUXAN® (Rituximab) full prescribing information*; Genentech, Inc.: 2010.

10. Shire, S. J.; Shahrokh, Z.; Liu, J., Challenges in the Development of High Protein Concentration Formulations. *J. Pharm. Sci.* **2004,** 93, (6), 1390-1402.

11. Dani, B.; Platz, R.; Tzannis, S. T., High Concentration Formulation Feasibility of Human Immunoglubulin G for Subcutaneous Administration. *J. Pharm. Sci.* **2007,** 96, (6), 1504-1517.

12. Neal, B. L.; Asthagiri, D.; Lenhoff, A. M., Molecular Origins of Osmotic Second Virial Coefficients of Proteins. *Biophys J* **1998,** 75, 2469-2477.

13. Chi, E. Y.; Krishnan, S.; Kendrick, B. S.; Chang, B. S.; Carpenter, J. F.; Randolph, T. W., Roles of conformational stability and colloidal stability in the aggregation of recombinant human granulocyte colony-stimulating factor. *Protein Science* **2003,** 12, 903-913.

14. Harn, N.; Allan, C.; Oliver, C.; Middaugh, C. R., Highly Concentrated Monoclonal Antibody Solutions: Direct Analysis of Physical Structure and Thermal Stability. *J. Pharm. Sci.* **2007,** 96, (3), 532-546.

15. Young, T. M.; Roberts, C. J., Structure and thermodynamics of colloidal protein cluster formation: Comparison of square-well and simple dipolar models. *J Chem Phys* **2009,** 131, 125104.

16. Liu, J.; Nguyen, M. D. H.; Andya, J. D.; Shire, S. J., Reversible Self-Association Increases the Viscosity of a Concentrated Monoclonal Antibody in Aqueous Solution. *J. Pharm. Sci.* **2005,** 94, (9), 1928-1940.

17. Sear, R. P., Interactions in protein solutions. *Current Opinion in Colloid & Interface Science* **2006,** 11, 35-39.

18. Curtis, R. A.; Prausnitz, J. M.; Blanch, H. W., Protein-Protein and Protein-Salt Interactions in Aqueous Protein Solutions Containing Concentrated Electrolytes. *Biotechnology and Bioengineering* **1998,** 57, (1), 11-21.

19. Miller, M. A.; Wilson, B.; Vier, D.; Rodrigues, M.; Ferrer, D. A.; Maynard, J. A.; Johnston, K. P., Weakly interacting nanoclusters of stabe protein at high concentration. **in preparation**.

20. Scherer, T. M.; Liu, J.; Shire, S. J.; Minton, A. P., Intermolecular Interactions of IgG1 Monoclonal Antibodies at High Concentrations Characterized by Light Scattering. *J Phys Chem B* **2010,** 114, 12948-12957.

21. Kendrick, B. S.; Carpenter, J. F.; Cleland, J. L.; Randolph, T. W., A transient expansion of the native state precedes aggregation of recombinant human interferon-γ. *PNAS* **1998,** 95, 14142-14146.

22. Wang, W.; Nema, S.; Teagarden, D., Protein aggregation- Pathways and influencing factors. *Int J Pharm* **2010,** 390, (2), 89-99.

23. Miller, M. A.; Engstrom, J. D.; Ludher, B. S.; Johnston, K. P., Low Viscosity Highly Concentrated Injectable Nonaqueous Suspensions of Lysozyme Microparticles. *Langmuir* **2010,** 26, (2), 1067-1074.

24. Defelippis, M. R.; Akers, M. J., Peptides and Proteins as Parenteral Suspensions: an Overview of Design, Development, and Manufacturing Considerations. In *Pharmaceutical Formulation Development of Peptides and Proteins*, Frokjaer, S.; Hovgaard, L., Eds. Taylor & Francis Limited: Philadelphia, 2000; pp 113-143.

25. Shenoy, B.; Wang, Y.; Shan, W.; Margolin, A. L., Stability of Crystalline Proteins. *Biotechnology and Bioengineering* **2001,** 73, (5), 358-369.

26. Foster, T. P.; Moseley, W. M.; Caputo, J. F.; Alaniz, G. R.; Leatherman, M. W.; Yu, X.; Claflin, W. H.; Reeves, D. R.; Cleary, D. L.; Zantello, M. R.; Krabill, L. F.; Wiest, J. R., Sustained elevated serum somatotropin concentrations in Holstein steers following subcutaneous delivery of a growth hormone releasing factor analog dispersed in water, oil or microspheres. *J. Controlled Release* **1997,** 47, 91-99.

27. Putney, S. D.; Burke, P. A., Improving protien therapeutics with sustained-release formulations. *Nature Biotechnology* **1998,** 16, 153-157.

28. Fu, K.; Klibanov, A. M.; Langer, R., Protein stability in controlled-release systems. *Nature Biotechnology* **2000,** 18, 24-25.

29. Zhu, G.; Mallery, S. R.; Schwendeman, S. P., Stabilization of proteins encapsulated in injectable poly(lactide-co-glycolide). *Nature Biotechnology* **2000,** 18, 52-57.

30. Gombotz, W. R.; Pettit, D. K., Biodegradable Polymers for Protein and Peptide Drug Delivery. *Bioconjugate Chem.* **1995,** 6, (4), 332-351.

31. Ye, M.; Kim, S.; Park, K., Issues in long-term protein delivery using biodegradable microparticles. *J Controlled Release* **2010,** 146, (2), 241-260.

32. Singh, M.; Li, X.-M.; McGee, J. P.; Zamb, T.; Koff, W.; Wang, C. Y.; O'Hagan, D. T., Controlled release microparticles as a single dose hepatitis B vaccine: evaluation of immunogenicity in mice. *Vaccine* **1997,** 15, (5), 475-481.

33. Miller, M. A.; Borwankar, A.; Khan, T.; Dinin, A.; Kaczorowski, K. J.; Wilson, B.; Truskett, T. M.; Maynard, J. A.; Johnston, K. P., Concentrated active protein by crowding into clusters. **in preparation**.

34. Cheung, J. K.; Truskett, T. M., Coarse-Grained Strategy for Modeling Protein Stability in Concentrated Solutions. *Biophys J* **2005,** 89, 2372-2384.

35. Shen, V. K.; Cheung, J. K.; Errington, J. R.; Truskett, T. M., Insights into Crowding Effects on Protein Stability from Coarse-Grained Model. *Journal of Biomechanical Engineering* **2009,** 131, 071002 (7pg).

36. Sato, H.; Ito, A.; Chiba, J.; Sato, Y., Monoclonal antibody against pertussis toxin: effect on toxin activity and pertussis infections. *Infect Immun* **1984,** 46, 422-428.

37. Sutherland, J. N.; Maynard, J. A., Characterization of a Key Neutralizing Epitope on Pertussis Toxin Recognized by Monoclonal Antibody 1B7. *Biochemistry* **2009,** 48, 11982-11993.

38. Webb, S. D.; Cleland, J. L.; Carpenter, J. F.; Randolph, T. W., Effects of Annealing Lyophilized and Spray-Lyophilized Formulations of Recombinant Human Interferon-γ. *J Pharm Sci* **2003,** 92, (4), 715-729.

39. Engstrom, J. D.; Simpson, D. T.; Cloonan, C.; Lai, E. S.; Williams III, R. O.; Kitto, G. B.; Johnston, K. P., Stable high surface area lactate dehydrogenase particles produced by spray freezing into liquid nitrogen. *European Journal of Pharmaceutics and Biopharmaceutics* **2007,** 65, 163-174.

40. Engstrom, J. D.; Lai, E. S.; Ludher, B. S.; Chen, B.; Milner, T. E.; Williams, R. O., III; Kitto, G. B.; Johnston, K. P., Formation of Stable Submicron Protein Particles by Thin Film Freezing. *Pharm. Res.* **2008,** 25, (6), 1334-1346.

41. Ryoo, W.; Webber, S. E.; Johnston, K. P., Water-in-Carbon Dioxide Microemulsions with Methylated Branched Hydrocarbon Surfactants. *Ind. Eng. Chem. Res.* **2003,** 42, 6348-6358.

42. Garidel, P.; Hegyi, M.; Bassarab, S.; Weichel, M., A rapid, sensitive and economical assessment of monoclonal antibody conformational stability by intrinsic tryptophan fluorescence spectroscopy. *Biotechnol. J.* **2008,** 3, 1201-1211.

43. Giteau, A.; Venier-Julienne, M.-C.; Marchal, S.; Courthaudon, J.-L.; Sergent, M.; Montero-Menei, C.; Verdier, J.-M.; Benoit, J.-P., Reversible protein precipitation to ensure stability during encapsulation within PLGA microspheres. *Eur. J. Pharm. Biopharm.* **2008,** 70, 127-136.

44. Sutherland, J. N.; Yoder, S. M.; Rock, M. T.; Maynard, J. A., Antibodies recognizing protective pertussis toxin epitopes are preferentially elicited by natural infection versus acellular immunization. **in preparation**.

45. Gillenius, P.; Jaatmaa, E.; Askelof, P.; Granstrom, M.; Tiru, M., The standardization of an assay for pertussis toxin and antitoxin in microplate culture of Chinese hamster ovary cells. *Journal of Biological Standardization* **1985,** 13, 61-66.

46. Maa, Y.-F.; Prestrelski, S. J., Biopharmaceutical powders: particle formation and formulation considerations. *Current Pharmaceutical Biotechnology* **2000,** 1, 283-302.

47. Engstrom, J. D.; Simpson, D. T.; Lai, E. S.; Williams III, R. O.; Johnston, K. P., Morphology of protein particles produced by spray freezing of concentrated solutions. *European Journal of Pharmaceutics and Biopharmaceutics* **2007,** 65, 149-162.

48. Carpenter, J. F.; Chang, B. S.; Randolph, T. W., Physical Damage to Proteins During Freezing, Drying and Rehydration. In *Lyophilization of Biopharmaceuticals*, Costantino, H. R.; Pikal, M. J., Eds. AAPS Press: 2005; pp 423-442.

49. Chen, B.; Bautista, R.; Yu, K.; Zapata, G. A.; Mulkerrin, M. G.; Chamow, S. M., Influence of Histidine on the Stability and Physical Properties of a Fully Human Antibody in Aqueous and Solid Forms. *Pharm. Res.* **2003,** 20, (12), 1952-1960.

50. Harn, N.; Spitznagel, T.; Perkins, M.; Allan, C.; Shire, S.; Middaugh, C. R., Biophysical Signatures of Monoclonal Antibodies. In *Current Trends in Monoclonal*

Antibody Development and Manufacturing, Shire, S. J., Ed. DOI 10.1007/978-0-387-76643-0_14: 2010; pp 229-246.

51. Souillac, P. O.; Middaugh, C. R.; Rytting, J. H., Investigation of protein/carbohydrate interactions in the dried state. 2. Diffuse reflectance FTIR studies. *Int J Pharm* **2002,** 235, 207-218.

52. Wang, B.; Tchessalov, S.; Warne, N. W.; Pikal, M. J., Impact of Sucrose level on Storage Stability of Proteins in Freeze-Dried Solids: I. Correlation of Protein-Sugar Interaction with Native Structure Preservation. *J Pharm Sci* **2009,** 98, (9), 3131-3144.

53. Timasheff, S. N., Stabilization of Protein Structure by Solvent Additives. In *Stability of Protein Pharmaceuticals: Part B.*, Ahern, T. J.; Manning, M. C., Eds. Springer: 1992; Vol. 3, pp 265-285.

54. Carpenter, J. F.; Crowe, J. H., The Mechanism of Cryoprotection of Proteins by Solutes. *Cryobiology* **1988,** 25, (3), 244-255.

55. Allison, S. D.; Chang, B. S.; Randolph, T. W.; Carpenter, J. F., Hydrogen Bonding between Sugar and Protein is Responsible for Inhibition of Dehydration-Induced Protein Unfolding. *Archives of Biochemistry and Biophysics* **1999,** 365, (2), 289-298.

56. Yu, Z.; Johnston, K. P.; Williams III, R. O., Spray freezing into liquid versus spray-freeze drying: Influence of atomization on protein aggregation and biological activity. *Eur. J. Pharm. Sci.* **2006,** 27, 9-18.

57. Kueltzo, L. A.; Wang, W.; Randolph, T. W.; Carpenter, J. F., Effects of Solution Conditions, Processing Parameters and Container Materials on Aggregation of a Monoclonal Antibody during Freeze-Thawing. *Journal of Pharmaceutical Sciences* **2008,** 97, (5).

58. Costantino, H. R.; Langer, R.; Klibanov, A. M., Moisture-Induced Aggregation of Lyophilized Insulin. *Pharm Res* **1994,** 11, (1), 21-29.

59. Jossang, T.; Feder, J.; Rosenqvist, E., Photon Correlation Spectroscopy of Human IgG. *Journal of Protein Chemistry* **1988,** 7, (2), 165-171.

60. Zaharoff, D. A.; Barr, R. C.; Li, C.-Y.; Yuan, F., Electromobility of plasmid DNA in tumor tissues during electric field-mediated gene delivery. *Gene Therapy* **2002,** 9, 1286-1290.

61. Yadav, S.; Liu, J.; Shire, S. J.; Kalonia, D. S., Specific Interactions in High Concentration Antibody Solutions Resulting in High Viscosity. *J Pharm Sci* **2010,** 99, (3), 1152-1168.

62. Kulkarni, A. M.; Dixit, N. M.; Zukoski, C. F., Ergodic and non-ergodic phase transitions in globular protein suspensions. *Farady Discuss.* **2003,** 123, 37-50.

63. Lu, P. J.; Zaccarelli, E.; Ciulla, F.; Schofield, A. B.; Sciortino, F.; Weitz, D. A., Gelation of particles with short-range attraction. *Nature* **2008,** 453, 499-503.

64. Boncina, M.; Rescic, J.; Vlachy, V., Solubility of Lysozyme in Polyethylene Glycol-Electrolyte Mixtures: The Depletion Interaction and Ion-Specific Effects. *Biophys. J.* **2008,** 95, 1285-1294.

65. Shulgin, I. L.; Ruckenstein, E., Preferential hydration and solubility of proteins in aqueous solutions of polyethylene glycol. *Biophysical Chemistry* **2006,** 120, 188-198.

66. Hiemenz, P. C.; Rajagopalan, R., *Principles of Colloid and Surface Chemistry*. 3rd ed.; Marcel Dekker, Inc.: New York, 1997; p 650.

67. Porcar, L.; Falus, P.; Chen, W.-R.; Faraone, A.; Fratini, E.; Hong, K.; Baglioni, P.; Liu, Y., Formation of the Dynamic Clusters in Concentrated Lyoszyme Protein Solutions. *J. Phys. Chem. Lett.* **2010,** 1, 126-129.

68. Lafleche, F.; Durand, D.; Nicolai, T., Association of Adhesive Spheres Formed by Hydrophobically End-Capped PEF. 1. Influence of the Presence of Single End-Capped PEO. *Macromolecules* **2003,** 36, 1331-1340.

69. Kanai, S.; Liu, J.; Patapoff, T. W.; Shire, S. J., Reversible Self-Association of a Concentrated Monoclonal Antibody Solution Mediated by Fab-Fab Interaction That Impacts Solution Viscosity. *J Pharm Sci* **2008,** 97, (10), 4219-4227.

70. Cantor, C. R.; Schimmel, P. R., *BioPhysical Chemistry. Part II: Techniques for the Study of Biological Structure and Function*. W. H. Freeman and Company: San Francisco, 1980; p 846.

71. Saluja, A.; Kalonia, D. S., Nature and consequences of protein-protein interactions in high protein concentration solutions. *Int. J. Pharm.* **2008,** 358, 1-15.

72. Gabrielson, J. P.; Brader, M. L.; Pekar, A. H.; Mathis, K. B.; Winter, G.; Carpenter, J. F.; Randolph, T. W., Quantitation of Aggregate Levels in a Recombinant Humanized Monoclonal Antibody Formulation by Size-Exclusion Chromatography,

Asymmetrical Flow Field Flow Fractionation, and Sedimentation Velocity. *J Pharm Sci* **2007,** 96, (2), 268-279.

73. Maas, C.; Hermeling, S.; Bouma, B.; Jiskoot, W.; Gebbink, M. F., A role for protein misfolding in immunogenicity of biopharmaceuticals. *J Biol Chem* **2007,** 282, (4), 2229-2236.

74. Cheung, M. S.; Klimov, D.; Thirumalai, D., Molecular crowding enhances native state stability and refolding rates of globular proteins. *PNAS* **2005,** 102, (13), 4753-4758.

75. Pincus, D. L.; Thirumalai, D., Crowding Effects on the Mechanical Stability and Unfolding Pathways of Ubiquitin. *J Phys Chem B* **2009,** 113, 359-368.

76. Desai, U. R.; Klibanov, A. M., Assessing the Structural Integrity of a Lyophilized Protein in Organic Solvents. *J Am. Chem. Soc.* **1995,** 117, 3940-3945.

77. Roberts, C. J.; Debenedetti, P. G., Engineering Pharmaceutical Stability with Amorphous Solids. *AIChE Journal* **2002,** 48, (6), 1140-1144.

78. Krishnan, S.; Chi, E. Y.; Webb, J. N.; Chang, B. S.; Shan, D.; Goldenberg, M.; Manning, M. C.; Randolph, T. W.; Carpenter, J. F., Aggregation of Granulocyte Colony Stimulating Factor under Physiological Conditions: Characterization and Thermodynamic Inhibition. *Biochemistry* **2002,** 41, 6422-6431.

79. Webb, S. D.; Cleland, J. L.; Carpenter, J. F.; Randolph, T. W., A New Mechanism for Decreasing Aggregation of Recombinant Human Interferon-gamma by a Surfactant: Slowed Dissolution of Lyophilized Formulations in a Solution Containing 0.03% Polysorbate 20. *Journal of Pharmaceutical Sciences* **2002,** 91, (2), 543-558.

80. Zhou, H.-X.; Rivas, G.; Minton, A. P., Macromolecular Crowding and Confinement: biochemical, biophysical and potential physiological consequences. *Annu. Rev. Biophys.* **2008,** 37, 375-397.

81. Wang, W.; Wang, E. Q.; Balthasar, J. P., Monoclonal Antibody Pharmacokinetics and Pharmacodynamics. *Clinical Pharmacology & Therapeutics* **2008,** 84, 548-558.

82. O'Connor, T. F.; Debenedetti, P. G.; Carbeck, J. D., Stability of proteins in the presence of carbohydrates; experiments and modeling using scaled particle theory. *Biophysical Chemistry* **2007,** 127, 51-63.

Chapter 5: Flocculated Amorphous Itraconazole Nanoparticles for Enhanced in vitro Supersaturation and in vivo Bioavailability

Rapid flocculation of nanoparticle dispersions of a poorly water soluble drug, itraconazole (Itz), was utilized to produce amorphous powders with desirable dissolution properties for high bioavailability in rats. Antisolvent precipitation (AP) was utilized to form Itz nanodispersions with high drug loadings stabilized with hydroxypropylmethylcellulose (HPMC) or the pH-sensitive Eudragit® L100-55 (EL10055). The HPMC dispersions were flocculated by desolvating the polymer through the addition of a divalent salt, and the enteric EL10055 by reducing the pH. The formation of open flocs by essentially diffusion limited aggregation, facilitated redispersion of the flocs at pH 6.8. Upon redispersion of the flocculated nanoparticles at pH 6.8, the particle size was modestly larger than the original size, on the order of 1 μm. High *in vitro* supersaturation (AUC) of the flocculated nanoparticle dispersions was observed in micellar media at pH 6.8, after 2 hours initial exposure at pH 1.2 to simulate the stomach, relative to the AUC for a commercially available solid dispersion Itz formulation, Sporanox. Greater *in vivo* bioavailability in rats was correlated directly to the higher *in vitro* AUC at pH 6.8 with micelles during the pH shift experiment for the flocculated nanoparticle dispersions relative to Sporanox. The ability to generate and sustain high supersaturation in micellar media at pH 6.8, as shown with the *in vitro* pH shift dissolution test, is beneficial for increasing bioavailability of Itz by oral delivery.

5.1 INTRODUCTION

A major challenge in oral drug delivery is the low bioavailability of poorly-water soluble therapeutics.[1-3] Two known mechanisms to increase the bioavailability of poorly-water soluble drugs are to increase the surface area and to create stable amorphous particles. A higher surface area increases dissolution rates, while an amorphous form of the drug allows for high supersaturation in a metastable state relative to the crystalline equilibrium solubility.[4-6] From configurational heat capacities of the amorphous state, predictions indicate that supersaturation for amorphous drugs may reach as high as 1,600 times the crystalline solubility.[6-9] Increases in supersaturation have also been found to lead to greater flux through biomembranes further increasing the bioavailability of the drug.[10, 11] Amorphous solid solutions and dispersions have been created by numerous techniques including co-grinding[12], solvent evaporation[13-16], hot-melt extrusion[17, 18], and antisolvent precipitation[5]. Many of these amorphous forms are stabilized against crystallization during formation, storage and dissolution with high quantities (>50% of the formulation) of polymers such as hydroxypropylmethylcellulose (HPMC) and poly(vinylpyrolidone).[6-8, 12, 13, 15, 19-22]

In previous work, dispersions with high surface areas produced by antisolvent precipitation (AP), up to 50 m^2/g, rapidly dissolve to high supersaturations close to the predicted supersaturation from the configurational heat capacity.[5, 6] These formulations also increase the drug to polymer ratio able to form a stable amorphous formulation (less than 15% excipients).[5, 6] What remains a formidable challenge for AP and other methods

used to produce aqueous dispersions of particles is the ability to recover the particles in the amorphous state as a dry powder. Common techniques include spray drying, ultrafiltration, and freeze drying. High processing temperatures near the glass transition (T_g) of the drug can increase the crystallinity of the recovered powder.[23] We have previously presented a method to rapidly flocculate with salt and filter the nanoparticle dispersions. During salt flocculation the overall volume fraction of solids is constant such that the flocs are formed rapidly prior to filtration. Otherwise, slow increases in the volume fraction of the particles during removal of water may cause irreversible coagulation of the particles.[23] The temperature was well below the T_g of the drug, which allows for the recovery of filtered and dried (at room temperature) stable amorphous particles.[23] However, in some cases the increase in salinity is not sufficient to reach the cloud point of the polymer at a reduced temperature; therefore there is a need to explore other methods to rapidly flocculate these amorphous nanoparticles. For example, in the case of polymers where a change in dissociation with pH influences solvation, the cloud point temperature can be readily accessible near room temperature. Previously, flocculation by electrostatic self-assembly of nanoparticles has been achieved from the addition of positively charged nanoparticles to a dispersion of strongly negatively charged nanoparticles.[24]

To better understand *in vivo* bioavailability of poorly water soluble drugs such as itraconaozle (Itz), a number of recent studies have explored the implications of high supersaturation values produced by amorphous drugs.[5, 23, 25-27] Previous experimental *in*

vitro dissolution tests have been performed based on sink conditions or high values of supersaturation relative to equilibrium crystalline solubility in a variety of medias to simulate the stomach, intestines or both.[5, 23, 25, 26, 28-31]. Many of these dissolution tests do not account for permeation. When an *in vivo* bioavailability study is run concurrently with the *in vitro* dissolution test, neither an increased rate of dissolution under sink conditions nor a higher maximum supersaturation value were found to correspond directly to an increase in bioavailability.[25, 26] To further complicate the correlation between an *in vitro* dissolution test and the *in vivo* bioavailability, the bioavailability measured for the same formulation may not change directly proportional to the dose administered to the animal[32, 33] or remain the same if the diet provided to the animal is changed prior to administration[32, 34, 35]. Future efforts to create more reliable *in vitro – in vivo* correlations will likely hinge on designing amorphous nanoparticles with better morphologies to provide greater control over the levels of superaturation values generated and maintained upon their dissolution.

For Itz, previous studies have indicated that the primary site of absorption is the proximal small intestine.[25, 26, 29] In the small intestine, the addition of bile salts and the change in pH from the stomach result in a slight decrease in solubility of Itz. However, if the bile salt micelles are neglected, an abrupt change of 3 orders of magnitude in solubility is predicted and seen experimentally.[36] Thus, micelles are an integral part of the overall solubility of Itz in the small intestines. Previous, supersaturated dissolution tests at pH 6.8 with the addition of sodium dodecyl sulfate (SDS) micelles of Itz and HPMC

dry powders, show that a surface area of 2-5 m^2/g was optimum for maintaining supersaturation over a 4 hour experiment. The higher area under the curve (AUC) for these experiments is due to the rapid generation of high supersaturation and the relatively slow subsequent growth of precipitate from solution by coagulation and condensation.[27]

The main objective of this study was to improve the oral delivery of the poorly water soluble drug, Itz by using amorphous dry powders formed by antisolvent precipitation (AP), which were then flocculated, filtered and dried at room temperature. Stable nanoparticles are coated with negatively charged EL10055 at a pH (pH 6.8) well above the pKa of the polymer (pH 5.5).[27] As previously reported for AP, the hydrophilic polymer is oriented towards the particle surface and provides steric stabilization at low levels, for example, high drug loadings up to 94%.[5] Rapid flocculation of the nanoparticle dispersion occurred upon decreasing the pH of the dispersion to 2.5 where the polymer was no longer charged. As in previous reports of nanoparticle dispersions flocculated with salt, the rapid and strong increase in interparticle attraction with the pH change caused essentially diffusion limited aggregation of the nanoparticle dispersion under constant volume fraction resulting in relatively large open flocs.[23, 27, 37] As for salt flocculation, crystallization of Itz was minimal, since the large flocs were rapidly filtered at room temperature.[23, 27] For the pH flocculated particles high drug loadings were maintained from AP through the flocculation and filtration process. Upon redispersion at pH 6.8, solvation of the enteric polymer results in only a slight increase in size of the EL10055 stabilized nanoparticles. An advantage of the pH flocculation process relative to

previous studies of flocculation with divalent salts, is the potential for a significant decrease in salt impurities in the final product.[23, 37]

A series of *in vitro* dissolution tests and an *in vivo* bioavailability study were used to compare flocculated amorphous Itz particle formulations, either formed by pH flocculation with EL10055, or by salt flocculation with HPMC, with a commercially marketed form of Itz, Sporanox®. The multiparticulate capsule form of Sporanox is produced by drug layering of Itz and HPMC onto sugar spheres which results in a 21% drug loading.[26] A pH shift dissolution test was established, starting at simulated stomach conditions (pH 1.2) for 2 hours, followed by a pH shift to small intestine conditions, pH 6.8. A micellar solution was utilized to simulate micelles formed with bile salts in the pH 6.8 media. The *in vivo* bioavailability for each formulation was compared with the AUC in the neutral media with micelles from the pH shift *in vitro* test at supersaturated conditions. The good *in vitro – in vivo* correlation suggests that the high initial supersaturation of Itz in the rat stomach and the properties of the supersaturated solutions in the intestines are captured reasonably well by the pH shift *in vitro* model.

5.2 MATERIALS AND METHODS

5.2.1 Materials

B.P. grade itraconazole (Itz) was purchased from Hawkins, Inc. (Minneapolis, MN). HPMC E5 (viscosity of 5 cP at 2% aqueous 25°C solution) grade was a gift from The Dow Chemical Corporation and methacrylic acid-ethyl acrylate copolymer (1:1 ratio), Eudragit® L100-55 (EL10055), was donated by Degussa Röhm America LLC

(Piscataway, NJ). Sporanox capsules were purchased from Janssen Pharmaceutica Products, L.P. (Titusville, NJ). Stabilized p.a. grade 1,3-dioxolane was obtained from Acros Organics (Morris Plains, NJ). HPLC grade acetonitrile (ACN) and HPLC grade methanol were used as received from Fisher Chemicals (Fairlawn, NJ). N. F. grade sodium taurocholate (NaTC) was purchase from Spectrum Chemical Mfg. Corp. (Gardena, CA). All other chemicals utilized in this study were ACS grade chemicals purchased from Fisher Chemicals.

5.2.2 Antisolvent Precipitation (AP) of Amorphous Itz

Antisolvent precipitation of Itz was used to produce nanoparticle dispersions of Itz stabilized by HPMC or EL10055. Deionized water (50 g) was used as the antisolvent phase into which 15 g of 1,3-dioxolane containing 3.3% (wt) Itz was injected to form a fine precipitate through a 19G syringe. For the HPMC stabilized dispersion, 0.25 g of HPMC was added to the deionized water prior to the addition of the dioxolane containing Itz, producing a final 2:1 ratio of Itz:HPMC as reported previously.[23, 27] For the EL10055 stabilized dispersion, 0.25 g of EL10055 was added to an aqueous pH 6.8 buffer composed of a 1:3 volume ratio of 0.2M tribasic sodium phosphate to 0.1N HCl, which was used in place of the 50g of deionized water as the antisolvent. Particle size was immediately quantified using the Malvern Mastersizer-S, as described below.

5.2.3 Flocculation to produce a Dry Powder

Immediately after the dispersion particle size was quantified, a desolvating solution was added. As previously described for the HPMC stabilized dispersions, 120 ml

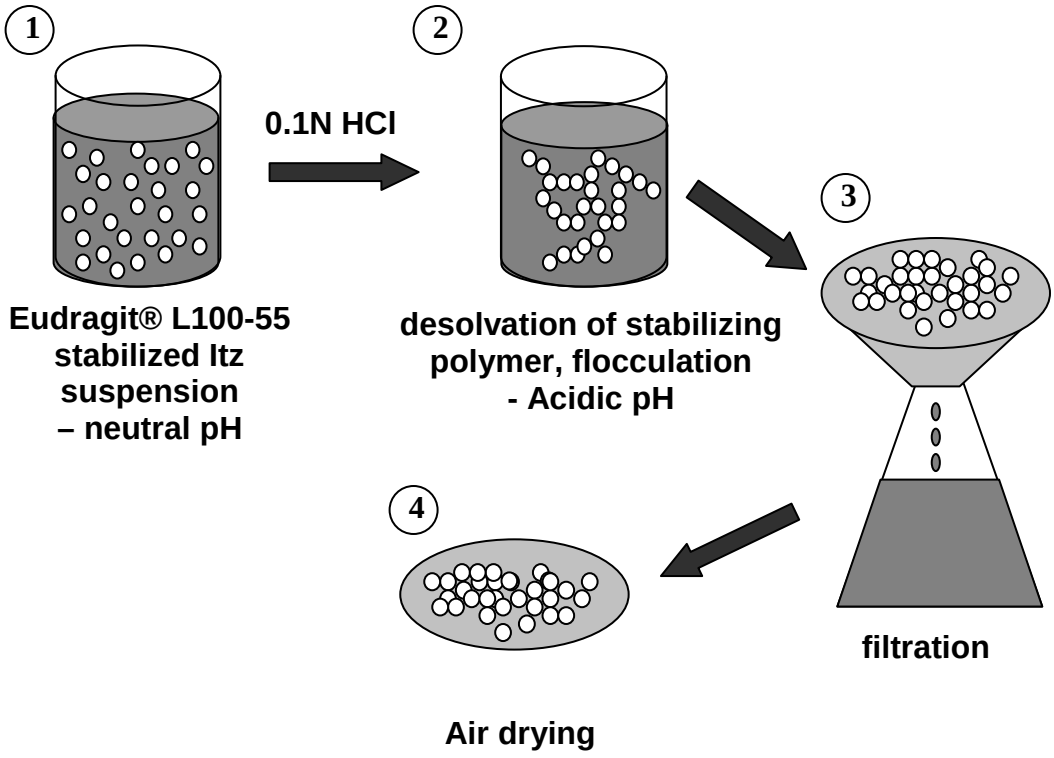

Figure 5.1 Schematic of the pH flocculation process to create particles by rapid flocculation (2), filtration (3) and drying (4).

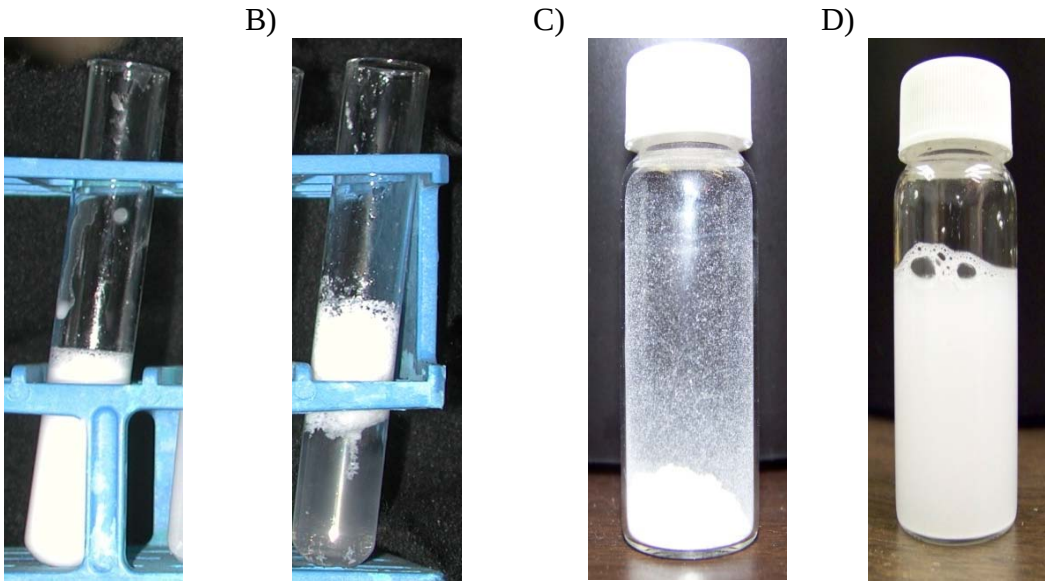

Figure 5.2 Images of the particles throughout the pH flocculation process: A) immediately after AP of ITZ with Eudragit®L100-55 stabilizer B) after flocculation and creaming by addition of HCl C) dried powder, scraped off the filter and placed in a vial D) resuspended suspension of ITZ particles stabilized by Eudragit®L100-55 in neutral pH DI water

of a 1.5M solution of Na_2SO_4 was added, producing a final SO_4^{-2} concentration of 1.0M in the mixture.[23, 27] For the EL10055 stabilized dispersion, 20 ml of 0.1N HCl was added to lower the pH of the final mixture to 2.5 ± 0.5 (Figure 5.1). In both cases, the dispersions sat for 3 minutes, allowing the flocculated dispersion to cream (Figures 5.1 and 5.2A and B). The large flocs were then filtered through an 11 cm diameter P2 filter paper (Fisher Scientific, Fairlawn, NJ) under vacuum. Filtration continued until no liquid was observed on top of the filter cake, typically between 5 and 10 minutes. The HPMC stabilized flocculated dispersion was then rinsed with a chilled solution of 5mg/ml HPMC, as described previously.[23, 27] The EL10055 stabilized flocculated dispersion was not rinsed. The filter cake was then allowed to dry overnight at atmospheric conditions after which the dried powder was obtained by gently scraping the filter paper (Figure 5.2C).

5.2.4 Determination of Particle Size and Morphology

Particle size distributions were measured by light scattering using a Malvern Mastersizer-S (Malvern Instruments Inc., Southborough, MA). For the particle dispersions, ~5 ml of the suspension was diluted with 500 ml of pure deionized water to produce an obscuration between 10-15%. For the dried powders, ~0.1g of the dried particles was added to 20 mL of DI water and sonicated for 1 minute using a Branson Sonifier 450 (Branson Ultrasonics Corporation, Danbury, CT) with a 102 converter and tip operated in pulse mode at 35 W. This suspension was then diluted into 500 ml of pure

deionized water to produce an obscuration between 10-15%. Distributions, based on volume fractions, were calculated using the refractive index of itraconazole (1.610 [38]).

Powder specific surface area was measured using a Quantichrome Instruments Nova 2000 series surface area analyzer (Boynton Beach, FL) using nitrogen as the adsorbate gas. Six points, taken over a range of relative pressures from 0.05 to 0.25, were used to fit with the Brunauer-Emmett-Teller (BET) equation to quantify the specific surface area of the powder. A correlation coefficient greater than 0.999 indicated a good linear fit to the data.

Approximate particle size and morphology was also determined by scanning electron microscopy (SEM). Immediately after AP, the organic phase was separated from the aqueous dispersion via vacuum distillation at 40 torr and 38°C. A few drops of the aqueous dispersion were then flash frozen onto aluminum SEM stages maintained at -200°C with liquid nitrogen. Lyophilization with 24 h. of primary drying at -35°C followed by 36h. of secondary drying at 25°C left a dried powder sample on the SEM stage. For dry powder samples, a small quantity was placed on adhesive carbon tape to form a thin film. All samples were gold-palladium sputter coated for 40 seconds. Micrographs were taken using a Hitachi S-4500 field emission scanning electron microscope with an accelerating voltage of 15 kV.

5.2.5 Determination of powder amorphous content

Dried powder samples of ~5 mg were placed in hermetically sealed aluminum pans in a 2920 modulated differential scanning calorimeter (mDSC) (TA Instruments,

New Castle, DE) with a refrigerated cooling system. The samples were purged with nitrogen at a flowrate of 150 ml/min. For temperatures from 20-200ºC, an amplitude of 1°C, a period of 1 min, and an underlying heating rate of 5°C/min were used to determine both total and reverse heat flow. The percent crystallinity ($\%_{cryst}$) was quantified by integration under the recrystallization peak around 120°C (Δh_{cryst}) and the melting endotherm around 168°C(Δh_{melt}) according to equation 5.1.

$$\%_{cryst} = \frac{\Delta h_{melt} - \Delta h_{cryst}}{\Delta h_{meltITZ}} \qquad (5.1)$$

$\Delta h_{meltITZ}$ is the heat of melting for pure crystalline ITZ. This equation assumes that the heat necessary to melt equivalent amounts of crystalline Itz and amorphous Itz are the same.

5.2.6 Drug and Salt Content Determination

The drug concentration of the final powder form was determined for the EL10055 samples by dissolving 3 separate ~10mg measured quantities of the powder. Each sample was dissolved in a solution of 14 ml ACN, 6 ml DI water, and 10 ml of methanol. After stirring the solutions overnight, 3 aliquots from each solution were taken and diluted by 2 with ACN. These 9 samples were then analyzed by HPLC for Itz concentration as described below. 3 samples of ~10 mg were also measured to determine salt content. These samples were exposed to 0.2ml of deionized water and shaken frequently for 2 weeks. The remaining powder was then filtered out using 0.2 μm syringe filter, and the solvent was tested for osmolarity using a μOsmette™ (Precision Systems, Inc. Natick,

MA) calibrated with 100 and 500 mOsmol standards. The drug and salt content determination for the HPMC samples was conducted as reported previously.[23]

5.2.7 Contact Angle Measurements

50 mg ± 1 mg of each dried powder was compacted with ~500 kg weight using a Model M Carver Laboratory Press (Fred S. Carver, Inc., Menomeonee Falls, WI) to form a flat sided pellet. Solutions of pH 1.2, pH 6.8 media, and pH 6.8 media with 0.17% SDS were made as described previously.[5, 23, 27] A media containing 30 mM (1.6wt%) NaTC was prepared in deionized water with the ionic strength of Na^+ ion adjusted to 0.1M with NaCl, as prepared by Crisp *et al.* and Bakatselou *et al.*[39, 40] A 10 µl drop of the solution was placed in the center of one side of the tablet and the contact angle was measured within 15 seconds using a contact angle goniometer, described previously for high pressure.[41] Briefly, the tablet was placed on a stand attached to an optical rail with a light source (Chiu Technical Corporation, model HG-DM) illuminating the solution droplet onto a Sony CCD camera (model XC-73CE) attached to a computer. The images were analyzed using a software package from KSV Instruments Ltd. (Helsinki, Finland) to estimate the air/water/tablet contact angle using the Young-Laplace method. Measurements were made in quadruplicate with the average and standard deviation reported. Sides where cracks or visible imperfections were observed were disregarded since they can dramatically alter the measured contact angle.

5.2.8 Dissolution under Supersaturated Conditions

Rates of supersaturation for metastable amorphous dry powder formulations were measured in pH 6.8 phosphate buffer with 0.17 % (*w/v*) SDS preheated to 37.2°C. The equilibrium crystalline solubility was 14 μg/ml in this media.[23] A sample weight equivalent to approximately 25-times the crystalline solubility (17.6 mg Itz) was added to 50 ml of the media. Sample aliquots (~1ml) were taken after 10, 20, 30, 60, 120, and 240 minutes, filtered and diluted for analysis. For the pH shift experiments, dry powder (10 mg Itz for the 45x acid supersaturation and 17.6 mg Itz for the 80x acid supersaturation) was added to 60 ml of 0.1N HCl (pH 1.2) and sample aliquots were taken after 10, 20, 30, 60, and 120 minutes. After 120 minutes, 20 ml of 0.2M tribasic sodium phosphate with or without 0.68% SDS added was added to shift the pH to ~6.8 and either 0 or 0.17% SDS. Sample aliquots were taken at 10, 20, 30, 60, and 120 minutes after the pH shift. For all dissolution experiments, the USP paddle method was adapted to accommodate small sample sizes using a ValKel VK6010 Dissolution Tester (VanKel, Cary, NC) equipped with small 100 ml capacity dissolution vessels (Varian Inc., Cary, NC) with a Vanderkamp VK650A heater/circulator (VanKel, Cary, NC). Each 0.8ml aliquot was filtered immediately using a 0.2 μm syringe filter and diluted with 0.8 ml of ACN. In all cases, the filtrate was completely clear upon visual inspection and dynamic light scattering of select samples of the filtrate gave negligible count rates. The drug concentration of each sample was quantified by HPLC as described below.

5.2.9 *In Vivo* Bioavailability in Sprague-Dawley Rats

An institutionally approved in vivo study was conducted using pre-catheterized (vascular catheter surgically inserted into the jugular vein) CD IGS Sprague-Dawley rats (Charles River Laboratories, Inc., Wilmington, MA). All rats received weighed ~300 g. For the duration of the study, the animals were stored in individual cages and subjected to 12h.-12h. cycles of light and darkness with access to food and water *ad libitum*. The catheter was flushed daily with 0.3ml of 50 U/ml heparinized normal saline. After an acclimatization period of at least 3 days, an aqueous dispersion of the engineered formulations at a dose of 15 mg Itz/kg body weight was administered by oral gavage to the rats (n=6 per formulation). Immediately prior to dosing, each formulation was dispersed in deionized water to a concentration of 4.5 mg Itz/ml to provide volumetric doses below 4 ml/kg body weight to prevent spontaneous release through the pyloric sphincter.[26, 42] The Sporanox control test was reported previously with other studies run concurrently.[26] The only difference between the *in vivo* tests was that the Sporanox® pellets were filled into a size 9 porcine gelatine capsule to achieve the target dose of 4.5 mg Itz per capsule and dosed using an oral capsule dosing syringe (Torpac, Inc., Fairfield, NJ) followed by administration of 200 µl of deionized water by oral gavage. Blood samples (~0.3 ml each) were withdrawn through the jugular vein catheter at 0, 2, 3, 3.5, 4, 4.5, 5, 5.5, 6, 8, 12, and 24 hours after dosing and replaced with an equal volume of heparinized saline. Blood samples were placed in pre-heparinized microcentrifuge tubes, where plasma was harvested by centrifugation of the blood at

3,000*g* for 15 minutes, transferred into a clean 1.5 ml microcentrifuge tube, and kept at -20°C until it was analyzed.

Calibration standards and plasma samples were analyzed as was previously reported.[29, 43, 44] In summary, upon thawing, a volume of harvested plasma was transferred to a clean 1.5 ml microcentrifuge tube. To each microcentrifuge tube, 50 µl of each 0.3N barium hydroxide and 0.4N zinc sulfate heptahydrate solution were added prior to vortex mixing for 30 seconds to precipitate water-soluble proteins. As an internal standard, 1 ml of ACN containing 1,200 ng/ml ketoconazole was added to each sample followed by an additional 1.5 minutes of vortex mixing. The samples were then centrifuged at 3,000*g* for 15 minutes. Afterwards, the supernatant was extracted and transferred to a clean 1.5 ml centrifuge tube and dried in an aluminum heat block at 70°C under a stream of nitrogen. The dried samples were then reconstituted with 250 µl of a 62% ACN: 38% 0.05M potassium phosphate monobasic buffer adjusted to pH 6.7 with NaOH (mobile phase for *in vivo* study). The reconstituted sample was vortex mixed for 1 minute and then centrifuged for an additional 15 minutes. A 150 µl aliquot of the supernatant was extracted and filled into a low volume HPLC vial insert and analyzed by HPLC as described below.

5.2.10 High Performance Liquid Chromatography (HPLC)

In vitro dissolution study samples and dissolved dried powders were analyzed for drug concentration using a Shimadzu LC-10 liquid chromatography (Shimadzu Corporation, Columbia, MD) with an Alltech 5 µm Inerstsil ODS-2 C18 reverse-phase

column (Alltech Associates, Itc., Deerfield, IL). The mobile phase of ACN/water/DEA 70:30:0.05 by volume set at a flowrate of 1 ml/min. Using a detection wavelength of 263 nm, the Itz peak eluted at ~5.5 min. The standard curve linearity was verified from 500 to 1 μg/ml with an r^2 value of at least 0.999 and reproducibility of replicate injections was within 2% relative standard deviation (RSD).

In vivo bioavailabilities were analyzed for drug concentration using a Waters HPLC system (Milford, MA) equipped with a photodiode array detector (Model 996), a model 717 Plus auto sampler, and the Empower® Version 5.0 software. A Phenomenex® Luna 5 μm C18(2) 100Å HPLC column (250x 4.6 mm) was used and maintained at 37°C for the duration of the injection set. The mobile phase was 62% ACN and 38% 0.05M potassium phosphate monobasic buffer adjusted to pH 6.7 with NaOH at an isocratic flowrate of 1 ml/min. Using the detection wavelength of 263nm and a sample injection volume of 100 μl, the retention times of ketoconazole and Itz were approximately 5.5 min and 14.7 min with limits of detection of 10ng/ml and 30 ng/ml, respectively. Each individual run maintained suitable limits for linearity ($r^2 \geq 0.999$) and reproducibility of replicate injections (% RSD $\leq$ 2.0%). Additional samples run concurrently are found in DiNunzio *et al.*[26]

5.2.11 Pharmacokinetic Analysis

Blood plasma concentrations were analyzed with WinNonlin v4.1 software (Pharsight Corporation, Mountain View, CA) using non-compartmental analysis for extravascular input. Specifically, T_{max} and C_{max} were determined directly from empirical

data, AUC was calculated by the linear trapezoidal method, and $t_{1/2}$ was determined by calculating the lambda z parameter. For statistical significance of the AUC, t_{max}, and c_{max} values, a t-test was performed using $p \leq 0.05$ as the criteria for statistical significance.

5.3 Results and Discussion

5.3.1 Particle Morphology of pH Flocculated Samples

Particle size and morphology for the EL10055 stabilized particles was determined before and after flocculation by light scattering, BET, and SEM. Prior to flocculation, ~300nm primary particles are observed in the SEM images (Figure 5.3a) and are consistent with the high specific surface area (35 m^2/g) measured by BET.[27] By light scattering in a pure aqueous environment without pH control, 90% of the particles (by volume) were between 1-4 μm with an average diameter of 2μm prior to flocculation. The pH of the dispersion diluted into pure water was between 5-6, where some of the methacrylic acid groups on the polymer will be protonated. The reduced charge stabilization of the nanoparticle dispersion results in slight aggregation of the particles. After flocculation and drying, the redispersed particles in distilled water have a slightly larger average particle diameter of ~ 5μm on the basis of light scattering. In the same manner, the slightly lower specific surface area (7.7 m^2/g) measured by BET corroborates the ~1 μm small nanoparticle aggregates visible on the SEM. Light scattering, BET surface area, and SEM all confirm that slight particle growth is observed between the initial nanoparticles formed by AP and the final dry powder after flocculation, filtration and drying. In the future, the particle size could be further controlled by studies in various

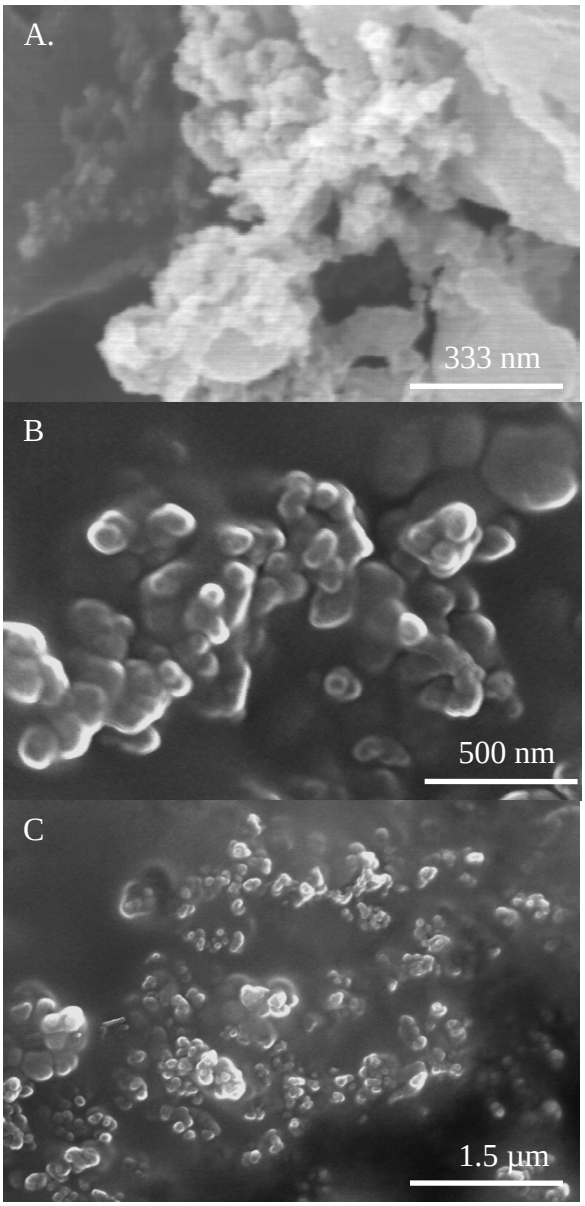

Figure 5.3 SEM of 2:1 Itz:Eudragit®L100-55 formulation: A) flash frozen and lyophilized immediately after precipitation B) and C) final particles formed after pH flocculation and drying at various magnifications

buffers at higher pH values where the particles are more fully charged. However, the current study clearly illustrates the behavior of the pH flocculation process, and the particles produced are shown to offer high supersaturation *in vitro* and enhanced bioavailability *in vivo*.

Open fractal flocs form upon rapid, diffusion limited flocculation of the nanoparticle dispersions under very poor solvent conditions.[23, 45] In the case of an EL10055 stabilized nanoparticle dispersion, poor solvent conditions occur upon lowering the pH well below the pKa of the polymer (pH 5.5), which results in protonation of the methacrylic acid groups. Almost instantaneous flocculation of the EL10055 stabilized nanoparticle dispersions is observed upon lowering the pH due to a change in turbidity. Previously reported HPMC stabilized and HPMC/poloxamer 407 stabilized Itz nanoparticle dispersions flocculated with salt were found to undergo similar rapid changes in turbidity.[23, 27] In the case of salt flocculated Itz/HPMC/poloxamer 407 dispersions, the fractal dimension of the floc (1.76) approaches that of open fractal flocs produced by rapid diffusion-limited aggregation (1.7).[23] The change in turbidity upon flocculation and the extent of creaming after flocculation at equal concentrations for the salt flocculated Itz/HPMC/poloxamer 407 dispersions and the pH flocculated EL10055 stabilized dispersions were similar. Open fractal flocs were produced in both cases. Upon returning the flocculated, filtered and dried nanoparticle dispersions to good solvent conditions at high pH, the polymer chains are recharged and the flocs break up into

dispersions of small particles. In contrast, denser flocs with a fractal dimension ~2.9 out of a maximum of 3 are produced by spray drying.[23] The denser flocs may not redisperse as effectively into primary particles during redispersion in drug delivery.[23]

Slight particle growth was observed for the pH flocculated EL10055 stabilized particles upon redispersion in pure water and by specific surface area and SEM particle size measurements following flocculation and filtration. Similar behavior has been reported previously for salt flocculated HPMC-stabilized particles upon redispersion.[27] However, no growth in particle size after flocculation and redispersion was seen when a combination of HPMC and poloxamer 407 polymer stabilizers were used.[23] Poloxamer 407 is a triblock copolymer consisting of a central hydrophobic block of polypropylene glycol surrounded by hydrophilic blocks of polyethylene glycol. When poloxamer 407 is used to stabilize the hydrophobic Itz domains, the drug nanoparticle will primarily associate with the more hydrophobic central block. Thus, the more hydrophilic end blocks will sterically stabilize the individual nanoparticle domains throughout the flocculation and filtration process.[27] In a similar manner, silica nanoparticles flocculated with crosslinked poly(N-vinylformamide) redisperse due to increased steric stabilization after hydrolysis of the crosslinking agent, bis[2,2'-di(N-vinylformamido)ethoxy] propane.[46] Both HPMC and EL10055, unlike poloxomer 407, associate with the individual nanoparticle domains over the entire length of the polymer. As a result, when the HPMC or EL10055 stabilized nanoparticles are desolvated by either addition of salt or change in pH, some of the Itz domains can irreversibly aggregate during the

flocculation and filtration process due to reduced steric stabilization. Thus, polymers can be chosen to tune the surface area and size of the final dry powder formulation.

As shown in Figure 2.4A, two separate glass transition temperatures are indicated for both a 2:1 and 4:1 ratio of Itz to EL10055. The first, at ~59°C, is consistent with that of pure itraconazole[31, 47], while the second, at ~105°C, is consistent with a solid solution of approximately 30% Itz in EL10055.[31] These two distinct glass transition temperatures indicate the formation of two separate phases, a polymer rich phase and a pure drug phase, consistent with previous AP formulations.[5, 23, 27] To further characterize the two distinct phases, the contact angle of the formulation is compared to that of the pure drug and polymers. The data indicate a characteristic contact angle for the formulations which was significantly closer to that of the pure polymer than pure Itz (Table 5.1). Thus, the exposed area of the final particles is primarily that of the polymer rich phase, which is also consistent with previous work with AP particles (Table 5.1).[5, 23] During particle formation, the hydrophilic polymer migrates towards the particle surface for favorable interactions with water. Thus, relatively small loading of polymer provide stabilization of the nanoparticles, unlike the case for more conventional solid dispersions.
Previously, mixtures of Itz and EL10055 have been found to produce solid solutions with Itz up to a drug loading of 70%.[31] Therefore, it is significant that AP followed by flocculation and drying produces particles containing two separate domains at ratios where a solid solution is still theoretically possible. This morphology will improve wetting over a solid solution when the polymer is soluble[5], as seen in the contact angle

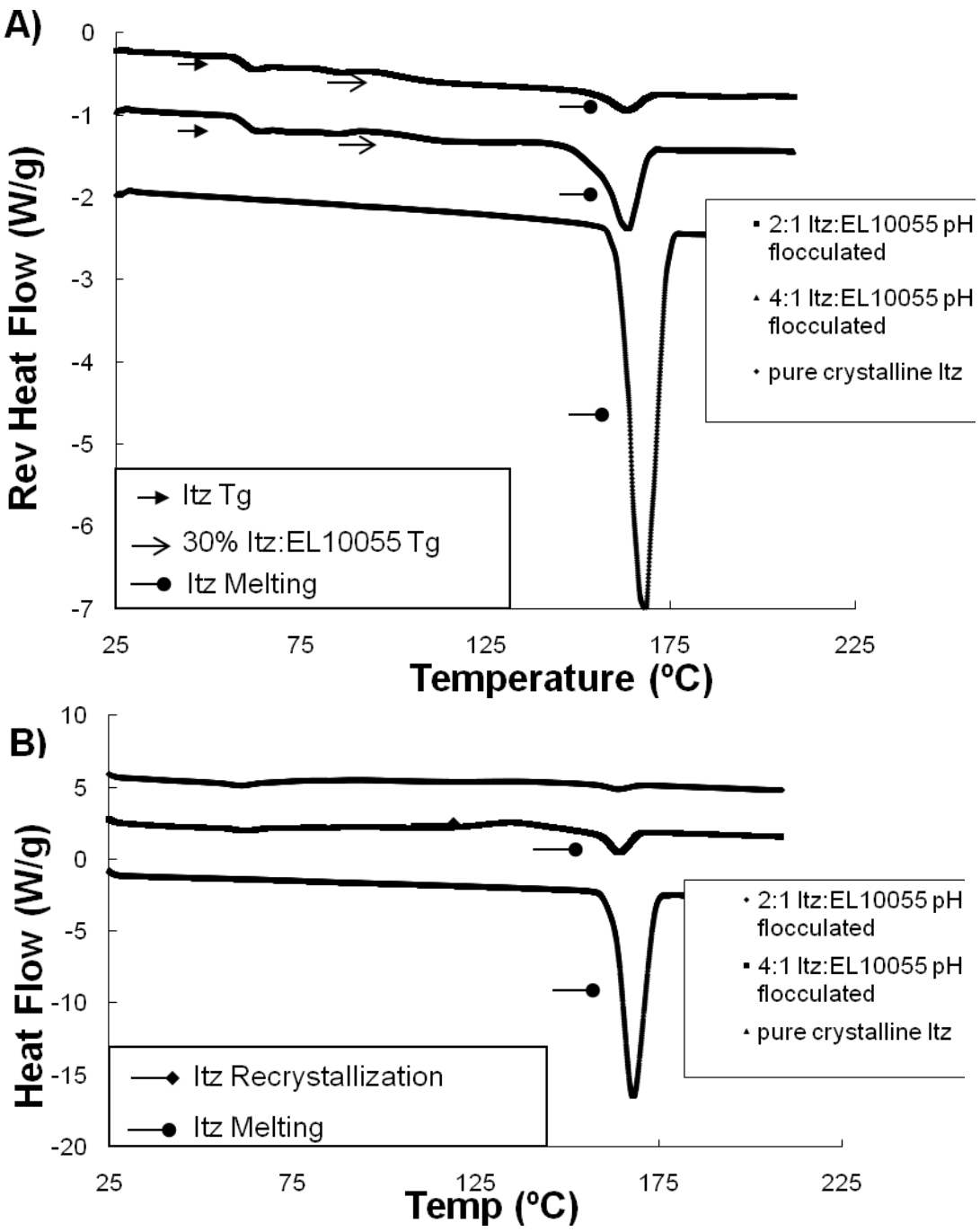

Figure 5.4 MDSC of pH flocculated formulations and pure Itz control: A) reverse heat flow B) total heat flow

Table 5.1 Contact angle of formulations in various media, pH 1.2, pH 6.8 pure buffer, pH 6.8 with SDS micelles, and pH 6.8 with NaTC micelles

Sample	**Media**	**Average Contact Angle**	**% RSD**
Micronized Itz	pH 1.2	109.9	9%
HPMC		100.9	5%
EL10055		67.4	6%
2:1 Itz: EL10055 pH flocculated		84.5	6%
2:1 Itz:HPMC salt flocculated		60.1	25%
Micronized Itz	pH 6.8 with no added surfactant	64.4	18%
HPMC		91.3	5%
EL10055		75.4	15%
2:1 Itz: EL10055 pH flocculated		76.1	16%
2:1 Itz:HPMC salt flocculated		83.2	7%
Micronized Itz	pH 6.8 with 0.17% SDS	47.1	13%
HPMC		78.3	5%
EL10055		37.3	15%
2:1 Itz: EL10055 pH flocculated		35.5	13%
2:1 Itz:HPMC salt flocculated		75.0	8%
Micronized Itz	30 mmol NaTC buffer	40.4	16%
HPMC		87.5	6%
EL10055		46.1	14%
2:1 Itz: EL10055 pH flocculated		46.3	11%
2:1 Itz:HPMC salt flocculated		60.5	9%

measurements in neutral media (Table 5.1). In addition, since the Itz domains are surrounded by a shell composed of mostly polymer, the enteric effect of the pH flocculated particles should be enhanced over pure solid solutions containing the same drug loading.

The amorphous nature of the pH flocculated and filtered particles is further confirmed by the small melting peaks observed in the DSC total heat flow measurements. The minor Itz melting peak for the 2:1 EL10055 stabilized pH flocculated formulation gave a $\%_{cryst}$ of 5%, indicating an almost fully amorphous Itz formulation. Since the 4:1 EL10055 stabilized pH flocculation formulation showed a recrystallization peak at ~125°C in addition to a melting peak at ~160°C, the $\%_{cryst}$ was determined to be even lower at ~3% by equation 1 (Figure 5.4B).

The low processing temperature (25°C) utilized in the pH flocculation process helps to preserve the amorphous morphology of Itz and reduces the excipients needed in the formulation. In hot-melt extrusion formulations, solutions formed with a methacrylate based polymer, such as EL10055, must use a plasticizing agent such as triethyl citrate to lower the processing temperature to 130°C.[25, 48] The use of these high temperatures during processing will cause partial crystallization of Itz during cooling, leading to lower dissolution and bioavailability. To prevent the partial crystallization of Itz, low drug to polymer ratios for hot-melt extrusion typically around 1:2, are used.[25] In contrast due to

room temperature processing during flocculation and filtration, much higher drug to polymer ratios (up to 4:1) can be used while retaining the amorphous nature of the Itz.

Recovery of particles after flocculation and drying was found to be near 100% as previously reported.[23] For the pH flocculated samples, the potency of the dried powder formed by flocculation and filtration according to HPLC remained at ~ 66% for the 2:1 ratio of drug to polymer initially added and 80% for the 4:1 ratio. Besides Itz and the polymer stabilizer, the only additional components present during AP flocculation, filtration and drying are the relatively dilute buffer ions, sodium, hydrogen phosphate and phosphate. To induce flocculation, hydrochloric acid was added with H and Cl concentrations of $10^{-2.5}$ M. The residual salt remaining in the dried formulation after flocculation and filtration, measured by osmolality was less than 0.15% even without washing. Most of the salt ions are presumed to be filtered out of the dry powder during the filtration step, as was observed previously for samples that were flocculated with salt.[23, 37] When compared to previous samples flocculated with a divalent salt with much higher ion concentrations of 1.5M, the residual salt present in the pH flocculated formulation is an order of magnitude lower.[23]

5.3.2 *In Vitro* Generation and Depletion of Supersaturation in Dissolution Media

To maintain the same initial ratio of drug to polymer, *in vitro* dissolution studies and the subsequent *in vivo* study were conducted with a 2:1 drug to polymer ratio for both the pH flocculated EL10055 and the HPMC stabilized salt flocculated formulation. Both of these Itz powders were also compared to the commercial Sporanox® formulation.

Dissolution experiments at supersaturated conditions were conducted by adding 25 times the crystalline solubility of Itz to pH 6.8 media with 0.17% SDS (sufficient to form micelles). In this media (Figure 5.5), all flocculated formulations produced supersaturation values greater than 7x (12-17x), the maximum supersaturation of the Sporanox® beads. The HPMC stabilized salt flocculated formulation obtained the highest maximum supersaturation at ~ 17x[27], followed by the EL10055 pH flocculated and lyophilized AP formulations both with ~ 12x. When the pH flocculated and the lyophilized AP formulations are compared, the decrease in the decay rate in supersaturation results in a higher overall AUC for the pH flocculated formulation versus the lyophilized AP formulation. This phenomena has also been observed for the salt flocculated HPMC sample when compared to an HPMC stabilized lyophilized control at the same drug to polymer ratio.[27]

As described in detail previously, the micron-sized flocculated particles have been found to produce an overall higher AUC in pH 6.8 media with SDS micelles versus higher surface area AP lyophilized nanoparticles.[27] The higher AUC is a manifestation of the negligible change in the maximum supersaturation followed by a dramatic decrease in the rate of heterogeneous nucleation and growth out of the supersaturated solution.[27] Significantly larger microparticles are not shown to increase the overall AUC due to the low surface area available for initial supersaturation. Previously, large 100 μm particles are shown to crystallize during the slow dissolution given their low surface areas.[7] The solvent mediated crystallization of the large amorphous particles lowers solubilities

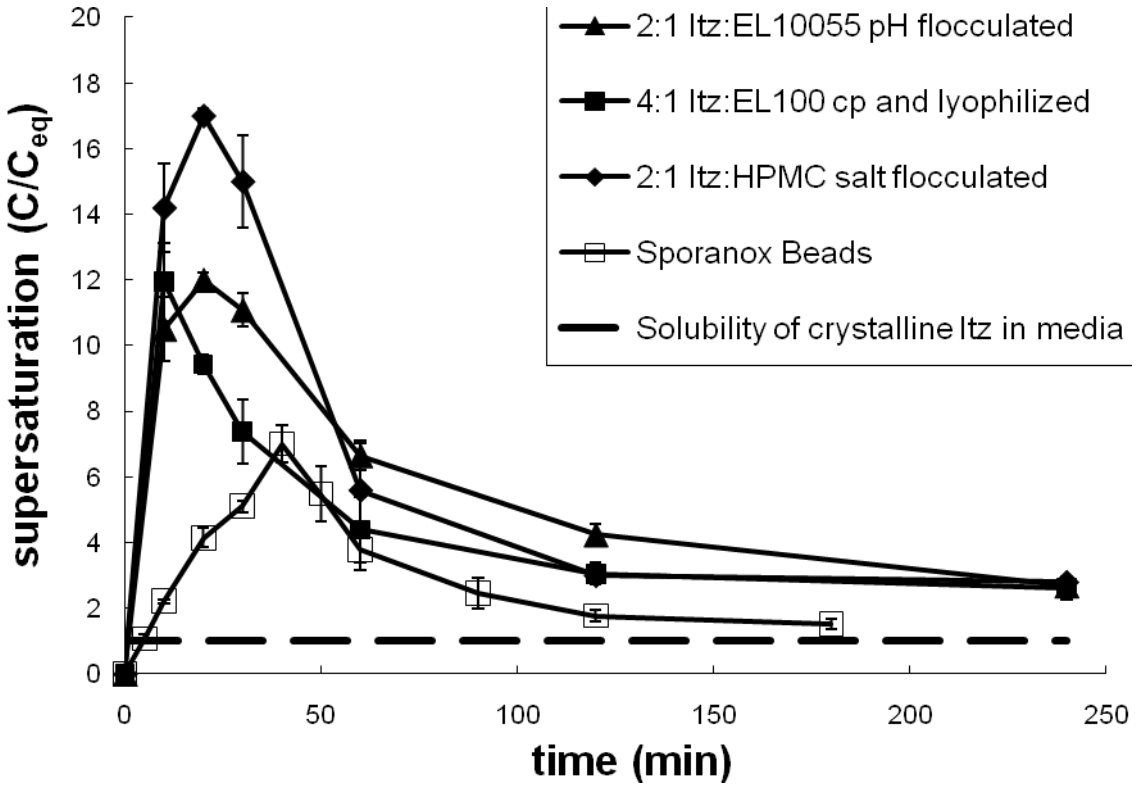

Figure 5.5 Dissolution of drug formulations (pH flocculated, salt flocculated[27], and Eudragit lyophilized control[27]) and Sporanox® Bead control in pH 6.8 media with 0.17% SDS

markedly relative to the results predicted for the initial amorphous form from the configurational heat capacities.[6] The lower surface area particles decrease the available surface area for nucleation and growth after the maximum supersaturation has been achieved.[27] Thus, an optimum range of dry powder specific surface area of ~ 2-5 m^2/g has been shown to achieve the highest *in vitro* AUC in the pH6.8 media with SDS micelles.[27]

Additional experiments were performed to establish how the dissolution history of the formulation in the acidic media affected the depletion of supersaturation following a pH shift to neutral pH media with or without micelles. As shown in Figure 5.6A, the HPMC stabilized salt flocculated formulation rapidly supersaturated the acidic media at either loading (45x or 80x crystalline solubility) to the point where few particles were visible in the remaining solution. The maximum supersaturation achieved was 34x when 45x was loaded and 57x when 80x was loaded. When no micelles were present in the neutral pH media, the supersaturation obtained in the acid phase rapidly decayed in the first 10 minutes following the pH shift to a level below 1 μg/ml. This result was observed with hot melt extruded particles stabilized by HPMC E5 in previous work.[25, 30] When SDS micelles were added to the pH 6.8 media to simulate micelles in the intestines, the extent of supersaturation was maintained at ~8x for 2 hours for the initial loading of 45x. With the higher initial loading of Itz (80x in the acidic media), 7x the crystalline solubility in the pH 6.8 media with micelles remained solubilized for 2 hours beyond the

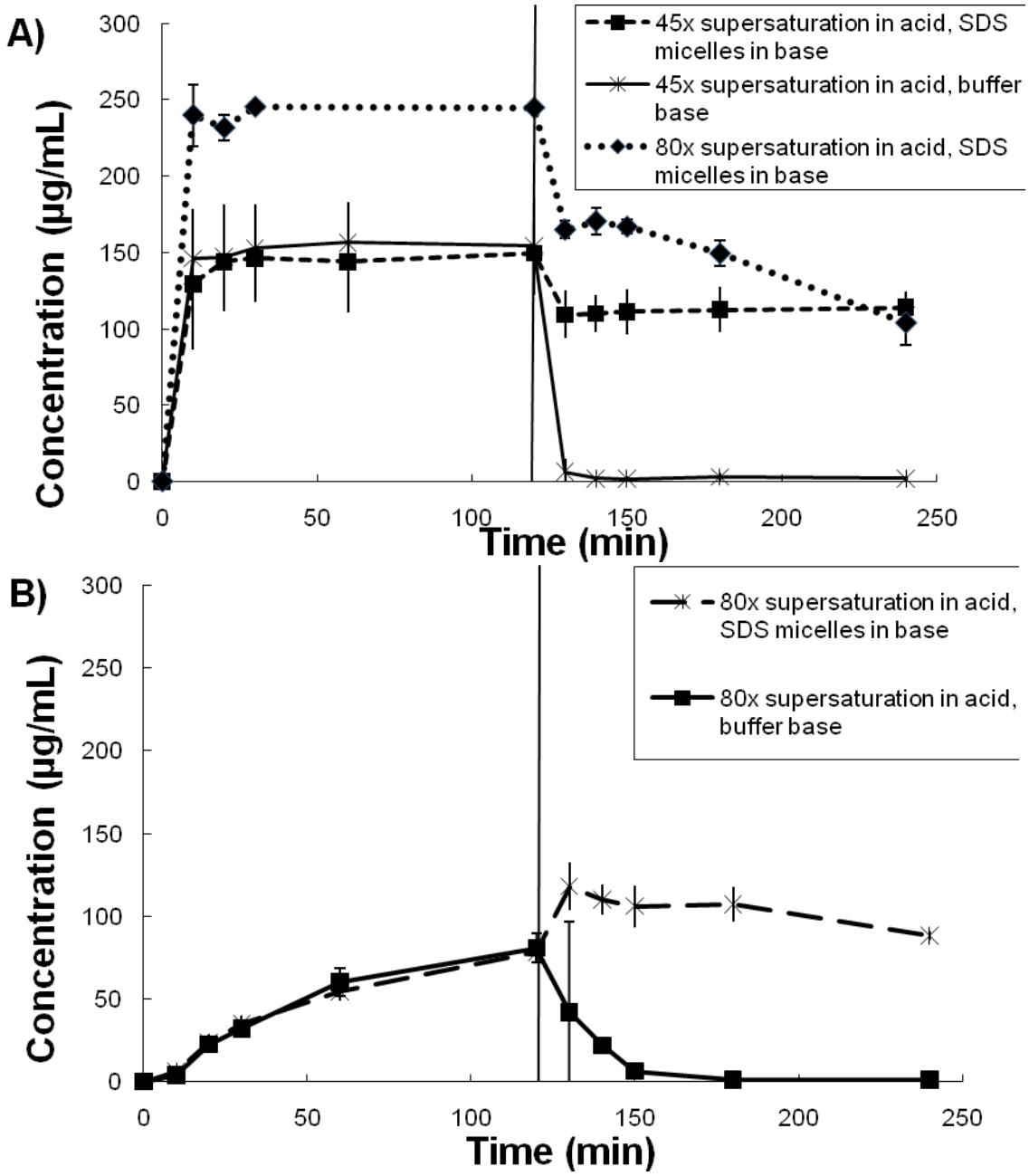

Figure 5.6 Dissolution of A) 2:1 Itz:HPMC salt flocculated formulation B)2:1 Itz:EL10055 pH flocculated formulation at various doses in pH 1.2 media for 120 minutes followed by rapid pH shift to 6.8 media with or without micelles.

pH shift due to constant decay in supersaturation. Since the temperature (T), molar volume (V_m), and surface tension (γ) are equal in the two experiments, homogeneous nucleation (B_o) at the higher loading increases based on the higher degree of supersaturation (S), as demonstrated in equation 5.2.

$$B_o = C \exp\left\{\frac{-16\pi\gamma^3 V_M N_A}{3(RT)^3[\ln(S)]^2}\right\} \qquad (5.2)$$

Subsequently, for the higher initial loading, the higher homogenous nucleation rate allows for additional growth out of solution. This results in a higher stable supersaturation level obtained for a lower initial loading after 2 h.

Given the small charge on the polymer at low pH, the supersaturation for the EL10055 pH flocculated formulation was limited in the acidic media. The percent of the Itz dissolved in the acid phase, ~19%, was comparable to that for a EL10055 hot melt extrusion formulation containing a much higher (1:2) Itz: polymer ratio.[25] The core-shell morphology of the flocculated AP particles allows for less of the Itz to be exposed to the pH 1.2 media on the surface of the particles than for the hot melt extrusion formulation. Because the Itz in the pH flocculated particles is surrounded by a shell of the enteric EL10055 polymer, reduced exposure of Itz to the pH 1.2 media minimizes dissolution of the drug. As a result, a significantly higher drug to polymer ratio has the same enteric effect as a hot melt extrusion formulation with lower drug loading. After the pH shift to neutral media without surfactant, slower depletion in supersaturation for the EL10055 stabilized particles relative to the HPMC formulation was observed. A level below 1

μg/ml was only seen after 60 minutes which is consistent with the results for EL10055 stabilized hot melt extrusion particles.[29] When experiments were performed with SDS micelles in the neutral media, the dissolved concentration of Itz increased to a maximum supersaturation of ~8x and then decreased over the 2 hour period to ~6.5x for the EL10055 stabilized pH flocculated formulation.

Previous studies demonstrate that Sporanox® almost fully dissolves to a supersaturation of 70x when 80x the crystalline solubility in acidic media at pH 1.2. Upon the pH shift with micelles, the high amount of Itz solubilized in the acidic media results in high supersaturation over the micellular solubility of Itz at pH 6.8 (22x). A high supersaturation of 22x causes rapid nucleation and growth out of the supersaturated solution. Thus a relatively low supersaturation of only 2x remains after only 30 min in the pH 6.8 media with micelles.[27] Therefore, very high supersaturation of the acidic media (70x) aides in the rapid nucleation and growth out of solution following the pH change.

While the solubility of Itz in the neutral media with SDS micelles is higher than the solubility in the acidic media (Table 2.2), the stability of the supersaturation values is inherently lower in the former. For supersaturation of Itz in micellar solutions (relative to the equilibrium solubility without micelles), the enhanced solubility is a consequence of the hydrophobic micelles cores.[49] The decreased stability of supersaturation in the pH 6.8 micellular media versus the pH 1.2 solution media is especially noticeable for Itz. A formulation with a stable supersaturation in acidic media near 90x can only achieve a

Table 5.2 Itraconazole solubility in a various media

Media	**Solubility of Itraconazole (µg/mL)**	**Source**
pH 1.2	4.4	experimental
pH 6.8 buffer	0.001	Brewster et al. *J Incl Phenom Macroycycl Chem* (2007) 57
pH 6.8 buffer with 0.17% SDS	14	experimental
30 mmol NaTC buffer	0.55	Derived from Mithani et al. *Pharm Res* (1996) 13(1)

Table 5.3 *In vitro* AUC over 2 hours in pH 6.8 media and *in vivo* AUC, C_{max}, and T_{max}.
[1]Sporanox *in vivo* data from[26]

Sample	***In vitro* AUC_{2h} (µg*min/ml)**	***In vivo* AUC (ng*hr/ml)**	**Cmax (ng/ml)**	**Tmax (hr)**
2:1 Itz: HPMC salt flocculated	17743 ± 1050	5084 ± 1970	389 ± 169	8.3 ± 3.3
2:1 Itz: EL10055 pH flocculated	12265 ± 988	2526 ± 714	350 ± 226	4.3 ± 1.4
Sporanox reference[1]	5646 ± 1183	2132 ± 1273	359 ± 261	5.5 ± 2.3

maximum supersaturation of 14x in the neutral media with SDS micelles followed by rapid decay due to nucleation and growth.[5, 23] Based on the AUC in the neutral pH media with SDS micelles of the pH shift experiment, the HPMC stabilized formulation is superior to the EL10055 formulation and both flocculated formulations are superior to the Sporanox® reference (Table 5.3).

5.3.3 *In Vivo* bioavailability of Itz from engineered formulation

As shown in Table 5.3, a dramatic result is that the higher *in vivo* bioavailability for the 2:1 Itz: HPMC salt flocculated formulation is statistically significant relative to the current marketed Sporanox® solid dosage formulation at a constant dose of 15 mg/kg (Table 5.3). While oral administration of the 2:1 Itz: EL10055 formulation did not lead to a statistically significant higher bioavailability, a >40% decrease in the standard deviation of the AUC_{24hr} and the shift in t_{max} are significant and will be discussed in more detail below (Table 5.3, Figure 5.7). Both of the flocculated nanoparticle formulations have much higher drug loadings, in this case to 67%, relative to ~21% for Sporanox® which can lead to decreased side effects from the excipients.[5]

In general, comparison between animal studies conducted by different protocols and at different initial doses is difficult, especially for a drug such as Itz where bioavailability is dose-dependant.[33] Itz bioavailability has also been found to be vary by food intake[26, 32, 34, 35, 50], making comparisons even more difficult. However, Itz bioavailability for the HPMC salt flocculated formulation and a previous 1:2 Itz:HPMC ratio micronized extrudate particles[30], can be compared as both of these studies were run

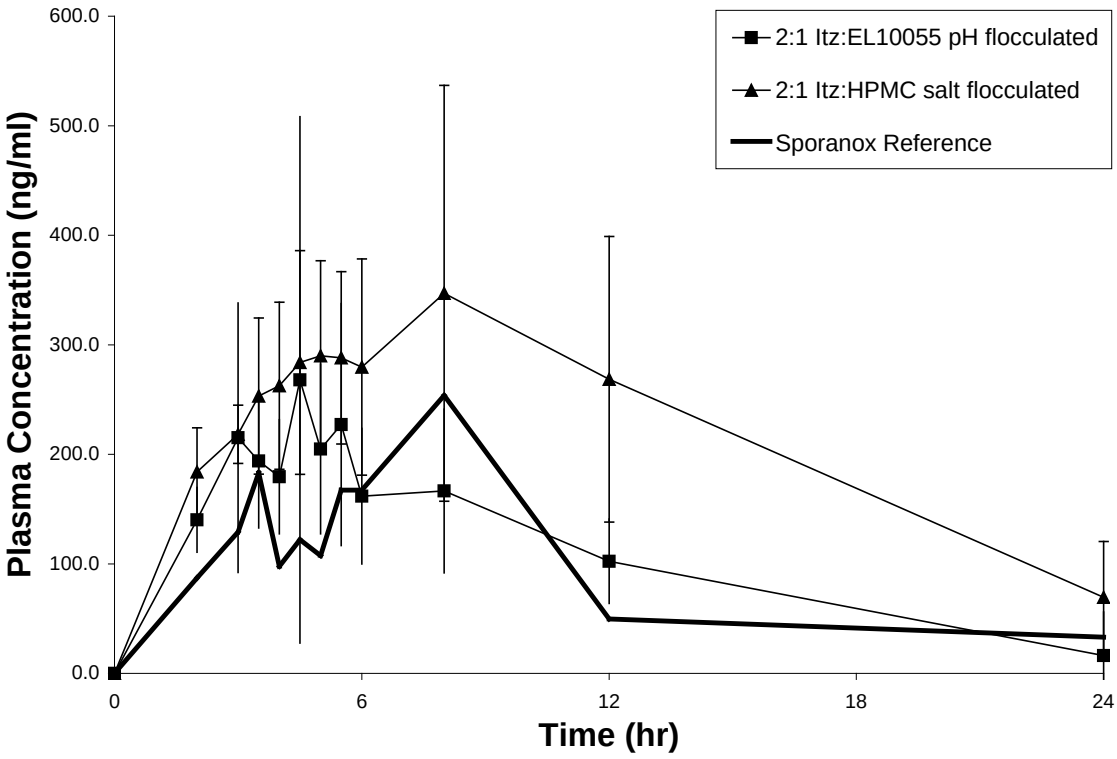

Figure 5.7 Plasma concentration over time for the 2:1 EL10055 stabilized pH flocculated and 2:1 HPMC stabilized salt flocculated Itz formulations and Sporanox® reference[26]

under similar conditions. In the current HPMC salt flocculated formulation, the actual AUC was twice as high, while the actual amount dosed was half as much.[30] In another study with Methocel™ E50, a higher viscosity grade HPMC, at a 1:2 drug to polymer ratio, the AUC was similar to that for the HPMC salt flocculated particles, with twice the dose.[25] Higher loadings of Itz result in similar or increase bioavailability for the HPMC salt flocculated formulation when compared to the 1:2 drug to polymer ratio of the extruded particles.[25, 30]

Previously, the bioavailability was studied for an EL10055 stabilized formulation made by hot-melt extrusion at the low 1:2 drug to polymer ratio.[25] Again, this previous study as well as the current study were run under similar conditions, with the only difference being the dose. In the previous study using hot-melt extrusion, the mean AUC appears significantly larger then that achieved for the EL10055 pH flocculated. However, the standard deviation was greater than the mean, leading to inconclusive results.[25] The large standard deviation may be have been caused by acidity resulting from the 20% triethyl citrate plasticizer, also known as citric acid, which may lower the dissolution of the enteric polymer in the small intestines.[25] The reduced dissolution of the particles may result in the high mean plasma concentrations noted after 12 and 24h.[25] Since the pH flocculated samples have no need for a plasticizing agent, this effect will not occur, which will result in more reproducible release kinetics for a pH sensitive polymer stabilized formulation. The enteric nature of both EL10055 formulations leads to a dependence on the pH in the gastrointestinal tract of the individual animals. Therefore,

for the pH flocculated formulation, the increased loading of the drug results in a decreased quantity of enteric polymer that must be solubilized to release the drug. As a result, the pH flocculated formulation may give a more reproducible result with a significantly decreased standard deviation when compared to the hot-melt extruded particles.

5.3.4 Comparison of *In Vitro* and *In Vivo* Results

The order of the values for the AUC_{2hr} for the pH shift experiment in the neutral media containing SDS is the same as for the bioavailability results from the animal study (Table 5.3). However, the AUC_{2hr} values from the neutral media without micelles are low and do not provide insight into the bioavailability. Alternately, the AUC_{4hr} solely in pH 6.8 media without a pH shift, for both the pH flocculated EL10055 and the HPMC salt flocculated formulations would incorrectly predict similar *in vivo* bioavailabilities.

Based on the dosage delivered to the rats, high supersaturation in the stomach and intestines is expected. Given the dosage to the animal (15 mg/kg body weight) in rats that weigh ~ 300 g, a total of ~4.5 mg Itz per rat was delivered. Since a rats stomach can hold ~2.5 ml[51], a total supersaturation in the stomach of 400x the crystalline solubility at low pH is expected. This high degree of supersaturation indicates that Itz is likely supersaturated, even after substantial dilution while in the gastrointestinal tract.

For the *in vitro* supersaturation experiment, the use of micelles turned out to be important. In general, the solubilization from the micelles is additive with the solution solubility at the particular pH (Equation 5.3).

$$S_{TOT} = S_W + \kappa C_{MIC} \quad (5.3)$$

S_{TOT} is the total molar mass of the solute, S_W is the water solubility, κ is the molar solubilization capacity of the surfactant, and C_{MIC} is the molar concentration of the micellular surfactant.[52] In the case of Itz, an increase in solubility of the 3 orders of magnitude is observed by adding micelles to the neutral media (Table 5.2). This dramatic change in solubility results in a significant change in dissolution behavior at pH 6.8, regardless of the particle composition (Figure 5.6).

Previously, *in vitro* dissolution tests have been studied in simulated stomach and intestinal fluids containing the appropriate bile salts for the fed and fasted states.[53-56] However, as a screening technique for multiple formulations, an inexpensive alternate micellular media is desired.[28] Recently this has been demonstrated for formulations of cilostazol using sodium lauryl sulfate (SLS) where the percent SLS used in the dissolution media was chosen based on matching surface tension measurements with the simulated intestinal fluid in a fed state.[28] While the contact angles measured in the media with NaTC and SDS are not equal (Table 5.1), they are very similar for Itz, the pure polymers and the flocculated formulations tested. In addition, the dissolution of a similar drug, danazol, was found to be primarily rate limited by the surface reaction for both NaTC and SDS micellular medias.[39] As a result, SDS can be considered an appropriate model surfactant to be used in the screening process.

The dissolution rate of Itz into the media is not the only important factor governing the overall *in vitro* AUC and *in vivo* bioavailability. The current *in vitro*

studies were conducted at supersaturated conditions where nucleation and growth are also important to determine the AUC in the neutral media.[27] The high 400x supersaturation dosed to the stomach of the rat compared to the lower stability of Itz supersaturation (~90x in acidic media and ~7x in pH 6.8 media with micelles) indicates that the decay in supersaturation may be highly significant. Thus, especially in the pH 6.8 media containing micelles, nucleation and growth kinetics of Itz out of solution may decrease the bioavailability of Itz. As the primary site for Itz absorption is the proximal small intestine[25, 29], the decreased soluble Itz concentration in the small intestines, due to nucleation and growth out of solution in the pH 6.8 media is expected to be an important factor.

Nucleation and growth of Itz from the neutral media containing micelles is dependent on the available surface area for heterogeneous nucleation and the initial dose of particles added. Thus the maintenance of supersaturation for high *in vivo* bioavailability will be dose-dependent.[32, 33] When comparing Figures 5.5 and 5.6, the enteric nature of the EL10055 coating results in similar dissolution and subsequent nucleation and growth out of the pH 6.8 media with SDS micelles, regardless of previous exposure to acidic media. Since the EL10055 does not dissolve in acidic media, the available particle surface area for nucleation and growth out of solution will be similar whether or not the particles were previously in an acidic environment. Thus, if only comparing enteric Itz formulations, a pH shift dissolution with SDS or a direct dissolution test in pH 6.8 media may be expected to give similar results. However, the

immediate release HPMC formulation will rapidly supersaturate the acidic media thereby changing both the dissolution and nucleation and growth behavior in the pH 6.8 media with SDS. Thus to compare immediate to enteric release polymers, *in vitro* dissolution tests should be designed to account for the natural pH shift between the stomach and the small intestines as well as the increased solubility due to the bile salt micelles. In addition, these tests should also provide high *in vitro* supersaturation in micelles to allow for loss of supersaturation by nucleation and growth to alter the AUC in the neutral media.

5.4 CONCLUSIONS

Nanoparticle dispersions of poorly water soluble drugs, in this case Itz, stabilized with an enteric polymer, Eudragit® L100-55, were flocculated, filtered and dried at room temperature to recover high yields (close to 100%) of amorphous particles. The negative charge on the enteric polymer coating, which stabilized the nanoparticle dispersions at pH 6.8 electrosterically, was neutralized by lowering the pH to 2.5 by adding HCl to flocculate the particles. The large flocs were filtered rapidly at room temperature, and at this low temperature, Itz did not crystallize. For the nanoparticle dispersions formed by antisolvent precipitation, high drug to polymer ratios were achieved. Here only small amounts of hydrophilic polymer oriented towards the particle surface are required for steric stabilization.[5] For the pH flocculation/filtration process, this high drug to polymer (66-80% Itz) loading is maintained. The rapid and strong increase in interparticle

attraction with the pH change produced diffusion limited flocculation of the nanoparticle dispersion under constant volume fraction, and consequently relatively open flocs. Upon reionizing the COOH groups on the enteric polymer at netural pH conditions, the open floccs redisperse to form ~1 μm particles with a surface area of ~7.7 m^2/g. Similar results were reported previously for salt flocculation of HPMC coated Itz upon redispersion.[27] In contrast, drying of nanoparticle dispersions by common techniques, such as spray drying, often produce densely packed flocs, which do not redisperse as well. Unlike related previous studies where nanoparticles were flocculated with high concentrations of salts[23, 27], the flocculation with pH introduces far less salt impurities in the final dried powder.

The dissolution behavior of both the HPMC and EL10055 flocs was tested by starting at simulated stomach conditions pH 1.2, followed by a pH shift to small intestine conditions, pH 6.8 with micelles to simulate bile salts. The HPMC based flocs generated a highest overall higher AUC_{2hr} followed by the EL10055 based flocs and lastly, the commercial Itz formulation, Sporanox. The higher AUC_{2hr} for the HPMC salt flocculated formulation, when compared to Sporanox, is a manifestation of slower decay in supersaturation at pH 6.8. This slower decay was determined for a control study of supersaturation versus time for dissolution experiments performed at a single pH, 6.8. The *in vivo* bioavailability was highest for the HPMC salt flocculated formulation, second for the EL10055 pH flocculated formulation and lowest for Sporanox. The same order was followed for the *in vitro* pH shift experiments to determine AUC_{2hr} in the

micelles at neutral pH. This correlation suggests that the high supersaturation for amorphous nanoparticles was important, which would not be available for crystalline drugs. The *in vivo* data were not correlated to the *in vitro* data without micelles, which may be expected given the presence of bile salts in the intestines. The 3 order of magnitude increase in Itz solubility from the micelles in the pH 6.8 media, and the minimization of nucleation and growth of Itz crystals from the supersaturated solution, appear to play an important role in achieving high *in vitro* AUCs that are more closely correlated to the *in vivo* bioavailability. The improved bioavailability of amorphous flocs produced by flocculation and filtration relative to the sugar-based solid dispersion, Sporanox, provides an alternative for more effective oral delivery of poorly water soluble drugs.

5.5 REFERENCES

1. Chen, H.; Wan, J.; Wang, Y.; Mou, D.; Liu, H.; Xu, H.; Yang, X., A facile nanoaggregation strategy for oral delivery of hydrophobic drugs by utilizing acid-base neutralization reactions. *Nanotechnology* **2008,** 19.

2. Fahr, A.; Liu, X., Drug delivery strategies for poorly water-soluble drugs. *Expert Opi. Drug Deliv.* **2007,** 4, (4), 403-416.

3. Lipinski, C., Solubility in the Design of Combinatorial Libraries. In *Analysis and Purification Methods in Combinatorial Chemisty*, Yan, B., Ed. John Wiley & Sons, Inc.: Hoboken, NJ, 2004; pp 407-434.

4. Lindfors, L.; Skantze, P.; Skantze, U.; Westergren, J.; Olsson, U., Amorphous Drug Nanosuspensions. 3. Particle Dissolution and Crystal Growth. *Langmuir* **2007,** 23, 9866-9874.

5. Matteucci, M. E.; Brettmann, B. K.; Rogers, T. L.; Elder, E. J.; Williams III, R. O.; Johnston, K. P., Design of Potent Amorphous Drug Nanoparticles for Rapid Generation of Highly Supersaturated Media. *Molecular Pharmaceutics* **2007,** 4, (5), 782-793.

6. Matteucci, M. E.; Miller, M. A.; Williams III, R. O.; Johnston, K. P., Highly Supersaturated Solutions of Amorphous Drugs Approaching Predictions from Configurational Thermodynamic Properties. *Journal of Physical Chemistry B* **2008,** 112, (51), 166675-16681.

7. Hancock, B. C.; Parks, M., What is the True Solubility Advantage for Amorphous Pharmaceuticals? *Pharm Res* **2000,** 17, (4), 397-404.

8. Gupta, P.; Chawla, G.; Bansal, A. K., Physical Stability and Solubility Advantage from Amorphous Celecoxib: The Role of Thermodynamic Quantities and Molecular Mobility. *Molecular Pharmaceutics* **2004,** 1, (6), 406-413.

9. Parks, G. S.; Snyder, L. J.; Cattoir, F. R., Studies on Glass. XI. Some Thermodynamic Relations of Glassy and Alpha-Crystalline Glucose. *Journal of Chemistry and Physics* **1934,** 2, 595-598.

10. Raghavan, S. L.; Trividic, A.; Davis, A. F.; Hadgraft, J., Crystallization of hydrocortisone acetate: influence of polymers. *Int J Pharm* **2001,** 212, 213-221.

11. Kumprakob, U.; Kawakami, J.; Adachi, I., Permeation Enhancement of Ketoprofen Using a Supersaturated System with Antinucleant Polymers. *Biological Pharmaceutical Bulletin* **2005,** 28, 1684-1688.

12. Yamada, T.; Saito, N.; Imai, T.; Otagiri, M., *Chemical & Pharmaceutical Bulletin* **1999,** 47, (9), 1311-1313.

13. Yamashita, K.; Nakate, T.; Okimoto, K.; Ohike, A.; Tokunaga, Y.; Ibuki, R.; Higaki, K.; Kimura, T., *Int J Pharm* **2003,** 267, 79-91.

14. Hasegawa, A.; Kawamura, R.; Nakagawa, H.; Sugimoto, I., Physical Properties of Solid Dispersions of Poorly Water-Soluble Drugs with Enteric Coating Agents. *Chem. Pharm. Bull.* **1985,** 33, (8), 3429-3435.

15. Okimoto, K.; Miyake, M.; Ibuki, R.; Yasumura, M.; Ohnishi, N.; Nakai, T., *Int J Pharm* **1997,** 159, 85-93.

16. Suzuki, H.; Sunada, H., Comparison of Nicotinamide, Ethylurea and Polyethylene Glycol as Carriers for Nifedipine Solid Dispersion Systems. *Chemical & Pharmaceutical Bulletin* **1997,** 45, 1688-1693.

17. Zhu, Y.; Shah, N. H.; Malick, A. W.; Infeld, M. H.; McGinity, J. W., Controlled Release of a Poorly Water-Soluble Drug from Hot-Melt Extrudates Containing Acrylic Polymers. *Drug Development and Industrial Pharmacy* **2006,** 32, 569-583.

18. Aitken-Nichol, C.; Zhang, F.; McGinnity, J. W., Hot-melt extrusion of acrylic films. *Pharm Res* **1996,** 13, 804-808.

19. Six, K.; Berghmans, H.; Leurner, C.; Cressman, J.; Van Werde, K.; Mullens, J.; Benoist, L.; Thimon, M.; Meublat, L.; Verreck, G.; Peeters, J.; Brewster, M. E.; Van den Mooter, G., *Pharm Res* **2003,** 20, (7), 1047-1054.

20. Verreck, G.; Six, K.; Van den Mooter, G.; Baert, L.; Peeters, J.; Brewster, M. E., *Int J Pharm* **2003,** 251, 165-174.

21. Six, K.; Verreck, G.; Peeters, J.; Brewster, M. E.; Van den Mooter, G., *J Pharm Sci* **2004,** 93, (1), 124-131.

22. Suzuki, H.; Sunada, H., *Chemical & Pharmaceutical Bulletin* **1998,** 46, (3), 482-487.

23. Matteucci, M. E.; Paguio, J. C.; Miller, M. A.; Williams III, R. O.; Johnston, K. P., Flocculated Amorphous Nanoparticles for Highly Supersaturated Solutions. *Pharm Res* **2008,** 25, (11), 2477-2487.

24. Shi, L.; Plumley, C. J.; Berkland, C., Biodegradable Nanoparticle Flocculates for Dry Powder Aerosol Formulation. *Langmuir* **2007,** 23, (22), 10897-10901.

25. Miller, D. A.; DiNunzio, J. C.; Yang, W.; McGinity, J. W.; Williams III, R. O., Enhanced In Vivo Absorption of Itraconazole via Stabilization of Supersaturation Following Acidic-to-Neutral pH Transition. *Drug Development and Industrial Pharmacy* **2008,** 34, (8), 890-902.

26. DiNunzio, J. C.; Miller, D. A.; Yang, W.; McGinity, J. W.; Williams III, R. O., Amorphous Compositions Using Concentration Enhancing Polymers for Improved Bioavailibility of Itraconazole. *Molecular Pharmaceutics* **2008,** 5, (6), 968-980.

27. Matteucci, M. E.; Paguio, J. C.; Miller, M. A.; Williams III, R. O.; Johnston, K. P., Highly Supersaturated Solutions from Dissolution of Amorphous Itraconazole Microparticles at pH 6.8. *Molecular Pharmaceutics* **2009,** 6, (2), 375-385.

28. Jinno, J.-i.; Kamada, N.; Miyake, M.; Yamada, K.; Mukai, T.; Odomi, M.; Toguchi, H.; Liversidge, G. G.; Higaki, K.; Kimura, T., In vitro-in vivo correlation for wet-milled tablet of poorly water-soluble cilostazol. *J Controlled Release* **2008,** 130, 29-37.

29. Miller, D. A.; DiNunzio, J. C.; Yang, W.; McGinity, J. W.; Williams III, R. O., Targeted Intestinal Delivery of Supersaturated Itraconazole for Improved Oral Absorption. *Pharm Res* **2008,** 25, (6), 1450-1459.

30. Miller, D. A.; McConville, J. T.; Yang, W.; Williams III, R. O.; McGinity, J. W., Hot-Melt Extrusion for Enhanced Delivery of Drug Particles. *J Pharm Sci* **2007,** 96, (2), 361-376.

31. Overhoff, K. A.; Moreno, A.; Miller, D. A.; Johnston, K. P.; Williams III, R. O., Solid dispersions of itraconazole and enteric polymers made by ultra-rapid freezing. *Int J Pharm* **2007,** 336, 122-132

32. Hardin, T. C.; Graybill, J. R.; Fetchinck, R.; Woestenborghs, R.; Rinaldi, M. G.; Kuhn, J. G., *Antimicrob. Agents Chemother.* **1988,** 32, (9), 1310-1313.

33. Shin, J. H.; Choi, K. Y.; Kim, Y. C.; Lee, M. G., *Antimicrob. Agents Chemother.* **2004,** 48, (5), 1756-1762.

34. Lohitnavy, M.; Lohitnavy, O.; Thangkeattiyanon, O.; Srichai, W., *J Clin Pharm Ther* **2005,** 30, (3), 201-206.

35. Jaruratanasirikul, S.; Keepkaew, A., *Eur J Clin Pharmacol* **1997,** 52, (3), 235-237.

36. Brewster, M. E.; Vandecruys, R.; Peeters, J.; Neeskens, P.; Verreck, G.; Loftsson, T., Comparative interaction of 2-hydroxypropyl-β-cyclodextrin and sulfobutylether-β-cyclodextrin with itraconazole: Phase-solubility behavior and stabilization of supersaturated drug solutions. *Eur J Pharm Sci* **2008,** 34, 94-103.

37. Chen, X.; Matteucci, M. E.; Lo, C. Y.; Johnston, K. P.; Williams III, R. O., Flocculation of polymer stabilized nanocrystal suspensions to produce

redispersible powders. *Drug Development and Industrial Pharmacy* **2009,** 35, (3), 283-296.

38. Wong, J.; Papadopoulos, P.; Werling, J.; Rebbeck, C.; Doty, M.; Kipp, J.; Konkel, J.; Neuberger, D., Itraconazole suspension for intravenous injection: determination of the real component of complete refractive index for particle sizing by static light scattering. *PDA J Pharm Sci Technol.* **2006,** 60, (5), 302-313.

39. Crisp, M. T.; Tucker, C. J.; Rogers, T. L.; Williams III, R. O.; Johnston, K. P., Turbidimetric measurement and prediction of dissolution rates of poorly soluble drug nanocrystals. *J Controlled Release* **2007,** 117, 351-359.

40. Bakatselou, V.; Oppenheim, R. C.; Dressman, J. B., Solubilization and Wetting Effects of Bile Salts on the Dissolution of Steroids. *Pharm Res* **1991,** 8, (12), 1461-1469.

41. Dickson, J. L.; Gupta, G.; Horozov, T. S.; Binks, B. P.; Johnston, K. P., Wetting Phenomena at the CO2/Water/Glass Interface. *Langmuir* **2006,** 22, 2161-2170.

42. Alban, L.; Dahl, A. K.; Hejgaard, K. C.; Jensen, A. L.; Kragh, M.; Thomsen, P.; Stennsgaard, P., *Anim. Welfare* **2001,** 10, 303-314.

43. Gubbins, P. O.; Gurley, B. J.; Bowman, J., Rapid and sensitive high performance liquid chromatographic method for determination of itraconazole and its hydroxyl-metabolie in human serum. *J Pharm Biomed Anal* **1998,** 16, 1005-1012.

44. Vaughn, J. M.; McConville, J. T.; Burgess, D.; Peters, J. I.; Johnston, K. P.; Talbert, R. L.; Williams III, R. O., Single dose and multiple dose studies of itraconazole nanoparticles. *Eur J Pharm Biopharm* **2006,** 63, (2), 95-102.

45. Hiemenz, P. C.; Rajagopalan, R., *Principles of Colloid and Surface Chemistry*. 3rd ed.; Marcel Dekker, Inc.: New York, 1997; p 650.

46. Shi, L.; Berkland, C., pH-Triggered Dispersion of Nanoparticle Clusters. *Adv. Mater*. **2006,** 18, 2315-2319.

47. Six, K.; Verreck, G.; Peeters, J.; Binnemans, K.; Berghmans, H.; Augustijns, P.; Kinget, R.; Van den Mooter, G., Investigation of thermal properties of glassy itraconazole: identification of a monotropic mesophase. *Thermochimica Acta* **2001,** 376, 175-181.

48. Petereit, H.-U.; Weisbrod, W., Formulation and process considerations affecting the stability of solid dosage forms formulated with methacrylate copolymers. *Eur J Pharm Biopharm* **1999,** 47, 15-25.

49. Liu, R.; Sadrzadeh, N.; Constantinides, P. P., Micellization and Drug Solubility Enhancement. In *Water-Insoluble Drug Formation*, Liu, R., Ed. Interpharm Press: Denver, 2000; pp 213-277.

50. Hong, J.-Y.; Kim, J.-K.; Song, Y.-K.; Park, J.-S.; Kim, C.-K., A new self-emulsifying formulation of itraconazole with improved dissolution and oral absorption. *J Controlled Release* **2006,** 110, 332-338.

51. Zhang, X.; Tsang, A. M.; Okino, M. S.; Power, F. W.; Knaak, J. B.; Harrison, L. S.; Dary, C. C., A Physiologically Based Pharmacokinetic/Pharmacodynamic Model for Carbofuran in Sprague-Dawley Rats Using the Exposure-Related Dose Estimating Model. *Toxicological Sciences* **2007,** 100, (2), 345-359.

52. Jain, A.; Ran, Y.; Yalkowsky, S. H., Effect of pH-Sodium Lauryl Sulfate Combination on Solubilization of PG-300995 (an Anti-HIV Agent): A Technical Note. *AAPS PharmSciTech* **2004,** 5, (3), 1-3.

53. Six, K.; Daems, T.; de Hoon, J.; Van Hecken, A.; Depre, M.; Bouche, M.-P.; Prinsen, P.; Verreck, G.; Peeters, J.; Brewster, M. E.; Van den Mooter, G., Clinical study of solid dipsersions of itraconazole prepared by hot-stage extrusion. *Eur J Pharm Sci* **2005,** 24, 179-186.

54. Schamp, K.; Schreder, S.-A.; Dressman, J., Development of an in vitro/in vivo correlation for lipid formulations of EMD 50733, a poorly soluble, lipophilic drug substance. *Eur J Pharm Biopharm* **2006,** 62, 227-234.

55. Naylor, L. J.; Bakatselou, V.; Dressman, J. B., Comparison of the Mechanism of Dissolution of Hydrocortisone in Simple and Mixed Micelle Systems. *Pharm Res* **1993,** 10, (6), 865-870.

56. Suzuki, H.; Ogawa, M.; Hironaka, K.; Ito, K.; Sunada, H., A Nifedipine Coground Mixture with Sodium Deoxycholate. II. Dissolution Characteristics and Stability. *Drug Development and Industrial Pharmacy* **2001,** 27, (9), 951-958.

Chapter 6: Highly Supersaturated Solutions of Amorphous Drugs Approaching Predictions from Configurational Thermodynamic Properties

Dissolution of pure solid itraconazole in metastable amorphous states was used to produce high supersaturation in low pH media. For a pre-wet dispersion of particles on the order of 1 μm produced by antisolvent precipitation, an experimental supersaturation of 63 times the crystalline solubility was achieved. This experimental value approached the calculated value of 95 from the configurational free energy, G_{conf}, which was determined from modulated differential scanning calorimetry measurements. A high fragility, quantitatively determined by the fragility parameter, γ_{cp}, is dependant on the configurational heat capacity, C_{pconf}, favoring a high G_{conf} and thus high supersaturation. However, high fragility also increases the driving force for crystallization of the solid during dissolution. The relatively fragile pre-wet dispersions dissolved rapidly and produced high supersaturation without crystallizing, in contrast with much lower supersaturation values for slowly dissolving particles with low wetted-surface areas formed by spray drying or lyophilization of aqueous dispersions.

6.1 INTRODUCTION

Over one-third of presently discovered drugs are poorly water-soluble, resulting in poor or highly variable bioavailability from oral absorption as well as other forms of delivery.[1] For biopharmaceutical classification system (BCS) type II drugs, the level of dissolved drug may be enhanced by engineering particles with accelerated dissolution rates and enhanced thermodynamic driving forces for dissolution.[2-5] The dissolution rate is described by the well-known Noyes-Whitney equation

$$\frac{dm}{dt} = \frac{DA}{h}\left(C_{sat} - C\right) \qquad (6.1)$$

where D is the diffusivity, A is the specific surface area of the particles , h is the diffusional path length in the boundary layer about the particle, C_{sat} is the solubility of the drug, and C is the concentration of drug in solution. Formation of a high energy metastable state, amorphous or semicrystalline, has the potential to increase the solubility, C_{sat}, and absorption of the drug substantially relative to its crystalline form.[3] For example, in some cases, the predicted solubility of the amorphous drug is as much as 1600-times that of its crystalline form, based on Gibbs free energy calculations.[3,6,7] In addition to increasing the dissolution rate via C_{sat}, the higher solubility will also enhance the permeation rate through biomembranes in the gastrointestinal tract.[8,9] However, these high energy amorphous polymorphs are kinetically unstable and relax towards the equilibrium liquid's disordered structure of lower energy and entropy and by surpassing the free energy barrier may nucleate to the lowest energy crystalline state during storage or during the dissolution process upon exposure to aqueous media.[10] In addition, different techniques will produces non-crystalline states with different free energies.[11]Therefore, the formation, characterization and stabilization of these high energy polymorphs in the solid phase is a major goal for improving dissolution in oral delivery.[2,12,13]

The configurational thermodynamic properties of amorphous drugs relative to their crystalline state, such as enthalpy, entropy, and free energy, can be used to predict the solubility ratio of the amorphous to crystalline forms.[3,6,7] In studies that have compared experimentally measured solubility ratios with the predicted values, the amorphous drug was typically made by quench cooling the melt or by solvent evaporation from solution. Typically, the particle size was on the order of 100 μm and the

Table 6.1 Different poorly-water soluble drugs, their theoretical and measured solubility ratios, the method the drug particles were produced, and the media the solubility was measured in. {[1]Hancock 2000, [2]Mosharraf 1999, [3]Elamin 1994, [4]Corrigan 1984, [5]Stagner 1979, [6]Gupta 2004}

Drug	**Predicted Solubility Ratio***	**Measured Solubility Ratio**	**Method used to produce particles**	**Solubility media**
Celecoxib[6]	7-21[6]	1.3-1.5	Quench-cooled	35°C, 45°C, 55°C, 65°C, 75°C, water
Indomethacin[1]	38-301	4.4	Quench-cooled	5°C, water
	25-104	4.5	Quench-cooled	25°C, water
	16-41	2.8	Quench-cooled	45°C, water
Glibenclamide[2]	112-1652	14	Quench-cooled	23°C, pH 7.4 buffer (Aq.)
Griseofulvin[2]	38-441	5.5	Quench-cooled	23°C, pH 7.4 buffer (Aq.)
Griseofulvin[3]	38-441	1.4	Quench-cooled	21°C, water
Hydrochlorthiazide[4]	21-113	1.1	Spray drying	37°C, HCl & PVP (Aq.)
Iopanoic Acid[5]	12-19	3.7	Solvent evaporation	37°C, phosphate buffer (Aq.)
Polythiazide[4]	48-455	9.8	Spray drying	37°C, HCl & PVP (Aq.)

experimental solubility ratios of these particles was typically less than 20% of the predicted values (Table 6.1).[3,14-17] For example, in the case of ~125 μm indomethacin particles, the predicted solubility ratio in water ranged from 25-104, while the experimentally measured value was only 4.5.[3] The experimental values were reduced by crystallization in the solid phase during wetting and dissolution.[3,7] Novel strategies are needed to address these limitations.

The objective of the current study was to design pure drug amorphous particles to achieve experimental solubilities approaching theoretical values predicted from configurational thermodynamic properties. The particle dispersions were made by antisolvent precipitation (AP), in which rapid nucleation and slow growth quenches the pure drug in the amorphous state as a fine particle dispersion in aqueous media. The dissolution behavior of the drug formed by AP was determined in acidic media, where the drug is more soluble, for two cases: (1) the original aqueous dispersion, and (2) dried particles formed by rapid freezing of the dispersion followed by lyophilization. In the first case, the particle dispersion was added dropwise to 0.1N HCl (pH 1.2) media in order to minimize buildup of excess undissolved particles and generate sustained levels of supersaturation relative to the crystalline solubility for up to 4 hours. In the second case, when the dispersions were frozen and lyophilized to produce a powder, the supersaturation achieved was much lower given poor wetting of the powder decreasing the dissolution rate and the partial crystallization of the powder form.

A comparison of two solid powder forms, the AP lyophilized powder and a spray dried powder will show the effect of different configurational thermodynamic properties in the amorphous state on the theoretical and experimental solubility ratios. Finally, the

result for the pure drug dispersion is compared with recent results for similar particles made by AP with a polymer stabilizer, hydroxypropylmethylcellulose (HPMC) to aid wetting of dried particles, reduce the particle size and reduce crystallization to maximize levels of supersaturation.[18] However, the configurational properties of the amorphous drug could not be measured for the polymer-stabilized samples given the contributions of the HPMC to these properties. Depending on the future application of the particles, it can be desirable in actual practice to use polymeric stabilizers to aid particle stabilization and wetting during dissolution.

6.2 MATERIALS AND METHODS

6.2.1 Materials

B.P. grade itraconazole (ITZ) was purchased from Hawkins, Inc. (Minneapolis, MN). HPMC E5 (viscosity of 5 cP at 2% aqueous 25°C solution) grade and spray dried intraconazole were gifts from the Dow Chemical Corporation. Stabilized p.a. grade 1,3-dioxolane was purchased from Acros Organics (Morris Plains, NJ). HPLC grade acetonitrile (ACN), A.C.S. grade hydrochloric acid (HCl), and diethanolamine (DEA) were used as received from Fisher Chemicals (Fairlawn, NJ).

6.2.2 Antisolvent Precipitation (AP) of Amorphous Itraconazole

Deionized water (50 g) was used as the anti-solvent phase into which 15 g of 1,3-dioxolane containing 3.3% (wt) ITZ was injected to form a fine precipitate. The organic phase was separated from the aqueous suspension via vacuum distillation. To recover the particles, the dispersion was added dropwise to liquid nitrogen and lyophilized to form a powder using a Virtis Advantage Tray Lyophilizer (Virtis Company, Gardiner, NY) with

24 hours of primary drying at -35 °C followed by 36 hours of secondary drying at 25 °C. Dried powders were stored in a 13% relative humidity environment.

6.2.3 Temperature Modulated Differential Scanning Calorimetry (MDSC)

Dried powder samples of approximately 5 mg were placed in hermetically sealed aluminum pans. Using a 2920 modulated DSC (TA Instruments, New Castle, DE) with a refrigerated cooling system, the samples were purged with nitrogen at a flow rate of 150 mL/min. The amplitude of 1°C, the period 1 min, and the underlying heating rate of 5°C/min were used. Crystallinity in the original sample (prior to DSC heating) was estimated from the total heat flow curve by integrating the area under the ITZ melting endotherm at 168°C and crystallization peak at approximately 120°C by

$$x_{cryst} = \frac{\Delta h_{melt} - \Delta h_{cryst}}{\Delta h_{meltItz}} \qquad (6.2)$$

where x_{cryst} is the percent crystallinity, Δh_{melt} is the heat of melting, Δh_{cryst} is the heat of crystallization, and the denominator, $\Delta h_{meltItz}$, is used to normalize the results by the heat of melting for pure crystalline ITZ. This equation is based upon the assumption that the heat necessary to melt 1 g of crystalline ITZ and to crystallize 1 g of amorphous ITZ are equal. For a purely crystalline sample, a crystallization peak is not present, $\Delta h_{cryst} = 0$, and $\Delta h_{melt} = \Delta h_{meltItz}$, giving $x_{cryst} = 1$. For a completely amorphous material, the crystallization peak area will be equal to the melting peak area, such that $x_{cryst} = 0$.

6.2.4 Quench Cooling of Molten ITZ Using MDSC

In order to form a purely amorphous ITZ sample, the bulk drug was placed in a hermetically sealed aluminum pan and heated at a rate of 5°C/min using the modulated DSC (MDSC). Upon reaching 200°C, the sample was then quench cooled to 0°C at a rate

of 40°C/min. Reheating the amorphous ITZ using the MDSC indicated 0% crystallinity as no melting peak was observed at ~168°C.

6.2.5 Calculation of Heat Capacity

The heat capacity as a function of temperature was determined by de-convoluting the total heat flow curve into the non-reversing and heat capacity signals using TA Instruments Universal Analysis Software. Heat capacities of amorphous materials were measured between 25 and 200 °C.

6.2.6 Dissolution under Supersaturated Conditions

Metastable solubility limits were measured in 0.1 N HCl (pH 1.2) media at 37.2°C. A USP paddle method was adapted to accommodate smaller sample sizes using a VanKel VK6010 Dissolution Tester with a Vanderkamp VK650A heater/circulator (VanKel, Cary, NC). Dissolution media (50 mL) was preheated in small 100 mL capacity dissolution vessels (Varian Inc., Cary, NC). Particle dispersions were added dropwise to the dissolution media at a rate of approximately 10 drops/min to reduce the excess particle dosing. The drops were no longer added when particles could barely be detected by the naked eye, minimizing heterogeneous sites for nucleation of the supersaturated solutions. In the case of dried powder dissolution, a sample weight (~17.6 mg drug) equivalent to approximately 80-times the crystalline equilibrium solubility (4.4 μg/mL[18]) of ITZ in 0.1 N HCl was added to the media. Sample aliquots (1.5 mL) were taken at various time points. The aliquots were filtered immediately using a 0.2 μm syringe filter and 0.8 mL of the filtrate was subsequently diluted with 0.8 mL of ACN to double the volume. In all cases, the filtrate was completely clear upon visual inspection and dynamic light scattering of the filtrate gave a count rate of less than 20 kcps (too low for particle

size analysis) indicating that not even nanoparticles were coming through the filter. For all samples, the drug concentration was quantified by high performance liquid chromatography as described below.

6.2.7 High Performance Liquid Chromatography (HPLC)

ITZ concentrations were quantified using a Shimadzu LC-600 HPLC (Columbia, MD). The mobile phase was ACN:water:DEA 70:30:0.05 and the flow rate was 1 mL/min. Using a detection wavelength of 263 nm, the ITZ peak eluted at 5.4 min. The standard curve linearity was verified from 1 to 500 μg/mL with an r^2 value of at least 0.999.

6.2.8 Scanning Electron Microscopy (SEM)

Dried powders were placed on double sided adhesive carbon tape and gold-palladium sputter coated for 35 sec. Micrographs were taken using a Hitachi S-4500 field emission scanning electron microscope with an accelerating voltage of 10-15 kV.

6.2.9 Dispersion Particle Size Analysis

Particle size of the dispersion was measured by multiangle laser light scattering using the Malvern Mastersizer-S (Malvern Instruments, Ltd., Worcestershire, UK). The prewet AP dispersion was diluted in water in the large recirculation cell (~500ml) immediately after the particles were prepared giving an obscuration between 10-15 % for the measurement. The refractive index of pure water was used as the refractive index of the solvent and the refractive index of itraconazole was used as the refractive index of the particles to calculate the particle size.

6.2.10 X-ray Diffraction (XRD)

A sample of powder was pressed onto a portion of a glass slide to form a flat sample surface where wide angle X-ray scattering was used to detect the crystallinity of the dried drug powder. A Philips PW 1720 X-ray generator (Philips Analytical Inc., Natick, MA) giving Cu $K\alpha_1$ radiation at a wavelength of 1.54054 Å at 40 kW and 20 mA was used and the reflected intensity was measured at a 2θ angle between 1 and 30° with a step size of 0.05° and a dwell time of 4 s.

6.3 THEORY

6.3.1 Prediction of Amorphous Solubility with Excess Thermodynamic Properties

In the method of Parks,[6] the solubility ratio ($\sigma_{amorph}/\sigma_{cryst}$) of the amorphous and crystalline form may be described by

$$G_{conf} = RT \ln\left(\frac{\sigma_{amorph}}{\sigma_{cryst}}\right) \qquad (6.3)$$

where G_{conf} is the configurational free energy difference of the two forms, R is the gas law constant, and T is the temperature. Here, the Gibbs free energy difference between crystalline and amorphous forms is directly proportional to the natural log of the thermodynamic activity ratio, which is approximated as the solubility ratio under dilute solution conditions.[7] The value of G_{conf} can then be related to other thermal properties by

$$G_{conf} = H_{conf} - TS_{conf} \qquad (6.4)$$

where the configurational enthalpy (H_{conf}) and entropy (S_{conf}) may be determined from the crystalline drug enthalpy of fusion (ΔH_f) and the configurational heat capacity (C_{pconf}).

$$H_{conf} = \Delta H_f - \int_T^{T_m} C_{p\,conf}\, dT \qquad (6.5)$$

$$S_{conf} = \Delta S_f - \int_T^{T_m} \frac{C_{p\,conf}}{T} dT \qquad (6.6)$$

$$\Delta S_f = \frac{\Delta H_f}{T_m} \qquad (6.7)$$

C_{pconf} is defined as the difference in heat capacity between the amorphous and crystalline drug forms and represents the temperature dependence of nonvibrational molecular mobility.[7,19]

The values of H_{conf} and S_{conf} may be estimated by choosing a constant value of C_{pconf}, specifically at the T_g (C_{pconf}^{Tg})[3]

$$H_{conf}* = \Delta H_f - C_{pconf}^{Tg}\left(T_m - T\right) \qquad (6.8)$$

$$S_{conf}* = \Delta S_f - C_{pconf}^{Tg}\left(\ln\left(\frac{T_m}{T}\right)\right) \qquad (6.9)$$

This simplified calculation has been shown to give values in good agreement with those from equations 2-6 for solubility ratios at temperatures above T_g.[3]

6.3.2 Fragility of the Amorphous State from Heat Capacity Measurement

The concept of fragility for a glass was proposed by Angell.[20] The fragility is defined as deviation from Arrhenious-type behavior of the relaxation time dependence on temperature. This relationship can be modeled by a modified Vogel-Tamman-Fulcher (VTF) equation [20]

$$\tau = A\exp\left(\frac{DT_o}{T - T_o}\right) \qquad (6.10)$$

where A is a constant representing the time scale of vibrational motions, D is the strength parameter, and T_o is the temperature at which molecular mobility is negligible.[7] For a strong glass (large D value), the mobility (characterized by the log of viscosity in poise

which is proportional to the relaxation time) increases approximately linearly with 1/T. A classic example of a strong glass, molten SiO_2, has a nearly constant activation energy that indicates a uniform mechanism throughout presumed to be the breaking and reforming of Si-O bonds.[21] For a glass characterized as fragile (low D values), the log of viscosity increases more rapidly with 1/T and the glass can reorganize to a wide variety of molecular arrangements and coordination states.[7] The fragility of an amorphous (glassy) drug provides insight into the physical stability of the solid dosage form in terms of its tendency to crystallize upon storage or in the presence of solvent during dissolution.[7,19,22,23]

An alternative method for determining the fragility of an amorphous material uses its difference in heat capacity from the crystalline state. The fragility parameter, γ_{Cp}, is defined as

$$\gamma_{Cp} = \frac{C_p^{\,l} - C_p^{\,g}}{C_p^{\,l} - C_p^{\,x}} \qquad (6.11)$$

where l, g, and x indicate the equilibrium supercooled liquid, glass, and crystalline states with the heat capacities calculated at the T_g.[7,19] γ_{Cp} ranges from 0 to 1, where a value approaching 1 indicates a strong glass with a C_p similar to that of the crystal. When γ_{Cp}=0, the glass is considered fragile, as the C_p is nearly equal to that of the equilibrium liquid. This simplified correlation between γ_{cp} and the fragility is not the case with hydrogen-bonded liquids.[19] However, for pharmaceuticals similar to those analyzed, this simplified relationship has been used successfully.[7,19]

6.4 RESULTS

6.4.1 Morphology of pure ITZ particles

The morphology of three pure drug samples, AP/lyophilized, spray dried, and bulk crystalline ITZ, was investigated. According to XRD, crystallinity was detected in all three pure ITZ dry powder samples, as evident by peaks at 20.5, 23.5, and 25.5 degrees 2θ (Figure 6.1). Further analysis by MDSC confirmed the presence of crystallinity demonstrated by the melting peaks seen for all three samples. The % crystallinity was estimated as the area under the crystallization and melting peaks described in equation 6.2 (Table 6.2). Removal of water by lyophilization of the frozen AP dispersion resulted in 44% crystallinity, and spray drying lead to 24% crystallinity. The amorphous ITZ, made by quench cooling the molten drug using the MDSC, contained no crystallinity. The bulk ITZ, assumed to be 100% crystalline, was used as a basis for calculating the % crystallinity of the other samples. As seen in Figure 6.2, SEM of the dried powders revealed that the pure ITZ particles made by AP were polydisperse in size, ranging from 1-5 μm. This is confirmed by the particle size (5.21 μm) of the prewet dispersion prior to lyophilization measured by static light scattering. The spray dried ITZ particles were 200 nm to 1 μm. The dried particle sizes were not measured by static light scattering since they could not be redispersed in water in order to make the measurement.

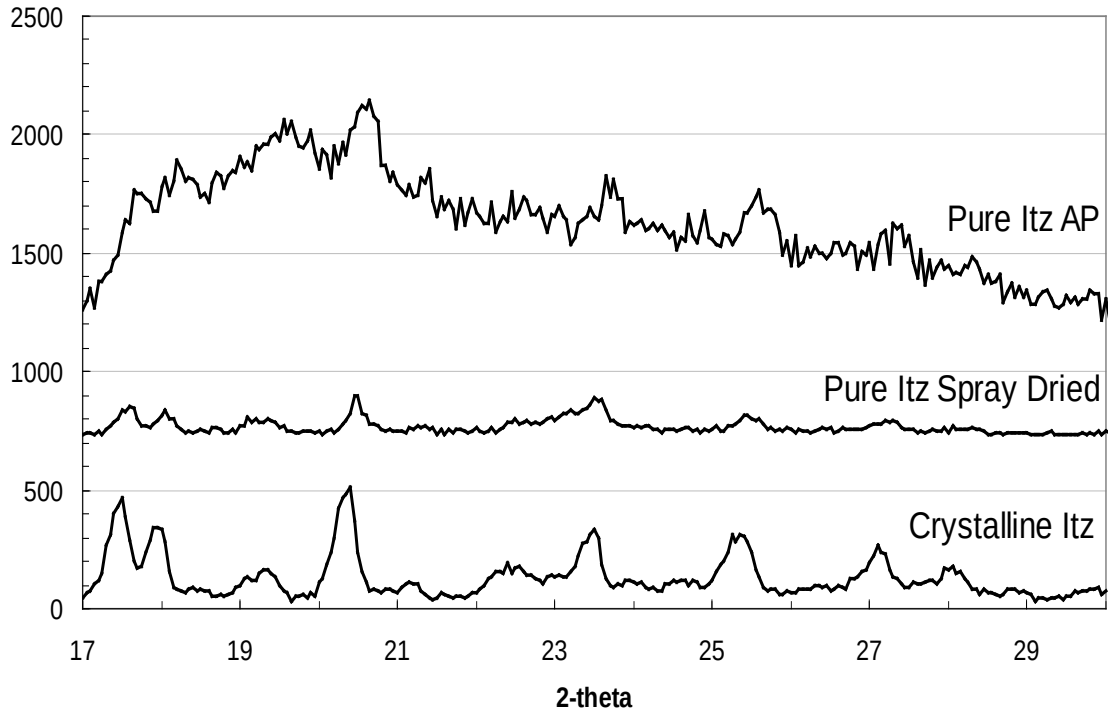

Figure 6.1 X-ray diffraction of antisolvent precipitated (AP) ITZ, spray dried ITZ, and crystalline ITZ powders

Table 6.2 C_{pconf}, solubility ratios, and γ_{Cp} of DSC quench-cooled, spray dried, and AP lyophilized amorphous ITZ powders compared with Indomethacin {[1]Hancock, 2000; [2]Shamblin, 1999; [3]Gupta, 2004}.

	Pure amorphous Itz (DSC quenched)	**Spray dried**	**AP lyophilized**	**Indomethacin**
T_g (°C)	59	63	60	42[1]
C_{pconf} at T_g (J/gK)	0.3949	0.2425	0.3229	0.41[1]
σ_{amorph} / σ_{cryst} at 37°C using eq. 3-7	125	175	25	~80
σ_{amorph} / σ_{cryst} at 37°C using C_{pconf} at T_g	95	237	147	28
Experimental solubility	63*	10	16	2.8-4.5[1]
% crystallinity	0	28	44	NA
γ_{Cp}	0.79	0.66	0.72	0.92[2]
T_m (°C)	168	168	168	162[3]
$(T_c-T_g)/(T_m-T_g)$	0.56	0.51	0.54	0.42[3]

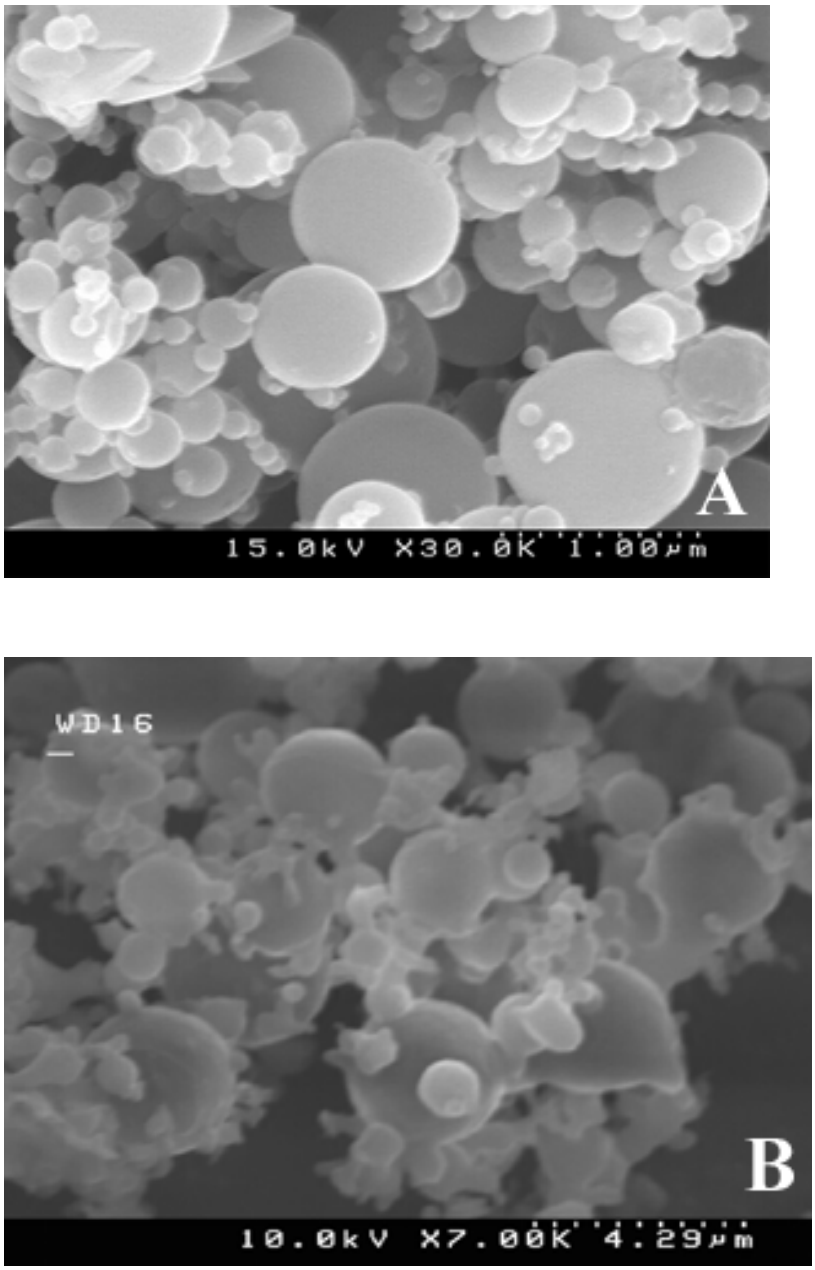

Figure 6.2 SEM of 100% ITZ (A) spray dried (B) AP lyophilized powders

6.4.2 Predicted Solubility Ratios and γ_{Cp} of Amorphous ITZ Particles

The heat capacity versus temperature profile for the three pure ITZ samples is shown in Figure 6.3. The resulting C_{pconf} versus temperature profile is shown in Figure 6.4. Predicted solubility ratios of pure ITZ particles were calculated by two methods, as reported in Table 6.2. The first method used equations 6.3-7, where C_{pconf} of amorphous ITZ particles was integrated over the appropriate temperature range (T to T_m). The second calculation method used equations 6.8 and 6.9, where C_{pconf}^{Tg} was determined for each sample at the T_g of ITZ, assumed to be the mid-point in the rise of the C_{pconf} near the reported T_g of ITZ, ~58.5°C,[24] and used as a constant over all temperatures. From the first method, the excess enthalpy, entropy, and Gibbs free energy were estimated over a temperature range from 25 to 168°C as shown in Figure 6.5. The resulting solubility ratio versus temperature profile is shown in Figure 6.6, where the vertical line indicates the temperature at which dissolution experiments were conducted, 37°C. The experimentally measured solubility ratios reported in Table 6.2 are also shown. The solubility ratio decreases with increasing temperature since the difference between T and T_m decreases. For the samples formed by DSC quench cooling and spray drying, the calculated solubility ratios by the two methods equations 6.3-7 versus equations 6.8 and 6.9, were much closer to each other than for the lyophilized AP particles. The values of γ_{Cp} for each sample are given in Table 6.2. The spray dried amorphous ITZ was slightly more fragile, at γ_{Cp} = 0.66, compared to 0.79 and 0.72 for the DSC quench cooled and AP samples,

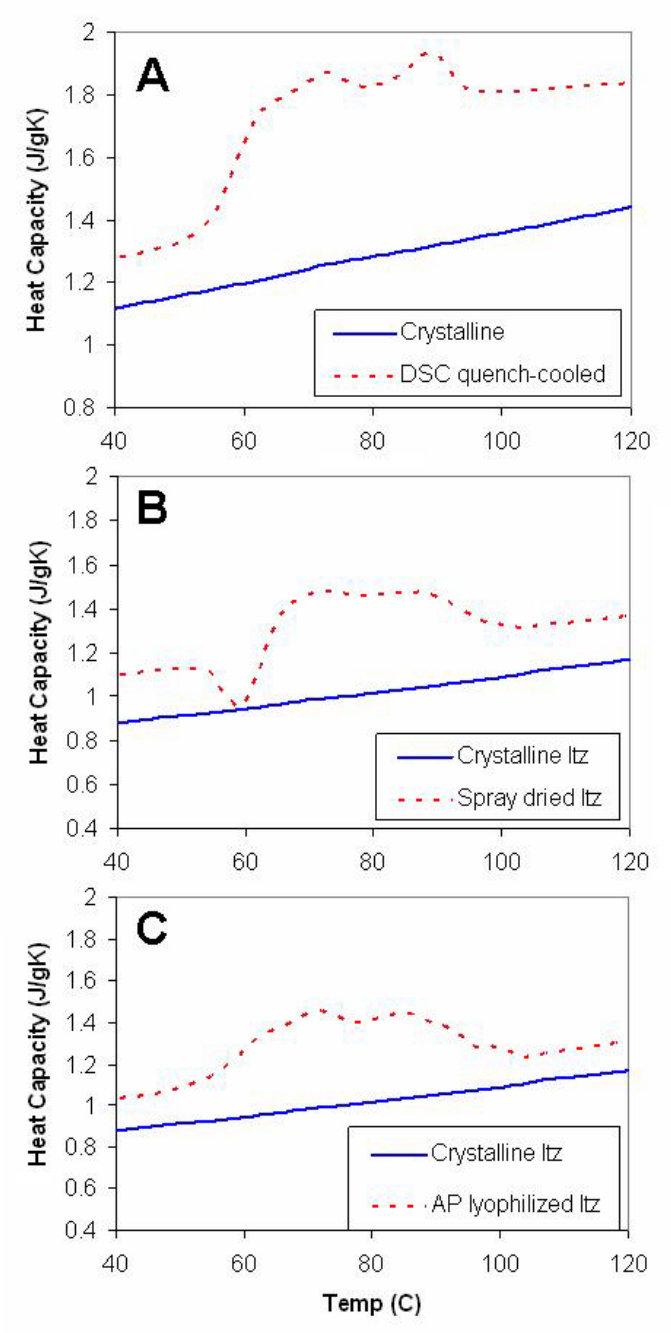

Figure 6.3 Heat capacity of a) DSC quench-cooled amorphous, b) spray dried partially amorphous, c) antisolvent precipitated (AP) lyophilized partially amorphous and crystalline ITZ as measured by mDSC

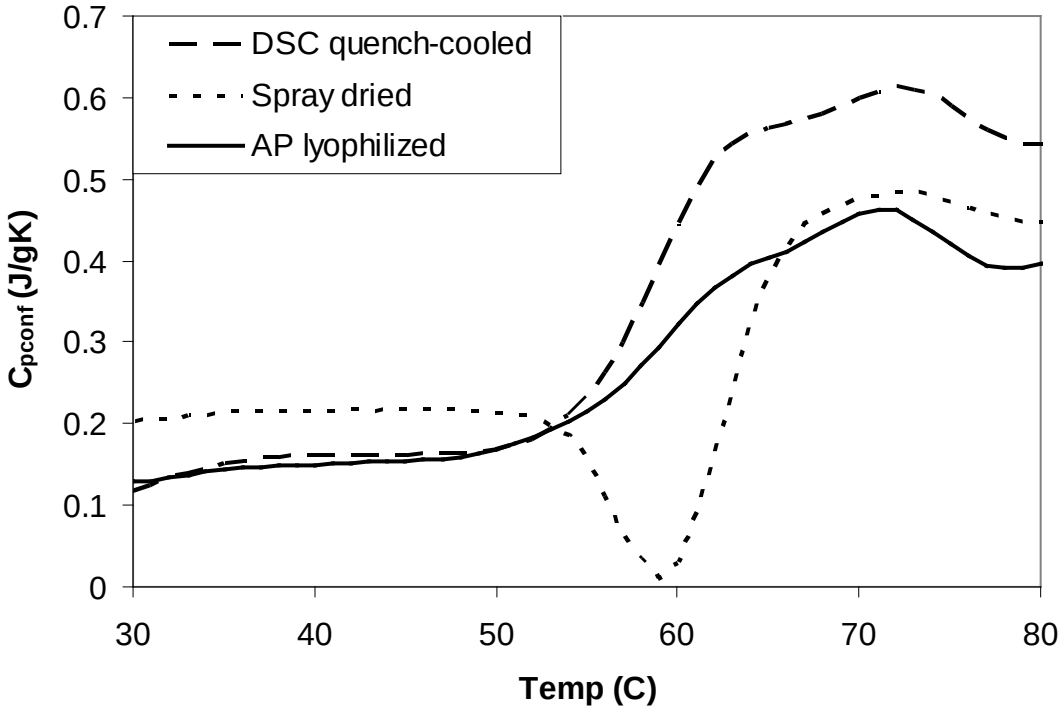

Figure 6.4 Configurational heat capacity of DSC quench-cooled, spray dried, and antisolvent precipitated (AP) lyophilized amorphous ITZ

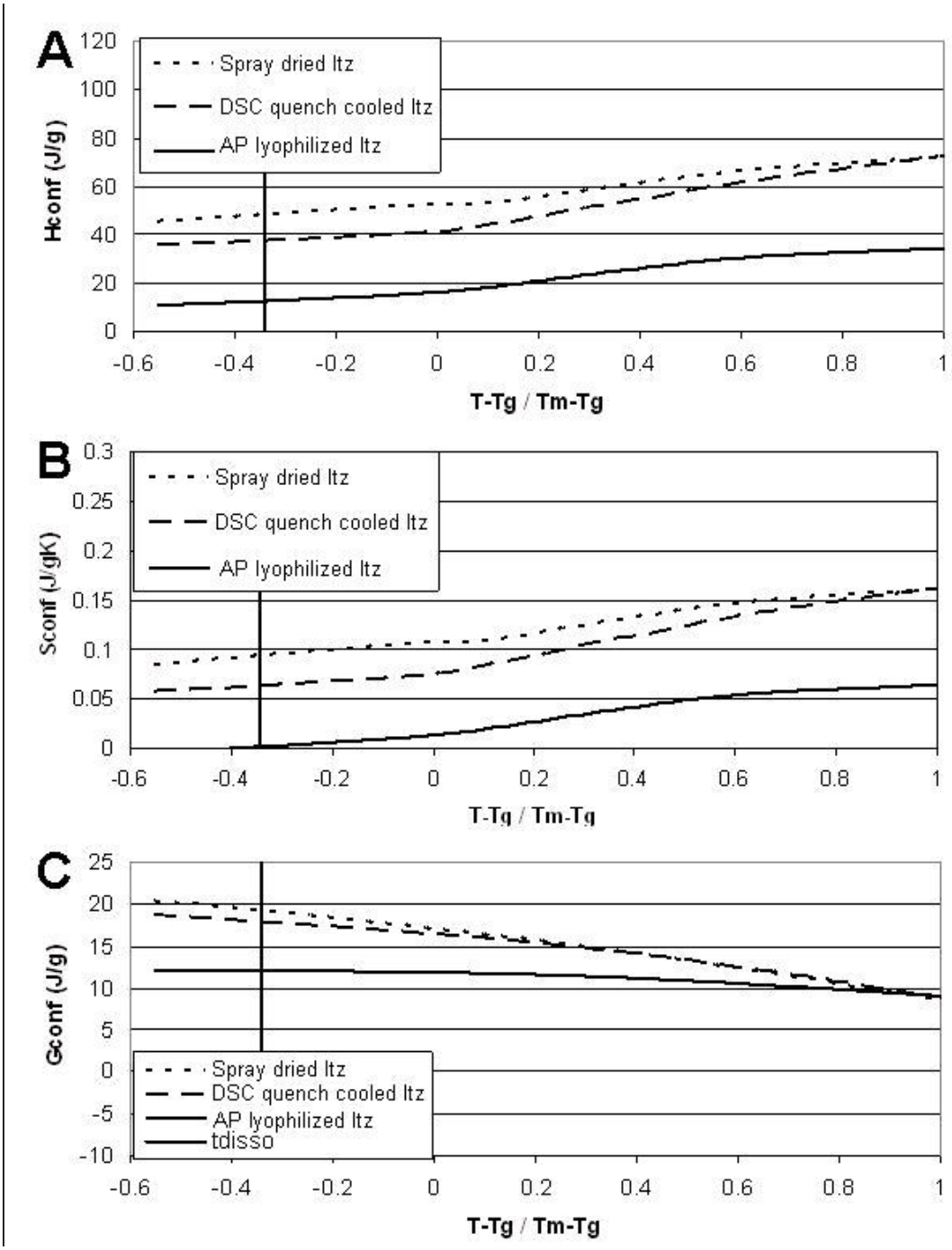

Figure 6.5 Configurational a) enthalpy, b) entropy, and c) free energy as a function of reduced temperature (vertical line indicates temperature of dissolution, 37.2°C)

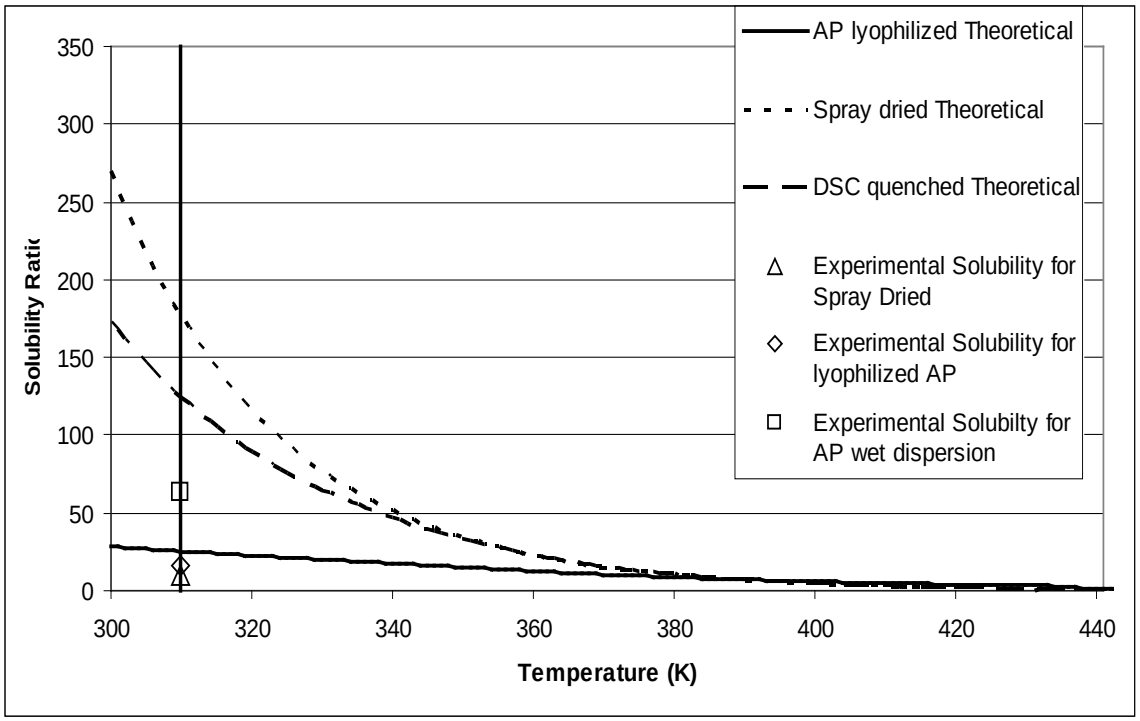

Figure 6.6 Predicted solubility ratios as a function of temperature and experimentally measured solubility ratios at 37°C

respectively. For comparison, the solubility ratio and thermal properties for another poorly water soluble drug, indomethacin, are also provided in Table 6.2.

6.4.3 Supersaturated Acidic Aqueous Media from Dissolution of ITZ Particles

Pure ITZ particles were dissolved for 4 hours to generate supersaturated solutions in 0.1 N HCl (Figure 6.7). In the case of spray dried and AP lyophilized pure ITZ particles, solubility ratios were only 10 and 16, respectively. These dried particles remained on the surface of the dissolution medium and few particles dispersed into the medium even after 4 h. Alternatively, the pure ITZ AP particle dispersion was added to the dissolution medium immediately after removal of the organic solvent (without drying). In this case, the particle dispersion was added dropwise until particles no longer instantly dissolved upon contacting the dissolution medium. Visually, the particles in dispersion were observed to rapidly disperse into the medium and immediately dissolve. The resulting supersaturation level of 63 was nearly 4-times higher than that from dissolution of the lyophilized AP particles.

For comparison, additional dissolution curves for both the pre-wet dispersion of particles made by AP with HPMC as a polymer stabilizer in a 1:2 ITZ/HPMC ratio and the final lyophilized particles are also shown in Figure 7.[18] In this case, when the lyophilized dried particles were added to the dissolution media, the degree of supersaturation over the crystalline solubility reached a level of 73, even higher then that of the pre-wet dispersion of pure ITZ.[18] An even higher supersaturation of 91 was achieve when the pre-wet dispersion of the 1:2 ITZ/HPMC particles was added in the same manner described above.[18]

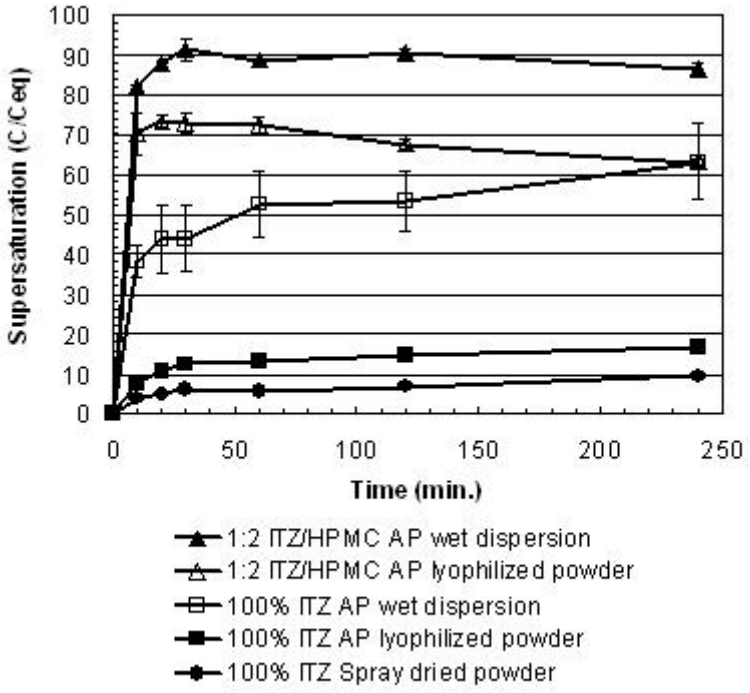

Figure 6.7 Supersaturation in pH 1.2 media from dissolution of 100% ITZ AP before and after freeze drying, 1:2 ITZ/HPMC AP before freeze drying, and spray dried 100% ITZ

6.5 DISCUSSION

6.5.1 Predicted Solubility of Pure Amorphous Itraconazole

The C_{pconf}, plotted in Figure 4 verses T, increases markedly near the T_g reflecting a rise in the molecular specific volume at the glass transition temperature.[7,19] The larger the increase in mobility between the glassy and supercooled states, as reflected in C_{pconf}^{Tg}, is an indication of the fragility that can be quantitatively described by γ_{Cp}. In this case, the similarity of the jump (0.24-0.39 J/gK) relative to indomethacin (0.46 J/gK) can indicate a relatively strong glass.[19] Backing this up are the γ_{cp} values calculated for the three amorphous forms, all of which fall between 0.66-0.79, which also indicate a moderately strong glass, since a value of 0.46 for celecoxib was classified as having moderately fragile behavior (Table 6.2).[7]

Similar basic trends for the H_{conf}, S_{conf}, and G_{conf} are observed for all three amorphous forms (Figure 6.5). The enthalpy of crystallization for the glass $-(H_{conf})$ becomes more favorable with increasing temperature. Likewise, the entropy barrier to crystallization, $-S_{conf}$, or the loss in the disorder of the glass upon crystallization, becomes more unfavorable. As a net result of enthalpy-entropy compensation, the configuration free energy or thermodynamic driving force for crystallization decreases as the temperature increases. All these basic trends are similar to those found for other amorphous pharmaceuticals.[22] As a result of the decrease in G_{conf}, the theoretical solubility ratios also decreased as the temperature increased. However, at physiologically relevant temperatures, the theoretical solubility ratio was still substantial ranging from 25-175 depending on the formulation (Figure 6.6).

6.5.2 Experimental Solubility of Pure Amorphous Itraconazole

The experimental solubility ratio of the pure ITZ AP pre-wet dispersion came within 66% of predicted values for the pure DSC quench-cooled amorphous ITZ. This agreement surpasses previous studies of pure amorphous drugs using configurational thermodynamic properties for solubility prediction (Table 6.1). The majority of the particles utilized in these previous studies were quench cooled with liquid nitrogen resulting in diameters on the order of 100 μm.[3] In comparison, the AP amorphous ITZ particles were on the order of 1 μm. The smaller particle size has been shown to increase the degree of supersaturation achievable for amorphous particles.[18] The increase in particle specific surface area by decreasing particle size increases the dissolution rate (see equation 1 above), thus reducing the time for the undissolved solid phase to crystallize, especially in the presence of a solvent. The lower degree of crystallization during dissolution can lead to higher supersaturation levels.[18]

A comparison of the pre-wet dispersion of pure AP ITZ to the spray dried and lyophilized powder samples probes the effects of the degree of crystallinity and wetting on the potential to achieve the theoretical solubility ratio predicted by thermodynamics. Supersaturation of both powder samples appeared to level off to a plateau indicating that the dissolution attained a meta-stable thermodynamic state (Figure 6.7). It appeared that the supersaturated solution did not precipitate to any significant level over four hours, consistent with our previous study.[18] However, the achieved solubility ratio is far below the predicted values (Table 6.1). On first glace, the partial crystallinity of these powders causes the resulting achievable experimental solubility for both powders to lie somewhere between the solubility of a pure amorphous and pure crystalline formulation.[25]

In addition, the fact that the non-dissolved powder was hydrophobic and therefore floated at the top of the dissolution vessel decreased the surface area exposed to the dissolution media, thereby decreasing the initial dissolution rate. As a result, the decrease in the initial dissolution rate increases the time allowed for additional crystallization of the particles from exposure to the solvent. Therefore, for a hydrophobic drug like ITZ, a powder rapidly dispersed in the media at the start of the measurement should increase the dissolution rate and therefore the achievable experimental solubility ratio demonstrating how wetting can reduce the achievable experimental solubility ratio.

Comparing the AP lyophilized and spray dried formulations demonstrates how the configurational free energy (G_{conf}) can explain the difference in experimental solubility ratio measured. Only considering that the spray dried powder has a slightly smaller particle size and lower % crystallinity indicates that the spray dried sample should, from previous arguments, have a higher solubility ratio than the AP lyophilized sample.[17,18] When comparing two methods of producing amorphous material, looking at the configurational free energy at the temperature of interest for dissolution, 37°C, can compare the samples for their different propensity to crystallize. However, since the G_{conf} of the spray dried formulation is the highest, at dissolution conditions, it will have the highest overall driving force for crystallization. As a result, the higher driving force for crystallization caused the lowest measured solubility ratio of the three amorphous ITZ samples analyzed.

6.5.3 Comparison to Amorphous Indomethacin

A comparison of the thermodynamic characteristics of ITZ and indomethacin shows that both have similar melting temperatures; however indomethacin has a lower

T_g(Table 6.1). Using this information and looking at the reduced crystallization temperature ((T_c-T_g)/(T_m-T_g)), which represents a normalized measure of how far a compound must be heated for spontaneous crystallization to occur[22], indicates that indomethacin should be more likely to crystallize than itraconazole. In addition, indomethacin has been shown to produce a stronger glass according to its γ_{cp} value (Table 6.2). The higher γ_{cp} value indicates that the average degree of mobility is less sensitive to temperature at temperatures below the T_g.[23] This confirms that indomethacin will have a reduced configurational free energy, which will lead to a lower predicted solubility ratio. In addition, obtaining the predicted solubility ratio for indomethacin will be more difficult and require an even faster initial dissolution rate than ITZ due to the faster crystallization predicted from the reduced crystallization temperature. In a previous study, the larger particle size used did allow solvent-mediated crystallization to occur and was confirmed by analysis of the indomethacin particles left after the solubility study. These particles were reanalyzed and showed all three solid forms, the amorphous, γ-crystals and α-crystals after being exposed to the media for only 2 hours.[3]

6.5.4 Surface Stabilization with Polymer for Measurement of Higher Metastable Solubility

As was shown previously, the only pure ITZ sample that exceeded 50% of the theoretical supersaturation was an aqueous dispersion that was dissolved immediately in acidic media after being prepared. After drying, the experimental supersaturation was about 4 fold smaller, as a result of poor wetting and partial crystallization of the particles. No stabilizing polymers were used in forming these dispersions as they would have complicated the analysis of C_{pconf}, due to drug-polymer interactions.

To create a practical formulation for drug delivery, it is important to protect the dosage form from crystallization during storage in the amorphous state, for example with a high T_g polymer.[26-28] In addition, the polymer may be utilized to increase the wetability of the powder [18,26] and decrease the particle size to accelerate the generation of supersaturation.[7,18] Recently we reported supersaturation values up to 91 for ITZ AP particles stabilized with HPMC, in contrast with a value of only 63 in the current study for the pure ITZ AP suspension.[18] Considering that polymer-drug interactions do not contribute significantly to the increase in solubility ratio[18], this supersaturation is in the range of that predicted by theory for the pure amorphous ITZ. Comparing the pure ITZ lyophilized formulation with the ITZ:HPMC lyophilized sample demonstrates how the polymer reduces particle size, increases wettability and reduces crystallization, leading to an experimental solubility ratio of 73, almost complete solubility of the 80 times supersaturation added in this test.[18]

6.6 CONCLUSIONS

The higher C_{pconf} values typical for a more fragile glass, when integrated over temperature, produce a larger G_{conf} and thus a larger supersaturation than for a stronger glass. However, fragile glasses are more likely to crystallize during storage and dissolution. Thus, it is beneficial to design fragile glass particles with high surface areas and rapid wetting to produce high supersaturation values during dissolution, before the undissolved solid crystallizes. Typically, the high supersaturation values for amorphous drugs, predicted from configurational thermodynamic properties, have not been achieved experimentally. For example, slowly dissolving large particles, formed by quench cooling in liquid nitrogen, produced solubilities less than 20% of the theoretical value (Table 6.1).

[3,7,14-17] In the present study, a similar limitation in supersaturation was observed for particles produced by spray drying and lyophilization of aqueous dispersions resulting from poor wetting and slow dissolution. In contrast, supersaturation values reached 63 for dissolution of a pre-wet amorphous dispersion of pure ITZ micron-sized particles in acidic media, relative to a predicted value of 95. With even smaller particles stabilized with HPMC during antisolvent precipitation, supersaturation values reached 90.[18] The high predicted values of supersaturation from configurational properties are thus reasonable goals for amorphous particles designed with sufficient wetting and high surface areas for rapid dissolution.

6.7 REFERENCES

1. Lipinski, C. A., Poor aqueous solubility- an industry wide problem in drug discovery. *Am. Pharm. Rev.* **2002,** 5, 82-85.

2. Leuner, C.; Dressman, J., Improving drug solubility for oral delivery using solid dispersions. *European Journal of Pharmaceutics and Biopharmaceutics* **2000,** 50, 47-60.

3. Hancock, B. C.; Parks, M., What is the True Solubility Advantage for Amorphous Pharmaceuticals? *Pharmaceutical Research* **2000,** 17, (4), 397-404.

4. Horter, D.; Dressman, J. B., Influence of physicochemical properties on dissolution of drugs in the gastrointestinal tract. *Advanced Drug Delivery Reviews* **2001,** 46, 75-87.

5. Rogers, T. L.; Gillespie, I. B.; Hitt, J. E.; Fransen, K. L.; Crowl, C. A.; Tucker, C. J.; Kupperblatt, G. B.; Becker, J. N.; Wilson, D. L.; Todd, C.; Broomall, C. F.; Evans, J. C.; Elder, E. J., Development and Characterization of a Scalable Controlled Precipitation Process to Enhance the Dissolution of Poorly Water-Soluble Drugs. *Pharmaceutical Research* **2004,** 21, (11), 2048-2057.

6. Parks, G. S.; Snyder, L. J.; Cattoir, F. R., Studies on Glass. XI. Some Thermodynamic Relations of Glassy and Alpha-Crystalline Glucose. *J. Chem. Phys.* **1934,** 2, (9), 595-598.

7. Gupta, P.; Chawla, G.; Bansal, A. K., Physical Stability and Solubility Advantage from Amorphous Celecoxib: The Role of Thermodynamic Quantities and Molecular Mobility. *Molecular Pharmaceutics* **2004,** 1, (6), 406-413.

8. Raghavan, S. L.; Trividic, A.; Davis, A. F.; Hadgraft, J., Effect of cellulose polymers on supersaturation and in vitro membrane transport of hydrocortisone acetate. *International Journal of Pharmaceutics* **2000,** 193, 231-237.

9. Raghavan, S. L.; Kiepfer, B.; Davis, A. F.; Kazarian, S. G.; Hadgraft, J., Membrane transport of hydrocortisone acetate from supersaturated solutions; the role of polymers. *International Journal of Pharmaceutics* **2001,** 221, 95-105.

10. Gunawan, L.; Johari, G. P.; Shanker, R. M., Structural Relaxation of Acetaminophen Glass. *Pharmaceutical Research* **2006,** 23, (5), 967-979.

11. Tombari, E.; Presto, S.; Johari, G. P.; Shanker, R. M., Molecular Mobility, Thermodynamics and Stability of Griseofulvin's Ultraviscous and Glassy States from Dynamic Heat Capacity. *Pharmaceutical Research* **2008,** 25, (4), 902-912.

12. Sertsou, G.; Butler, J.; Hempenstall, J.; Rades, T., Solvent change co-precipitation with hydroxypropylmethylcellulose phthalate to improve dissolution characteristics of a poorly water-soluble drug. *Journal of Pharmacy and Pharmacology* **2002,** 54, (8), 1041-1047.

13. Roberts, C. J.; Debenedetti, P. G., Engineering Pharmaceutical Stability with Amorphous Solids. *AIChE J.* **2002,** 48, (6), 1140-1144.

14. Stagner, W. C.; Guillory, J. K., Physical Characterization of Solid Iopanoic Acid Forms. *Journal of Pharmaceutical Sciences* **1979,** 68, (8), 1005-1009.

15. Corrigan, O. I.; Holohan, E. M.; Sabra, K., Amorphous forms of thiazide diuretics prepared by spray-drying. *International Journal of Pharmaceutics* **1984,** 18, 195-200.

16. Elamin, A. A.; Ahlneck, C.; Alderborn, G.; Nystrom, C., Increased metastable solubility of milled griseofulvin, depending on the formation of a disordered surface structure. *International Journal of Pharmaceutics* **1994,** 111, 159-170.

17. Mosharraf, M.; Nystrom, C., The effect of dry mixing on the apparent solubility of hydrophobic, sparingly soluble drugs. *European Journal of Pharmaceutical Sciences* **1999,** 9, 145-156.

18. Matteucci, M. E.; Brettmann, B. K.; Rogers, T. L.; Elder, E. J.; Williams III, R. O.; Johnston, K. P., Design of Potent Amorphous Drug Nanoparticles for Rapid Generation of Highly Supersaturated Media. *Molecular Pharmaceutics* **2007,** 4, (5), 792-799.

19. Shamblin, S. L.; Tang, X.; Chang, L.; Hancock, B. C.; Pikal, M. J., Characterization of the Time Scales of Molecular Motion in Pharmaceutically Important Glasses. *J. Phys. Chem. B* **1999,** 103, 4113-4121.

20. Angell, C. A., Relaxation in liquids, polymers and plastic crystals - strong/fragile patterns and problems. *Journal of Non-Crystalline Solids* **1991,** 131-133, 13-31.

21. Debenedetti, P. G.; Stillinger, F. H., Supercooled liquids and the glass transition. *Nature* **2001,** 410, 259-267.

22. Zhou, D.; Zhang, G. G. Z.; Law, D.; Grant, D. J. W.; Schmitt, E. A., Physical Stability of Amorphous Pharmaceuticals: Importance of Configurational Thermodynamic Quanitites and Molecular Mobility. *Journal of Pharmaceutical Sciences* **2002,** 91, (8), 1863-1872.

23. Hancock, B. C.; Shamblin, S. L., Molecular mobility of amorphous pharmaceuticals determined using differential scanning calorimetry. *Thermochimica Acta* **2001,** 380, 95-107.

24. Six, K.; Berghmans, H.; Leuner, C.; Dressman, J.; Van Werde, K.; Mullens, J.; Benoist, L.; Thimon, M.; Meublat, L.; Verreck, G.; Peeters, J.; Brewster, M.; Van den Mooter, G., Characterization of Solid Dispersions of Itraconazole and Hydroxypropylmethylcellulose Prepared by Melt Extrusion, Part II. *Pharmaceutical Research* **2003,** 20, (7), 1047-1054.

25. Mosharraf, M.; Sebhatu, T.; Nystrom, C., The effects of disordered structure on the solubility and dissolution rates of some hydrophilic, sparingly soluble drugs. *International Journal of Pharmaceutics* **1999,** 177, 29-51.

26. Verreck, G.; Six, K.; Van den Mooter, G.; Baert, L.; Peeters, J.; Brewster, M., Characterization of solid dispersions of itraconazole and hydroxypropylmethylcellulose prepared by melt extrusion - part I. *International Journal of Pharmaceutics* **2001,** 251, 165-174.

27. Yamashita, K.; Nakate, T.; Okimoto, K.; Ohike, A.; Tokunaga, Y.; Ibuki, R.; Higaki, K.; Kimura, T., Establishment of new preparation method for solid

dispersion formulation of tacrolimus. *International Journal of Pharmaceutics* **2003,** 267, 79-91.

28. Zhu, Z.; Anacker, J. L.; Ji, S.; Hoye, T. R.; Macosko, C. W.; Prud'homme, R. K., Formation of Block Copolymer-Protected Nanoparticles via Reactive Impingement Mixing. *Langmuir* **2007,** 23, 10499-10504.

Chapter 7: Conclusions and Recommendations

This chapter summarizes the key advances made by the research described in this dissertation as well as recommendations for future research. In the first section, suspensions and dispersions of protein particles formed by multiple techniques suspended in either aqueous or non-aqueous solvents are used to demonstrate the potential of subcutanenous injections of a highly concentrated protein therapeutic. Understanding mechanisms which allow for the formation of the dispersions while simultaneously retaining the activity of the protein and a low viscosity formulation provide the basis to increase the use of protein therapeutics. The second section improves upon the mechanistic understanding of amorphous particle formation and how to enhance poorly-water soluble drug concentrations *in vivo*. The final section demonstrates the need to understand freezing of a bulk monoclonal antibody solution for long term storage stability.

7.1 Conclusions

7.1.1 Dispersions of protein particles for subcutaneous delivery

In chapter 2, viscosities below 50cp for concentrated suspensions up to 300-400 mg/ml of ~10 μm milled particles of the model protein, lysozyme, were obtained for subcutaneous injection through a 25 to 27-gauge needle. The apparent viscosity of these suspensions was correlated with volume fraction at all conditions according to the Krieger-Dougherty equation resulting in an intrinsic viscosity close to 2.5, indicating weak interparticle interactions. The various factors that produce large increases in viscosity for proteins in aqueous solution, including an increase in ϕ from solvation, and

deviations of the particle shape from a spherical geometry, have almost negligible effects for the non-aqueous protein suspensions in this study.

In chapter 3, a polyclonal antibody, sheep IgG, forms equilibrium nanoclusters that simultaneously provide a low dispersion viscosity at high protein concentrations (up to 270 mg/ml) and preserve the native folded state of the protein. These equilibrium clusters are formed by balancing attraction from specific short-range attractive protein interactions and extrinsic crowders against very weak electrostatic charging near the isoelectric point of the protein. The hierarchy of strong intracluster interactions used to form the nanoclusters and the weak intercluster interactions result in high colloidal stability and low viscosities. The highly self-crowded environment within the nanocluster prevents unfolding of the protein, as predicted previously.[1, 2]

In chapter 4, the formation, dissolution and bioavailability of a nanocluster dispersion of a protein monoclonal antibody is characterized to deliver highly concentrated monoclonal antibodies via a subcutaneous injection. In this case, highly concentrated 190 mg/ml aqueous-based dispersions of a therapeutically relevant antibody, 1B7[3], were formed from particles formed by SWIFT. *In vitro* stability was confirmed within the dispersion by tryptophan fluorescence and upon dilution into a pure buffer by ELISA, DLS and SDS-PAGE. Upon *in vivo* injection, similar distribution and elimination half-lives were measured from the dispersion and solution formulations at similar doses, while the time to peak serum concentration (t_{max}) was delayed for the SQ injections, consistent with the expected slower diffusion kinetics from this injection site. In the terminal serum samples, testing for specific PTx binding activity by ELISA, as

well as an *in vitro* PTx neutralization test, was unable to detect a loss in 1B7 activity or development of anti-1B7 immune responses.

In conclusion from chapters 3 and 4, nanoclusters formed from the balancing attraction from specific short-range attractive protein interactions and depletion attraction from extrinsic crowders against very weak electrostatic charging near the isoelectric point of the protein are suitable for subcutaneous injections. The hierarchy of strong intracluster interactions used to form the nanoclusters and the weak intercluster interactions to limit their size result in high colloidal and molecular stability and low viscosities. The hierarchical protein nanocluster concept is based on general scaling of short-ranged and crowding intermolecular and repulsive intercluster interactions, and thus, has been expanded to multiple proteins and multiple crowding agents. As a result, this concept may be expected to be applicable to a wide variety of protein and peptides.

7.1.2 Oral delivery of amorphous itraconazole

In chapter 5, nanoparticle dispersions of itraconazole stabilized with an enteric polymer, Eudragit® L100-55, were flocculated, filtered and dried at room temperature to recover high yields (close to 100%) of amorphous particles. Flocculation of the particles occurred by neutralizing the negative charge on the polymer by lowering the pH to 2.5. By remaining at room temperature throughout processing, crystallization of the antisolvent precipitated nanoparticles of itraconaozle was prevented. The *in vitro* dissolution behavior and *in vivo* bioavailability of the pH-flocculated particles was compared to previously analyzed salt flocculated particles[4] and the commercially available itraconazole formulation, Sporanox. The *in vivo* bioavailability was highest for the salt flocculated formulation, second for the pH flocculated formulation and lowest for

Sporanox. The same order was followed for the *in vitro* pH shift experiments to determine AUC_{2hr} in the micelles at neutral pH. This correlation suggests that the high supersaturation for amorphous nanoparticles was important, which would not be available for crystalline drugs. The improved bioavailability of amorphous flocs produced by flocculation and filtration relative to the sugar-based solid dispersion, Sporanox, provides an alternative for more effective oral delivery of poorly water soluble drugs.

Analysis of the increase in suspersaturation of amorphous particles based on configurational thermodynamic properties is found in Chapter 6. The higher configuration heat capacity for a more fragile glass, when integrated over temperature, produced a larger configuration free energy and thus a larger supersaturation than for a stronger glass. However, fragile glasses are more likely to crystallize during storage and dissolution. Thus, it is beneficial to design fragile glass particles with high surface areas and rapid wetting to produce high supersaturation values during dissolution, before the undissolved solid crystallizes.

7.2 RECOMMENDATIONS AND FUTURE RESEARCH

7.2.1 Dispersions of protein particles

Biopharmaceutics and delivery of these types of therapeutic agents is an active area of research as few of the conventional delivery techniques, such as oral delivery, for small molecule drugs work.[5-7] In chapters 2-4, a novel method to formulate protein therapeutics into nanoclusters of proteins is demonstrated for use in subcutaneous delivery. The research presented in this section is one that has many future applications for the delivery of biopharmaceutics. First off, additional characterization of proteins of

various sizes from small peptides and antibody fragments[8] to larger multi-domain proteins could further confirm the generality of the approach described in this dissertation. In addition, future work can involve tracing the antibody once it is injected *in vivo* to quantitatively show the protein concentration in any part of the body.[9] This method could help demonstrate the specificity of the protein utilized to the therapeutic target and show relative ratio of the active drug compound to the total drug injected, demonstrating the percentage of the drug remaining at the injection site. Beyond verifying the protein characteristics, further research could be done on different methods of delivery for these nanocluster dispersions, including pulmonary[10] to find how to best utilize the biopharmaceutics. These alternative methods of delivery have shown promise *in vitro* however would need to be expanded to the *in vivo* studies to demonstrate pharmacokinetics and efficacy.

In addition, while the research in this dissertation does not show an immune response, further animal studies to test for immunogenicity would be necessary using multiple injections and tracer molecules to track the dissolution of the particles throughout the host. Beyond proving the lack of an immune response to the nanoclusters, larger nanoclusters can be potentially created to act as a vaccine. Larger nanoparticles which do not dissolve as rapidly can elicit an immune response without the need to add an adjuvant.[11] As a result, this mechanism can be utilized for vaccine production and injection, especially for a large molecular weight biologic molecule.

While much colloidal characterization has been obtained, a better understanding of the exact protein volume fraction would require specialized imaging devices. Understanding the details of the exact final protein volume fraction within clusters of

various sizes can increase the understanding of the mechanism leading to their formation. This knowledge can be used to increase the understanding of several degenerative human diseases including Alzheimer's[12] and eye cataracts[13]. In these cases, protein aggregation and the formation of a highly ordered superstructure of the protein lead to changes in a humans biological response. Misfolding of the proteins which leads to the formation of the fibrils can be analyzed within the context of the formation of misfolded proteins into nanoclusters. By purposely misfolding the protein, the aggregation kinetics and influence of solution parameters such as pH and tonicity can be independently varied. Increased understanding of the factors affecting protein aggregation can result in novel techniques utilized to combat diseases such as Alzheimers and eye cateracts that result from an increase in protein aggregation. The realm of possibilities is still open and hopefully just the stepping stone to future ideas.

7.2.2 Recommendations to extend oral delivery of amorphous poorly-water soluble drugs

The use of amorphous forms of poorly-water soluble drugs has greatly expanded over the last 10 years and significant advances have been made.[14] Specific to the flocculation project, future work would be to expand the techniques of antisolvent precipitation and flocculation by both pH and salt to a greater number of drug molecules and polymers. pH sensitive polymers that have shown increased *in vivo* bioavailability without the use of higher surface area powders would be of great interest.[15] In addition, the variation in surface area and resulting pharmacokinetics from compressing the powder into a tablet or enclosing the powder in a capsule would be of great interest. These simple steps would significantly advance the work to truly understand the

relationship between sustained supersaturation of the drug molecule and resulting *in vivo* bioavailability.

Beyond simple additional experiments, the addition of a mucoadhesives to the formulation can be analyzed. Since a mucoadhesive will adhere to the mucosal layer lining of the body, including the gastrointestinal tract, the combined drug molecule will be slowed through the gastrointestinal tract resulting in an increase in residence time of the drug molecule.[16, 17] An increase in residence time of the drug molecule to the absorption surface of the gastrointenstinal tract, will result in an increase in the bioavailability of the drug.[18] To date, little research has utilized the combination of a mucoadhesive with high surface area drug particles. Such a combination could result in the prolonged supersaturation of the drug molecule and higher bioavailability.

7.3 REFERENCES

1. Cheung, J. K.; Truskett, T. M., Coarse-Grained Strategy for Modeling Protein Stability in Concentrated Solutions. *Biophys J* **2005,** 89, 2372-2384.

2. Shen, V. K.; Cheung, J. K.; Errington, J. R.; Truskett, T. M., Insights into Crowding Effects on Protein Stability from Coarse-Grained Model. *Journal of Biomechanical Engineering* **2009,** 131, 071002 (7pg).

3. Sutherland, J. N.; Maynard, J. A., Characterization of a Key Neutralizing Epitope on Pertussis Toxin Recognized by Monoclonal Antibody 1B7. *Biochemistry* **2009,** 48, 11982-11993.

4. Matteucci, M. E.; Paguio, J. C.; Miller, M. A.; Williams III, R. O.; Johnston, K. P., Flocculated Amorphous Nanoparticles for Highly Supersaturated Solutions. *Pharm Res* **2008,** 25, (11), 2477-2487.

5. Brown, L. R., Commercial challenges of protein drug delivery. *Expert Opin. Drug Deliv.* **2005,** 2, (1), 29-42.

6. Pawar, R.; Ben-Ari, A.; Domb, A. J., Protein and peptide parenteral controlled delivery. *Expert Opin. Biol. Ther.* **2004,** 4, (8), 1203-1212.

7. Liu, J.; Nguyen, M. D. H.; Andya, J. D.; Shire, S. J., Reversible Self-Association Increases the Viscosity of a Concentrated Monoclonal Antibody in Aqueous Solution. *Journal of Pharmaceutical Sciences* **2005,** 94, (9), 1928-1940.

8. Maynard, J. A.; Maassen, C. B. M.; Leppla, S. H.; Brasky, K.; Patterson, J. L.; Iverson, B. L.; Georgiou, G., Protection against anthrax toxin by recombinant antibody fragments correlates with antigen affinity. *Nature Biotechnology* **2002,** 20, 597-601.

9. Zintchenko, A.; Susha, A. S.; Concia, M.; Feldmann, J.; Wagner, E.; Rogach, A. L.; Ogris, M., Drug Nanocarriers Labeled with Near-infrared-emitting Quantum Dots (Quantoplexes): Imaging Fast Dynamics of Distribution in Living Animals. *Molecular Therapy* **2009,** 17, (11), 1849-1856.

10. Engstrom, J. D.; Tam, J. M.; Miller, M. A.; Williams III, R. O.; Johnston, K. P., Templated Open Flocs of Nanorods for Enhanced Pulmonary Delivery with Pressurized Metered Dose Inhalers. *Pharm Res* **2009,** 26, (1), 101-117.

11. Cox, J. C.; Coulter, A. R., Adjuvants - a classification and review of their modes of action. *Vaccine* **1997,** 15, (3), 248-256.

12. Nguyen, H. D.; Hall, C. K., Spontaneous Fibril Formation by Polyalanines; Discontinuous Molecular Dynamics Simulations. *JACS* **2006,** 128, 1890-1901.

13. Berland, C. R.; Thurston, G. M.; Kondo, M.; Broide, M. L.; Pande, J.; Ogun, O.; Benedek, G. B., Solid-liquid phase boundaries of lens protein solutions. *Proc. Natl. Acad. Sci.* **1992,** 89, 1214-1218.

14. Lipinski, C. A., Avoiding investment in doomer drugs, is poor solubility an industry wide problem? *Current Drug Discovery* **2001**, 17-19.

15. DiNunzio, J. C.; Miller, D. A.; Yang, W.; McGinity, J. W.; Williams III, R. O., Amorphous Compositions Using Concentration Enhancing Polymers for Improved Bioavailibility of Itraconazole. *Molecular Pharmaceutics* **2008,** 5, (6), 968-980.

16. Chowdary, K. P. R.; Rao, Y. S., Mucoadhesive Microspheres for Controlled Drug Delivery. *Biological and Pharmaceutical Bulletin* **2004,** 27, (11), 1717-1724.

17. Nagai, T.; Machida, Y., Mucosal adhesive dosage forms. *Pharm. Int.* **1985,** 6, 196.

18. Ponchel, G.; Irache, J.-M., Specific and non-specific bioadhesive particulate systems for oral delivery to the gastrointestinal tract. *Advanced Drug Delivery Reviews* **1998,** 34, 191-219.

Appendix A: Supplemental Information for Various Chapters

A.1 Supplemental Information for chapter 2

A.1.1 Time to draw 1 ml of solution correlation to the viscosity for 25 and 27 g needles

Each graph in the figure below (Figure A.1.1) contains four points on the line containing the known viscosities of perfluorodecalin, benzyl benzoate, ethyl oleate and olive oil compared to their measured time to draw 1mL through the respective needle gauge. As described in the text, this correlation is backed up by the basic Hagen-Poiseuille flow equation, and has been used previously as a measure of viscosity by Shire and coworkers.

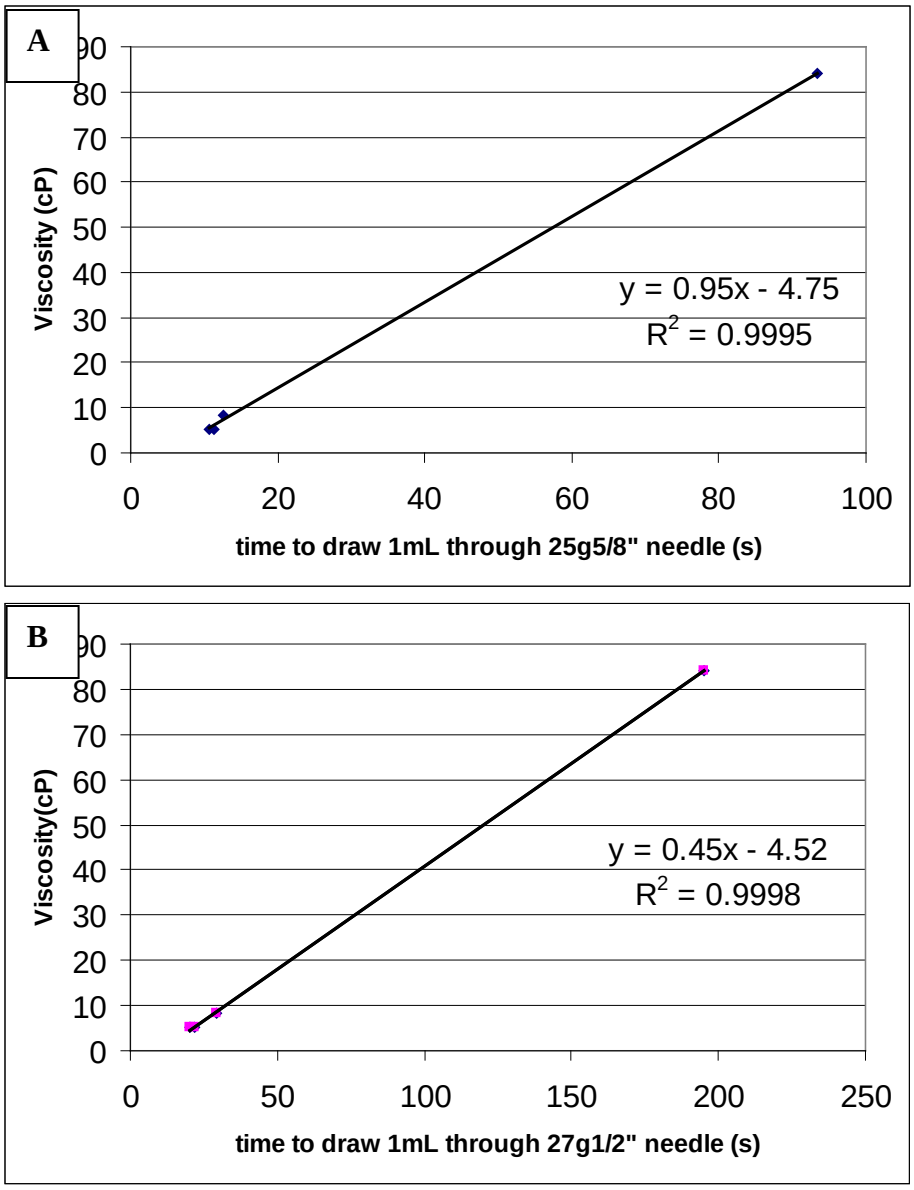

Figure A.1 Linear plots of the time to draw 1 mL of a suspension through a) a 25g 5/8" needle and b) a 27g 1/2" needle.

A.1.2 Optical Density Absorbance Values

The actual optical density values measured using the method described in the "Optical Density Measurement" section of the Materials and Methods are below in Table A.1. The low %RSD indicates the very similar results from the multiple samples and all samples are very close to the standard measured. Since the absorbance values are relatively high, additional standards and a sample that clearly aggregated were compared to the diluted 50 mg/ml concentrations in the safflower oil and benzyl benzoate as well as the pure benzyl benzoate solvent using a Falcon UV transparent 96-well plate. Absorbance of the standard was lowered to 0.047 ± 0.005 however the sample that aggregated had an absorbance of 0.24, above the absorbance of any sample reported in table A1.1. The absorbance of the two extracted and diluted 50 mg/ml lysozyme samples in the safflower oil and benzyl benzoate and pure benzyl benzoate solvents were 0.052 and 0.051 respectively, within the deviation for the standard.

Table A.1 Optical Density values for the various formulations diluted to 1 mg/ml using standard 96-well plates measured in the μQuant spectrophotometer at 350 nm. (Benzyl Benzoate is abbreviated BB and Lysozyme is abbreviated LYS)

	A_{350}	% RSD
Standard	0.1025	0.56%
100 mg/mL LYS in 50/50 Safflower Oil/BB	0.106	1.16%
200 mg/mL LYS in 50/50 Safflower Oil/BB	0.1016	0.54%
300 mg/mL LYS in 50/50 Safflower Oil/BB	0.1026	0.87%
50 mg/mL LYS in Water with BB	0.1032	1.06%
50 mg/mL LYS in BB	0.105	0.80%
100 mg/mL LYS in BB	0.1036	0.53%
200 mg/mL LYS in BB	0.1016	1.49%
400 mg/mL LYS in BB	0.1004	1.94%

A.1.3 Calculation for Entry Distance to Poiseuille Flow in Capillary

Using the Equation

$$X = \frac{\mathrm{Re}}{30} d \quad \text{(A.1.1)}$$

where, X is the entry distance, Re is the Reynold's Number, and d is the diameter of the capillary, should give the entry distance to the point where the maximum velocity in the tube is within 5% of the theoretical maximum.[1] Assuming the viscosity and density of pure benzyl benzoate (μ = 8.8 cP and ρ = 1.128 g/cm^3), the Reynolds number through the syringe (assuming constant flow to get the velocity) is 0.139. Using the equation above for a 25 gauge needle (ID = 0.0241 cm), the entry distance required should be $1.12*10^{-4}$ cm, much smaller than the actual length of the needle.

A.1.4 References

1. Jacobson, B. O., *Rheology and Elastohydrodynamic Lubrication*. Elsevier Publishing Company: 1991; Vol. 19.

A.2 Supplemental Information for Chapter 3

A.2.1 Supplemental Methods

A.2.1.1 Protein purification

The IgG was reconstituted to 20 mg/ml in pH 7.0 phosphate buffer and further purified to >99% monomeric protein via FPLC size-exclusion chromatography. Injections of ~ 20 mg IgG were separated by a Superdex S200 Column (GE Healthcare, Uppsala, Sweden) using phosphate buffer with sodium chloride as the eluent. The

purified monomer was concentrated and the buffer was exchanged to a pH 5.5 or pH 7.0 histidine buffer with 50,000 MWCO Amicon Ultra-15 (Millipore, Billerica, MA) centrifugal concentrator to yield a final IgG concentration of 20 mg/ml with a 1:1 (wt) ratio of α-α trehalose in histidine buffer, pH 5.5 or 7.0.

A.2.1.2 Determination of the isoelectric point

The pI of the IgG was determined by measuring the zeta potential of the protein in a 20mM histidine buffer at pHs 5.5, 6.4, and 7.4 on a Brookhaven Instruments ZetaPlus dynamic light scattering apparatus at a scattering angle of 90° and temperature of 25 °C. The average zeta potential reported is the average of 30 runs with the standard deviation reported as the error bars (Figure 3A). In addition, the pI of the IgG was confirmed by isoelectric focusing (IEF) gel electrophoresis. In a precast IEF gel (Bio-Rad product 161-1111) with a pH range of 3-10, 5-10 μg of the purified IgG diluted in a loading buffer of 50% glycerol with pure DI water was separated based on pI for 1 h. at 100V followed by 2 h. at 250V using a cathode buffer containing 20mM lysine and 20mM arginine and an anode buffer containing 7mM% phosphoric acid. The IEF gel was stained with silver staining and the image captured prior to drying.

A.2.1.3 Images of the particles before and after forming dispersions

Samples of the dry powders after lyophilization for scanning electron microscopy (SEM) analysis were placed on adhesive carbon tape to fix the sample to the SEM stub. A drop of the final dispersion diluted to 40 mg/ml was placed on an SEM stub or lacey-carbon transmission electron microscope (TEM) grid, blotted to remove the excess liquid and rapidly frozen by immersing it in liquid nitrogen. The stages were then dried using a Virtis Advantage Tray Lyophilizer with 2 hours of primary drying at -40^{o}C followed by a

12 hour ramp to +25^{o}C and then 2 hours of secondary drying at 25^{o}C. Each sample for SEM was platinum-palladium sputter coated using a Cressington 208 bench top sputter coater to a thickness of 10nm. Micrographs were taken using a Zeiss Supra 40 VP scanning electron microscope with an accelerating voltage of 5 kV. Z-contrast scanning transmission electron microscopy (STEM), using a high-angle annular dark field (HAADF) detector visualized the particles at 200 kV on a FEI Tecnai TF20 transmission electron microscope.

A.2.1.4 Determination of irreversible denaturation and aggregation of IgG

The percent of monomeric protein present in IgG samples was analyzed by dynamic light scattering as described above. Samples of the initial purified IgG powder, dissolved lyophilized particles and the dissolved particles from the dispersions were adjusted to ~1 mg/ml in phosphate buffer. The amount of active antibody in a sample was quantified using a polyclonal capture enzyme-linked immunosorbent assay (ELISA). For the ELISA test, high-binding ELISA plates (Costar No. 3590) were coated with 12.5 µg/ml rabbit anti-sheep IgG (Southern Biotech No. 6150-01) and incubated at 4ºC overnight, then blocked with PBS-1% milk for 1 hr at room temperature. After triplicate washing with PBS-0.05% Tween20, sheep IgG samples were serially diluted from 100 µg/ml using a √10 dilution scheme with PBS-milk as the diluent. After room temperature equilibration for 1 h and an additional wash step, peroxidase-conjugated rabbit anti-sheep IgG (MP Biomedical No. 55814) at 0.125 µl/ml was added. After additional equilibration and washing steps, substrate (tetramethylbenzidine dihydrochloride (Pierce, Rockford, IL)) was added and color allowed to develop for 30 seconds before quenching the reaction with 1N HCl. The absorbance at 405nm was recorded on a SectraMax M5

instrument. EC_{50} (50% effective concentration) values were calculated from the linear range of the dose-response curve as the sheep antibody concentration corresponding to 50% of the maximum absorbance. For comparison of IgG samples, relative EC_{50} values were calculated as the ratio of the treated to reference EC_{50}. Each sample was analyzed in triplicate with the mean and standard deviation reported. Denatured IgG, heated to 70°C for 1 hr, was used as a non-binding negative control.

A.2.1.5Determination of the dn/dc for a protein nanocluster dispersion

The refractive index of the solvent was measured using a refractometer and confirmed by using optical coherence tomography. The refractive index of the solvent was confirmed by calculating the predicted refractive index using the Lorenz-Lorenz mixing rule:

$$\frac{(n_{mix}-1)^2}{(n_{mix}+2)^2} = \sum \varphi_i (n_i-1)^2/(n_i+2)^2 \text{ (eq. A.2.1)}$$

The measured value from the refractometer and by OCT differed by less than 1% due to the difference between measuring the phase refractive index (measured by a refractometer) and the group refractive index (measured by OCT). Figure A1.2.7 shows the slope, indicating the dn/dc, for a BSA dispersion in 25% PEG300 and 20% Ethanol. Due to the amount of protein needed for this test, it was not replicated for the IgG. Since the absolute values corresponded with the predicted values by the Lorenz-Lorenz rule, and the dn/dc was the same as that for a BSA solution ($0.183 cm^3/g$ [1]), the calculated values for the solvent refractive index and reported literature values for the dn/dc of an IgG solution ($0.185 cm^3/g$ [2, 3]) were used in the calculations.

A.2.2 Supplemental Figures and Tables

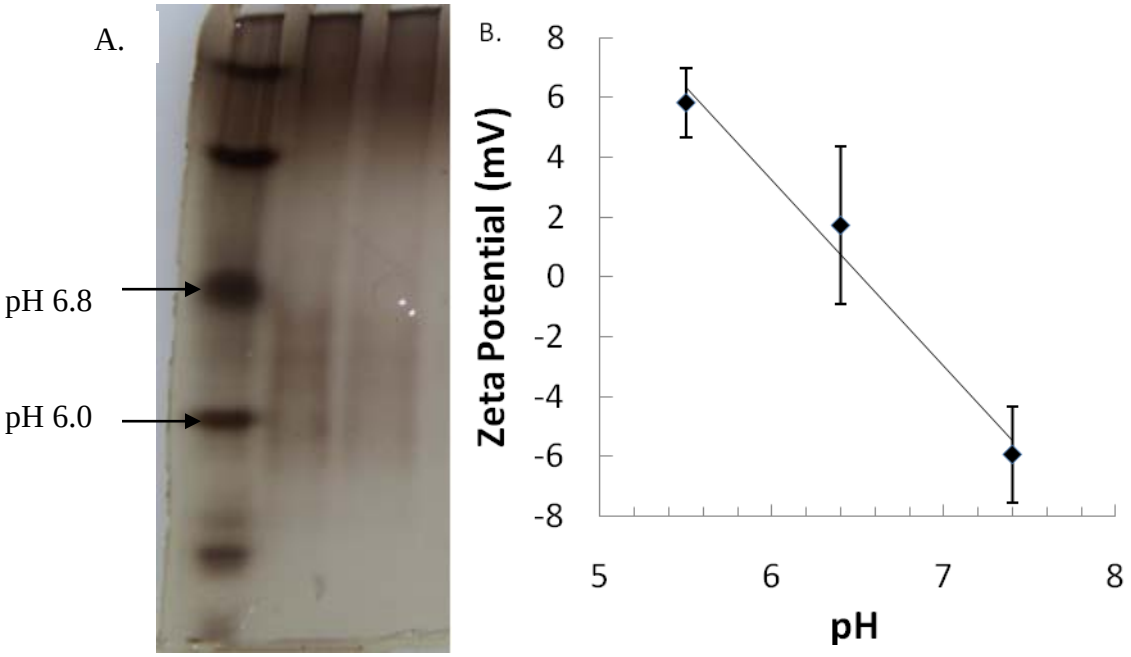

Figure A.2.1 A) IEF analysis of sheep IgG solution, from left to right lanes are IEF markers (Bio-Rad), 2μg sheep IgG and 1 μg sheep IgG. B) Zeta potential measurements on sheep IgG solution.

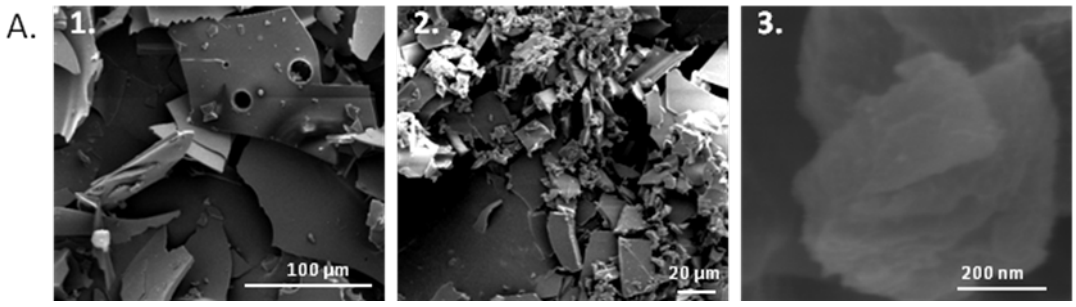

Figure A.2.2 SEMs of dried powders frozen at 20 mg/ml IgG with a 1:1 ratio of trehalose after lyophilization of the slow frozen, lyophilized IgG

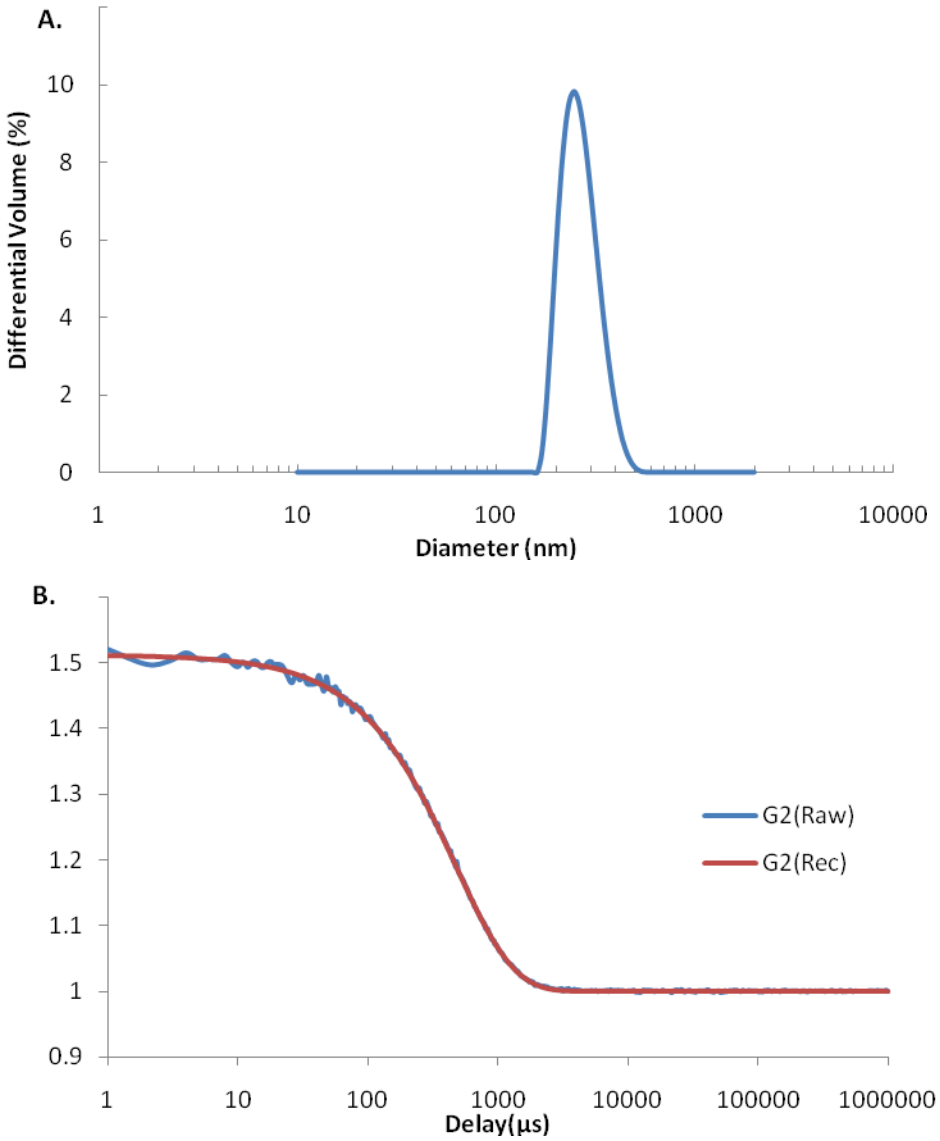

Figure A.2.3 A) Concentrated DLS on a 10% solids weight polystyrene standard of 298nm spheres. B) Correlation function for sample in A, raw data (G2(Raw)), and fit using CONTIN algorithm (G2(Rec)).

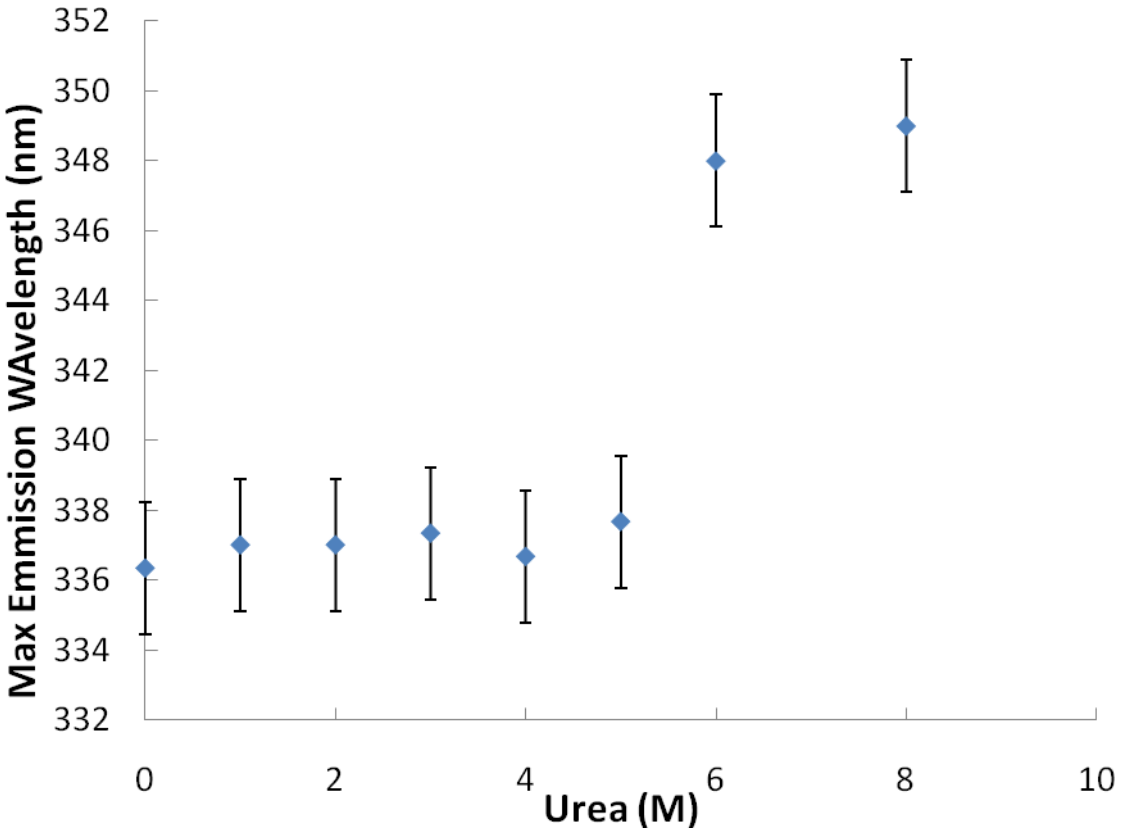

Figure A.2.4 Unfolding of IgG measured as maximum emission wavelength (λ_{max}) at various urea concentrations.

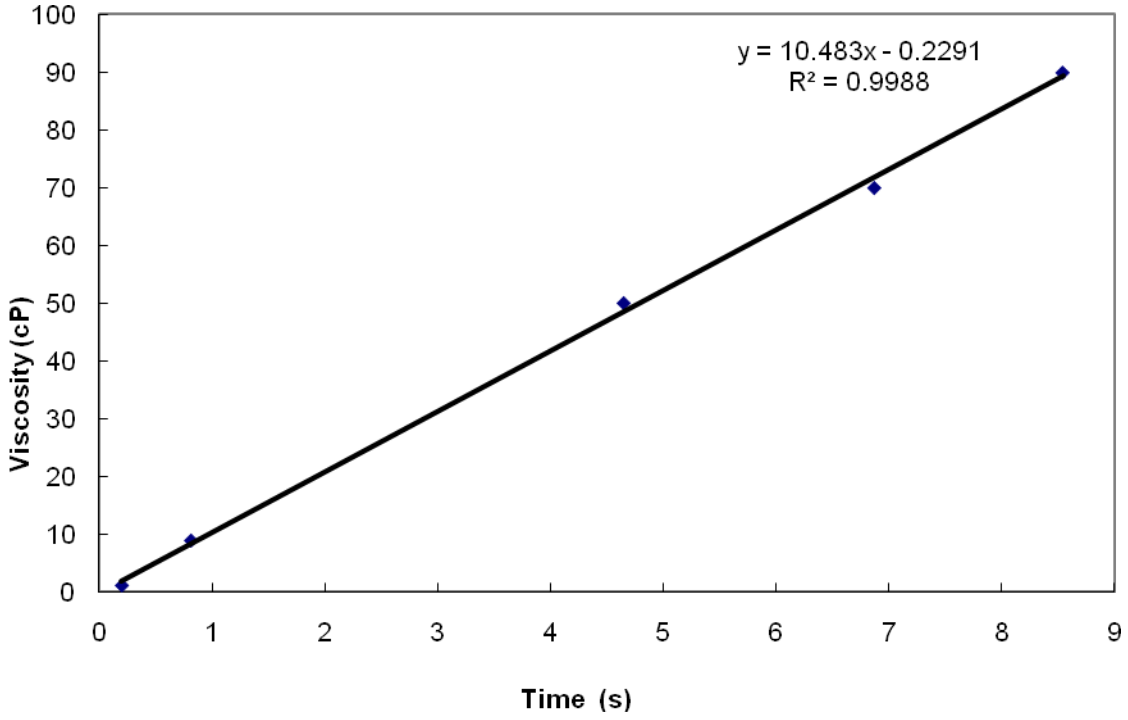

Figure A.2.5 Calibration curve for small conical vials from various solution standards DI water (η_o = 1 cP), PEG200 (η_o = 50 cP), PEG300 (η_o = 70 cP), PEG400 (η_o = 90 cP), and benzyl benzoate (η_o = 8.8 cP). The time for the liquid level to be drawn from 0.4" to 0.1" in small conical vial was measured from a video of the solution converted to a stack of images with 30 images per second.

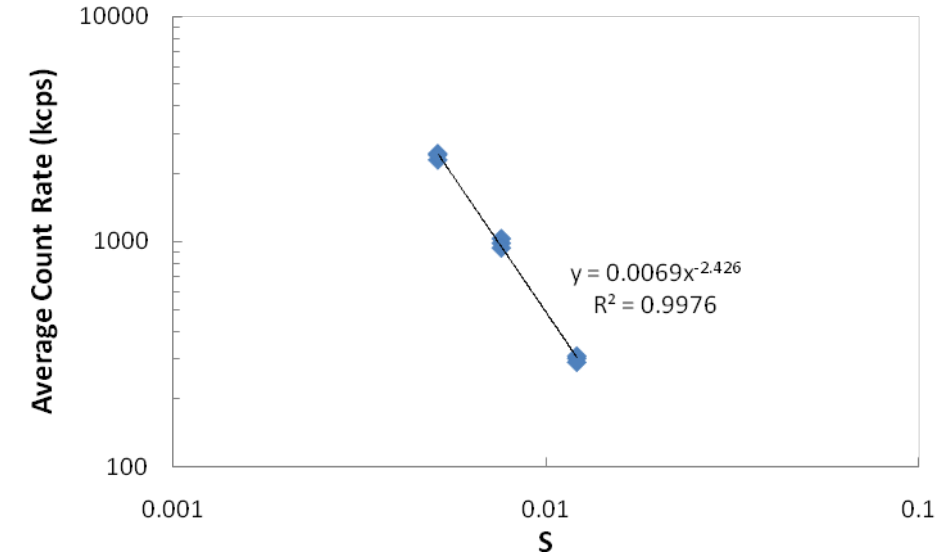

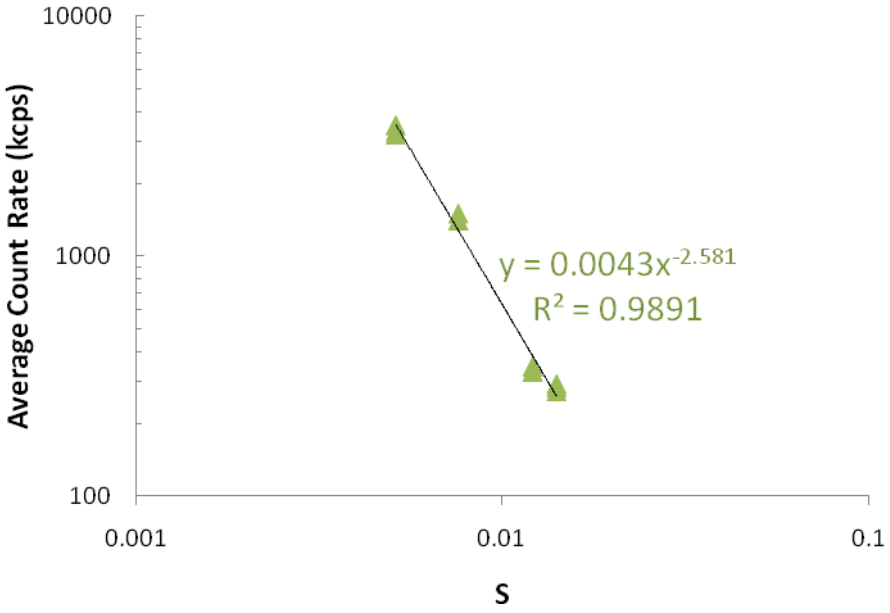

Figure A.2.6 Static light scattering at various angles to determine porosity for A) Nanoclusters formed with 50 mg/ml IgG at 250 mg/ml trehalose B) Nanoclusters formed at 10 mg/ml IgG with 8% PEG300/16% NMP

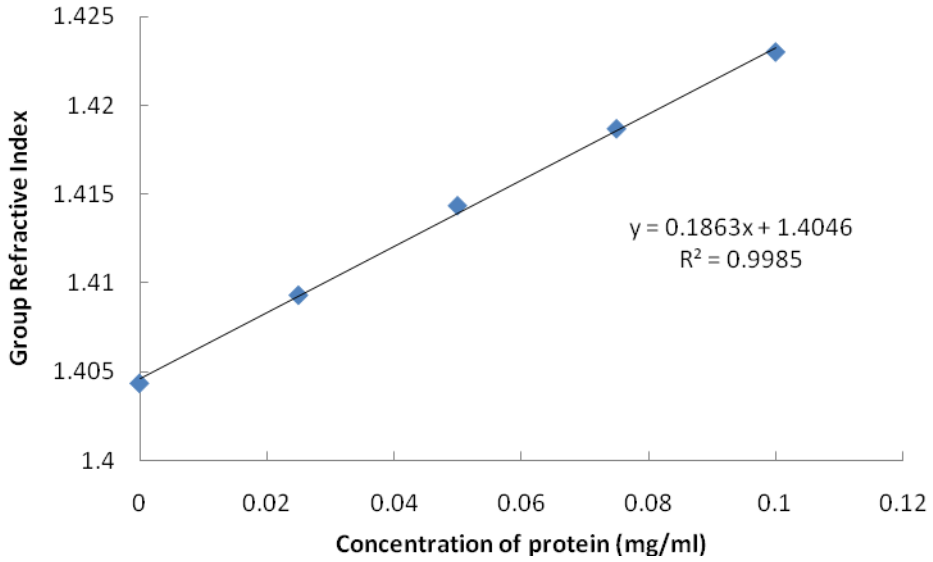

Figure A.2.7 Group refractive index versus concentration of protein particles for a BSA dispersion with 25% PEG300 and 20% Ethanol. The slope of the line indicates the measured dn/dc used in the calculation of the B_2 by SLS. The standard deviation of each measurement was 0.0001 so error bars are not visible.

Table A.2.1 Material balance from actual measured powder weight and added dispersion volume and resulting volume fraction of protein and other crowders. To approximate the volume fraction mass density of the IgG (1.34 g/ml) was estimated from the partial molar volume of a native IgG[4] and density of trehalose (1.64 g/ml) was estimated from the partial molar volume of trehalose[5]. Trehalose is included in all samples at a 1:1 wt ratio with the IgG concentration.

Name of sample	**Actual weight of 1:1 IgG: trehalose powder (mg)**	**Actual volume of total solvent added (ml)**	**Composition of actual solvent added (excluding dissolved sugar)**	**Volume of IgG (µl)**	**Volume of trehalose (µl)**	**Volume of pure buffer (µl)**	**Volume of PEG300 (µl)**	**Volume of NMP (µl)**	**Total volume of all components (µL)**
214 mg/ml	60.2	0.100	50 mM phosphate buffer	23	18	100	0	0	141
275 mg/ml	79.3	0.090	50mM phosphate buffer	30	24	90	0	0	144
157 mg/ml – 0.16 φ_P	40.4	0.100	20%(v/v) PEG300 in 50mM phosphate buffer	15	12	80	20	0	127
162 mg/ml – 0.24 φ_P	41.4	0.100	30%(v/v) PEG300 in 50mM phosphate buffer	15	13	70	30	0	128
157 mg/ml – 0.08 φ_P/0.16 φ_N	39.8	0.100	20%(v/v) NMP, 10%(v/v) PEG300 in 50mM phosphate buffer	15	12	70	10	20	127
204 mg/ml – 0.08 φ_P/0.16 φ_N	56.5	0.100	20%(v/v) NMP, 10%(v/v) PEG300 in 50mM phosphate buffer	21	17	70	10	20	138

Table A.2.2 Summary of various individual DLS samples run for average colloid sizes in Table 3.1.

IgG or Trehalose Concentration (mg/ml)	**Additional Crowders**	**Run**	**Mean diameter (nm)**	**% standard deviation over mean**
214	-	Run 1	103	9
		Run 2	68	21
275	-	Run 1	92	8
		Run 2	78	8
		Run 3	94	9
157	0.16 φ_P	Run 1	95	9
		Run 2	93	9
		Run 3	140	23
162	0.24 φ_P	Run 1	118	10
		Run 2	103	16
157	0.08 φ_P 0.16 φ_N	Run 1	280	8
		Run 2	259	12
		Run 3	256	8
		Run 4	220	5
		Run 5	275	6

Table A.2.3 Comparison of % monomer of 157 mg/ml IgG dispersions in pH 6.4 50mM phosphate buffer with 10% PEG300 and 20% N-methyl-2-pyrrolidone (NMP) by volume to unprocessed purified material

Sample name	**% monomer after purification**	**% monomer after dilution**
157 mg/ml - 0.08 φ PEG, 0.16 φ NMP	96.2 ± 0.6	97.0 ± 0.1

Table A.2.4 Summary of means and standard deviations for individual DLS runs for clusters formed along path 1 in Figure 3.5A.

Trehalose Concentration (mg/mL)	**Run**	**Mean diameter (nm)**	**Standard Deviation (nm)**	**% standard deviation over mean**
50	1	6.3	0.6	9
	2	6.0	1.0	16
	3	15.2	7.9	52
100	1	10.9	1.0	9
	2	9.4	0.7	8
	3	6.1	1.5	24
	4	11.3	1.6	15
150	1	5.3	1.5	28
	2	5.8	0.6	11
	3	7.0	0.3	4
	4	7.9	0.4	5
	5	9.1	0.5	5
200	1	26.5	5.8	22
	2	27.6	6.9	25
	3	27.3	4.1	15
	4	19.5	7.9	41
	5	35.7	8.6	24
225	1	51.9	2.7	5
	2	38.7	2.8	7
	3	39.9	4.1	10
240	1	67.0	4.8	7
	2	52.1	3.0	6
	3	50.7	2.6	5
250	1	83.5	6.7	8
	2	88.3	7.1	8
	3	104.6	6.8	7
300	1	84.4	7.8	9
	2	129.4	6.3	5
	3	110.1	4.9	5

Table A.2.5 Values of the protein B_2/B_2^{HS} and resulting ε/kT, including van der Waals interactions as well as short-range attraction, values for proteins of various molecular weights at or near the isoelectric point

Protein	**B_2 (10^4 mol-ml/g^2)**	**Molecular Weight (kDa)**	**Hydrodynamic Radius (nm)**	**B_2/B_2^{HS}**	**ε/k_BT**
Ribonuclease A[1]	-0.9	13.7	1.5	**-0.52**	**1.26**
Lysozyme[2]	-3.21	14.7	1.9	**-1.00**	**1.70**
Ovalbumin[3]	-0.8	43.5	3.0	**-0.56**	**1.91**
mAb[4]	-0.5	125.0	5.5	**-0.62**	**1.86**
mAb[3]	-0.9	144.0	5.5	**-1.11**	**2.76**

1. Tessier, PM et al. *Protein: Structure, Function and Genetics* 50(2), 303-311 (2003)
2. Tessier, PM et al. *Biophy J* 82 1620-1631 (2002)
3. H Bajaj et al. *Pharm Res* 23(6) 1382-1394 (2006)
4. Salinas et al. *Pharm Sci* 99(1) 82-93 (2010)

A.2.3 Supplemental Results and Discussion

A.2.3.1 Determination of the porosity of the nanocluster dispersions

A plot of the log of intensity versus the log of magnitude of the scattering vector gives a straight line with the exponent being the fractal dimension of the scattering particle.[6] In this case, the fractal dimension was measured for two separate systems as 2.4 and 2.6 for the concentrated sugar crowder and NMP/PEG crowders respectively (Figure A1.2.6).

The fractal dimension of a floc, D_f, characterizes the floc structure by relating the volume fraction of solid in the floc, φ_k to the primary particle diameter, d, and the floc diameter, d_k.[7] For a floc composed of densely packed particles, D_f approaches 3.

$$\phi_k = \left(\frac{d_k}{d}\right)^{D_f - 3} \quad \text{Eq. A1.2.2}$$

Assuming primary particles of 50nm as appear to be present under SEM, a φ_k for the NMP/PEG crowder system is estimated to be 0.53. This is consistent with the appearance from the SEM and STEM images in Figure 4. As the smallest primary particles would be the individual 11nm proteins, the calculated volume fraction of IgG within the nanocluster is 0.29. The sample value of 0.29 is estimated for the pure sugar crowder system with 85nm diameter flocs with 11nm diameter particles and a Df of 2.4.

A.2.3.2 Formation of Aqueous Dispersions – additional comments

Dissolution of the protein monomer in the aqueous phase is prevented with the addition of precipitants typical for protein purification.[8-17] Like PEG300 described in the text, by adding various precipitants at different ratios, it is possible to control the total attraction thus removes protein dependence from specific attraction. As a result since various proteins will have different extent of attractions, the formation of an aqueous

dispersion can be generalized for different proteins. PEG was chosen for these studies because of various polymers, PEG found to best ppt for proteins.[18] For PEG, solubility can vary order of magnitude with > 10% increase in low MW PEG for many different types of molecules including monoclonal antibodies.[8-14, 19] The mechanism to decrease the solubility of a protein by the addition of PEG is due to depletion-attraction.[12-14, 20] Solubility has been characterized by models based in statistical mechanics[13] and from a preferential binding parameter model [14]

Ethanol precipitation is common for purification of proteins, however other water-soluble organic molecules can be used as well. The primary mechanism for the decrease of protein solubility due to an organics is the decrease dielectric constant.[21]

A.2.3.3 Stability of the protein molecules in the lyophilized powder

Lyophilized solid state protein powders are known to be stable after freezing and lyophilization.[22] During freezing however, several studies have shown that proteins can have both reversible and non-reversible changes to secondary and tertiary structure in the frozen[23] and dried[22, 24] state. The addition of a stabilizing carbohydrate such as trehalose [22, 25, 26] or stabilizing amino acid such as histidine[27] prevent the secondary structure changes of the protein, thus prevent an aggregation prone state from being present upon rehydration of the dried powder.

A.2.4 References

1. Tumolo, T.; Angnes, L.; Baptista, M. S., Determination of the refractive index increment (dn/dc) of molecule and macromolecule solutions by surface plasmon resonance. *Analytical Biochemistry* **2004,** 333, (2), 273-279.
2. Saluja, A.; Badkar, A. V.; Zeng, D. L.; Nema, S.; Kalonia, D. S., Ultrasonic Storage Modulus as a Novel Parameter for Analyzing Protein-Protein Interactions in High Protein Concentration Solutions: Correlation with Static and Dynamic Light Scattering Measurements. *Biophys J* **2007,** 92, 234-244.

3. Salinas, B. A.; Sathish, H. A.; Bishop, S. M.; Harn, N.; Carpenter, J. F.; Randolph, T. W., Understanding and Modulating Opalescence and Viscosity in a Monoclonal Antibody Formulation. *J Pharm Sci* **2010,** 99, (1), 82-92.

4. Pilz, I.; Puchwein, G.; Kratky, O.; Herbst, M.; Haager, O.; Gall, W. E.; Edelman, G. M., Small Angle X-Ray Scattering of a Homogeneous γG1 Immunoglobulin. *Biochemistry* **1970,** 9, (2), 211-219.

5. Miller, D. P.; de Pablo, J. J.; Corti, H., Thermophysical Properties of Trehalose and its Concentrated Aqueous Solutions. *Pharmaceutical Research* **1997,** 14, (5), 578-590.

6. Hiemenz, P. C.; Rajagopalan, R., *Principles of Colloid and Surface Chemistry*. 3rd ed.; Marcel Dekker, Inc.: New York, 1997; p 650.

7. Larson, R. G., *The Structure and Rheology of Complex Fluids*. Oxford University Press Inc.: New York, 1999.

8. Juckes, I. R. M., Fractionation of Proteins and Viruses with Polyethylene glycol. *Biochim. Biophys. Acta* **1971,** 229, 535-546.

9. Ingham, K. C., Precipitation of Proteins with Polyethylene Glycol: Characterization of Albumin. *Arch. Biochem. Biophys.* **1978,** 186, (1), 106-113.

10. Miekka, S. I.; Ingham, K. C., Influence of Self-Association of Proteins on Their Precipitation by Poly(ethylene glycol). *Arch. Biochem. Biophys.* **1978,** 191, (2), 525-536.

11. Middaugh, C. R.; Tisel, W. A.; Haire, R. N.; Rosenberg, A., Determination of the Apparent Thermodynamic Activities of Saturated Protein Solutions. *the Journal of Biological Chemistry* **1979,** 254, (2), 367-370.

12. Arakawa, T.; Timasheff, S. N., Mechanism of Poly(ethylene glycol) Interaction with Proteins. *Biochemistry* **1985,** 24, 6756-6762.

13. Mahadevan, H.; Hall, C. K., Experimental analysis of protein precipitation by polyethylene glycol and comparison with theory. *Fluid Phase Equilibria* **1992,** 78, 297-321.

14. Shulgin, I. L.; Ruckenstein, E., Preferential hydration and solubility of proteins in aqueous solutions of polyethylene glycol. *Biophysical Chemistry* **2006,** 120, 188-198.

15. Cohn, E. J.; Edsall, J. T., *Proteins, Amino Acids and Peptides as Ions and Dipolar Ions*. Reinhold Publishing Corporation: New York, 1943.

16. Green, A. A.; Hughes, W. L., Protein fractionation on the basis of solubility in aqueous solutions of salts and organic solvents. *Methods Enzymol* **1955,** 1, 67-90.

17. Liu, W.; Bratko, D.; Prausnitz, J. M.; Blanch, H. W., Effect of alcohols on aqueous lysozyme-lysozyme interactions from static light-scattering measurements. *Biophysical Chemistry* **2004,** 107, (3), 289-298.

18. Polson, A.; Potgeiter, G. M.; Largier, J. F.; Mears, G. E. F.; Joubert, F. J., The fractionation of protein mixtures by linear polymers of high molecular weight. *Biochim. Biophys. Acta* **1964,** 82, 463-475.

19. Ahamed, T.; Esteban, B. N. A.; Ottens, M.; van Dedem, G. W. K.; van der Wielen, L. A. M.; Bisschops, M. A. T.; Lee, A.; Pham, C.; Thommes, J., Phase Behavior of an Intact Monoclonal Antibody. *Biophys J* **2007,** 93, 610-619.

20. Atha, D. H.; Ingham, K. C., Mechanism of Precipitation of Proteins by Polyethylene Glycols. *the Journal of Biological Chemistry* **1981,** 256, (23), 12108-12117.

21. Dumetz, A. C.; Chockla, A. M.; Kaler, E. W.; Lenhoff, A. M., Comparative Effects of Salt, Organic, and Polymer Precipitants on Protein Phase Behavior and Implications for Vapor Diffusion. *Crystal Growth & Design* **2009,** 9, (2), 682-691.

22. Carpenter, J. F.; Chang, B. S.; Randolph, T. W., Physical Damage to Proteins During Freezing, Drying and Rehydration. In *Lyophilization of Biopharmaceuticals*, Costantino, H. R.; Pikal, M. J., Eds. AAPS Press: 2005; pp 423-442.

23. Strambini, G. B.; Gabellieri, E., Proteins in Frozen Solutions: Evidence of Ice-Induced Partial Unfolding. *Biophys. J.* **1996,** 70, (2), 971-976

24. Griebenow, K.; Klibanov, A. M., Lyophilization-induced reversible changes in the secondary structure of proteins. *PNAS* **1995,** 92, 10969-10976.

25. Souillac, P. O.; Middaugh, C. R.; Rytting, J. H., Investigation of protein/carbohydrate interactions in the dried state. 2. Diffuse reflectance FTIR studies. *Int J Pharm* **2002,** 235, 207-218.

26. Wang, B.; Tchessalov, S.; Warne, N. W.; Pikal, M. J., Impact of Sucrose level on Storage Stability of Proteins in Freeze-Dried Solids: I. Correlation of Protein-Sugar Interaction with Native Structure Preservation. *J Pharm Sci* **2009,** 98, (9), 3131-3144.

27. Tian, F.; Middaugh, C. R.; Offerdahl, T.; Munson, E.; Sane, S.; Rytting, J. H., Spectroscopic evaluation of the stabilization of humanized monoclonal antibodies in amino acid formulations. *Int J Pharm* **2007,** 335, 20-31.

A.3 SUPPLEMENTAL INFORMATION FOR CHAPTER 4

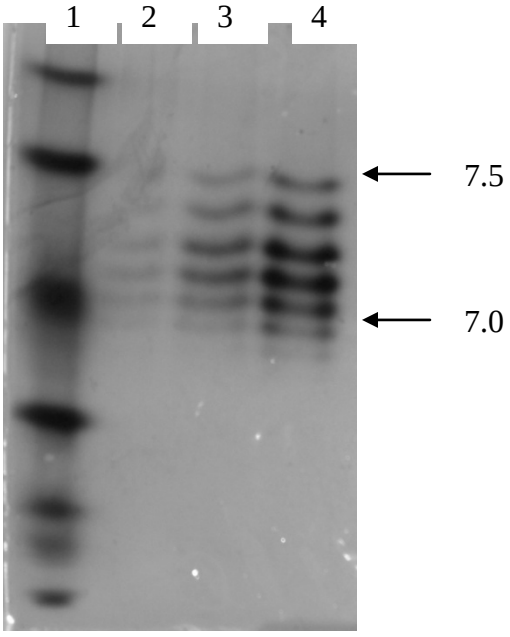

Figure A.3.1 Iso-electric focusing (IEF) gel to determine the isoelectric point (pI) of mAb 1B7. Lane **1:** 5 mg/ml 1B7; **2**: 2 mg/ml 1B7; **3**: 1 mg/ml 1B7, **4**: IEF standards, ranging from 4.45 to 9.6 (BioRad).

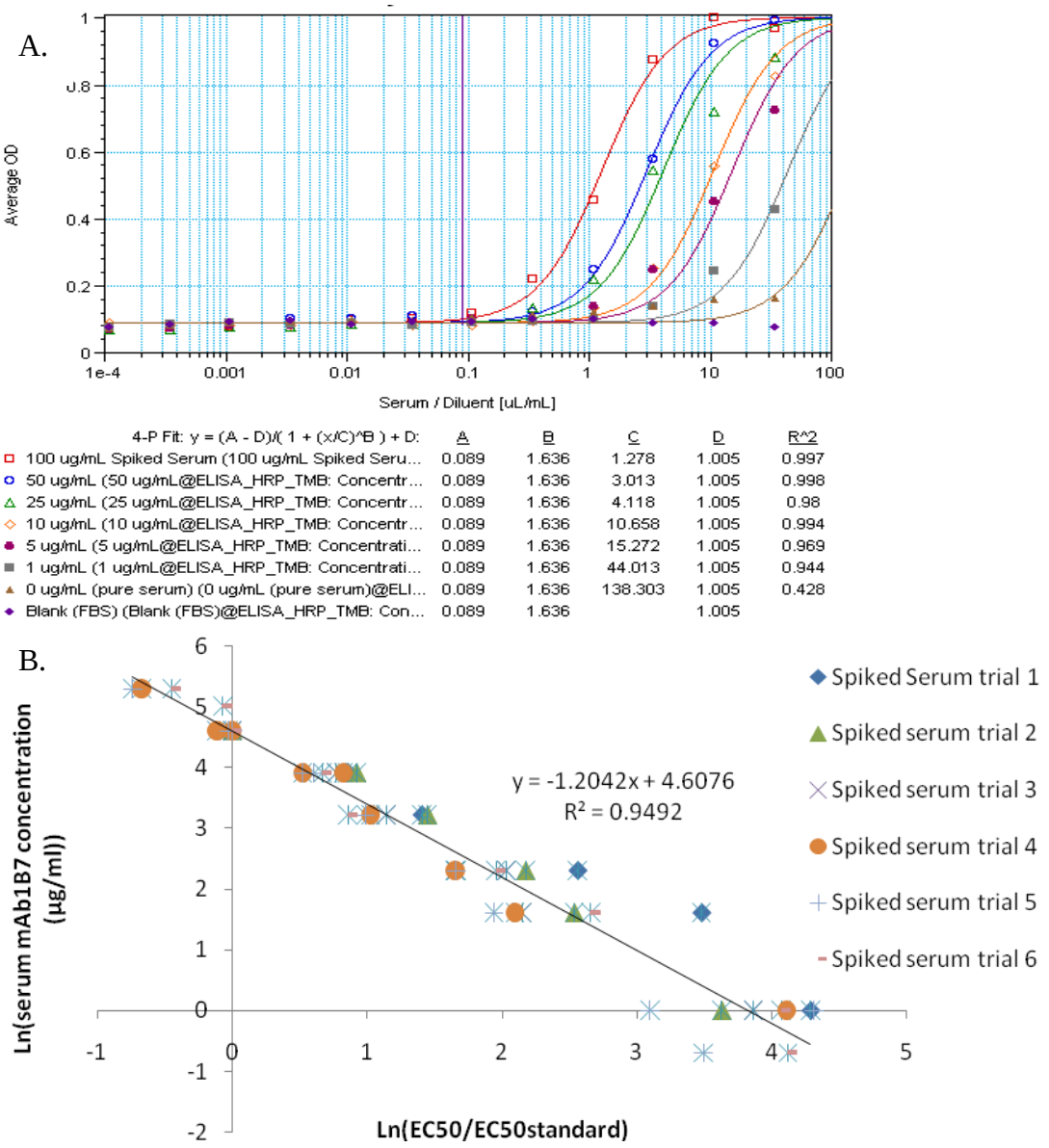

Figure A.3.2 **Calibration data for the anti-pertussis toxin activity ELISA.** ***A)*** Sample spiked serum pertussis ELISA assay analyzed using parallel line fit to a 100 µg/ml spiked serum standard to determine EC_{50} in SpectraMax Pro software. ***B)*** Measure of the correlation between standards: natural log of the sample EC_{50} divided by the EC_{50} of the 100 µg/ml spiked serum standard versus the spiked serum concentration. For each sample, the natural log of the Ec50/EC50 of the 100 µg/ml standard and used to determine the serum mAb1B7 concentration.

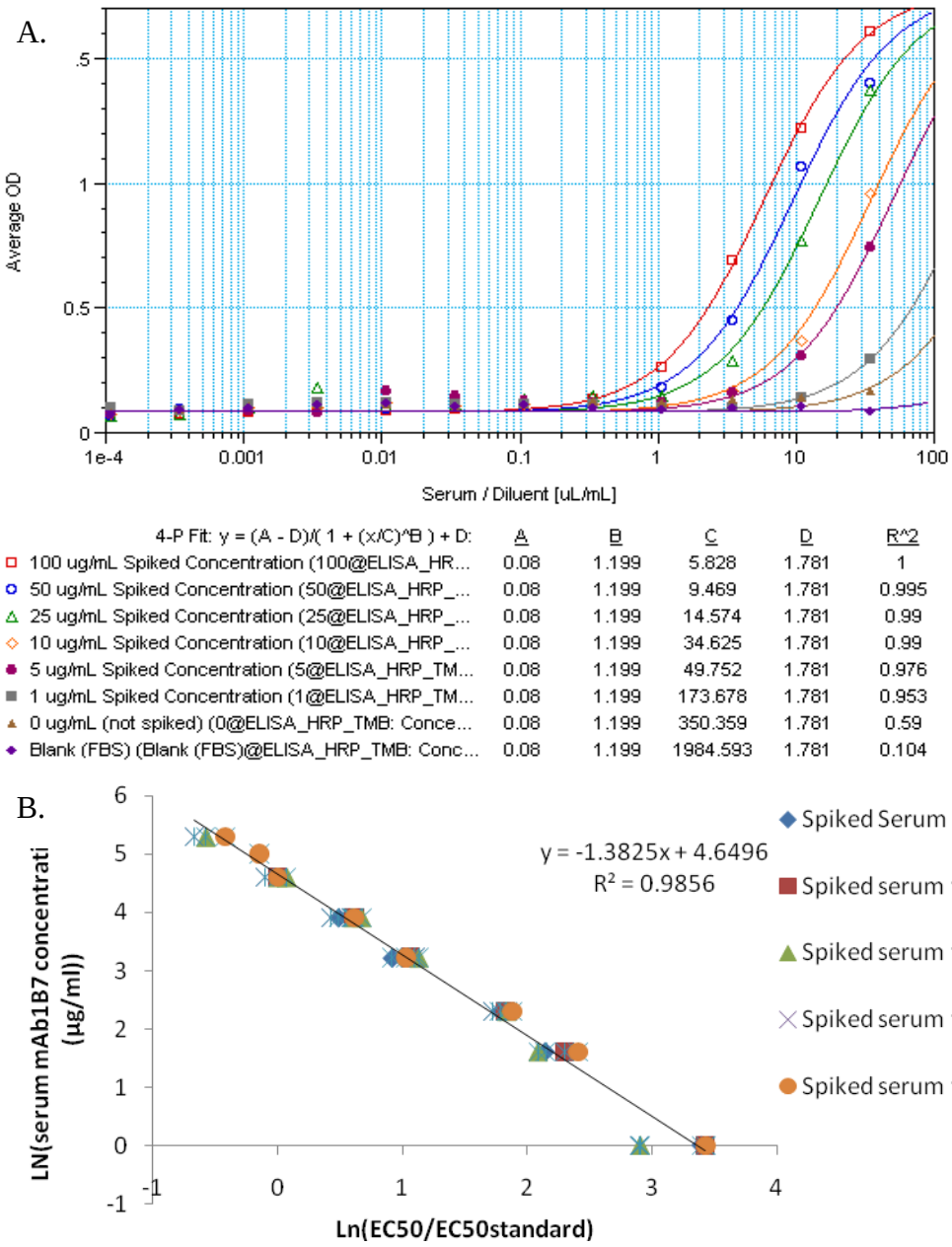

Figure A.3.3 **Calibration data for the streptavidin total protein ELISA.** ***A)*** Sample spiked serum streptavidin ELISA assay analyzed using parallel line fit to a 100 µg/ml spiked serum standard to determine the sample EC_{50}. ***B)*** Measure of the correlation between samples and standards: natural log of the EC_{50} divided by the EC_{50} of the 100 µg/ml spiked serum standard.

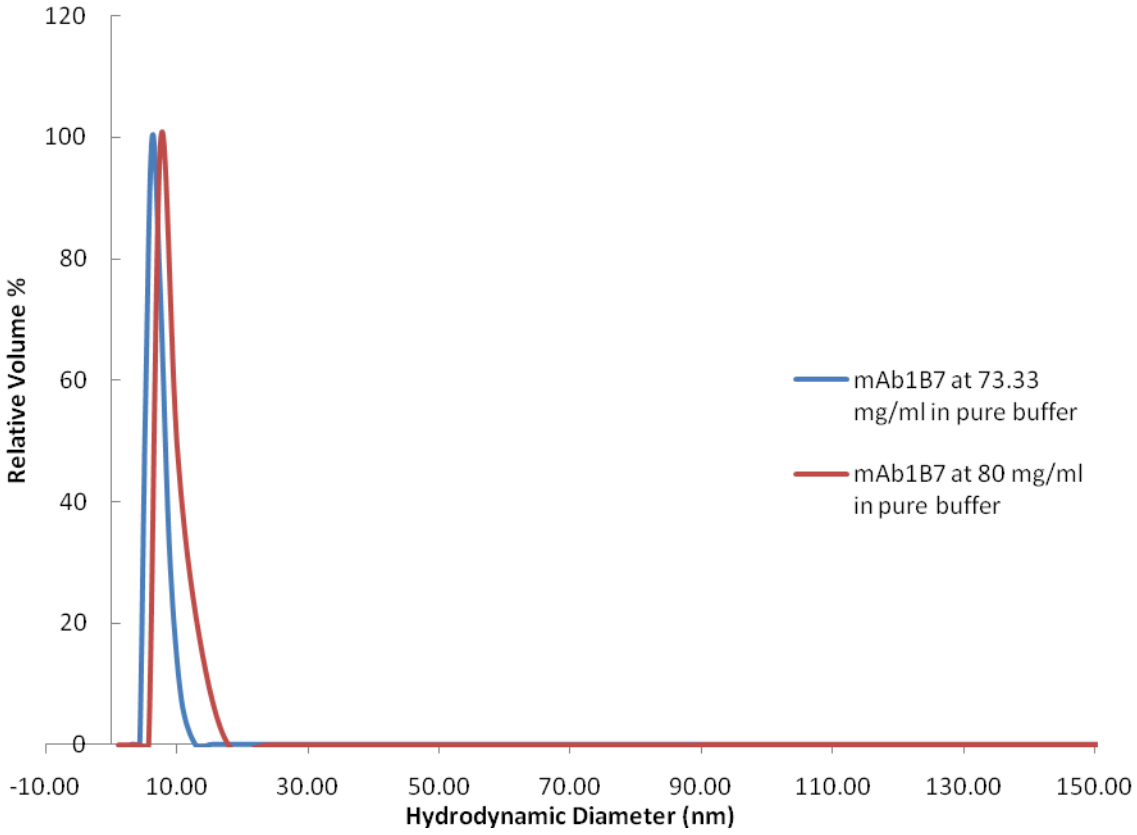

Figure A.3.4 DLS curves for two separate samples of mAb1B7 diluted in pH 7.2 50mM phosphate buffer. The concentration of solubilized trehalose in these samples will be equal to that of the protein as no addition trehalose was added beyond what was in the initial particles.

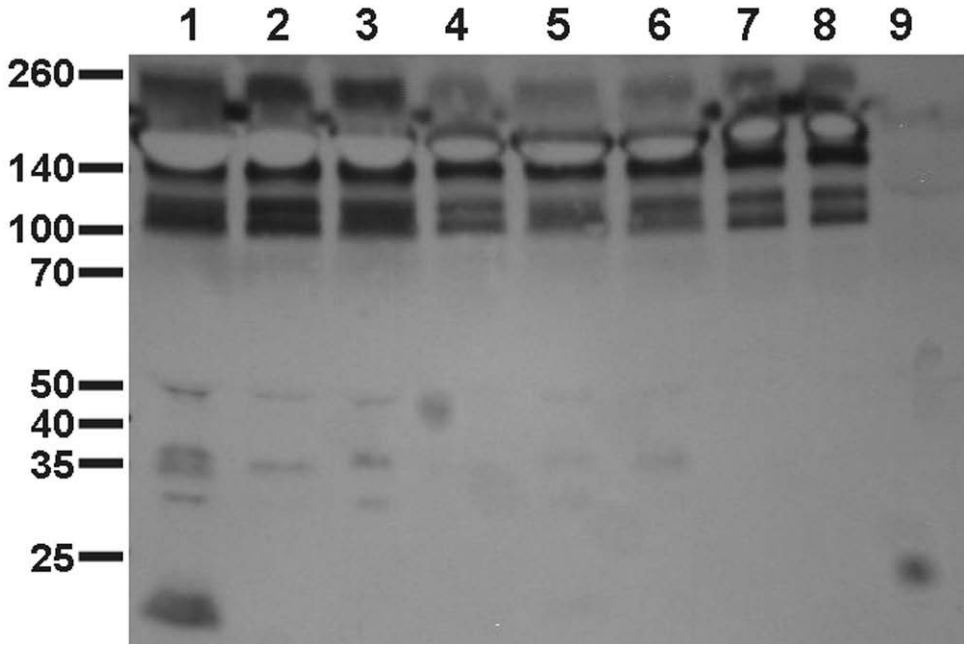

Figure A.3.5 **Non-reducing western blot to detect biotinylated 1B7 in the terminal serum samples.** 4 μg of 1B7 from serum samples were combined with non-reducing SDS-PAGE loading buffer, boiled and applied to a 4-20% SDS-PAGE gel. After separation and transfer to a PVDF membrane, the blot was blocked with 5% BSA and probed with SA-HRP to detect intact and fragments of mAb 1B7. Lanes contain the following mouse samples: **1:** IV solution, mouse #2; **2:** IV solution #5; **3:** SQ solution #7; **4:** SQ solution #10; **5:** SQ low dose dispersion #13; **6:** SQ low dose dispersion #17; **7:** SQ high dose dispersion #20; **8:** SQ high dose dispersion #24; **9:** SQ dispersion buffer only #18. The amount of serum used for lane 9 corresponded to amount of serum used in the most dilute sample (SQ low dose dispersion #13).

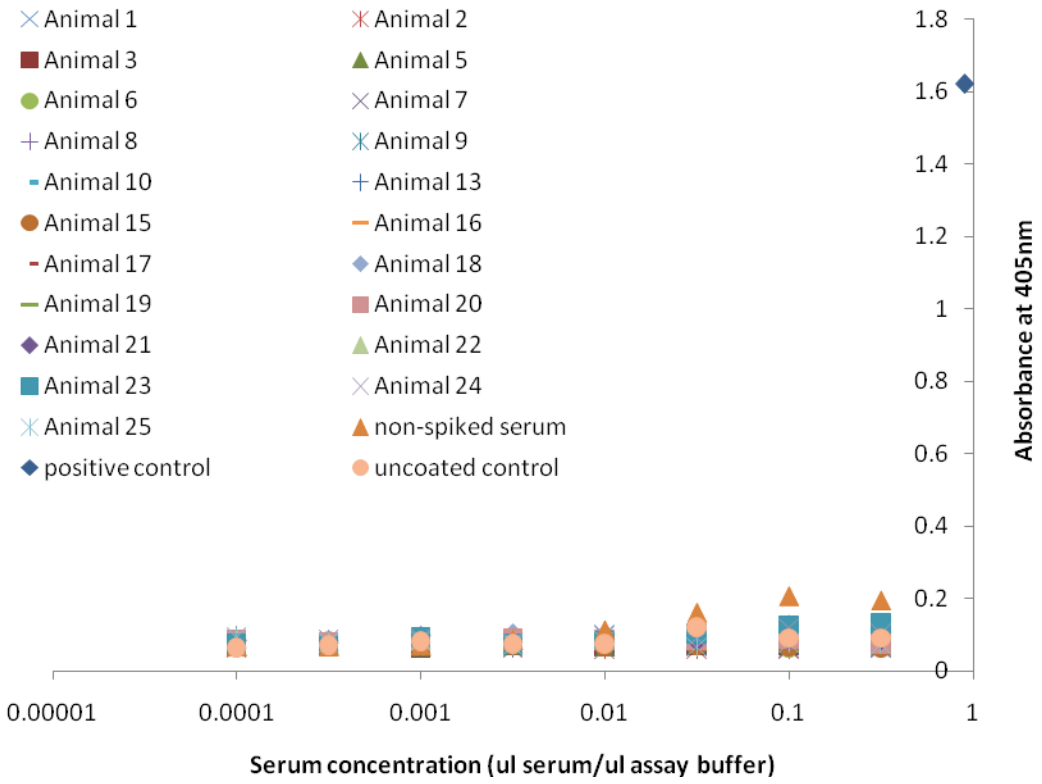

Figure A.3.6 **Mouse anti-mAb 1B7 responses.** Serum from the terminal time point was used to measure IgG1 antibody concentrations recognizing the mAb 1B7 using an ELISA. A positive response was defined as a signal greater than twice the background. Only the positive control obtained such a response.

Table A.3.1 PK analysis using total protein ELISA to measure 1B7 concentrations

Type of injection	$t_{1/2,\beta}$ ***(hours)***
IV solution injection	195.4 ± 15.3
SQ solution injection	181.3 ± 10.5
SQ dispersion injection	191.6 ± 8.7
SQ dispersion injection	191.4 ± 8.5

Appendix B: SWIFT freezing

B.1 METHODS

B.1.1 Formation of SWIFT powder

For SWIFT freezing, the direction of the rotation was changed every ~3 revolutions resulting in a spiral towards the center of the vial. For the vials with only 1 ml of solution, the change in direction did not affect the rotation paper, however for larger volumes, the rotation patter resulted in a spiral inverting in direction every 3 rotations. This did not appear to affect the resulting powder or dispersion from the powder in any measurement and is thus, not distinguished in the manuscript. All samples, whether SWIFT or slow frozen were then lyophilized for 12 hours at -40°C at 100mTorr, followed by a 6 hour ramp to 25°C at 50 mTorr, and maintained for secondary drying at 25°C at 50 mTorr for at least an additional 6 hours. 1 mg of powder was then weighed out and reconstituted at 1 mg/ml in phosphate buffer for stability analysis by size exclusion chromatography, SDS-PAGE gel, and enzyme-linked immunosorbant assay (ELISA) as described in the main text. The temperature of the freezing liquid near the center of the vial was measured by placing a type T 1/20” thermocouple (Omega), through a small hole placed in the center of the cap of the vial. The temperature was monitored and recorded using a NI 9211 board and NI SignalExpress software (National Instruments). The thickness for a single layer of the freezing protein solution was measured by freezing a single layer within the same 8 ml cylindrical vial, removing the unfrozen liquid and measuring the difference in weight from the empty vial and the vial with 1 layer frozen. The thickness of the annular area was then calculated based on the known height and inner radius of the cylindrical vial.

B.1.2 Determination of film thickness (t) for SWIFT freezing

Weight of 1 annulus layer frozen on the inside of the vial was calculated from the difference between the weight of the vial with 1 layer frozen on the inside and the weight of the dried vial (Δw)

$$\frac{\Delta w}{\rho} = \pi H(R^2 - (R-t)^2) \qquad \text{Eq. B.1}$$

Average weight from 4 trials: 0.5666 ± 0.0835 g

Inner radius of cylindrical vial (R): 1.0 cm

Height of inside of cylindrical vial (H) : 4.8 cm

B.1.3 Determination of freezing time by SWIFT freezing

As shown in Figure B.1, the plateau temperature at the freezing point of water, 0°C, accounts for the time from the first ice nuclei to form in the solution until the entire contents of the vial are frozen. For 2 ml of liquid solution, the freezing time was ~15 seconds whereas for 4ml of liquid solution, the freezing time increased to ~30 seconds. Dividing by the number of ml of solution, this gives an average freezing time of ~7.5 s/ml.

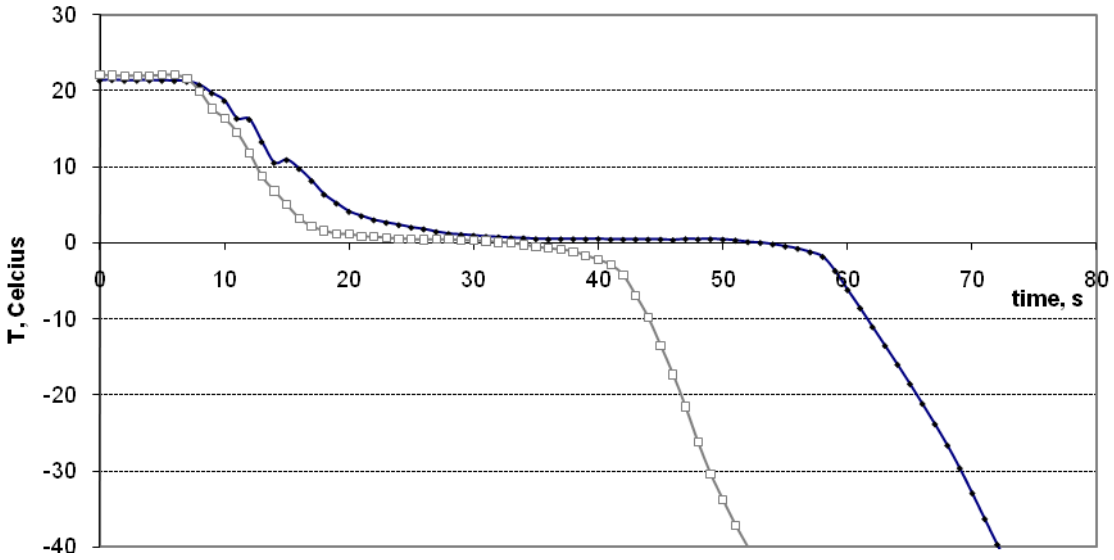

Figure B.1. Freezing temperature profiles of lysozyme solutions (10 mg/ml) inside vials. The solutions were frozen in different film thicknesses 2.6 mm and 0.6 mm corresponding to the total liquid volume of 4 ml and 2.6 ml in vials with 15 mm diameter. The coolant temperature was 80 K and the vial rotation speed was 30 rpm.

B.2 SWIFT FREEZING RESULTS AND DISCUSSION

The rotation of the vial creates thin frozen solution films at the bottom of the vial in contact with liquid nitrogen. During rotation these films will freeze in a spiral towards the center of the vial until the full volume is frozen. The freezing time for a volume of 2 and 4 ml in an 8 ml vial was estimated to be a total of 20 and 40 seconds respectively, in the same 8 ml glass vial. Thus, by this process, each ml of sample will take ~10 seconds to fully freeze. In comparison, upon scaling from the time to freeze 1 drop by TFF, the time to freeze 1 ml by TFF will be 25 seconds[1], indicating both processes freeze protein solutions at similar rates, ~10^2 K/s. The submicron particle size and high stability of the reconstituted protein for SWIFT may be expected, as the film thickness, on the order of 200μm for each film (one revolution) and cooling rate on the order of 10^2 K/s, are comparable to those in the similar processes, TFF and SFL, which have been analyzed in great detail.[1, 2] A freezing film thickness of ~200nm per revolution, calculated from the volume of a single freezing layer inside the vial, is comparable to the 210nm thickness for a similar process reported previously, thin film freezing (TFF).[1] In TFF, a small droplet (~3.6mm diameter) spreads and freezes on a cryogenically cooled surface and takes ~1s to freeze. To compare freezing times, the volume of the solution frozen must be equal, thus for a scale-up TFF disk at the same freezing rate, it would take ~5.1 s to freezing 1ml. For SWIFT, a comparable freezing time of ~7.5 seconds/ml of protein solution was measured from the total freezing time of various freezing volumes using temperature measurements from a thermocouple at the center of the vial (Figure B.1). As a result, similar morphology between TFF and SWIFT lyophilized particles frozen at the same protein solution concentration is observed as expected (Figure B.2).[1]

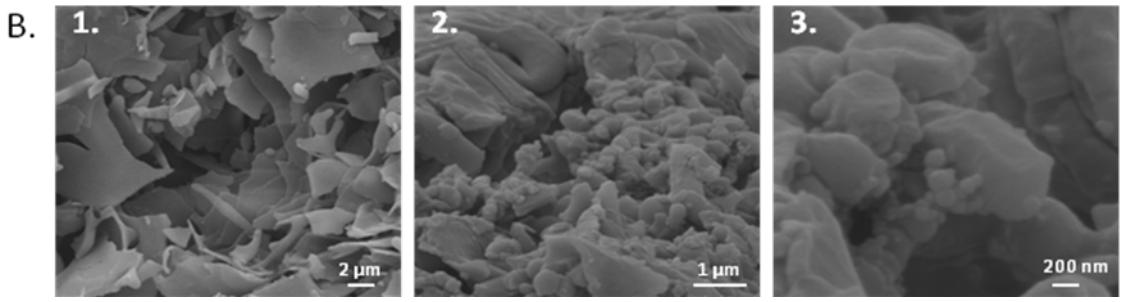

Figure B.2. Morphology of SWIFT powder after lyophilization by SEM

The greater number of ice nuclei leads to the formation of many thin liquid channels between the frozen water domains, containing the remaining unfrozen solution. The rapid vitrification of the thin liquid channels then decreases the number of collisions between protein and sugar particles thus inhibiting growth by coagulation of particles relative to lyophilization which contains much larger liquid channels.[1] In addition, as the concentrations of the protein and sugar are increased in the unfrozen liquid, the rapid increase in viscosity will further reduce the mobility of the growing particle nuclei. The formation of sub-micron particles has also been demonstrated with the extremely rapid (10^6 K/s) freezing process spray freeze drying(SFD).[3] By separately studying the effects of the spraying, freezing, and drying steps in SFD, the large gas-liquid interface in the spraying step was found to be the primary cause of protein aggregation for recombinant human interferon-γ and lysoyzme.[4, 5] The large area/volume of the gas-liquid interface of ~6000 cm^{-1} in SFD for 10 μm sprayed droplets can lead to protein adsorption, denaturation and aggregation.[1, 4, 6-8]

However, in addition to the gas-liquid interface, exposure to the ice-water interface has been shown to destabilize proteins at slow cooling rates (~100 C/min).[9] The protein denaturation in that case was attributed to an increase in the number of ice nuclei increasing the ice-water interface area prior to complete freezing. However, the protein must have time to adsorb to the interface and subsequently partially unfold to form aggregates.[4, 6, 7] As reported previously for rhIFN-γ using spray-lyophilization[4], the time scale for freezing was faster than the time scale for diffusion, thus preventing unfolding of the protein on the ice-water interface. For a diffusion coefficient on the order of 10^{-7} cm^2/s, based on a 5 nm protein molecule in a solvent with a viscosity of 2 cp, the diffusion length, $2*(Dt)^{1/2}$, is on the order of 1 μm in 0.1s. Since each film layer in

SWIFT is on the order of 0.2 mm, the protein will only diffuse a fraction of the film thickness. Furthermore, the diffusion coefficient will decrease markedly as the viscosity increases upon freeze concentration and vitrification of the unfrozen liquid. Finally, the time available for adsorption of protein molecules to an ice interface will be less than 0.1 s for each film layer formed upon a revolution of the vial. In the case for SWIFT freezing, the ice-water interface area was approximated as the specific surface area (SSA) of the final dried powder.[1, 4] Given that the SEM in Figure B.2, resemble those from TFF[1], it is reasonable to assume that our ice-water interface has an area on the order of 10 m^2/g. With this level of ice-water interfacial area, the freezing was sufficiently rapid that protein diffusion and adsorption at this interface did not lead to denaturation and aggregation, as seen by SEC, consistent with the earlier results for TFF[1]. Once the protein solution in fully frozen below the T_g', protein stability is anticipated to be retained due to the decreased mobility preventing further aggregation.[10]

High retention of antibody tertiary structure and activity for the SWIFT powder and for the protein diluted and dissolved from the aqueous dispersion, is shown in Table B.1, from a series of biophysical and biochemical assays including SEC HPLC, SDS-PAGE and ELISA. As the polyclonal sheep IgG used in these initial studies does not bind a single target, a polyclonal rabbit anti-sheep IgG capture ELISA was used to monitor loss of conformational epitopes due to denaturation.[11, 12] The relative EC_{50} (relative to the purified never frozen IgG material) of slightly less than 1.0, indicates an insignificant change in activity as these values are significantly smaller than the >70 value measured for the heat-treated denatured IgG (30 min. at 70^{o}C).

Table B.1. Relative turbidity, % monomer and relative EC_{50} of SWIFT frozen powders at different pHs at an original IgG concentration of 20 mg/ml with a 1:1 (wt) ratio of trehalose to IgG, reconstituted to 1 mg/ml in pH 7.0 phosphate buffer

pH of original solution	**Phase diluted (dispersion) or reconstituted (dry powder)**	**Relative turbidity* for dry powder A_{350}**	**% monomer after purification**	**% monomer after dilution**	**relative EC_{50}****
5.5	dry powder	1.13	97.7 ± 0.0	97.8 ± 0.0	0.9 ± 0.3
7.4	dry powder	1.08	98.1 ± 0.1	98.4 ± 0.1	0.8 ± 0.2

*Relative turbidity is defined as the ratio of the absorbance at 350nm of the reconstituted SWIFT frozen powder to the purified solution prior to processing.

**Relative EC_{50} was calculated as the difference between the EC_{50} of the reconstituted dry powder to the original purified solution prior to processing.

According to HPLC-SEC measurements, the change in % monomer from the original purified IgG solution was negligible (Table B.1). The lack of irreversible aggregates is further confirmed by a single band on the SDS-PAGE gel (Figure B.3)

One practical advantage of SWIFT freezing is the ability to freeze directly in the final dosage vial when compared to SFL or TFF. This prevents the need for costly, solid transfer steps while maintaining aseptic conditions. In this case, if a dosage of 80 mg of the protein is required, at a concentration of 20 mg/ml, the 8 ml vial used in the study can serve both as the freezing vial and then the reconstitution vial following lyophilization. However, since the cooling rate in the case of SWIFT freezing is governed by the liquid cryogen used and the thickness of the glass on the vial, as well as the heat transfer coefficients of the materials used, the vial can easily be scaled-up or scaled-down to the proper size for the dosage necessary. In addition, by removing the transfer step to the final vial, 100% of the protein added to the vial can be recovered after lyophilization and utilized in the formation of the final dosage form.

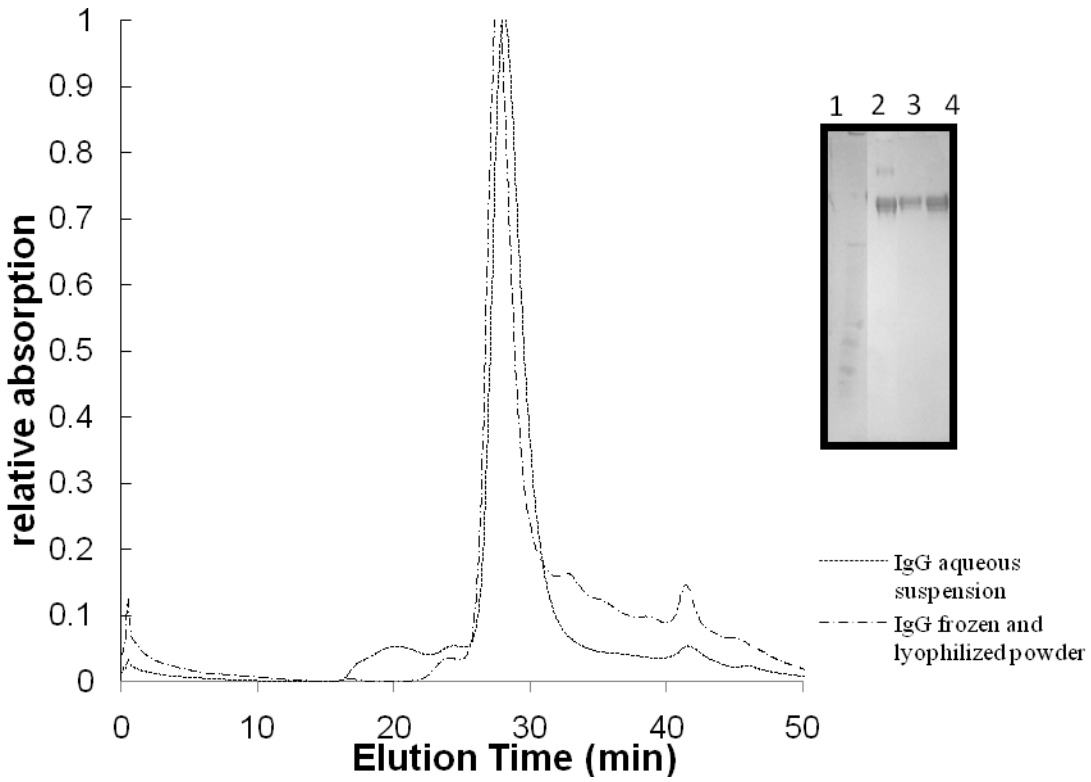

Figure B.3 Size-exclusion chromatograph of purified IgG SWIFT frozen at pH 5.5, lyophilized powder reconstituted and the subsequent 200 mg/ml aqueous suspension diluted in pH 7.0 phosphate buffer as measured on FPLC. Insert shows the SDS-PAGE gel of the IgG reconstituted as received (lane 2) followed by the purified reconstituted lyophilized powder (lane 3) and purified IgG diluted aqueous suspension (lane 4) in the chromatographs.

B.3 REFERENCES

1. Engstrom, J. D.; Lai, E. S.; Ludher, B. S.; Chen, B.; Milner, T. E.; Williams, R. O., III; Kitto, G. B.; Johnston, K. P., Formation of Stable Submicron Protein Particles by Thin Film Freezing. *Pharm. Res.* **2008,** 25, (6), 1334-1346.

2. Engstrom, J. D.; Simpson, D. T.; Cloonan, C.; Lai, E. S.; Williams III, R. O.; Kitto, G. B.; Johnston, K. P., Stable high surface area lactate dehydrogenase particles produced by spray freezing into liquid nitrogen. *European Journal of Pharmaceutics and Biopharmaceutics* **2007,** 65, 163-174.

3. Sonner, C.; Maa, Y.-F.; Lee, G., Spray-Freeze-Drying for Protein Powder Preparation: Particle Characterization and a Case Study with Trypsinogen Stability. *J Pharm Sci* **2002,** 91, (10), 2122-2139.

4. Webb, S. D.; Cleland, J. L.; Carpenter, J. F.; Randolph, T. W., Effects of Annealing Lyophilized and Spray-Lyophilized Formulations of Recombinant Human Interferon-γ. *J Pharm Sci* **2003,** 92, (4), 715-729.

5. Yu, Z.; Johnston, K. P.; Williams III, R. O., Spray freezing into liquid versus spray-freeze drying: Influence of atomization on protein aggregation and biological activity. *Eur. J. Pharm. Sci.* **2006,** 27, 9-18.

6. Carpenter, J. F.; Chang, B. S.; Randolph, T. W., Physical Damage to Proteins During Freezing, Drying and Rehydration. In *Lyophilization of Biopharmaceuticals*, Costantino, H. R.; Pikal, M. J., Eds. AAPS Press: 2005; pp 423-442.

7. Kueltzo, L. A.; Wang, W.; Randolph, T. W.; Carpenter, J. F., Effects of Solution Conditions, Processing Parameters and Container Materials on Aggregation of a Monoclonal Antibody during Freeze-Thawing. *Journal of Pharmaceutical Sciences* **2008,** 97, (5).

8. Costantino, H. R.; Langer, R.; Klibanov, A. M., Moisture-Induced Aggregation of Lyophilized Insulin. *Pharm Res* **1994,** 11, (1), 21-29.

9. Strambini, G. B.; Gabellieri, E., Proteins in Frozen Solutions: Evidence of Ice-Induced Partial Unfolding. *Biophys. J.* **1996,** 70, (2), 971-976

10. Ahamed, T.; Esteban, B. N. A.; Ottens, M.; van Dedem, G. W. K.; van der Wielen, L. A. M.; Bisschops, M. A. T.; Lee, A.; Pham, C.; Thommes, J., Phase Behavior of an Intact Monoclonal Antibody. *Biophys J* **2007,** 93, 610-619.

11. Yang, M. X.; Shenoy, B.; Disttler, M.; Patel, R.; McGrath, M.; Pechenov, S.; Margolin, A. L., Crystalline monoclonal antibodies for subcutaneous delivery. *PNAS* **2003,** 100, (12), 6934-6939.

12. Brickelmaier, M.; Hochman, P. S.; Baciu, R.; Chao, B.; Cuervo, J. H.; Whitty, A., ELISA methods for the analysis of antibody responses induced in multiple sclerosis patients treated with recombinant interferon-beta. *J Immunol Methods* **1999,** 227, (1-2), 121-135.

References

Adamczyk, Z.; Jachimska, B.; Kolasinska, M., Structure of colloid silica determined by viscosity measurements. *J Colloid Interface Sci* **2004,** 273, 668-674.

Aitken-Nichol, C.; Zhang, F.; McGinnity, J. W., Hot-melt extrusion of acrylic films. *Pharm Res* **1996,** 13, 804-808.

Alban, L.; Dahl, A. K.; Hejgaard, K. C.; Jensen, A. L.; Kragh, M.; Thomsen, P.; Stennsgaard, P., *Anim. Welfare* **2001,** 10, 303-314.

Allison, S. D.; Chang, B. S.; Randolph, T. W.; Carpenter, J. F., Hydrogen Bonding between Sugar and Protein is Responsible for Inhibition of Dehydration-Induced Protein Unfolding. *Archives of Biochemistry and Biophysics* **1999,** 365, (2), 289-298.

Amidon, G. L.; Lennernas, H.; Shah, V. P.; Crison, J. R., A Theoretical Basis for a Biopharmaceutical Drug Classification: The Correlation of in Vitro Drug Product Dissolution and In Vivo Bioavailability. *Pharm Res* **1995,** 12, (3), 413-420.

Angell, C. A., Relaxation in liquids, polymers and plastic crystals - strong/fragile patterns and problems. *Journal of Non-Crystalline Solids* **1991,** 131-133, 13-31.

Bajaj, H.; Sharma, V. K.; Kalonia, D. S., A High-Throughput Method for Detection of Protein Self-Association and Second Virial Coefficient Using Size-Exclusion Chromatography Through Simultaneous Measurement of Concentration and Scattered Light Intensity. *Pharm. Res.* **2007,** 24, (11), 2071-2083.

Bakatselou, V.; Oppenheim, R. C.; Dressman, J. B., Solubilization and Wetting Effects of Bile Salts on the Dissolution of Steroids. *Pharm Res* **1991,** 8, (12), 1461-1469.

Ballard, B. E., Biopharmaceutical Considerations in Subcutaneous and Intramuscular Drug Administration. *J. Pharm. Sci.* **1968,** 57, (3), 357-378.

Banerjee, P. S.; Hosny, E. A.; Robinson, J. R., Parenteral Delivery of Peptide and Protein Drugs. In *Peptide and Protein Drug Delivery*, Lee, V. H. L., Ed. 1991; Vol. 4, pp 487-543.

Barnes, H. A.; Hutton, J. F.; Walters, K., *An Introduction to Rheology*. Elsevier: New York, 1989; Vol. 3, p 199.

Bender, J. W.; Wagner, N. J., Optical Measurement of the Contributions of Colloidal Forces to the Rheology of Concentrated Suspensions. *J. Colloid Interface Sci.* **1995,** 172, 171-184.

Bergstrom, L., Shear thinning and shear thickening of concentrated ceramic suspensions. *Colloids Surf., A* **1998,** 133, 151-155.

Berland, C. R.; Thurston, G. M.; Kondo, M.; Broide, M. L.; Pande, J.; Ogun, O.; Benedek, G. B., Solid-liquid phase boundaries of lens protein solutions. *Proc. Natl. Acad. Sci.* **1992,** 89, 1214-1218.

Boncina, M.; Rescic, J.; Vlachy, V., Solubility of Lysozyme in Polyethylene Glycol-Electrolyte Mixtures: The Depletion Interaction and Ion-Specific Effects. *Biophys. J.* **2008,** 95, 1285-1294.

Brewster, M. E.; Vandecruys, R.; Peeters, J.; Neeskens, P.; Verreck, G.; Loftsson, T., Comparative interaction of 2-hydroxypropyl-β-cyclodextrin and sulfobutylether-β-cyclodextrin with itraconazole: Phase-solubility behavior and stabilization of supersaturated drug solutions. *Eur J Pharm Sci* **2008,** 34, 94-103.

Brickelmaier, M.; Hochman, P. S.; Baciu, R.; Chao, B.; Cuervo, J. H.; Whitty, A., ELISA methods for the analysis of antibody responses induced in multiple sclerosis patients treated with recombinant interferon-beta. *J Immunol Methods* **1999,** 227, (1-2), 121-135.

Brown, L. R., Commercial challenges of protein drug delivery. *Expert Opin. Drug Deliv.* **2005,** 2, (1), 29-42.

Buitenhuis, J.; Dhont, J. K. G.; Lekkerkerker, H. N. W., Static and Dynamic Light-scattering by Concentrated Colloidal Suspensions of Polydisperse Sterically stabilized Boehmite Rods Expeirments. *Macromolecules* **1994,** 27, (25), 7267-7277.

Cantor, C. R.; Schimmel, P. R., *BioPhysical Chemistry. Part II: Techniques for the Study of Biological Structure and Function*. W. H. Freeman and Company: San Francisco, 1980; p 846.

Carpenter, J. F.; Chang, B. S.; Garzon-Rodrigues, W.; Randolph, T. W., Rational design of stable lyophilized protein formulations: theory and practice. In *Pharmaceutical Biotechnology. 13. Rational Design of Stable Protein Formulations*, Carpenter, J. F.; Manning, M. C., Eds. Kluwer: New York, 2002; Vol. 13, pp 109-133.

Carpenter, J. F.; Chang, B. S.; Randolph, T. W., Physical Damage to Proteins During Freezing, Drying and Rehydration. In *Lyophilization of Biopharmaceuticals*, Costantino, H. R.; Pikal, M. J., Eds. AAPS Press: 2005; pp 423-442.

Carpenter, J. F.; Crowe, J. H., The Mechanism of Cryoprotection of Proteins by Solutes. *Cryobiology* **1988,** 25, (3), 244-255.

Carpenter, J. F.; Izutsu, K.-i.; Randolph, T. W., Freezing and drying induced perturbations of protein structure and mechanisms of protein protection by stabilizing additives. In *Freeze Drying/Lyophilization of Pharmaceutical and Biological Products*, Rey, L.; May, J. C., Eds. Marcel Dekker, Inc.: New York, 2004; Vol. 137, pp 147-186.

Chari, R.; Jerath, K.; Badkar, A. V.; Kalonia, D. S., Long- and Short-Range Electrostatic Interactions Affect the Rheology of Highly Concentrated Antibody Solutions. *Pharm. Res.* **2009,** 26, (12), 2607-2618.

Chaubal, M. V.; Zhao, Z.; Bruley, D. F., Novel injectable gels for the sustained release of protein C. In *Advances in Experimental Medicine and Biology*, Kluwer Academic/Plenum Publishers: Baltimore, 2003; Vol. 540 (Oxygen Transport to Tissue XXV), pp 147-155.

Chen, B.; Bautista, R.; Yu, K.; Zapata, G. A.; Mulkerrin, M. G.; Chamow, S. M., Influence of Histidine on the Stability and Physical Properties of a Fully Human Antibody in Aqueous and Solid Forms. *Pharm. Res.* **2003,** 20, (12), 1952-1960.

Chen, G.; Luk, A.; Houston, P.; Li, L.; Sharon, M.; Garley, M.; Bannister, R.; Hill, B.; Lucas, C.; Volkin, D.; Dalmonte, P.; Qi, P.; Khossravi, M.; Blasie, C.; Grousnick, K.; Huang, M.; Wang, D.; Zhao, H.; Zhu, Y.; Martin, P.; Treacy, G. In *Injectable nonaqueous suspension of highly concentrated proteins for non-IV administration*, AAPS Annual Meeting and Exposition, Nashville, TN, 2005; The AAPS Journal: Nashville, TN, 2005.

Chen, H.; Wan, J.; Wang, Y.; Mou, D.; Liu, H.; Xu, H.; Yang, X., A facile nanoaggregation strategy for oral delivery of hydrophobic drugs by utilizing acid-base neutralization reactions. *Nanotechnology* **2008,** 19.

Chen, X.; Matteucci, M. E.; Lo, C. Y.; Johnston, K. P.; Williams III, R. O., Flocculation of polymer stabilized nanocrystal suspensions to produce redispersible powders. *Drug Development and Industrial Pharmacy* **2009,** 35, (3), 283-296.

Chennamsetty, N.; Voynov, V.; Kayser, V.; Helk, B.; Trout, B. L., Design of therapeutic proteins with enhanced stability. *PNAS* **2009,** 106, (29), 11937-11942.

Cheung, M. S.; Klimov, D.; Thirumalai, D., Molecular crowding enhances native state stability and refolding rates of globular proteins. *PNAS* **2005,** 102, (13), 4753-4758.

Cheung, J. K.; Raverkar, P. S.; Truskett, T. M., Analytical model for studying how environmental factors influence protein conformational stability in solution. *Journal of Chemical Physics* **2006,** 125, (22).

Cheung, J. K.; Truskett, T. M., Coarse-grained strategy for modeling protein stability in concentrated solutions. *Biophysical Journal* **2005,** 89, (4), 2372-2384.

Chi, E. Y.; Krishnan, S.; Kendrick, B. S.; Chang, B. S.; Carpenter, J. F.; Randolph, T. W., Roles of conformational stability and colloidal stability in the aggregation of recombinant human granulocyte colony-stimulating factor. *Protein Science* **2003,** 12, 903-913.

Chowdary, K. P. R.; Rao, Y. S., Mucoadhesive Microspheres for Controlled Drug Delivery. *Biological and Pharmaceutical Bulletin* **2004,** 27, (11), 1717-1724.

Corrigan, O. I.; Holohan, E. M.; Sabra, K., Amorphous forms of thiazide diuretics prepared by spray-drying. *International Journal of Pharmaceutics* **1984,** 18, 195-200.

Costantino, H. R.; Firouzabadian, L.; Hogeland, K.; Wu, C. C.; Beganski, C.; Carrasquillo, K. G.; Cordova, M.; Griebenow, K.; Zale, S. E.; Tracy, M. A., Protein spray-freeze drying. Effect of atomization conditions on particle size and stability. *Pharm Res* **2000,** 17, 1374-1383.

Costantino, H. R.; Langer, R.; Klibanov, A. M., Moisture-Induced Aggregation of Lyophilized Insulin. *Pharm Res* **1994,** 11, (1), 21-29.

Cox, J. C.; Coulter, A. R., Adjuvants - a classification and review of their modes of action. *Vaccine* **1997,** 15, (3), 248-256.

Crisp, M. T.; Tucker, C. J.; Rogers, T. L.; Williams III, R. O.; Johnston, K. P., Turbidimetric measurement and prediction of dissolution rates of poorly soluble drug nanocrystals. *J Controlled Release* **2007,** 117, 351-359.

Curtis, R. A.; Prausnitz, J. M.; Blanch, H. W., Protein-Protein and Protein-Salt Interactions in Aqueous Protein Solutions Containing Concentrated Electrolytes. *Biotechnology and Bioengineering* **1998,** 57, (1), 11-21.

Dani, B.; Platz, R.; Tzannis, S. T., High Concentration Formulation Feasibility of Human Immunoglubulin G for Subcutaneous Administration. *J. Pharm. Sci.* **2007,** 96, (6), 1504-1517.

Davis-Searles, P. R.; Saunders, A. J.; Erie, D. A.; Winzor, D. J.; Pielak, G. J., Interpreting the Effects of Small Uncharged Solutes on Protein-Folding Equilibria. *Annu. Rev. Biophys. Biomol. Struct.* **2001,** 30, 271-306.

Dawson, K. A., The glass paradigm for colloidal glasses, gels, and other arrested states driven by attractive interactions. *Current Opinion in Colloid & Interface Science* **2002,** 7, 218-227.

Debenedetti, P. G.; Stillinger, F. H., Supercooled liquids and the glass transition. *Nature* **2001,** 410, 259-267Areas, E. P. G.; Areas, J. A. G.; Hamburger, J.; Peticolas, W. L.; Santos, P. S., On the High Viscosity of Aqueous Solution of Lysozyme Induced by Some Organic Solvents. *J Colloid Interface Sci* **1996,** 180, 578-589.

Defelippis, M. R.; Akers, M. J., Peptides and Proteins as Parenteral Suspensions: an Overview of Design, Development, and Manufacturing Considerations. In *Pharmaceutical Formulation Development of Peptides and Proteins*, Frokjaer, S.; Hovgaard, L., Eds. Taylor & Francis Limited: Philadelphia, 2000; pp 113-143.

Desai, U. R.; Klibanov, A. M., Assessing the Structural Integrity of a Lyophilized Protein in Organic Solvents. *J Am. Chem. Soc.* **1995,** 117, 3940-3945.

Dickson, J. L.; Gupta, G.; Horozov, T. S.; Binks, B. P.; Johnston, K. P., Wetting Phenomena at the CO2/Water/Glass Interface. *Langmuir* **2006,** 22, 2161-2170.

DiNunzio, J. C.; Miller, D. A.; Yang, W.; McGinity, J. W.; Williams III, R. O., Amorphous Compositions Using Concentration Enhancing Polymers for Improved Bioavailibility of Itraconazole. *Molecular Pharmaceutics* **2008,** 5, (6), 968-980.

Elamin, A. A.; Ahlneck, C.; Alderborn, G.; Nystrom, C., Increased metastable solubility of milled griseofulvin, depending on the formation of a disordered surface structure. *International Journal of Pharmaceutics* **1994,** 111, 159-170.

Engstrom, J. D.; Lai, E. S.; Ludher, B. S.; Chen, B.; Milner, T. E.; Williams, R. O., III; Kitto, G. B.; Johnston, K. P., Formation of Stable Submicron Protein Particles by Thin Film Freezing. *Pharm. Res.* **2008,** 25, (6), 1334-1346.

Engstrom, J. D.; Simpson, D. T.; Cloonan, C.; Lai, E. S.; Williams III, R. O.; Kitto, G. B.; Johnston, K. P., Stable high surface area lactate dehydrogenase particles produced by spray freezing into liquid nitrogen. *European Journal of Pharmaceutics and Biopharmaceutics* **2007,** 65, 163-174.

Engstrom, J. D.; Simpson, D. T.; Lai, E. S.; Williams III, R. O.; Johnston, K. P., Morphology of protein particles produced by spray freezing of concentrated

solutions. *European Journal of Pharmaceutics and Biopharmaceutics* **2007,** 65, 149-162.

Engstrom, J. D.; Tam, J. M.; Miller, M. A.; Williams III, R. O.; Johnston, K. P., Templated Open Flocs of Nanorods for Enhanced Pulmonary Delivery with Pressurized Metered Dose Inhalers. *Pharm Res* **2009,** 26, (1), 101-117.

Fahr, A.; Liu, X., Drug delivery strategies for poorly water-soluble drugs. *Expert Opi. Drug Deliv.* **2007,** 4, (4), 403-416.

Foster, T. P.; Moseley, W. M.; Caputo, J. F.; Alaniz, G. R.; Leatherman, M. W.; Yu, X.; Claflin, W. H.; Reeves, D. R.; Cleary, D. L.; Zantello, M. R.; Krabill, L. F.; Wiest, J. R., Sustained elevated serum somatotropin concentrations in Holstein steers following subcutaneous delivery of a growth hormone releasing factor analog dispersed in water, oil or microspheres. *J. Controlled Release* **1997,** 47, 91-99.

Frokjaer, S.; Otzen, D. E., Protein Drug Stability: A Formulation Challenge. *Nat. Rev. Drug Discovery* **2005,** 4, 298-306.

Fu, K.; Klibanov, A. M.; Langer, R., Protein stability in controlled-release systems. *Nature Biotechnology* **2000,** 18, 24-25.

Gabrielson, J. P.; Brader, M. L.; Pekar, A. H.; Mathis, K. B.; Winter, G.; Carpenter, J. F.; Randolph, T. W., Quantitation of Aggregate Levels in a Recombinant Humanized Monoclonal Antibody Formulation by Size-Exclusion Chromatography, Asymmetrical Flow Field Flow Fractionation, and Sedimentation Velocity. *J Pharm Sci* **2007,** 96, (2), 268-279.

Garidel, P.; Hegyi, M.; Bassarab, S.; Weichel, M., A rapid, sensitive and economical assessment of monoclonal antibody conformational stability by intrinsic tryptophan fluorescence spectroscopy. *Biotechnol. J.* **2008,** 3, 1201-1211.

Gast, A. P.; Hall, C. K.; Russel, W. B., Polymer-Induced Phase Separations in Nonaqueous Colloidal Suspensions. *J Colloid Interface Sci* **1983,** 96, (1), 251-267.

George, A.; Wilson, W. W., Predicting Protein Crystallization from a Dilute Solution Property. *Acta Cryst.* **1994,** D50, 361-365.

Gillenius, P.; Jaatmaa, E.; Askelof, P.; Granstrom, M.; Tiru, M., The standardization of an assay for pertussis toxin and antitoxin in microplate culture of Chinese hamster ovary cells. *Journal of Biological Standardization* **1985,** 13, 61-66.

Giteau, A.; Venier-Julienne, M.-C.; Marchal, S.; Courthaudon, J.-L.; Sergent, M.; Montero-Menei, C.; Verdier, J.-M.; Benoit, J.-P., Reversible protein precipitation to ensure stability during encapsulation within PLGA microspheres. *Eur. J. Pharm. Biopharm.* **2008,** 70, 127-136.

Gliko, O.; Pan, W.; Katsonis, P.; Neumaier, N.; Galkin, O.; Weikauf, S.; Vekilov, P. G., Metastable Liquid Clusters in Super- and Undersaturated Protein Solutions. *J Phys Chem B* **2007,** 111, 3106-3114.

Gombotz, W. R.; Pettit, D. K., Biodegradable Polymers for Protein and Peptide Drug Delivery. *Bioconjugate Chem.* **1995,** 6, (4), 332-351.

Groenewold, J.; Kegel, W. K., Anomalously Large Equilibrium Clusters of Colloids. *J Phys Chem B* **2001,** 105, 11702-11709.

Gubbins, P. O.; Gurley, B. J.; Bowman, J., Rapid and sensitive high performance liquid chromatographic method for determination of itraconazole and its hydroxyl-metabolie in human serum. *J Pharm Biomed Anal* **1998,** 16, 1005-1012.

Gunawan, L.; Johari, G. P.; Shanker, R. M., Structural Relaxation of Acetaminophen Glass. *Pharmaceutical Research* **2006,** 23, (5), 967-979.

Gupta, P.; Chawla, G.; Bansal, A. K., Physical Stability and Solubility Advantage from Amorphous Celecoxib: The Role of Thermodynamic Quantities and Molecular Mobility. *Molecular Pharmaceutics* **2004,** 1, (6), 406-413.

Halling, P. J., High-affinity binding of water by proteins is similar in air and in organic solvents. *Biochimica et Biophysica Acta* **1990,** 1040, 225-228.

Hancock, B. C.; Parks, M., What is the True Solubility Advantage for Amorphous Pharmaceuticals? *Pharmaceutical Research* **2000,** 17, (4), 397-404.

Hancock, B. C.; Shamblin, S. L., Molecular mobility of amorphous pharmaceuticals determined using differential scanning calorimetry. *Thermochimica Acta* **2001,** 380, 95-107.

Hardin, T. C.; Graybill, J. R.; Fetchinck, R.; Woestenborghs, R.; Rinaldi, M. G.; Kuhn, J. G., *Antimicrob. Agents Chemother.* **1988,** 32, (9), 1310-1313.

Harn, N.; Allan, C.; Oliver, C.; Middaugh, C. R., Highly Concentrated Monoclonal Antibody Solutions: Direct Analysis of Physical Structure and Thermal Stability. *J. Pharm. Sci.* **2007,** 96, (3), 532-546.

Harn, N. R.; Jeng, Y. N.; Kostelc, J. G.; Middaugh, C. R., Spectroscopic Analysis of Highly Concentrated Suspensions of Bovine Somatotropin in Sesame Oil. *J. Pharm. Sci.* **2005,** 94, (11), 2487-2495.

Harn, N.; Spitznagel, T.; Perkins, M.; Allan, C.; Shire, S.; Middaugh, C. R., Biophysical Signatures of Monoclonal Antibodies. In *Current Trends in Monoclonal Antibody Development and Manufacturing*, Shire, S. J., Ed. DOI 10.1007/978-0-387-76643-0_14: 2010; pp 229-246.

Harris, R. J.; Shire, S. J.; Winter, C., Commercial Manufacturing Scale Formulation and Analytical Characterization of Therapeutic Recombinant Antibodies. *Drug Dev. Res.* **2004,** 61, 137-154.

Hasegawa, A.; Kawamura, R.; Nakagawa, H.; Sugimoto, I., Physical Properties of Solid Dispersions of Poorly Water-Soluble Drugs with Enteric Coating Agents. *Chem. Pharm. Bull.* **1985,** 33, (8), 3429-3435.

Hiemenz, P. C.; Rajagopalan, R., *Principles of Colloid and Surface Chemistry*. 3rd ed.; Marcel Dekker, Inc.: New York, 1997; p 650.

Hong, J.-Y.; Kim, J.-K.; Song, Y.-K.; Park, J.-S.; Kim, C.-K., A new self-emulsifying formulation of itraconazole with improved dissolution and oral absorption. *J Controlled Release* **2006,** 110, 332-338.

Horn, F. M.; Richtering, W.; Bergenholtz, J.; Willenbacher, N.; Wagner, N. J., Hydrodynamic and Colloidal Interactions in Concentrated Charge-Stabilized Polymer Dispersions. *J Colloid Interface Sci* **2000,** 225, 166-178.

Horter, D.; Dressman, J. B., Influence of physicochemical properties on dissolution of drugs in the gastrointestinal tract. *Advanced Drug Delivery Reviews* **2001,** 46, 75-87.

Hunter, R. J., *Zeta Potential in Colloid Science*. Academic Press Inc.: New York, 1981; p 386.

Itakura, M.; Shimada, K.; Matsuyama, S.; Saito, T.; Kinugasa, S., A Convenient Method to Determine the Rayleigh RAtio with Uniform Polystyrene Oligomers. *Journal of Applied Polymer Science* **2006,** 99, 1953-1959.

Jain, A.; Ran, Y.; Yalkowsky, S. H., Effect of pH-Sodium Lauryl Sulfate Combination on Solubilization of PG-300995 (an Anti-HIV Agent): A Technical Note. *AAPS PharmSciTech* **2004,** 5, (3), 1-3.

Jaruratanasirikul, S.; Keepkaew, A., *Eur J Clin Pharmacol* **1997,** 52, (3), 235-237.

Jinno, J.-i.; Kamada, N.; Miyake, M.; Yamada, K.; Mukai, T.; Odomi, M.; Toguchi, H.; Liversidge, G. G.; Higaki, K.; Kimura, T., In vitro-in vivo correlation for wet-milled tablet of poorly water-soluble cilostazol. *J Controlled Release* **2008,** 130, 29-37.

Jossang, T.; Feder, J.; Rosenqvist, E., Photon Correlation Spectroscopy of Human IgG. *Journal of Protein Chemistry* **1988,** 7, (2), 165-171.

Kanai, S.; Liu, J.; Patapoff, T. W.; Shire, S. J., Reversible Self-Association of a Concentrated Monoclonal Antibody Solution Mediated by Fab-Fab Interaction That Impacts Solution Viscosity. *J Pharm Sci* **2008,** 97, (10), 4219-4227.

Kang, F.; Singh, J., In vitro release of insulin and biocompatibility of in situ forming gel systems. *Int. J. Pharm.* **2005,** 304, 83-90.

Kendrick, B. S.; Carpenter, J. F.; Cleland, J. L.; Randolph, T. W., A transient expansion of the native state precedes aggregation of recombinant human interferon-γ. *PNAS* **1998,** 95, 14142-14146.

Klibanov, A. M., Improving enzymes by using them in organic solvents. *Nature* **2001,** 409, 241-246.

Knepp, V. M.; Muchnik, A.; Oldmark, S.; Kalashnikova, L., Stability of Nonaqueous Suspension Formulations of Plasma Derived Factor IV and Recombinant Human Alpha Interferon at Elevated Temperatures. *Pharm. Res.* **1998,** 15, (7), 1090-1095.

Krishnan, S.; Chi, E. Y.; Webb, J. N.; Chang, B. S.; Shan, D.; Goldenberg, M.; Manning, M. C.; Randolph, T. W.; Carpenter, J. F., Aggregation of Granulocyte Colony Stimulating Factor under Physiological Conditions: Characterization and Thermodynamic Inhibition. *Biochemistry* **2002,** 41, 6422-6431.

Kueltzo, L. A.; Wang, W.; Randolph, T. W.; Carpenter, J. F., Effects of Solution Conditions, Processing Parameters and Container Materials on Aggregation of a Monoclonal Antibody during Freeze-Thawing. *Journal of Pharmaceutical Sciences* **2008,** 97, (5).

Kulkarni, A. M.; Dixit, N. M.; Zukoski, C. F., Ergodic and non-ergodic phase transitions in globular protein suspensions. *Farady Discuss.* **2003,** 123, 37-50.

Kumprakob, U.; Kawakami, J.; Adachi, I., Permeation Enhancement of Ketoprofen Using a Supersaturated System with Antinucleant Polymers. *Biological Pharmaceutical Bulletin* **2005,** 28, 1684-1688.

Lafleche, F.; Durand, D.; Nicolai, T., Association of Adhesive Spheres Formed by Hydrophobically End-Capped PEF. 1. Influence of the Presence of Single End-Capped PEO. *Macromolecules* **2003,** 36, 1331-1340.

Larson, R. G., *The Structure and Rheology of Complex Fluids*. Oxford University Press: New York, 1998; p 688.

Laven, J.; Vissers, J. P. C., The Hamaker and the Lifshitz approaches for the Van der Waals interaction between particles of composite materials dispersed in a medium. *Colloids and Surfaces A: Physicochemical and Engineering Aspects* **1999,** 152, 345-355.

Leach, W. T.; Simpson, D. T.; Val, T. N.; Anuta, E. C.; Yu, Z.; Williams III, R. O.; Johnston, K. P., Uniform encapsulation of stable protein nanoparticles produced by spray freezing for the reduction of burst release. *J Pharm Sci* **2005,** 94, 56-69.

Lee, J. C.; Timasheff, S. N., The stabilization of proteins by sucrose. *Journal of Biological Chemistry* **1981,** 256, (14), 7193-7201.

Lee, S. L.; Hafeman, A. E.; Debenedetti, P. G.; Pethica, B. A.; Moore, D. J., Solid-State Stabilization of alpha-Chymotrypsin and Catalase with Carbohydrates. *Ind. Eng. Chem. Res.* **2006,** 45, 5134-5147.

Leuner, C.; Dressman, J., Improving drug solubility for oral delivery using solid dispersions. *European Journal of Pharmaceutics and Biopharmaceutics* **2000,** 50, 47-60.

Lindfors, L.; Skantze, P.; Skantze, U.; Westergren, J.; Olsson, U., Amorphous Drug Nanosuspensions. 3. Particle Dissolution and Crystal Growth. *Langmuir* **2007,** 23, 9866-9874.

Lipinski, C., Solubility in the Design of Combinatorial Libraries. In *Analysis and Purification Methods in Combinatorial Chemisty*, Yan, B., Ed. John Wiley & Sons, Inc.: Hoboken, NJ, 2004; pp 407-434.

Lipinski, C. A., Avoiding investment in doomer drugs, is poor solubility an industry wide problem? *Current Drug Discovery* **2001**, 17-19.

Lipinski, C. A., Poor aqueous solubility - an industry wide problem in drug discovery. *Am. Pharm. Rev.* **2002,** 5, 82-85.

Liu, J.; Nguyen, M. D. H.; Andya, J. D.; Shire, S. J., Reversible Self-Association Increases the Viscosity of a Concentrated Monoclonal Antibody in Aqueous Solution. *Journal of Pharmaceutical Sciences* **2005,** 94, (9), 1928-1940.

Liu, R.; Sadrzadeh, N.; Constantinides, P. P., Micellization and Drug Solubility Enhancement. In *Water-Insoluble Drug Formation*, Liu, R., Ed. Interpharm Press: Denver, 2000; pp 213-277.

Liversidge, E. M.; Liversidge, G. G.; Cooper, E. R., Nanosizing: a formulation approach for poorly-water-soluble compounds. *Eur J Pharm Sci* **2003,** 18, 113-120.

Lohitnavy, M.; Lohitnavy, O.; Thangkeattiyanon, O.; Srichai, W., *J Clin Pharm Ther* **2005,** 30, (3), 201-206

Lopatin, P. V.; Safonov, V. P.; Litvinova, T. P.; Yakimenko, L. M., Use of Nonaqueous solvents to Prepare Injection Solutions. *Khim.-Farm. Zh.* **1972,** 6, (11), 36-47.

Lopez-Lopez, M. T.; Gomez-Ramirez, A.; Duran, J. D. G.; Gonzalez-Caballero, F., Preparation and Characterization fo Iron-Based Magnetorheological Fluids Stabilized by Addition of Organoclay Particles. *Langmuir* **2008,** 24, (14), 7076-7084.

Lu, P. J.; Conrad, J. C.; Wyss, H. M.; Schofield, A. B.; Weitz, D. A., Fluids of Clusters in Attractive Colloids. *Phys Rev Let* **2006,** 96, 028306.

Lu, P. J.; Zaccarelli, E.; Ciulla, F.; Schofield, A. B.; Sciortino, F.; Weitz, D. A., Gelation of particles with short-range attraction. *Nature* **2008,** 453, 499-503.

Maa, Y.-F.; Costantino, H. R., Spray freeze-drying of biopharmaceuticals: applications and stability considerations. In *Lyophilization of Biopharmaceuticals*, Costantino, H. R.; Pikal, M. J., Eds. American Association of Pharmaceutical Scientists: Arlington, 2004; Vol. 2.

Maa, Y.-F.; Prestrelski, S. J., Biopharmaceutical powders: particle formation and formulation considerations. *Current Pharmaceutical Biotechnology* **2000,** 1, 283-302.

Maas, C.; Hermeling, S.; Bouma, B.; Jiskoot, W.; Gebbink, M. F., A role for protein misfolding in immunogenicity of biopharmaceuticals. *J Biol Chem* **2007,** 282, (4), 2229-2236.

Mahadevan, H.; Hall, C. K., Experimental analysis of protein precipitation by polyethylene glycol and comparison with theory. *Fluid Phase Equilibria* **1992,** 78, 297-321.

Manning, M. C.; Patel, K.; Borchardt, R. T., Stability of Protein Pharmaceuticals. *Pharm Res* **1989,** 6, (11), 903-918.

Matteucci, M. E.; Brettmann, B. K.; Rogers, T. L.; Elder, E. J.; Williams III, R. O.; Johnston, K. P., Design of Potent Amorphous Drug Nanoparticles for Rapid Generation of Highly Supersaturated Media. *Molecular Pharmaceutics* **2007,** 4, (5), 782-793.

Matteucci, M. E.; Hotze, M. A.; Williams III, R. O.; Johnston, K. P., Drug Nanoparticles by Antisolvent Precipitation: Mixing Energy Versus Surfactant Stabilization. *Langmuir* **2006,** 22, (21), 8951-8959.

Matteucci, M. E.; Miller, M. A.; Williams III, R. O.; Johnston, K. P., Highly Supersaturated Solutions of Amorphous Drugs Approaching Predictions from Configurational Thermodynamic Properties. *Journal of Physical Chemistry B* **2008,** 112, (51), 166675-16681.

Matteucci, M. E.; Paguio, J. C.; Miller, M. A.; Williams III, R. O.; Johnston, K. P., Flocculated Amorphous Nanoparticles for Highly Supersaturated Solutions. *Pharm Res* **2008,** 25, (11), 2477-2487.

Matteucci, M. E.; Paguio, J. C.; Miller, M. A.; Williams III, R. O.; Johnston, K. P., Highly Supersaturated Solutions from Dissolution of Amorphous Itraconazole Microparticles at pH 6.8. *Molecular Pharmaceutics* **2009,** 6, (2), 375-385.

Maynard, J. A.; Maassen, C. B. M.; Leppla, S. H.; Brasky, K.; Patterson, J. L.; Iverson, B. L.; Georgiou, G., Protection against anthrax toxin by recombinant antibody fragments correlates with antigen affinity. *Nature Biotechnology* **2002,** 20, 597-601.

McMinn, J. H.; Sowa, M. J.; Charnick, S. B.; Paulaitis, M. E., The Hydration of Proteins in Nearly Anhydrous Organic Solvent Suspensions. *Biopolymers* **1993,** 33, 1213-1224.

Miller, D. A.; DiNunzio, J. C.; Yang, W.; McGinity, J. W.; Williams III, R. O., Enhanced In Vivo Absorption of Itraconazole via Stabilization of Supersaturation Following Acidic-to-Neutral pH Transition. *Drug Development and Industrial Pharmacy* **2008,** 34, (8), 890-902.

Miller, D. A.; DiNunzio, J. C.; Yang, W.; McGinity, J. W.; Williams III, R. O., Targeted Intestinal Delivery of Supersaturated Itraconazole for Improved Oral Absorption. *Pharm Res* **2008,** 25, (6), 1450-1459.

Miller, D. A.; McConville, J. T.; Yang, W.; Williams III, R. O.; McGinity, J. W., Hot-Melt Extrusion for Enhanced Delivery of Drug Particles. *J Pharm Sci* **2007,** 96, (2), 361-376.

Miller, D. P.; de Pablo, J. J.; Corti, H., Thermophysical Properties of Trehalose and its Concentrated Aqueous Solutions. *Pharmaceutical Research* **1997,** 14, (5), 578-590.

Miller, M. A.; Borwankar, A.; Khan, T.; Dinin, A.; Kaczorowski, K. J.; Wilson, B.; Truskett, T. M.; Maynard, J. A.; Johnston, K. P., Concentrated active protein by crowding into clusters. **in preparation**.

Miller, M. A.; Engstrom, J. D.; Ludher, B. S.; Johnston, K. P., Low Viscosity Highly Concentrated Injectable Nonaqueous Suspensions of Lysozyme Microparticles. *Langmuir* **2010,** 26, (2), 1067-1074.

Miller, M. A.; Wilson, B.; Vier, D.; Rodrigues, M.; Ferrer, D. A.; Maynard, J. A.; Johnston, K. P., Weakly interacting nanoclusters of stabe protein at high concentration. **in preparation**.

Minton, A. P., The Effective Hard Particle Model Provides a Simple, Robust, and Broadly Applicable Description of Nonideal Behavior in Concentrated Solutions of Bovine Serum Albumin and Other Nonassociating Proteins. *J. Pharm. Sci.* **2007,** 96, (12), 3466-3469.

Mittal, J.; Best, R. B., Dependence of Protein Folding Stability and Dynamics on the Density and Composition of Macromolecular Crowders. *Biophys J* **2010,** 98, 315-320.

Mosharraf, M.; Nystrom, C., The effect of dry mixing on the apparent solubility of hydrophobic, sparingly soluble drugs. *European Journal of Pharmaceutical Sciences* **1999,** 9, 145-156.

Mosharraf, M.; Sebhatu, T.; Nystrom, C., The effects of disordered structure on the solubility and dissolution rates of some hydrophilic, sparingly soluble drugs. *International Journal of Pharmaceutics* **1999,** 177, 29-51.

Muller, R. H.; Jacobs, C.; Kayser, O., Nanosuspensions as particulate drug formulations in therapy: Rationale for development and what we can expect for the future. *Advanced Drug Delivery Reviews* **2001,** 47, 3-19.

Nagai, T.; Machida, Y., Mucosal adhesive dosage forms. *Pharm. Int.* **1985,** 6, 196.

Nail, S. L.; Jiang, S.; Chongprasert, S.; Knopp, S. A., Fundamentals of freeze-drying. In *Pharmaceutical Biotechnology. 14. Development and Manufacture of Protein Pharmaceuticals*, Nail, S. L.; Akers, M. J., Eds. Kluwer Academic/Plenum Publishers: New York, 2002; pp 281-360.

Naylor, L. J.; Bakatselou, V.; Dressman, J. B., Comparison of the Mechanism of Dissolution of Hydrocortisone in Simple and Mixed Micelle Systems. *Pharm Res* **1993,** 10, (6), 865-870.

Neal, B. L.; Asthagiri, D.; Lenhoff, A. M., Molecular Origins of Osmotic Second Virial Coefficients of Proteins. *Biophys J* **1998,** 75, 2469-2477.

Nelson, A. L.; Dhimolea, E.; Reichert, J. M., Development trends for human monoclonal antibody therapeutics. *Nat Rev Drug Disc* **2010,** 9, 767-774.

Newcombe, A. R.; Cresswell, C.; Davies, S.; Watson, K.; Harris, G.; O'Donovan, K.; Francis, R., Optimised affinity purification of polyclonal antibodies from hyper immunised ovine serum using a syntehtic Protein A adsorbent, MAbsorbent® A2P. *Journal of Chromatography B* **2005,** 814, 209-215.

Nguyen, H. D.; Hall, C. K., Spontaneous Fibril Formation by Polyalanines; Discontinuous Molecular Dynamics Simulations. *JACS* **2006,** 128, 1890-1901.

Noyes, A. A.; Whitney, W. R., The rate of solution of solid substances in their own solutions. *Journal of the American Chemical Society* **1897,** 19, 930-934.

O'Connor, T. F.; Debenedetti, P. G.; Carbeck, J. D., Stability of proteins in the presence of carbohydrates; experiments and modeling using scaled particle theory. *Biophysical Chemistry* **2007,** 127, 51-63.

Okimoto, K.; Miyake, M.; Ibuki, R.; Yasumura, M.; Ohnishi, N.; Nakai, T., *Int J Pharm* **1997,** 159, 85-93.

Overhoff, K. A.; Moreno, A.; Miller, D. A.; Johnston, K. P.; Williams III, R. O., Solid dispersions of itraconazole and enteric polymers made by ultra-rapid freezing. *Int J Pharm* **2007,** 336, 122-132

Pan, W.; Vekilov, P. G.; Lubchenko, V., Origin of Anomalous Mesoscopic Phases in Protein Solutions. *J Phys Chem B* **2010,** 114, (22), 7620-7630.

Pandit, N.; Trygstad, T.; Croy, S.; Bohorquez, M.; Koch, C., Effect of Salts on the Micellization, Clouding, and Solubilization Behaviour of Pluronic F127 Solutions. *J Colloid Interface Sci* **2000,** 222, (2), 213-220.

Parks, G. S.; Snyder, L. J.; Cattoir, F. R., Studies on Glass. XI. Some Thermodynamic Relations of Glassy and Alpha-Crystalline Glucose. *Journal of Chemistry and Physics* **1934,** 2, 595-598.

Partridge, J.; Moore, B. D.; Halling, P. J., Alpha-Chymotrypsin stability in aqueous-acetonitrile mixture: is the native enzyme thermodynamically or kinetically stable under low water conditions? *J. Mol. Catal. B: Enzym.* **1999,** 6, 11-20.

Pawar, R.; Ben-Ari, A.; Domb, A. J., Protein and peptide parenteral controlled delivery. *Expert Opin. Biol. Ther.* **2004,** 4, (8), 1203-1212.

Pelton, R. H., Polystyrene and polystyrene-butadiene latexes stabilized by poly(N-isopropylacrylamide). *Journal of Polymer Science, Part A: Polymer Chemisty* **1988,** 26, (1), 9-18.

Pechenov, S.; Shenoy, B.; Yang, M. X.; Basu, S. K.; Margolin, A. L., Injectable controlled release formulations incorporating protein crystals. *J. Controlled Release* **2004,** 96, 149-158.

Petereit, H.-U.; Weisbrod, W., Formulation and process considerations affecting the stability of solid dosage forms formulated with methacrylate copolymers. *Eur J Pharm Biopharm* **1999,** 47, 15-25.

Pincus, D. L.; Thirumalai, D., Crowding Effects on the Mechanical Stability and Unfolding Pathways of Ubiquitin. *J Phys Chem B* **2009,** 113, 359-368

Ping, G.; Yang, G.; Yuan, J.-M., Depletion force from macromolecular crowding enhances mechanical stability of protein molecules. *Polymer* **2006,** 47, 2564-2570.

Ponchel, G.; Irache, J.-M., Specific and non-specific bioadhesive particulate systems for oral delivery to the gastrointestinal tract. *Advanced Drug Delivery Reviews* **1998,** 34, 191-219.

Porcar, L.; Falus, P.; Chen, W.-R.; Faraone, A.; Fratini, E.; Hong, K.; Baglioni, P.; Liu, Y., Formation of the Dynamic Clusters in Concentrated Lyoszyme Protein Solutions. *J. Phys. Chem. Lett.* **2010,** 1, 126-129.

Prausnitz, J. M., Molecular thermodynamics for some applications in biotechnology. *J Chem Thermodynamics* **2003,** 35, 21-39.

Putney, S. D.; Burke, P. A., Improving protien therapeutics with sustained-release formulations. *Nature Biotechnology* **1998,** 16, 153-157.

Radwan, M., In vivo screening model for excipients and vehicles used in subcutaneous injections. *Drug Dev. Ind. Pharm.* **1994,** 20, (17), 2753-2762.

Raghavan, S. L.; Kiepfer, B.; Davis, A. F.; Kazarian, S. G.; Hadgraft, J., Membrane transport of hydrocortisone acetate from supersaturated solutions; the role of polymers. *International Journal of Pharmaceutics* **2001,** 221, 95-105.

Raghavan, S. L.; Trividic, A.; Davis, A. F.; Hadgraft, J., Crystallization of hydrocortisone acetate: influence of polymers. *Int J Pharm* **2001,** 212, 213-221.

Raghavan, S. L.; Trividic, A.; Davis, A. F.; Hadgraft, J., Effect of cellulose polymers on supersaturation and in vitro membrane transport of hydrocortisone acetate. *International Journal of Pharmaceutics* **2000,** 193, 231-237.

Rasenack, N.; Muller, B. W., Dissolution Rate Enhancement by in Situ Micronization of Poorly Water-Soluble Drugs. *Pharm Res* **2002,** 19, (12), 1894-1900.

Reichert, J. M.; Rosensweig, C. J.; Faden, L. B.; Dewitz, M. C., Monoclonal antibody successes in the clinic. *Nature Biotechnology* **2005,** 23, (9), 1073-1078.

Reichert, J. M., Probabilities of success for antibody therapeutics. *mAbs* **2009,** 1, (4), 387-389.

Reid, R. C.; Prausnitz, J. M.; Sherwood, T. K., *The Properties of Gases and Liquids*. 3 ed.; McGraw-Hill Book Company: New York, 1977; p 688.

Roberts, C. J.; Debenedetti, P. G., Engineering Pharmaceutical Stability with Amorphous Solids. *AIChE Journal* **2002,** 48, (6), 1140-1144.

Rogers, T. L.; Gillespie, I. B.; Hitt, J. E.; Fransen, K. L.; Crowl, C. A.; Tucker, C. J.; Kupperblatt, G. B.; Becker, J. N.; Wilson, D. L.; Todd, C.; Broomall, C. F.; Evans, J. C.; Elder, E. J., Development and Characterization of a Scalable Controlled Precipitation Process to Enhance the Dissolution of Poorly Water-Soluble Drugs. *Pharmaceutical Research* **2004,** 21, (11), 2048-2057.

Rosenbaum, D. F.; Zukoski, C. F., Protein interactions and crystallization. *J Cryst Growth* **1996,** 169, 752-758.

Rosenbaum, D. F.; Kulkarni, A. M.; Ramakrishnan, S.; Zukoski, C. F., Protein interactions and phase behavior: Sensitivity to the form of the pair potential. *J Chem Phys* **1999,** 111, (21), 9882-9890.

Ross, P. D.; Minton, A. P., Analysis of Non-ideal Behavior in Concentrated Hemoglobin Solutions. *J. Mol. Biol.* **1977,** 112, 437-452.

Ross, P. D.; Minton, A. P., Hard Quasispherical Model for the Viscosity of Hemoglobin Solutions. *Biochem. Biophys. Res. Commun.* **1977,** 76, (4), 971-976.

Ruch, F.; Matijevic, E., Preparation of Micrometer Size Budesonide Particles by Precipitation. *J Colloid Interface Sci* **2000,** 229, 207-211.

Russel, W. B., Structure-Property Relations for the Rheology of Dispersions of Charged Colloids. *Ind. Eng. Chem. Res.* **2009,** 48, 2380-2386.

Russel, W. B., The rheology of suspensions of charged rigid spheres. *J Fluid Mech* **1978,** 85, (2), 209-232.

Russel, W. B.; Saville, D. A.; Schowalter, W. R., *Colloidal Dispersions*. Cambridge University Press: New York, 1995; p 525.

Ryoo, W.; Webber, S. E.; Johnston, K. P., Water-in-Carbon Dioxide Microemulsions with Methylated Branched Hydrocarbon Surfactants. *Ind. Eng. Chem. Res.* **2003,** 42, 6348-6358.

Salinas, B. A.; Sathish, H. A.; Bishop, S. M.; Harn, N.; Carpenter, J. F.; Randolph, T. W., Understanding and Modulating Opalescence and Viscosity in a Monoclonal Antibody Formulation. *J Pharm Sci* **2010,** 99, (1), 82-92.

Saluja, A.; Badkar, A. V.; Zeng, D. L.; Nema, S.; Kalonia, D. S., Application of High-Frequency Rheology Measurements for Analyzing Protein-Protein Interactions in High Protein Concentration Solutions using a Model Monoclonal Antibody (IgG2). *J. Pharm. Sci.* **2006,** 95, (9), 1967-1983.

Saluja, A.; Badkar, A. V.; Zeng, D. L.; Kalonia, D. S., Ultrasonic Rheology of a Monoclonal Antibody (IgG2) Solution: Implications for Physical Stability of Proteins in High Concentration Formulations. *J. Pharm. Sci.* **2007,** 96, (12), 3181-3195Shire, S. J.; Shahrokh, Z.; Liu, J., Challenges in the Development of High Protein Concentration Formulations. *Journal of Pharmaceutical Sciences* **2004,** 93, (6), 1390-1402.

Saluja, A.; Badkar, A. V.; Zeng, D. L.; Nema, S.; Kalonia, D. S., Ultrasonic Storage Modulus as a Novel Parameter for Analyzing Protein-Protein Interactions in High Protein Concentration Solutions: Correlation with Static and Dynamic Light Scattering Measurements. *Biophys J* **2007,** 92, 234-244.

Saluja, A.; Kalonia, D. S., Nature and consequences of protein-protein interactions in high protein concentration solutions. *Int. J. Pharm.* **2008,** 358, 1-15.

Sandler, S. R.; Karo, W.; Bonesteel, J.-A.; Pearce, E. M., *Polymer Syntehsis and Characterization: A Laboratory Manual*. 1 ed.; Academic Press: San Diego, 1998; p 212.

Santini, C. M. B.; Hatton, T. A.; Hammond, P. T., Solution Behavior of Linear-Dendritic Rod Diblock Copolymers in Methanol. *Langmuir* **2006,** 22, (18), 7487-7498.

Sato, H.; Ito, A.; Chiba, J.; Sato, Y., Monoclonal antibody against pertussis toxin: effect on toxin activity and pertussis infections. *Infect Immun* **1984,** 46, 422-428.

Schamp, K.; Schreder, S.-A.; Dressman, J., Development of an in vitro/in vivo correlation for lipid formulations of EMD 50733, a poorly soluble, lipophilic drug substance. *Eur J Pharm Biopharm* **2006,** 62, 227-234.

Scherer, T. M.; Liu, J.; Shire, S. J.; Minton, A. P., Intermolecular Interactions of IgG1 Monoclonal Antibodies at High Concentrations Characterized by Light Scattering. *J Phys Chem B* **2010,** 114, 12948-12957.

Sear, R. P., Interactions in protein solutions. *Current Opinion in Colloid & Interface Science* **2006,** 11, 35-39.

Sedgwick, H.; Egelhaaf, S. U.; Poon, W. C. K., Clusters and gels in systems of sticky particles. *J. Phys.: Condens. Matter* **2004,** 16, S4913-S4922.

Sertsou, G.; Butler, J.; Hempenstall, J.; Rades, T., Solvent change co-precipitation with hydroxypropylmethylcellulose phthalate to improve dissolution characteristics of a poorly water-soluble drug. *Journal of Pharmacy and Pharmacology* **2002,** 54, (8), 1041-1047.

Shamblin, S. L.; Tang, X.; Chang, L.; Hancock, B. C.; Pikal, M. J., Characterization of the Time Scales of Molecular Motion in Pharmaceutically Important Glasses. *J. Phys. Chem. B* **1999,** 103, 4113-4121.

Shen, V. K.; Cheung, J. K.; Errington, J. R.; Truskett, T. M., Insights into Crowding Effects on Protein Stability from Coarse-Grained Model. *Journal of Biomechanical Engineering* **2009,** 131, 071002 (7pg).

Shenoy, B.; Wang, Y.; Shan, W.; Margolin, A. L., Stability of Crystalline Proteins. *Biotechnology and Bioengineering* **2001,** 73, (5), 358-369.

Shi, L.; Berkland, C., pH-Triggered Dispersion of Nanoparticle Clusters. *Adv. Mater.* **2006,** 18, 2315-2319.

Shi, L.; Plumley, C. J.; Berkland, C., Biodegradable Nanoparticle Flocculates for Dry Powder Aerosol Formulation. *Langmuir* **2007,** 23, (22), 10897-10901.

Shin, J. H.; Choi, K. Y.; Kim, Y. C.; Lee, M. G., *Antimicrob. Agents Chemother.* **2004,** 48, (5), 1756-1762.

Shire, S. J.; Shahrokh, Z.; Liu, J., Challenges in the Development of High Protein Concentration Formulations. *J. Pharm. Sci.* **2004,** 93, (6), 1390-1402.

Shulgin, I. L.; Ruckenstein, E., Preferential hydration and solubility of proteins in aqueous solutions of polyethylene glycol. *Biophysical Chemistry* **2006,** 120, 188-198.

Sidebottom, D. L.; Tran, T. D., Universal patterns of equilibrium cluster growth in aqueous sugars observed by dynamic light scattering. *Physical Review E* **2010,** 82, 051904.

Singh, M.; Li, X.-M.; McGee, J. P.; Zamb, T.; Koff, W.; Wang, C. Y.; O'Hagan, D. T., Controlled release microparticles as a single dose hepatitis B vaccine: evaluation of immunogenicity in mice. *Vaccine* **1997,** 15, (5), 475-481.

Six, K.; Berghmans, H.; Leuner, C.; Dressman, J.; Van Werde, K.; Mullens, J.; Benoist, L.; Thimon, M.; Meublat, L.; Verreck, G.; Peeters, J.; Brewster, M.; Van den Mooter, G., Characterization of Solid Dispersions of Itraconazole and Hydroxypropylmethylcellulose Prepared by Melt Extrusion, Part II. *Pharmaceutical Research* **2003,** 20, (7), 1047-1054.

Six, K.; Daems, T.; de Hoon, J.; Van Hecken, A.; Depre, M.; Bouche, M.-P.; Prinsen, P.; Verreck, G.; Peeters, J.; Brewster, M. E.; Van den Mooter, G., Clinical study of solid dipsersions of itraconazole prepared by hot-stage extrusion. *Eur J Pharm Sci* **2005,** 24, 179-186.

Six, K.; Verreck, G.; Peeters, J.; Binnemans, K.; Berghmans, H.; Augustijns, P.; Kinget, R.; Van den Mooter, G., Investigation of thermal properties of glassy itraconazole: identification of a monotropic mesophase. *Thermochimica Acta* **2001,** 376, 175-181.

Six, K.; Verreck, G.; Peeters, J.; Brewster, M. E.; Van den Mooter, G., *J Pharm Sci* **2004,** 93, (1), 124-131.

Souillac, P. O.; Middaugh, C. R.; Rytting, J. H., Investigation of protein/carbohydrate interactions in the dried state. 2. Diffuse reflectance FTIR studies. *Int J Pharm* **2002,** 235, 207-218.

Spiegel, A. J.; Noseworthy, M. M., Use of Nonaqueous Solvents in Parenteral Products. *J. Pharm. Sci.* **1963,** 52, (10), 917-927.

Stagg, L.; Zhang, S.-Q.; Cheung, M. S.; Wittung-Stafshede, P., Molecular crowding enhances native structure and stability of α/β protein flavodoxin. *PNAS* **2007,** 104, (48), 18976-18981.

Stagner, W. C.; Guillory, J. K., Physical Characterization of Solid Iopanoic Acid Forms. *Journal of Pharmaceutical Sciences* **1979,** 68, (8), 1005-1009.

Stradner, A.; Sedgwick, H.; Cardinaux, F.; Poon, W. C. K.; Egelhaaf, S. U.; Schurtenberger, P., Equilibrium cluster formation in concentrated protein solutions and colloids. *Nature* **2004,** 432, 492-495.

Stevenson, C. L., Characterization of Protein and Peptide Stability and Solubility in Non-Aqueous Solvents. *Current Pharmaceutical Biotechnology* **2000,** 1, 165-182.

Strickley, R. G., Solubilizing Excipients in Oral and Injectable Formulations. *Pharm. Res.* **2004,** 21, (2), 201-230.

Studart, A. R.; Amstad, E.; Gauckler, L., Colloidal Stabilization of Nanoparticles in Concentrated Suspensions. *Langmuir* **2007,** 23, (3), 1081-1090.

Sutherland, J. N.; Maynard, J. A., Characterization of a Key Neutralizing Epitope on Pertussis Toxin Recognized by Monoclonal Antibody 1B7. *Biochemistry* **2009,** 48, 11982-11993.

Sutherland, J. N.; Yoder, S. M.; Rock, M. T.; Maynard, J. A., Antibodies recognizing protective pertussis toxin epitopes are preferentially elicited by natural infection versus acellular immunization. **in preparation**.

Suzuki, H.; Ogawa, M.; Hironaka, K.; Ito, K.; Sunada, H., A Nifedipine Coground Mixture with Sodium Deoxycholate. II. Dissolution Characteristics and Stability. *Drug Development and Industrial Pharmacy* **2001,** 27, (9), 951-958.

Suzuki, H.; Sunada, H., Comparison of Nicotinamide, Ethylurea and Polyethylene Glycol as Carriers for Nifedipine Solid Dispersion Systems. *Chemical & Pharmaceutical Bulletin* **1997,** 45, 1688-1693.

Suzuki, H.; Sunada, H., *Chemical & Pharmaceutical Bulletin* **1998,** 46, (3), 482-487.

Tam, J. M.; Murthy, A. K.; Ingram, D. R.; Nguyen, R.; Sokolov, K. V.; Johnston, K. P., Kinetic Assembly of Near-IR-Active Gold Nanoclusters Using Weakly Adsorbing Polymers to Control the Size. *Langmuir* **2010,** 26, (11), 8988-8999.

ten Wolde, P. R.; Frenkel, D., Enhancement of Protein Crystal Nucleation by Critical Density Fluctuations. *Science* **1997,** 277, 1975-1978.

Timasheff, S. N., Stabilization of Protein Structure by Solvent Additives. In *Stability of Protein Pharmaceuticals: Part B.*, Ahern, T. J.; Manning, M. C., Eds. Springer: 1992; Vol. 3, pp 265-285.

Tombari, E.; Presto, S.; Johari, G. P.; Shanker, R. M., Molecular Mobility, Thermodynamics and Stability of Griseofulvin's Ultraviscous and Glassy States from Dynamic Heat Capacity. *Pharmaceutical Research* **2008,** 25, (4), 902-912.

Trevino, S. R.; Scholtz, J. M.; Pace, C. N., Measuring and increasing protein solubility. *J Pharm Sci* **2008,** 97, (10), 4155-4166.

Tuinier, R.; Rieger, J.; De Kruif, C. G., Depletion-induced phase separation in colloid-polymer mixtures. *Advances in Colloid and Interface Science* **2003,** 103, 1-31.

Uchida, T.; Nagayama, M.; Gohara, K., Trehalose solution viscosity at low temperatures measured by dynamic light scattering method: Trehalose depresses molecular transportation for ice crystal growth. *J Crystal Growth* **2009,** 311, 4747-4752.

Vaughn, J. M.; McConville, J. T.; Burgess, D.; Peters, J. I.; Johnston, K. P.; Talbert, R. L.; Williams III, R. O., Single dose and multiple dose studies of itraconazole nanoparticles. *Eur J Pharm Biopharm* **2006,** 63, (2), 95-102.

Vekilov, P. G.; Feeling-Taylor, A. R.; Petsev, D. N.; Galkin, O.; Nagel, R. L.; Hirsch, R. E., Intermolecular Interactions, Nucleation and Thermodynamics of Crystallization of Hemoglobin C. *Biophys J* **2002,** 83, 1147-1156.

Verreck, G.; Six, K.; Van den Mooter, G.; Baert, L.; Peeters, J.; Brewster, M. E., *Int J Pharm* **2003,** 251, 165-174.

Verreck, G.; Six, K.; Van den Mooter, G.; Baert, L.; Peeters, J.; Brewster, M., Characterization of solid dispersions of itraconazole and hydroxypropylmethylcellulose prepared by melt extrusion - part I. *International Journal of Pharmaceutics* **2001,** 251, 165-174.

Vrij, A., Polymers at Interfaces and the Interactions in Colloidal Dispersions. *Pure & Appl. Chem.* **1976,** 48, 471-483.

Wang, B.; Tchessalov, S.; Warne, N. W.; Pikal, M. J., Impact of Sucrose level on Storage Stability of Proteins in Freeze-Dried Solids: I. Correlation of Protein-Sugar Interaction with Native Structure Preservation. *J Pharm Sci* **2009,** 98, (9), 3131-3144.

Wang, W., Instability, stabilization, and formulation of liquid protein pharmaceuticals. *Int. J. Pharm.* **1999,** 185, 129-188.

Wang, W., Lyophilization and development of solid protein pharmaceuticals. *Int. J. Pharm.* **2000,** 2000, 1-60.

Wang, W., Protein aggregation and its inhibition in biopharmaceutics. *Int. J. Pharm.* **2005,** 289, 1-30.

Wang, W.; Nema, S.; Teagarden, D., Protein aggregation- Pathways and influencing factors. *Int J Pharm* **2010,** 390, (2), 89-99.

Wang, W.; Wang, E. Q.; Balthasar, J. P., Monoclonal Antibody Pharmacokinetics and Pharmacodynamics. *Clinical Pharmacology & Therapeutics* **2008,** 84, 548-558.

Webb, S. D.; Cleland, J. L.; Carpenter, J. F.; Randolph, T. W., A New Mechanism for Decreasing Aggregation of Recombinant Human Interferon-gamma by a Surfactant: Slowed Dissolution of Lyophilized Formulations in a Solution Containing 0.03% Polysorbate 20. *Journal of Pharmaceutical Sciences* **2002,** 91, (2), 543-558.

Webb, S. D.; Cleland, J. L.; Carpenter, J. F.; Randolph, T. W., Effects of Annealing Lyophilized and Spray-Lyophilized Formulations of Recombinant Human Interferon-γ. *J Pharm Sci* **2003,** 92, (4), 715-729.

Webb, S. D.; Golledge, S. L.; Cleland, J. L.; Carpenter, J. F.; Randolph, T. W., Surface adsorption of recombinant human interferon-gamma in lyophilized and spray-lyophilized formulations. *J Pharm Sci* **2002,** 91, 1474-1487.

Weiss IV, W. F.; Young, T. M.; Roberts, C. J., Principles, Approaches, and Challenges for Predicting Protein Aggregation Rates and Shelf Life. *J. Pharm Sci.* **2009,** 98, (4), 1246-1277.

Wong, J.; Papadopoulos, P.; Werling, J.; Rebbeck, C.; Doty, M.; Kipp, J.; Konkel, J.; Neuberger, D., Itraconazole suspension for intravenous injection: determination of the real component of complete refractive index for particle sizing by static light scattering. *PDA J Pharm Sci Technol.* **2006,** 60, (5), 302-313.

Yadav, S.; Liu, J.; Shire, S. J.; Kalonia, D. S., Specific Interactions in High Concentration Antibody Solutions Resulting in High Viscosity. *J Pharm Sci* **2010,** 99, (3), 1152-1168.

Yamada, T.; Saito, N.; Imai, T.; Otagiri, M., *Chemical & Pharmaceutical Bulletin* **1999,** 47, (9), 1311-1313.

Yamashita, K.; Nakate, T.; Okimoto, K.; Ohike, A.; Tokunaga, Y.; Ibuki, R.; Higaki, K.; Kimura, T., Establishment of new preparation method for solid dispersion formulation of tacrolimus. *International Journal of Pharmaceutics* **2003,** 267, 79-91.

Yang, M. X.; Shenoy, B.; Disttler, M.; Patel, R.; McGrath, M.; Pechenov, S.; Margolin, A. L., Crystalline monoclonal antibodies for subcutaneous delivery. *PNAS* **2003,** 100, (12), 6934-6939.

Ye, M.; Kim, S.; Park, K., Issues in long-term protein delivery using biodegradable microparticles. *J Controlled Release* **2010,** 146, (2), 241-260.

Young, T. M.; Roberts, C. J., Structure and thermodynamics of colloidal protein cluster formation: Comparison of square-well and simple dipolar models. *J Chem Phys* **2009,** 131, 125104.

Yu, L. X.; Foster, T. P.; Sarver, R. W.; Moseley, W. M., Preparation, Characterization, and in Vivo Evaluation of an Oil Suspension of a Bovine Growth Hormone Releasing Factor Analog. *J. Pharm. Sci.* **1996,** 85, (4), 396-400.

Yu, Z.; Johnston, K. P.; Williams, R. O., III, Spray freezing into liquid versus spray-freeze drying: Influence of atomization on protein aggregation and biological activity. *Eur. J. Pharm. Sci.* **2006,** 27, 9-18.

Zaharoff, D. A.; Barr, R. C.; Li, C.-Y.; Yuan, F., Electromobility of plasmid DNA in tumor tissues during electric field-mediated gene delivery. *Gene Therapy* **2002,** 9, 1286-1290.

Zhang, F.; Skoda, M. W. A.; Jacobs, R. M. J.; Martin, R. A.; Martin, C. M.; Schreiber, F., Protein Interactions Studied by SAXS: Effect of Ionic Strength and Protein Concentration for BSA in Aqueous Solutions. *J Phys Chem B* **2007,** 111, 251-259.

Zhang, X.; Tsang, A. M.; Okino, M. S.; Power, F. W.; Knaak, J. B.; Harrison, L. S.; Dary, C. C., A Physiologically Based Pharmacokinetic/Pharmacodynamic Model for Carbofuran in Sprague-Dawley Rats Using the Exposure-Related Dose Estimating Model. *Toxicological Sciences* **2007,** 100, (2), 345-359.

Zhou, D.; Zhang, G. G. Z.; Law, D.; Grant, D. J. W.; Schmitt, E. A., Physical Stability of Amorphous Pharmaceuticals: Importance of Configurational Thermodynamic Quanitites and Molecular Mobility. *Journal of Pharmaceutical Sciences* **2002,** 91, (8), 1863-1872.

Zhou, H.-X.; Rivas, G.; Minton, A. P., Macromolecular Crowding and Confinement: biochemical, biophysical and potential physiological consequences. *Annu. Rev. Biophys.* **2008,** 37, 375-397.

Zhu, G.; Mallery, S. R.; Schwendeman, S. P., Stabilization of proteins encapsulated in injectable poly(lactide-co-glycolide). *Nature Biotechnology* **2000,** 18, 52-57.

Zhu, Y.; Shah, N. H.; Malick, A. W.; Infeld, M. H.; McGinity, J. W., Controlled Release of a Poorly Water-Soluble Drug from Hot-Melt Extrudates Containing Acrylic Polymers. *Drug Development and Industrial Pharmacy* **2006,** 32, 569-583.

Zhu, Z.; Anacker, J. L.; Ji, S.; Hoye, T. R.; Macosko, C. W.; Prud'homme, R. K., Formation of Block Copolymer-Protected Nanoparticles via Reactive Impingement Mixing. *Langmuir* **2007,** 23, 10499-10504.

Zintchenko, A.; Susha, A. S.; Concia, M.; Feldmann, J.; Wagner, E.; Rogach, A. L.; Ogris, M., Drug Nanocarriers Labeled with Near-infrared-emitting Quantum Dots (Quantoplexes): Imaging Fast Dynamics of Distribution in Living Animals. *Molecular Therapy* **2009,** 17, (11), 1849-1856.